Argus® II Retinal Prosthesis System: Clinical & Functional Outcomes

Yvonne Hsu-Lin Luo

Institute of Ophthalmology, University College of London and Moorfields Eye Hospital NHS Foundation Trust

Supervisors: Professor Lyndon da Cruz and Professor Peter J. Coffey

Thesis submitted for the degree of Doctor of Philosophy (Ph.D.) University College of London

October 2016

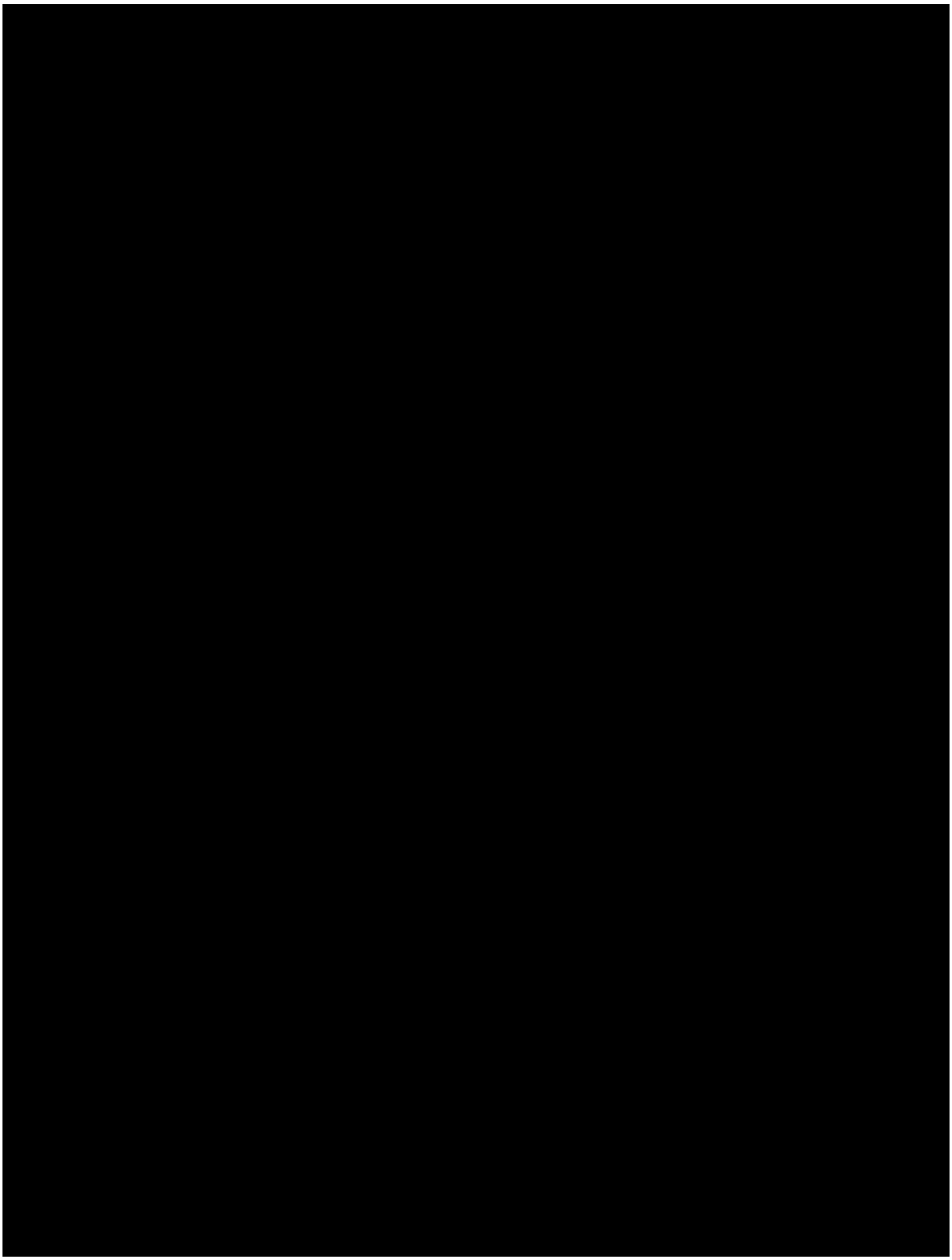

I, Yvonne Hsu-Lin Luo, confirm that the work presented in this thesis is my own. Where information has been obtained with the help of others, I confirm that this has been indicated below:

1. All the patients who received the Argus® II retinal prosthesis implantation at Moorfields Eye Hospital NHS Foundation Trust had their surgery performed by, and are under the care of, Professor Lyndon da Cruz.

2. Three patients who received the Argus® II retinal prosthesis implantation at Manchester Eye Hospital had their surgery performed by, and are under the care of, Professor Paulo Stanga.

3. Psychophysical tests for the Shapes Recognition Study in 2 of the subjects at Moorfields Eye Hospital and all the subjects at Manchester Royal Eye Hospital (n = 3) were performed by field engineers from Second Sight Medical Products, Inc. (Sylmar, CA, USA) (**Chapter 3**).

4. Psychophysical tests for Objects Recognition Study in one subject at Manchester site (n=1) was performed by a field engineer from Second Sight Medical Products, Inc. (Sylmar, CA, USA) (**Chapter 3**).

5. MATLAB® script used in analysing the 3D motion data from ProReflex® Motion Capture system (Qualysis, Sweden)(**Chapter 4**), and functional near-infrared spectroscopy (fNIRS) imaging analysis (**Chapter 7**) was written by Dr. Joe Jianjiang Zhong from Moorfields Eye Hospital

6. Images of the MRI of brain scans of Argus® II patients were reformatted and analysed by consultant neuro-radiologist, Dr. Indran Davagnanam at Moorfields Eye Hospital (**Chapter 6**).

7. Dr. Ilias Tachtsidis from the Medical Physics and Biomedical Engineering Department of University College London, provided expert advice on the interpretation of fNIRS imaging analysis (**Chapter 7**).

Yvonne Hsu-Lin Luo Date: 24th October 2016

Table of Contents

2. Luo, Y.H.-L., da Cruz, L., 2014. A review and update on the current status of retinal prostheses (bionic eye). Br. Med. Bull. 109, 31–44.
3. Luo, Y.H.-L., Fukushige, E., daCruz, L., 2016. The potential of the second sight system bionic eye implant for partial sight restoration. Expert Rev Med Dev 13, 673–681.
4. Luo, Y.H.-L., Davagnanam, I., daCruz, L., 2013. MRI Brain Scans in Two Patients with the Argus II Retinal Prosthesis. Ophthalmology 120, 1711–1711.e8.
5. Luo, Y.H.-L., Zhong, J.J., daCruz, L., 2015. The use of Argus® II retinal prosthesis by blind subjects to achieve localisation and prehension of objects in 3-dimensional space. Graefe's archive for clinical and experimental ophthalmology = Albrecht von Graefes Archiv fur klinische und experimentelle Ophthalmologie 253, 1907–1914.
6. Luo, Y.H.-L., Zhong, J.J., Clemo, M., daCruz, L., 2016. Long-term Repeatability and Reproducibility of Phosphene Characteristics in Chronically Implanted Argus® II Retinal Prosthesis Subjects. Am. J. Ophthalmol.

Abstract

Developing artificial visual systems to restore sight in blind patients has long been the dream of scientists, clinicians and the public at large. After decades of research, the greatest success in the field has been achieved with electronic retinal prostheses. To date, 3 retinal prosthetic systems have made the transition from laboratory / clinical research to entering the commercial market for clinical use, namely the Argus® II Retinal Prosthesis System (Second Sight), the alpha-IMS system (Retinal Implant AG), and the IRIS® II (Pixium Vision). The following body of work describes the Argus® II Retinal Prosthesis system, which obtained regulatory approval in the European Economic Area in 2011 (CE marking) and later on in the USA (FDA approval in February 2013), based on the results of an international multi-centre clinical feasibility trial (Clinical Trial identifier: NCT 00407602).

This thesis aims to examine the long-term clinical and functional outcomes in an early cohort of subjects chronically implanted with the Argus® II system, from the original feasibility study. A further aim is to elucidate the characteristics of the artificial vision that is perceived and its long-term repeatability and reproducibility in individual subjects. These two broad aims will assist in understanding the nature of the visual performance provided by this device, as well as to add to the current data that is defining the feasibility of constructing predictable pixelated patterns to achieve useful artificial vision in the future. Finally, we explored the feasibility of real-time imaging of visual cortex activation in response to electrical retinal stimulation with the Argus® II system, using functional near infra-red spectroscopy (fNIRS). Development of this real-time imaging tool will enable future investigations into the differences in the cortical activities in response to different stimulations and in different subjects. This may in turn help us understand the variability in their visual performance, as well as to further explore the extent and effect of cross-modal plasticity at the cortical level, in this cohort of patients who have been deprived of visual inputs for decades.

Visual function was assessed in terms of: a) form recognition and b) spatial localisation under both 2-dimensional (2D) screen-based laboratory settings and 3-dimensional (3D) paradigms simulating real-life settings. A prospective

study of 11 Argus® II subjects showed that the subjects could identify distinct geometric shapes presented in high contrast better with the prosthetic system switched on (median % of correct identification = 20.0%, IQR = 18.8), versus off (median = 12.5%, IQR = 5.0). The accuracy of shapes identification could be further improved by enhancing the outlines of the geometric shape (median = 33.1%, IQR = 21.6).

A further prospective study from a subset of 7 subjects showed that this 2D shape identification could be translated into improved identification of 3D objects. These subjects could identify 8 common daily-life objects presented in high contrast with the prosthetic system switched on (median = 31.3%, IQR = 20.3) versus off (median = 12.5%, IQR = 12.5). Scrambling of the transmission signals within the prosthetic system in order to separate light information from form information (i.e. “scrambled mode”) hindered the identification in some but not all subjects (median = 25.0%, IQR = 12.5). The accuracy of object identification could also be improved by enhancing the edges of objects (median = 43.8%, IQR = 15.6).

Previously published data showed that Argus® II subjects were able to locate and point to white squares presented on touch screens against a black background more accurately with the prosthetic system switched on versus off. We demonstrated with a prospective study of 5 subjects that they could localise an object on the table, reach out and grasp the object (prehension) with great accuracy (66.7 – 100%) when the prosthetic system was switched on, versus no object prehension (0%) with the system switched off.

A prospective study of 6 Argus® II subjects illustrated that while there was a wide variation in the shape and size of the phosphenes perceived by individual subjects, the elicited phosphenes were consistently reproducible in each subject using fixed stimulating parameters, with inter-stimuli intervals ranging from 20 minutes apart, down to 1 second. The perceived location of the phosphenes grossly matched retinotopic agreement, with 4 subjects drawing phosphenes in the same visual field quadrant as predicted by the relative stimulus-fovea position, and 2 subjects depicting phosphenes in the same hemi-field as the expected locations.

A retrospective study of 3 Argus® II subjects who underwent MRI brain scan

(for unrelated medical reasons) showed that MRI brain scans of up to 1.5 Tesla field strength appeared to have no detrimental effect on the subjects and their implant function. The Argus® II implant produced an artefact of around 50mm x 50mm in size which would prevent visualisation of structures within the orbit, but visualisation of surrounding tissues outside this areas are unaffected.

The use of functional MRI as a tool of exploring visual cortex activation in Argus® II subjects was discounted, due to concerns of signal interference from the radiofrequency telemetry of Argus® II system with that of MRI. Subsequently, we have demonstrated in a prospective study that an alternative neuro-imaging technique, functional near infra-red spectroscopy (fNIRS), was capable of capturing real-time cortical activation in 5 out of 6 Argus® II subjects, and maybe a feasible tool for future investigation into cortical function and interactions.

The work in this thesis has shown that the Argus® II retinal prosthesis system could improve visual function both in terms of form recognition, as well as object localisation in 3D in situations simulating real-life settings, in a cohort of patients with end-stage retinitis pigmentosa or other outer retinal diseases such as choroideremia. The wide variation in the visual performance level observed could in part be attributable to the diversity in the phosphene features perceived by these subjects. Nevertheless, the consistency and reproducibility with which these phosphenes could be elicited, with fixed stimulating parameters within each subject, provides an encouraging basis for the construction of more complicated pixelated images.

Future work to determine the underlying factors influencing the perceived phosphene characteristics, may allow for better prediction of functional outcome, which could in turn be useful for patient selection and tailored pre-operative counselling. For those subjects already implanted with the Argus® II system, future work into determining the suitable stimulating parameters for each electrode / quad stimulation may be required for individual subjects, to achieve the construction of optimised and useful, pixelated prosthetic vision.

Publications related to this thesis

Review articles presenting data from this thesis

- Luo, Y.H.-L., da Cruz, L., 2016. The Argus® II Retinal Prosthesis System. Prog Retin Eye Res 50, 89–107.
- Luo, Y.H.-L., da Cruz, L., 2014. A review and update on the current status of retinal prostheses (bionic eye). Br. Med. Bull. 109, 31–44.
- Luo, Y.H.-L., Fukushige, E., da Cruz, L., 2016. The potential of the second sight system bionic eye implant for partial sight restoration. Expert Rev Med Dev 13, 673–681.

Original articles also presenting data from this thesis

- Luo, Y.H.-L., Davagnanam, I., da Cruz, L., 2013. MRI Brain Scans in Two Patients with the Argus II Retinal Prosthesis. Ophthalmology 120, 1711–1711.e8.
- Luo, Y.H.-L., Zhong, J.J., da Cruz, L., 2015. The use of Argus® II retinal prosthesis by blind subjects to achieve localisation and prehension of objects in 3-dimensional space. Graefe's archive for clinical and experimental ophthalmology = Albrecht von Graefes Archiv fur klinische und experimentelle Ophthalmologie 253, 1907–1914.
- Luo, Y.H.-L., Zhong, J.J., Clemo, M., da Cruz, L., 2016. Long-term Repeatability and Reproducibility of Phosphene Characteristics in Chronically Implanted Argus® II Retinal Prosthesis Subjects. Am. J. Ophthalmol.

Conference oral presentations presenting data from this thesis

- Luo, Y.H.-L., Zhong, J.J., da Cruz, L. Subjects blinded by outer retinal dystrophies are able to differentiate a range of common objects using the Argus® II Retinal Prosthesis System. The 13th Euretina Congress (2013), Hamburg, Germany.
- Luo, Y.H.-L., Zhong, J.J., Clemo, M., da Cruz, L. Long-term characteristics of phosphenes in chronically implanted Argus® II retinal prosthesis subjects. The 16th Euretina Congress (2016), Copenhagen, Denmark.

Conference poster presentations presenting data from this thesis

- Luo, Y.H.-L., Davagnanam, I., da Cruz, L. Safety of MRI brain scans in Argus® II retinal prosthesis patients. The 2013 Annual Meeting of the Association for Research in Vision and Ophthalmology (ARVO), Seattle, USA. (Received ARVO NIHR Travel Grant Award)
- Luo, Y.H.-L., Zhong, J.J., Merlini, F., Anaflous, F., Asiero, M., Stanga, P., da Cruz, L. The use of Argus II Retinal Prosthesis to Identify Common Objects in Blind Subjects with Outer Retinal Dystrophies. The 2013 Annual Meeting of the American Academy of Ophthalmology (AAO), New Orleans, USA.
- Luo, Y.H.-L., Zhong, J.J., Clemo, M., da Cruz, L. Long-term characteristics of phosphenes produced by Argus® II retinal prosthesis. The 2015 Annual Meeting of the American Academy of Ophthalmology (AAO), Las Vegas, USA.

Acknowledgements

There are many people I am grateful to, without whom this work would not be possible.

Firstly, I would like to express my utmost gratitude to Professor Lyndon da Cruz for his continuing guidance, patience and encouragement throughout my Ph.D. His dedication and committed spirit to research is exemplary and has inspired and driven me. I am particularly grateful for his constructive comments and insightful advice on both my clinical and research work over the years. It has been a wonderful privilege to work with him. I am also grateful to Professor Pete Coffey for his support and tireless efforts in obtaining funding and practical guidance.

My gratitude also goes to Joe Zhong, whose expertise in computer programming, optics, engineering and psychophysics have provided invaluable technical support throughout my research. Joe's great sense of humour and optimistic yet pragmatic nature has made clinical experiments a productive while enjoyable experience. My research would also not have been possible if not for the generosity and altruism of all the Argus® II patients John, Ron, Phil, Eric, Richard and Kim and their families.

Special thanks to the staff at the Moorfields Eye Hospital Biomedical Research Centre Clinical Trials Unit: Monica Clemo, Vincent Rocco and the technical team – for capturing excellent images throughout the study; Roxanne Crosby-Nwaobi and the nursing team – for taking care and monitoring the well-being of the Argus® II patients during their study visits; Rahdika Krishnan and Wen Xing – for their statistical support and advice; David Stewart and Panayiotis Panayiotou – for their fantastic organisation and co-ordination of all the research patient visits. Many thanks also go to the Second Sight Medical Products Inc. field engineers and staff, in particular Fatima Anaflous, Francesco Merlini and Gregoire Cosendai, for their efforts in training and performing psychophysical testing on our Argus® II patients.

The supports from Dr. Aachal Kotecha on the use of the ProReflex® Motion Capture system (Qualisys, Sweden) were much appreciated. My thanks also go to Dr. Indran Davagnanam for his expert advice on MRI imaging and

interpretation; and to Dr. Ilias Tachtsidis on his invaluable advice and input on the acquisition of functional near infra-red spectroscopy imaging, as well as data analysis. I would also like to thank Monica Clemo for her technical help and support with the use of the Adobe® Creative Suite® 5 Photoshop® software.

I am indebted to the Moorfields Eye Hospital NIHR Biomedical Research Centre for Ophthalmology and the London Project to Cure Blindness for funding my research. I am also grateful for the Special Trustees of Moorfields Eye Hospital and the NIHR Biomedical Research Centre for Ophthalmology for providing support for travel to conferences and the infrastructure for clinical research at Moorfields Eye Hospital.

Most importantly, this thesis would not be possible without the love, support and sacrifices from my parents, who gave me the opportunity to come and study in England in 1993.

List of Abbreviations

2D	Two-dimensional
3D	Three-dimensional
AMD	Age-related macular degeneration
ASIC	Application-Specific-Internal-Circuit
BOLD	Blood oxygenation level-dependent
CE	Conformité Européene
EEG	Electroencephalography
EEP	Electrically evoked potentials
eVEP	Electrically elicited visual evoked potentials
FDA	Food and drug administration
FHS	First hand stop
fMRI	Functional magnetic resonance imaging
fNIRS	Functional near infra-red spectroscopy
HFS	High frequency stimulation
HHb	Deoxygenated haemoglobin
HRF	Haemodynamic response function
ICER	Incremental cost effectiveness ratio
iPSC	Induced pluripotent stem cell
IQR	Interquartile range
IR	Infra-red
LCD	Liquid crystal display

LED	Light emitting diode
LGN	Lateral geniculate nucleus
MPDA	Microphotodiode array
MRI	Magnetic resonance imaging
NIR	Near infra-red
NVC	Neurovascular coupling
OCT	Optical coherence tomography
O_2Hb	Oxygenated haemoglobin
QALY	Quality-adjusted life-year
QTM	Qualysis track manager
RF	Radio-frequency
RGC	Retinal ganglion cell
RP	Retinitis pigmentosa
RPE	Retinal pigment epithelium
SD	Standard deviation
VEP	Visually-evoked potentials
VPU	Visual processing unit

List of Figures

List of Tables

Chapter 1

Introduction and Overview

Prostheses are artificial replacements designed to substitute a destroyed or damaged part of the body in order to restore function and / or cosmesis. Using visual prostheses to restore visual function in blind patients has long been the dream of many scientists, clinicians and has captured the imagination of the public. Over the years, several devices have been developed with varying degrees of success, though none of these come close to emulating the complexity or resolution of the human visual system.

According to the Bulletin of World Health Organisation 2004 (Grover et al., 1999; Milam et al., 1998; Resnikoff et al., 2004), the prevalence of blindness worldwide in 2002 (defined as visual acuity of less than 3/60, or a corresponding visual field loss to less than 10 degrees in the better eye with best possible correction) was estimated to be 37 million people, of which 1.368 million were children under the age of 15. In the developed countries, retinal diseases are the leading cause of childhood and adult visual loss (Apte et al., 2001; Attebo et al., 1996; Dimitrov et al., 2003; Hartong et al., 2006; Klaver et al., 1998; Klein et al., 1995; Krumpaszky et al., 1999; Muñoz et al., 2000; Sakaguchi et al., 2012; Santos, 1997; Stone, 1992). Age-related macular degeneration (AMD), which peaks in the 8th and 9th decade of life (Klaver et al., 1998), contributes to more than half of blindness registration (Yong et al., 2006). Inherited retinal / macular dystrophy, on the other hand, while less common, can lead to blindness during the 2nd or 3rd decade of life (Liew et al., 2014). Of these, retinitis pigmentosa (RP) is the most common with a prevalence of 1 in 3000 worldwide (Hamel, 2006; Hartong et al., 2006; Humayun et al., 2012; Michaelides et al., 2003). Collectively, AMD and RP, diseases both affecting the outer retina (photoreceptors and RPE), are responsible for a large proportion of adult blindness. Replacement of outer retina function by means of a retinal prosthesis therefore represents a potential treatment target for prosthetic vision.

1.1 Visual Pathway & Visual Processing

Vision represents the outcome of a complex physiological process and the visual system is the most complex and developed sensory system in our body (Holmes, 1945; Perry and Morton, 1992; Wurtz and Kandel, 2013). To achieve optimal visual function, several principle steps are involved:

1. Capture of electromagnetic waves in the visible spectrum as emitted from or reflected by the physical world onto the retina as focused images;
2. Conversion of these electromagnetic waves into a voltage gradient in the photoreceptors;
3. Propagation of a neurological signal by means of action potentials along the visual pathway;
4. Simultaneous processing of the images to extract visual information along the visual pathway;
5. Interpretation of the visual information by the visual cortex.

1.1.1 Retina

The human retina is a complex neural network organised into multiple regular and integrated layers (see Figure 1.1). The deepest layer of this network is a layer of photosensitive photoreceptors. Electromagnetic energy that enters the eye as a focused pattern of visible light is converted into electrical energy in the photoreceptors. This transduced signal is then propagated via bipolar cells layer (with modification from amacrine and horizontal cells) to the ganglion cells layer. The axons of the ganglion cells aggregate to exit the eyeball as the optic nerve. Within the retina, image processing and information extraction begins and continues throughout the visual pathway (Bear et al., 2015; Kolb, 2003).

In a human with normal retinal anatomy, there are around 5 million cones and 120 million rods. Processing such a significant amount of input into the visual system requires complex intercellular interactions and involve summation and integration of signals from different cells (Carpenter and Reddi, 2012; Potts and Inoue, 1969; Potts et al., 1968; Wurtz and Kandel, 2013).

The first level of signal processing begins at the bipolar cells. There are two broad classes of bipolar cells: the rod bipolar cells, which receive signals from the rods (and later form the **magnocellular** pathway); and the cone bipolar cells, which synapse with the cones (and later form the **parvocellular** pathway). Summation of information occurs as many photoreceptors converge and synapse onto the same bipolar cells (except at the fovea, see Section 1.2.4). Together with modifications from the laterally communicating horizontal cells (which form synapses amongst neighbouring bipolar cells), integration of the summated photoreceptor signals (in the form of graded membrane potentials)

result in the concentric, antagonistic centre-surround receptive field of the bipolar cells. The ON bipolar cells depolarise when light is shone in their receptive field centre (and hyperpolarise when light is shone in the surrounding of their receptive field), while OFF bipolar cells hyperpolarise to light in their receptive field centre (and depolarise with the light in the surrounding).

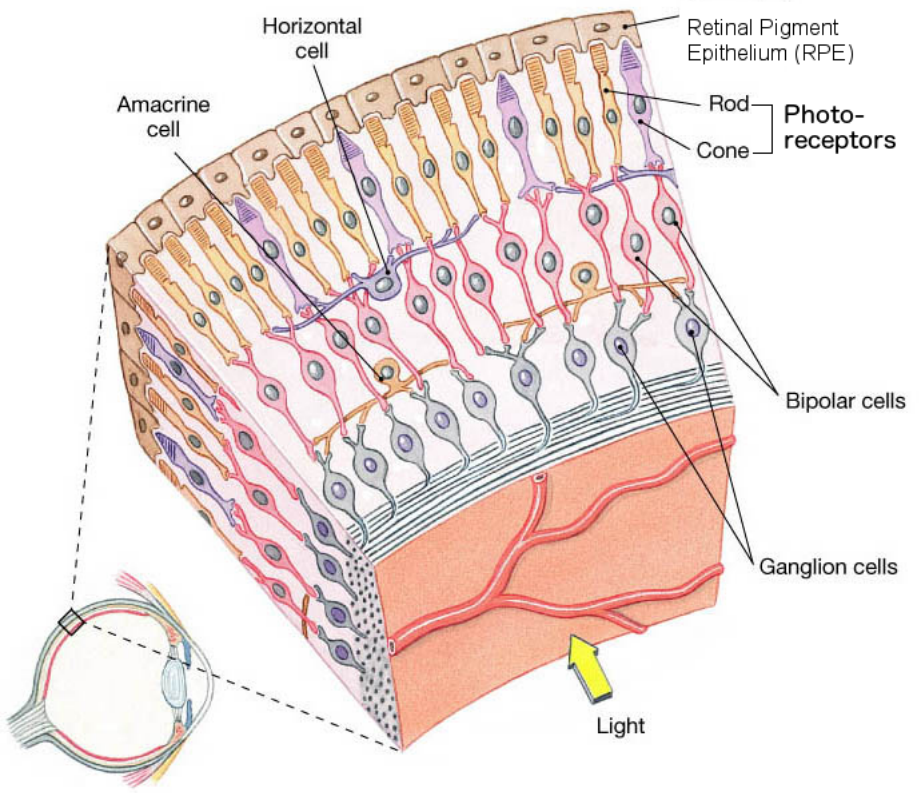

Figure 1.1: Schematic drawing of the different layers of retina. Electromagnetic visible light waves travel through the pupil and the virtually transparent retinal layers to activate the photosensitive photoreceptors. Conversion of electromagnetic light waves into electrical energy takes place in the photoreceptors, which then propagate the resultant signal to the bipolar cells layer, and then to the ganglion cells layer. The collective axons of the ganglion cells exit the globe as the optic nerve. In each of these retinal cell layers, summation and integration of information take place as part of visual processing. (Image from ("Special Senses," n.d.))

The next level of information summation and processing occurs at the ganglion cells layer, where information within each bipolar cell is further converged and synapsed onto the 1.5 million ganglion cells. The parvocellular **P-type** ganglion cells receive signals from cone bipolar cells; while the magnocellular **M-type** ganglion cells receive inputs from the rod bipolar cells. Again, with modification and integration of information from laterally communicating amacrine cells, ganglion cells exhibit various types of response to light. Some ganglion cells

maintain the concentric antagonistic centre-surround receptive fields as seen in bipolar cells. Others exhibit “on response” (transient burst of action potentials in response to an increase in illumination), “off response” (transient burst of action potentials to a decrease in illumination), “on-off response” (transient burst of action potentials at the commencement and at the cessation of a period of steady illumination), or “sustained response” (persistent action potentials when a steady illumination is on, and fades when the illumination is switched off).

1.1.2 Lateral Geniculate Nucleus (LGN) of the Thalamus

After interactions at the ganglion cells layer, ganglion cell axons bundle together to form the optic nerve and exit the eye to continue as the intracranial portion of the visual pathway. The first major synapse and relay of the intracranial visual pathway is the lateral geniculate nucleus (LGN) of the thalamus, where more than 90% of the ganglion cell axons terminate. The remaining 10% of the ganglion cell axons project to superior colliculus (which controls saccadic eye movements) and the pretectum in the midbrain (which controls pupillary reaction). This small proportion of ganglion cells are also thought to be responsible for *blindsight* – a limited residual vision which appears to function at a subconscious level, and will not be discussed further.

In primates, the LGN consists of 6 layers (see Figure 1.2). The magnocellular ganglion cells (containing inputs from rod bipolar cells) from the nasal hemi-retina project to layer 1 of the contralateral LGN; while those from the temporal hemi-retina project to layer 2 of the ipsilateral LGN. This magnocellular pathway contains information on **movement**, **depth**, and **brightness** (i.e. high sensitivity to luminance contrast), and transmits signals that are transient and rapid in nature. The parvocelluar ganglion cells (containing inputs from cone bipolar cells), on the other hand, project to levels 4 and 6 of the contralateral LGN (from nasal hemi-retina) and levels 3 and 5 of the ipsilateral LGN (from the temporal hemi-retina). This parvocellular pathway transmits information on **colour**, **form** and **fine details**, and the signals are slow and sustained in nature, with low sensitivity to luminance contrast. Further more, LGN cells driven by the same area of retina form a single radial column, thereby preserving the retinotopic organisation of the signals originating from the retinal images. Such preservation of retinotopy is crucial for later form construction and interpretation

in the primary visual cortex at the occipital lobe (see Figure 1.3). The LGN also receives substantial feedback from other brain areas, in particular the reticular formation and the visual cortex (in fact only 10 – 20% of the presynaptic inputs in the LGN are from the retina), thereby acting as a gateway for controlling the information passing from the retina to the cortex (Wurtz and Kandel, 2013).

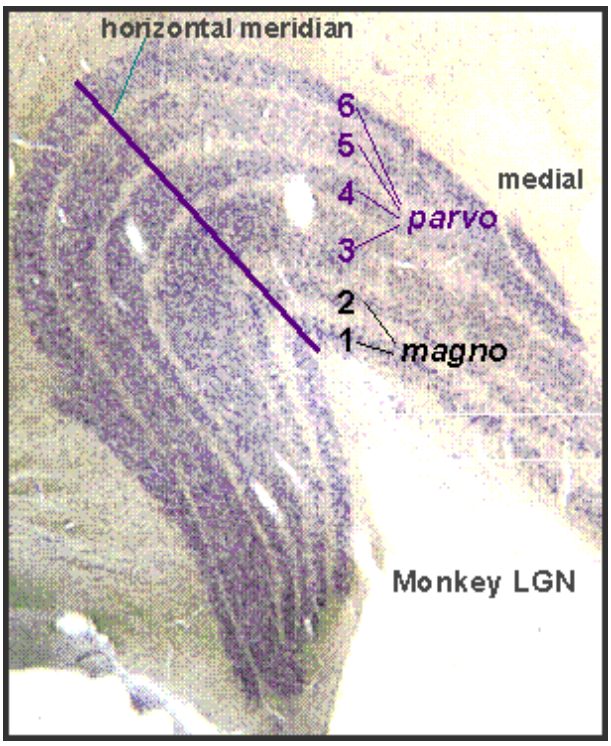

Figure 1.2: Histology slide of a coronoal section through the lateral geniculate nucleus (LGN) of the rhesus monkey. In primates, the LGN consists of 6 layers. The magnocellular ganglion cells from the nasal hemi-retina project to layer 1 of the contralateral LGN; while those from the temporal hemi-retina project to layer 2 of the ipsilateral LGN. This magnocellular pathway (labelled in black) contains information on **movement**, **depth**, and **brightness**, and transmits signals that are transient and rapid in nature. The parvocelluar ganglion cells project to levels 4 and 6 of the contralateral LGN (from nasal hemi-retina) and levels 3 and 5 of the ipsilateral LGN (from the temporal hemi-retina). This parvocellular pathway (labelled in purple) transmits information on **colour**, **form** and **fine details**, and the signals are slow and sustained in nature, with low sensitivity to luminance contrast. Further more, LGN cells driven by the same area of retina form a single radial column, thereby preserving the retinotopic organisation of the signals originating from the retinal images. (Image from ("Slide Show: The Neural Control of Vision D-1," n.d.))

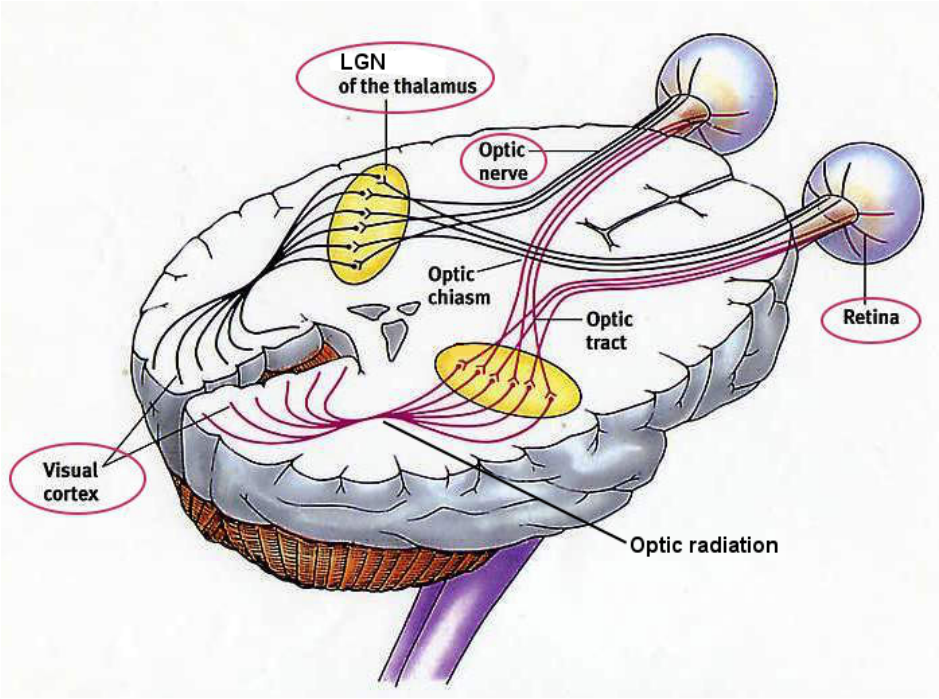

Figure 1.3: Schematic representation of the visual pathway from the retina to the visual cortex. Theoretically, electrical stimulation at any point along the visual pathway could elicit transient visual percepts known as phosphenes. Visual prostheses have been developed for direct electrical stimulation at the following sites (circled in red): retina, optic nerve, thalamus and the visual cortex. (Image from ("Neuroscience for Kids: the visual pathway Interesting information on what can happen if there's any damage | Teaching: Physics - Vision | Pinterest | Pathways…," n.d.))

1.1.3 Visual Cortex

From the LGN the neurones leave the thalamus, traversing the white matters of the brain (antero-posteriorly) as the optic radiations to arrive at the occipital lobe. Further inputs and outputs to other cortical regions also occur, to facilitate final processing and interpretation in the visual cortex.

The primary visual cortex (also known as striate cortex or Brodmann's area 17), is also composed of 6 layers (see Figure 1.4). Layer 4 is the main receiving layer and is subdivided into 4A, 4B and 4C. Layer 4Cα (a further sub-layer) receives input from the LGN magnocellular pathway (containing M-type cells), which relays to the 4B layer; while layer 4Cß receives input from the LGN parvocellular pathway (containing P-type cells), and relays onto layer 3. Apart from the predominate magnocellular and parvocellular pathways, a third koniocellular pathway is also present. Little is known about the function of this koniocellular pathway, but it is thought that they originate from non-M non-P

koniocellular ganglion cells in the retina, synapsing at the intra-laminar layers of the LGN, and terminate in the “blobs” areas of layers 2 and 3.

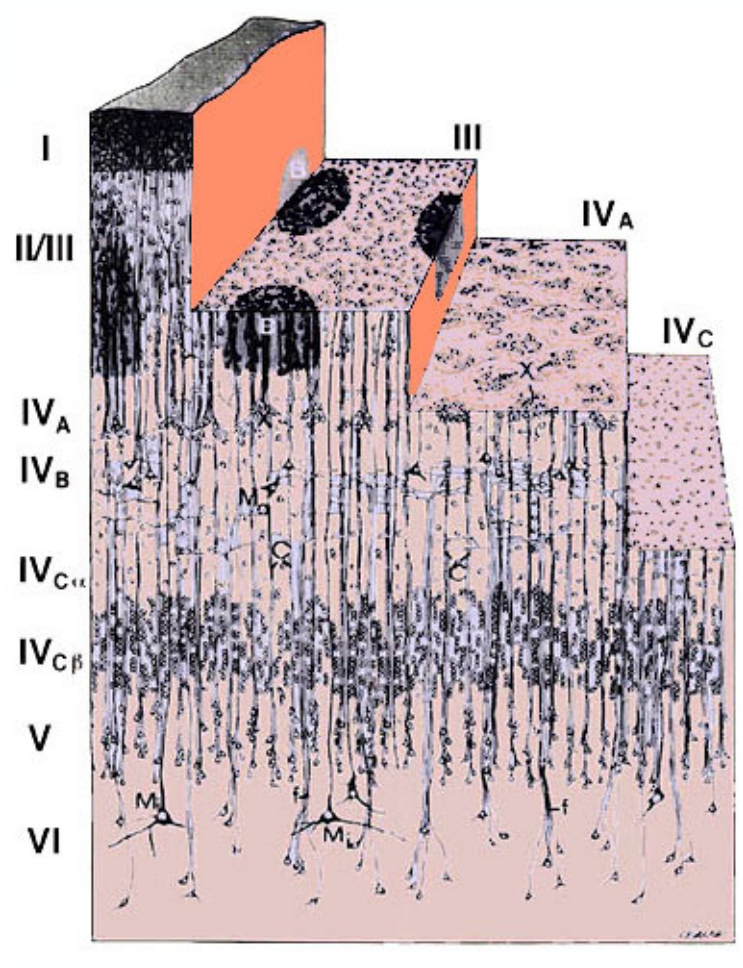

Figure 1.4: Schematic drawing of the 6 layers of the primary visual cortex. Layer 4 is the main receiving layer and is subdivided into 4A, 4B and 4C. Layer 4Cα (a further sub-layer) receives input from the LGN magnocellular pathway (containing M-type cells), which relays to the 4B layer; while layer 4Cß receives input from the LGN parvocellular pathway (containing P-type cells), and relays onto layer 3. Apart from the predominate magnocellular and parvocellular pathways, a third koniocellular pathway is also present. Little is known about the function of this koniocellular pathway, but it is thought that they originate from non-M non-P koniocellular ganglion cells in the retina, synapsing at the intra-laminar layers of the LGN, and terminate in the “blobs” areas of layers 2 and 3. (Image modified from (“The Primary Visual Cortex by Matthew Schmolesky – Webvision,” n.d.))

Once at the visual cortex, visual processing proceeds as 3 parallel channels, each focusing on extracting different aspects of the visual information (see Figure 1.5):

a) M channel

b) P-IB channel

c) Blob channel

a) M channel

The M channel processes information from the magnocellular pathway. Originating from magnocellular ganglion cells (which in turn receive inputs from rods), M-type cells have large, concentric, centre-surround antagonistic receptive fields, with particular sensitivity to movement and luminance contrast.

On arriving in the visual cortex at the 4C cortex, the information is relayed (via layer 4B) onto and processed by the **simple cells** in layers 2 and 3. Simple cells' receptive fields are linear and highly orientation specific, flanked by an antagonistic surround. As such, they can detect both the orientation and location of a stimulus.

From the primary visual cortex, the M channel projects to the middle temporal (MT) area in the posterior parietal lobe, where **motion detection** takes place. The M channel is therefore responsible for processing visual information related to **motion** and **localisation**, with high sensitivity under low luminance setting.

b) P-IB Channel

The P-IB channel processes information from the parvocellular pathway and consists of parvocellular ganglion cells (P-type cells), which receive inputs from cones. P-type cells have small, concentric centre-surround antagonistic receptive fields. 80% of the P-type cells are also sensitive to light wavelength changes (i.e. colour sensitive), and have red-green or blue-yellow centre-surround antagonistic receptive fields.

After arriving at the 4Cß layer of the primary visual cortex, the information flows to the "inter-blobs" (IB) areas of layers 2 and 3, to undergo further integration and processing by the **complex cells** at these layers.

Complex cells, in contrast to simple cells, respond to more complex sets of stimuli. The receptive fields of complex cells are generally larger than that of simple cells, as many complex cells receive inputs from several simple cells. In addition to being orientation specific, complex cells also respond to a target placed anywhere within their receptive field. They are therefore sensitive to changes in direction of movement, with some neurones showing responses to movement in the opposite direction. Some complex cells (**end-stopped complex cells**) require both the **orientation** as well as **length** of the stimulus to be correct to elicit a response. All in all, these responses allow extraction of information on **shapes** and **form** by the P-IB channel.

While simple cells always receive information from one eye, some complex cells receive information from both eyes, whereby they have receptive fields in both eyes. For some, the receptive fields are identically situated with respect to fovea in each eye; while in others, the receptive field location in one eye does not correspond with that in the other eye. Such retinal disparity provides information on **distance** judgement, as well as **depth** perception (stereopsis).

Beyond the primary visual cortex, information from the P-IB channel flows to the inferior temporal cortex where interactions with other cortical areas allow complex functions such as **objects** and **facial recognition**.

c) Blob Channel

Information from the parvocellular pathway is also processed in “blobs”. 80% of the retinal ganglion cells in this channel are parvocellular in origin (P-type cells), while the remaining consist some of the little known koniocellular ganglion cells. After arriving at the 4Cß layer of the primary visual cortex, the information is relayed to the “blobs” areas of layers 2 and 3. Cells in “blobs” areas are sensitive to changes in light wavelengths, thereby allowing **colour differentiation** in the inferior temporal cortex as the information flow proceeds there.

With these 3 channels of parallel information processing, the primary visual cortex is organised into functioning units called **cortical modules** (see Figure

1.5)**.** Each module has a surface area of 2mm x 2mm. Within layer 3, all the orientation specific simple cells and complex cells are grouped together in columns perpendicular to the cortical surface, such that all the cells in a particular column have the same preferred orientation (i.e. an **orientation column**). This orientation preference changes in a systematic way across the cortical surface, thereby encompassing the full range (360˚) of orientation with every 2mm of cortical surface. The 2mm x 2mm area also encompasses 16 “blobs” from layer 3 for colour recognition. In layer 4, the primary visual cortex receives 2 sets of alternating inputs from left and right eye (the ocular dominance columns) with every 2mm of cortical surface. Collectively, each cortical module therefore contains all the cells required to process all aspects of visual information from a particular point in the visual field. Communications amongst cortical modules (by virtue of horizontal connections within layer 3) allow patterns of synchronous activity in different patches of cortical modules to be compared and interpreted.

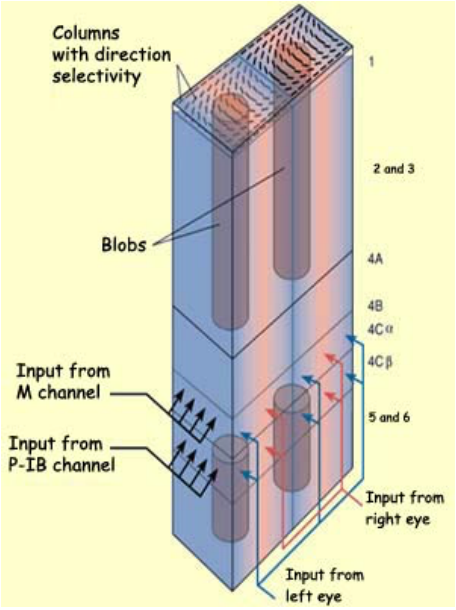

Figure 1.5: Schematic drawing of two cortical modules, one from each eye, representing the ocular dominance column. Each module has a surface area of 2mm x 2mm. Within layer 3, all the orientation specific simple cells and complex cells are grouped together in columns perpendicular to the cortical surface, such that all the cells in a particular column have the same preferred orientation (i.e. an **orientation column**). This orientation preference changes in a systematic way across the cortical surface, thereby encompassing the full range (360˚) of orientation with every 2mm of cortical surface. The 2mm x 2mm area also encompasses 16 “blobs” from layer 3 for colour recognition. In layer 4, the primary visual cortex receives 2 sets of alternating inputs from left and right eye (the ocular dominance columns) with every 2mm of cortical surface. Collectively, each cortical module therefore contains all the cells required to process all aspects of visual information from a particular point in the visual field. (Image from (“The Primary Visual Cortex by Matthew Schmolesky – Webvision,” n.d.))

From the primary visual cortex, information is believed the processed in two different streams (Goodale and Milner, 1992; Grover et al., 1999; Hartong et al., 2006; Klaver et al., 1998; Klein et al., 1995; Milam et al., 1998; Norman, 2002; Resnikoff et al., 2004; Stone, 1992). The dorsal stream (from occipital lobe to parietal lobe) is involved in the processing of motion and spatial information; while the ventral stream (from occipital lobe to temporal lobe) is involved in the processing of form representation and object recognition. Interconnections exist between these two streams, as well as with the multimodal association areas of parietal lobe, whereby information from all other sensory modalities are assimilated to form a coherent percept. This in turn allows the human brain to direct attention and coordinate behavioural responses accordingly (Perry and Morton, 1992; Wurtz and Kandel, 2013). Further analysis and integration of such activities in deeper subcortical regions may be the key to functional vision.

1.2 Development of Visual Prostheses

For a visual prosthesis to mimic natural vision as much as possible, it should ideally achieve the following steps:

1. Transformation of electromagnetic light wave energy into electrical impulses to set up action potentials in visual pathway neurones;
2. Visual processing to allow accurate presentation of information to the visual cortex and beyond for interpretation;
3. Completion of the above functions in “real-time” in order to allow accurate assessment of spatial-temporal relationships of the visualised scenes;
4. Coupling of the prosthetic vision with the subject’s eye movement to allow integration with proprioception and vestibular reflex, so the subject can accurately localise the visualised scene in relation to oneself.
5. The prostheses must also be made of biocompatible material with minimal toxicity and damage to the surrounding tissues despite prolonged stimulation.

The first documented method of external stimulation to elicit a visual response was by direct stimulation of the visual cortex with electric currents. As early as 1874, surgeons have been aware of the fact that electrical stimulations of the human brain could produce physical or “pschophysical” effects (Bartholow, 1874). Foerster (Foerster, 1929) and Krause & Schum (1932) (Krause et al., 1932; Stingl et al., 2013b) were the first to expose the occipital cortex and found that by stimulating a focal point on the occipital pole electrically, the subject saw a small spot of light which was localised in space. This reproducible visual phenomenon in response to direct electrical stimuli is known as a **phosphene**. Krause & Schum also showed that phosphenes could be elicited in a patient who had lost vision more than eight years previously from a gunshot wound to the optic radiation. This finding suggested that the adult visual cortex is capable of retaining some function despite prolonged deprivation of visual input.

Hodgkin and Huxley first described the electrical nature of signal propagation along all nervous systems by the means of action potentials in 1952 (Hodgkin and Huxley, 1952; Mokwa et al., 2008; Roessler et al., 2009). During electrical

stimulation of any nervous tissue with an external electrode, injection of electrical charges creates a localised depolarisation, activating the voltage-gated ion channels in the nearby nervous cell plasma membrane. Influx of sodium (Na^+) ions ensue, resulting in the opening of more Na^+ channels and delayed opening of potassium (K^+) channels for K^+ ions outflux to set up and complete an action potential cycle. This in turn depolarises the adjacent area of plasma membrane and the sequence of Na^+/K^+ ions movements repeat to allow propagation of the action potentials along the axons.

As voltage-gated ion channels are ubiquitous in all excitable tissues, electrical stimulation could theoretically be applied to anywhere along the visual pathway to elicit phosphenes. Over the past few decades, visual prostheses stimulating various sites along the visual pathway have been developed by different research groups including: the visual cortex, thalamus, optic nerve head and the retina (see Figure 1.2). Of these, development of retinal prostheses is the most advanced, followed by cortical prostheses.

Since propagation of the elicited signals requires normal functioning of the downstream pathway, the more distal the point of prosthetic stimulation, the greater the proportion of the visual pathway needs to be intact. Retinal prostheses could therefore only benefit patients in whom the outer retina is damaged with preservation of the rest of the visual pathway; while at the other end of spectrum, cortical prostheses could potentially benefit patients whose entire visual pathway is damaged but still have intact visual cortex function.

1.2.1 Cortical Prosthesis

The first ever visual prosthesis developed was a cortical prosthesis implanted by Brindley et al. in 1968, whereby the stimulating electrodes were placed directly on the primary visual cortex of a patient (Brindley and Lewin, 1968; Roessler et al., 2011). It consisted of an intracranial component of 80 platinum electrodes implanted over the calcarine and neighbouring cortex (see Figure 1.3). This intracranial implant was in turn connected to an extracranial component consisting of 80 radio receivers, which were secured to the skin beneath the pericranium.

To activate the electrodes, the patient had to wear a helmet containing 80 radio transmitters, corresponding to each of the 80 extracranial receivers. By selectively transmitting radio frequency pulses to individual receivers, individual intracranial electrodes could be activated. Brindley et al. demonstrated that while some electrodes produced single discrete phosphenes when activated, some gave rise to “a pair of points”; others also gave rise to “rows of three points” or “clusters of ten or more dim points”. Such diverse and ill-understood patterns of visual response to direct electric stimuli reflect the complexity of visual processing prior to the visual cortex, and the challenges we need to overcome to decipher this neural code before we can present comprehensible visual information to the visual cortex to gain useful vision.

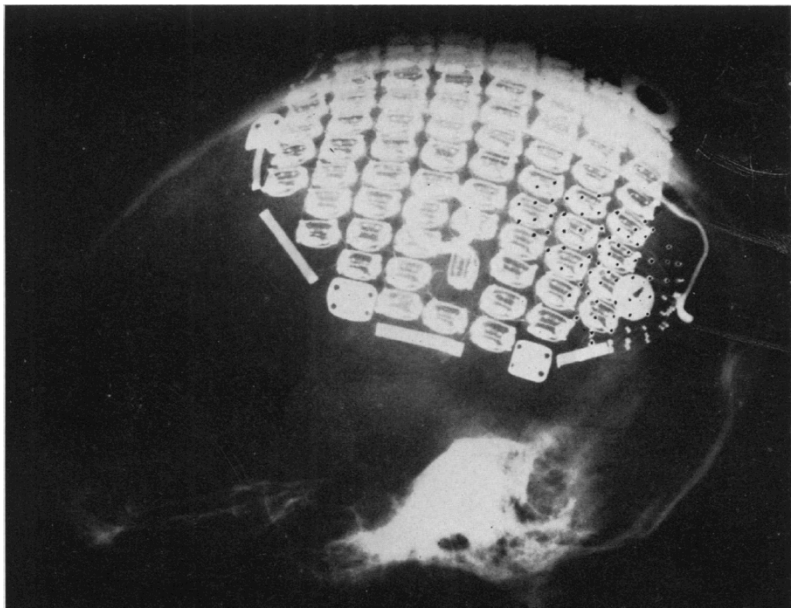

Figure 1.6: Skull x-ray of the patient implanted with the cortical prosthesis by Brindley et al. Eighty intracranial platinum electrodes were implanted over the calcarine and neighbouring cortex, which were in turn connected to 80 corresponding extracranial radio receivers, embedded under the pericranium. (Image from (Brindley and Lewin, 1968))

The next major step in cortical prosthesis development came with the development of the “Dobelle eye” by the late Dr. William H. Dobelle’s team. Dobelle et al. developed a platinum foil of 64 superficial cortical electrodes, each electrode connected by a wire to a connector contained in a carbon percutaneous pedestal (Dobelle, 2000; 1998; Dobelle et al., 1974; 1979). The patient wore a pair of sunglasses which had a mini-television camera built in. The image captured by the camera was transmitted to a sub-notebook computer either via cable or wirelessly via radio-frequency (RF) telemetry. Once

the visual image was processed by the sub-notebook computer, electric stimulation signals were sent to the implanted cortical electrode array via a micro-controller system. The first group of patients underwent surgery in the 1970s to receive temporary implants for a few days. Permanent electrode arrays were then implanted in 5 patients between 1974 and 1978. Two of the patients had their implants removed after 3 months and 14 years respectively, while the remaining 3 retained their implants for more than 20 years to date without infection or other complications. The Dobelle eye allowed previously blind patients to recognise 6-inch characters at 5 feet (approximately 20/1200 visual acuity). However, due to the density of neural pathways at the visual cortex, overlapping areas with uncontrolled numbers of phosphenes were observed with stimulation of each electrode (Henderson et al., 1979). Large electrodes also caused pain and occasionally acted as epileptic foci, resulting in partial seizures. Moreover, apart from the foveal region, the rest of the visual field project to areas of primary visual cortex lying deep within the calcarine fissure. To stimulate those neurones, higher stimulation charges are required, which may lead to further discomfort and damage to the underlying tissues.

To overcome these problems with superficial cortical electrodes, intracortical penetrating electrodes were devised, to allow for higher density and better-localised stimulation with finer electrodes. One group working on this area is the University of Utah research group led by Professor Normann (Normann et al., 2009). They devised a 100 electrode array 4 x 4 mm in size, with each electrode 0.4mm apart, termed the “Utah Electrode Array (UEA)” (see Figure 1.4). A scanning electron micrograph of UEA showed that the electrodes are essentially multiple silicon spikes, each 1.5mm in length, allowing them to reach and stimulate the 4Cβ layer of the visual cortex, the major input layer for the parvocellular pathway from LGN.

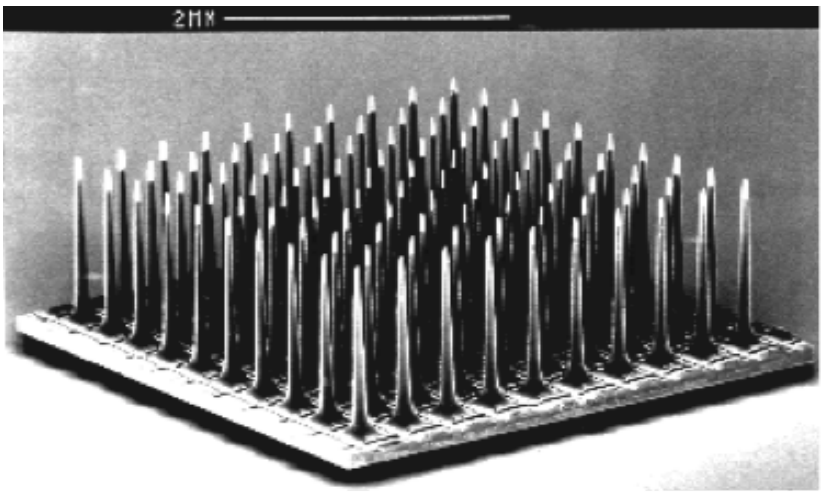

Figure 1.7: Scanning electron micrograph of the Utah Electrode Array (UEA). It contains 100 microelectrodes over an area of 4mm x 4mm. Each electrode is 1.5mm in length, separated from each other by 0.4mm. The length of the electrode allows penetration into and direct stimulation of the 4Cβ layer of the visual cortex. (Image from (Normann et al., 2009))

Experiments on primates have shown that this device is capable of producing phosphenes. However, concerns on the safety of long term stimulation, and accurate mapping of phosphenes to spatial orientation of stimuli need to be investigated before useful prosthetic vision could be achieved by cortical stimuli.

1.2.2 Thalamic Prosthesis

The LGN of the thalamus, being the first major synaptic relay centre of the optic nerve, has been explored as potential stimulation site. Potential patients include those suffering from end-stage glaucoma.

Experiments on Wistar rats (Panetsos et al., 2009) and pigs (Choi et al., 2014) showed that it is possible to elicit comparable responses in the visual cortex to that driven by natural visual stimuli, by electrically stimulating the animals' thalami. Further experiments on trained macaque monkeys showed that behaviourally, they responded to localised electrical stimulation of the LGN in the same manner as to a focal visual target, by making saccadic eye movements to the target. This indicates that focal electrical stimulations of the LGN can produce focal visual precepts in the visual field predicted by retinotopic arrangement within the LGN (Pezaris and Reid, 2007; Velikay-Parel et al., 2009).

However, due to the relative inaccessibility of the thalamus as a subcortical structure compared with the other more anatomically superficial sites, development of thalamic prostheses has been limited to animal experiments.

1.2.3 Optic Nerve Prosthesis

Optic nerve prosthesis can potentially benefit patients who have a damaged retina, such as diabetic retinopathy and inoperable retinal detachment. Three groups lead research in this field: the Université Catholique de Louvain (Brussels, Belgium), the Osaka University of Japan, and the Chinese Project for Sight (C-Sight) at Jiao-Tong University in Shanghai.

a) Université Catholique de Louvain

Two prototypes of optic nerve prostheses have been developed by this group. The first prototype was developed over 2 phases: the Microsystems-Based Visual Prosthesis (MiVip) project, from 1996 to 2000, culminating in the implantation of a self-sizing, 4 contact-electrode spiral cuff (designed by (Naples et al., 1988; Velikay-Parel et al., 2010) around the optic nerve, in a 59-year-old patient with end-stage RP in 1998. This prosthesis was implanted intracranially, through a pterional transsylvian approach. Phosphene perceptions were reliably reported and their locations corresponded to the expected quadrant of the visual field according to the point of optic nerve contact. Of all the phosphenes, 37% were reported to be “moving”. Moreover, attributes of the phosphenes elicited by the same contact electrode could be varied by changing pulse duration, current level or train frequencies (Chow et al., 2001; Veraart et al., 1998). A further operation was carried out in 2000 to implant a neuro-stimulator with an antenna for RF telemetry into the parietal cranium of the same patient (Chow et al., 2010; Delbeke et al., 2002).

The second phase, the Optic Nerve Visual Prosthesis (OPTIVIP) project (from 2000 to 2005), focused on studying the visual sensations produced by optic nerve stimulation. By altering the amplitude, duration and frequency, and number of pulses in stimulus trains, 109 reproducible phosphenes have been identified. The patient could perform recognition

tasks of 45 simple patterns with an accuracy of 63% and orientation discrimination of an L shaped pattern with 100% accuracy after training (Veraart et al., 2003).

More recently, a second prototype was implanted in a 68-year-old endstage RP patient in 2006 (Brelén et al., 2006). This prototype allowed intra-orbital implantation of the spiral nerve cuff via a medial canthotomy approach with detachment of the medial rectus and lateral canthotomy, thereby negating the need for craniotomy (i.e. less invasive), and greatly reduced the surgical as well as recovery time (see Figure 1.8). Results of preliminary assessments suggested that this intraorbitally implanted cuff electrode could work as well as the intracranially implanted electrode in the 1998 patient. As of 2009, the group is no longer active.

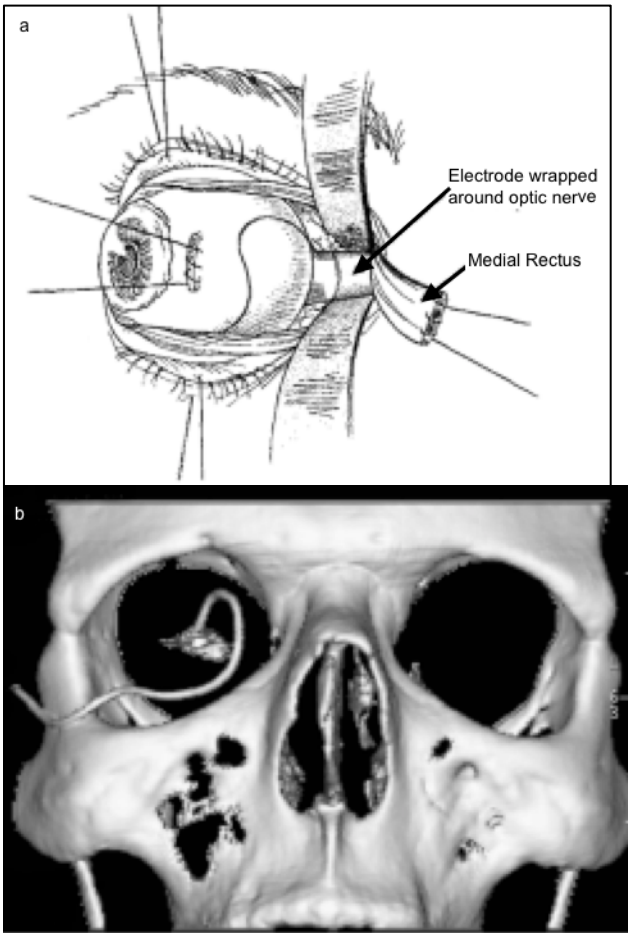

Figure 1.8: a) Schematic drawing illustrating the medial canthotomy approach of spiral optic nerve cuff implantation, negating the need for craniotomy and thereby greatly reducing the surgical and recovery time. The optic nerve cuff electrode was wrapped 2½ turns around the nerve and the cable was brought out underneath the globe. b) Coronal section of a CT head scan showing the cable leaving from underneath the globe, before running subcutaneously to the stimulator box embedded in the right parietal cranium (not shown). (Image modified from (Brelén et al., 2006))

a) Osaka University

The Osaka University Group first implanted a 3-wire electrodes system (AV-DONE) to directly stimulate the optic nerve in a blind RP patient with no light perception in 2009 (Sakaguchi et al., 2009). In this patient, phosphenes could be elicited by electric stimulation through each electrode and the phosphenes ranged in size from a match head to an apple. The phosphenes were also localised depending on the position of electrode used for stimulation, indicating that a useful visual prosthesis may be developed using more electrodes mapped to correct spatial orientation of the visual images.

More recently, a newer prototype composed of 7 wire stimulation electrodes, one return electrode, one manipulation rod and a cylindrical silicone board has been developed (see Figure 1.9). This device has been implanted in rabbits' eyes to explore the surgical techniques (Sakaguchi et al., 2012). To implant the device, it was first inserted into a vitrectomised eye via a 7mm pars plana sclerostomy using a trocar. The device was then manipulated with vitreoretinal forceps in the vitreous cavity and it was shown that the 7 wire electrodes could be inserted intra-papillarily into the optic disc head in one single move. Electrical stimulation via the electrodes of this implant showed evoked potentials (EEPs) at the visual cortex. The smooth experimental surgical implantation of this new device is an encouraging step towards human trials.

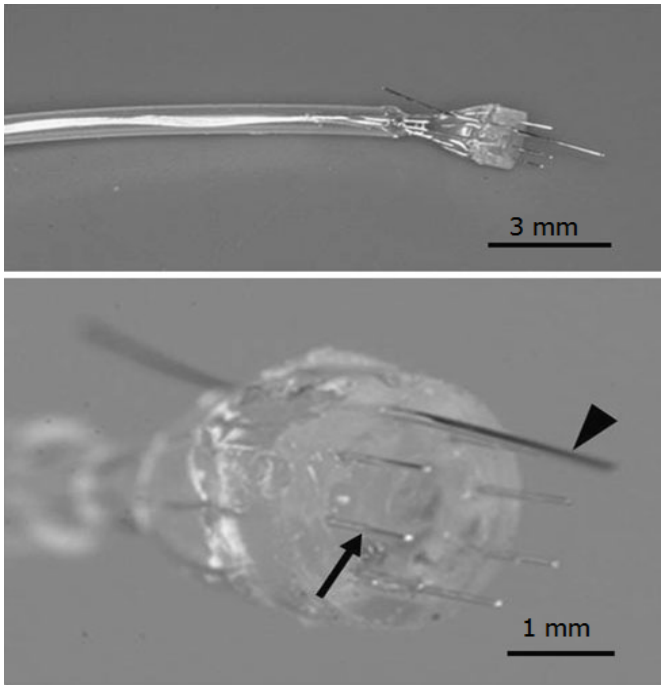

Figure 1.9: Photograph of the newer AV-DONE optic nerve prosthesis prototype. It consisted of 7 wire stimulating electrodes, one return electrode, one manipulation rod and a cylindrical silicone board (2.0 mm in diameter). The arrow points to the stimulating electrode, while the arrowhead indicates the manipulation rod. During the implantation surgery, the 7 wire electrodes were inserted intra-papillarily into the optic disc head after vitrectomy. This device has been implanted in rabbits' eyes to explore the surgical techniques. (Image from (Sakaguchi et al., 2012)).

c) C-Sight (Chinese Project for Sight) Group

Set up in 2004, the C-Sight Group at Jiao-Tong University at Shanghai developed a 13-channel, platiniridium penetrating microelectrode array to optimise contact and localisation with the optic nerve (see Figure 1.10). A micro-camera was designed to be implanted into the lens capsule (powered by a solar panel in front of the iris) to provide coupling of camera movement to eye movements. Both the micro-camera and the cuff electrode were connected to an external image-processing unit. Experiments have been carried out in rabbits and cats to determine the best stimulation position of electrodes on the optic nerve ("Special Senses," n.d.).

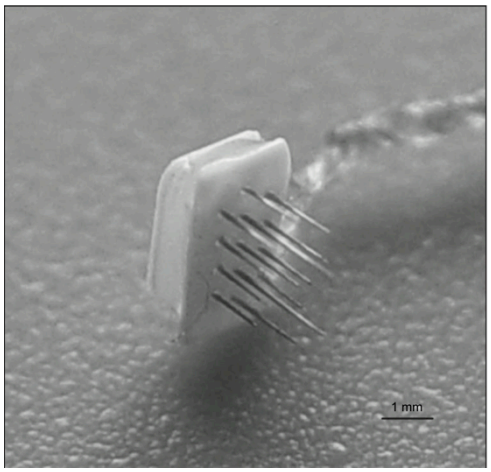

Figure 1.10: Photograph of the 13-channel, platiniridium penetrating microelectrodes for the optic nerve prosthesis, developed by the C-Sight Group at Jiao-Tong University at Shanghai (Image from (Chai et al., 2008)).

1.2.4 Retinal Prosthesis

While the development of thalamic prostheses is still in the animal experimental stage, and that of the cortical and optic nerve prostheses are in early acute human studies phase, research into the development of retinal prostheses has made the most progress.

There are many reasons for this and they can be best summarised as:

a) greater accessibility at lower surgical risk than the intracranial visual pathways;
b) straightforward monitoring of the device by direct visualisation; and

c) potentially predictable and reproducible retinotopy by applying stimulation at a pre-processing site.

With the advent of modern vitreoretinal surgical techniques, access to the retina and the subsequent implantation of stimulating electrodes are comparatively easier than other sites of implantation. This is exemplified by the widespread implantation of the Argus® II System in many countries by many different surgeons over a relatively short period, at a level of surgical morbidity acceptable to regulators (Humayun et al., 2012; Rizzo et al., 2014). Despite the relative accessibility and safety discussed here, implantation still requires advanced vitreoretinal surgical skills. Complications and problems were also easily identified during the Argus® II phase I/II clinical trials due to the ability to directly visualise the device (Humayun et al., 2012).

Two other advantages of a retinal prosthesis are: predictable retinotopy, and stimulation of the visual system at a site before significant processing of the signal has occurred. Brindley and Lewin (1968b) have demonstrated that although stimulation of cortical electrodes gave rise to phosphenes in locations in agreement with the classic Holmes' retinotopic map of the visual cortex (Holmes, 1945), many of the phosphenes were complex and non-discrete in nature. This was thought to be due to the fact that there was significant processing and integration carried out in the pre-cortical visual pathway. This was borne out with the discovery of organisational processing in the retina, as demonstrated by the antagonistic centre-surround responses of the retinal ganglion cell (RGC) receptive fields to light stimuli, as previously discussed in Section 1.1.1. Furthermore, as there are approximately 120 million photoreceptors and only 1.5 million ganglion cells, many photoreceptors converge onto a single bipolar cell *especially at the periphery*, with further convergence taking place from the bipolar cells to RGCs (Kolb, 2003). In contrast, within the macular region of the retina, the ratio of photoreceptor: bipolar cell: RGC approaches 1: 1: 1, with minimal convergence. It is thus envisaged that focal electrical stimulating patterns with a multi-electrode array in the macular region would more likely manifest retinotopic correlations along the visual pathway. There is, however, a particular limitation to this rationale, due to the arcuate displacement of axons and the piling up of ganglion cell bodies when approaching the fovea, if epiretinal stimulation is carried out.

The retina being a viable site for electrical stimulation to generate phosphene perception was first demonstrated by contact lens electrode stimulation in RP patients (Potts et al., 1968; Potts and Inoue, 1970; 1969; Zrenner et al., 2011). Currently, there are two main anatomical approaches to stimulating the retina: the epiretinal approach – whereby the multi-electrode array is placed on the retinal surface in direct contact with the nerve fibre layer; and secondly the subretinal approach – whereby the array is placed underneath the retina and is in closest contact with the bipolar cells. Both approaches have achieved reliable phosphene activation and have shown comparable functional improvements in human clinical trials.

The Argus® II retinal prosthesis system uses the epiretinal approach, as do the 2 German consortium groups who developed EPI-RET3 (Menzel-Severing et al., 2012; Wilke et al., 2011) and Intelligent Retinal Implant System (IRIS) (Besch et al., 2008; Velikay-Parel et al., 2009; 2013). The subretinal approach is used in the Artificial Silicon Retina (ASR) developed by the Optobionics (Chow et al., 2005; “Neuroscience for Kids: the visual pathway Interesting information on what can happen if there's any damage | Teaching: Physics - Vision | Pinterest | Pathways…,” n.d.; Wurtz and Kandel, 2013), and the alpha-IMS device (Stingl et al., 2013b; Wilke et al., 2011) developed by the German group headed by Professor E. Zrenner. The alpha-IMS obtained the CE mark in 2013.

As the functional outcomes of the Argus® II retinal prosthesis system is the main theme of this thesis, a detailed introduction and analysis of the system will be discussed in the following chapters. The other retinal prosthesis systems currently available clinically or undergoing human clinical trials are briefly outlined as follows:

a) EPI-RET3, EpiRet GmbH

Research into the development of EPI-RET3 started in 1995 as part of the German EPI-RET implant project. Subsequently, the implants came under the development of EpiRet GmbH, a German company founded in 2007. At present, 11 different partners from industry and universities are involved in the development of the third generation implant, the EPI-RET3. The EPI-RET3 consists of an external unit (with a video-camera

and an external coil mounted onto a glasses frame), and an internal unit (see Figure 1.11).

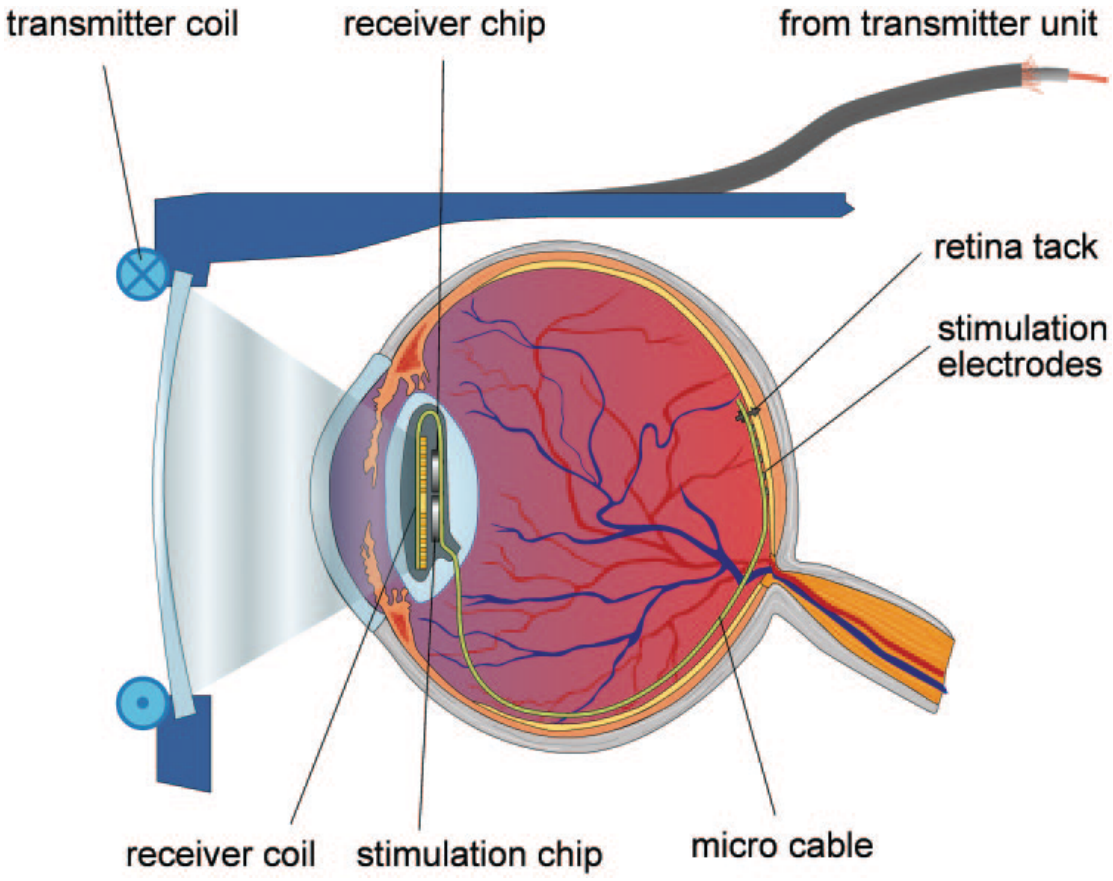

Figure 1.11: Schematic drawing of the EPI-RET3 system. Visual images captured by an external video camera are relayed to an external processing unit and transmitted back to an external transmitter coil situated at the side of the glasses frame. By RF telemetry, the external coil transmits the visual data and power to the internal receiver coil situated within the capsular bag. The final step of information rely consists of conversion of RF into electric pulses to stimulate the retina via the microelectrode array. (Image from (Roessler et al., 2009))

The internal unit of the EPI-RET3 implant has a micro-coil buried in a flexible substrate and all the electronic components are integrated into a compact package similar in dimension to that of an intraocular lens (Mokwa et al., 2008; Roessler et al., 2009). This compact internal unit is then inserted into the capsular bag or sulcus area like an intraocular lens, which is further stabilised by 2 trans-scleral 10/0 sutures. Once in situ, the electrode array (consisting of 25 electrodes connected to the micro-coil via a flexible cable) pierces through the posterior capsule to exit the

capsular bag and extends to rest on the retinal surface, where it is stabilised on the epiretinal surface by gold tacks (see Figure 1.12).

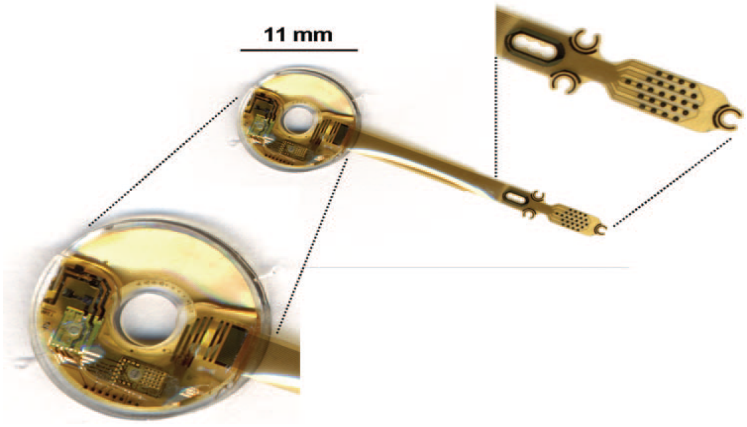

Figure 1.12 An illustration of the Epi-Ret3 internal unit with magnified views of the receiver module composed of microcircuits and a micro-coil (left), and that of the stimulating electrode array (right). The 3 C-shaped opening close to the electrode array is for insertion of retinal tacks to stabilise the electrode array onto the retinal surface. The total length of the system is 40 mm. (Image from (Roessler et al., 2011))

A distinct advantage of this design is that all the components of the internal unit are intraocular, without any trans-scleral wire connections between the intraocular electrode array and the usually more superficially located internal coil and circuitry (as seen in Argus® II retinal prosthetic system). This potentially minimises the risk of conjunctival erosion and infection, and is dubbed the “wireless retinal implant system”.

The first clinical trial for the EPI-RET3 retinal prosthesis started in 2007, when 6 patients registered as legally blind from RP were temporarily implanted with the device for 4 weeks before it was removed. The patients were tested with the implants activated on day 7, 14, and 27 post-operatively. All the patients reported perceiving phosphenes such as dots, arcs or lines and the required stimulation threshold were found to be low (Menzel-Severing et al., 2012; Stingl et al., 2013a).

b) IRIS® II, Pixium Vision

The earliest prototype of this device was manufactured by a Swiss company founded in 1998, the IMI Intelligent Medical Implant AG (Hornig et al., 2007a). It has an external unit consisting of a video camera,

processing unit and external coil, and an internal unit consisting of the receiver internal coil, processing circuitry and stimulating electrode array, which is attached to the epiretinal surface by a Titanium tack. The electrodes are made of polyimide with gold tracks.

A unique feature of this system is that it has a built-in “learning algorithm” in its image processing. “Learning” is achieved by fixing some of the filter parameters while changing others as images are presented to the test subject. Each time, the subject has to choose if one image is better than the other with the changing parameters. Simulations on normally sighted people have shown that after about 80 iterations of preferential choice, the presented image object can be recognised. In this way, fine-tuning of the parameters by each subject is simplified (Eckmiller et al., 2005).

From 2005 to 2006, a 50-electrode system was temporarily (up to 13 weeks) implanted into 4 patients in a clinical trial. The patients were able to discern simple lines and spots, as well as detect horizontal movements (Hornig et al., 2007b).

In 2007, a multi-centre clinical trial (ClinicalTrials.gov Identifier: NCT00427180) began for the implantation of the IRIS (Intelligent Retinal Implant System) into RP patients. This was a 61-electrode prototype system with visual field of up to 40p. The 4-month report of the first IRIS patient was published in 2009, whereby the patient reported reliable visual percepts with stimulation (Velikay-Parel et al., 2009). In 2010, further report showed that the electrodes in IRIS have stable thresholds with prolonged active stimulation (Velikay-Parel et al., 2010).

Lately, development of IRIS has been taken over by Pixium Vision, a French company. The next generation prototype, known as IRIS® II consisting of 150 electrodes, has recently started phase I clinical trial (ClinicalTrials.gov Identifier: NCT02670980) in multiple centres across Europe, and obtained CE mark in July 2016.

c) Artificial Silicon Retina (ASR), Optobionics

The Artificial Silicone Retina (ASR) is the first ever retinal prosthesis to be devised and patented in the 1980s by the Optobionics Corportaions.

This device is essentially a silicone microchip with microphotodiode-array, 25 μm in thickness and 2 mm in diameter. It is composed of 5000 micro-photodiodes (each linked to its individual electrode), and has been shown to be capable of converting light electromagnetic waves into electric impulses (photovoltaic) to stimulate the retinal ganglion cells in cats when inserted subretinally, akin to the natural function of the photoreceptors (Chow et al., 2001).

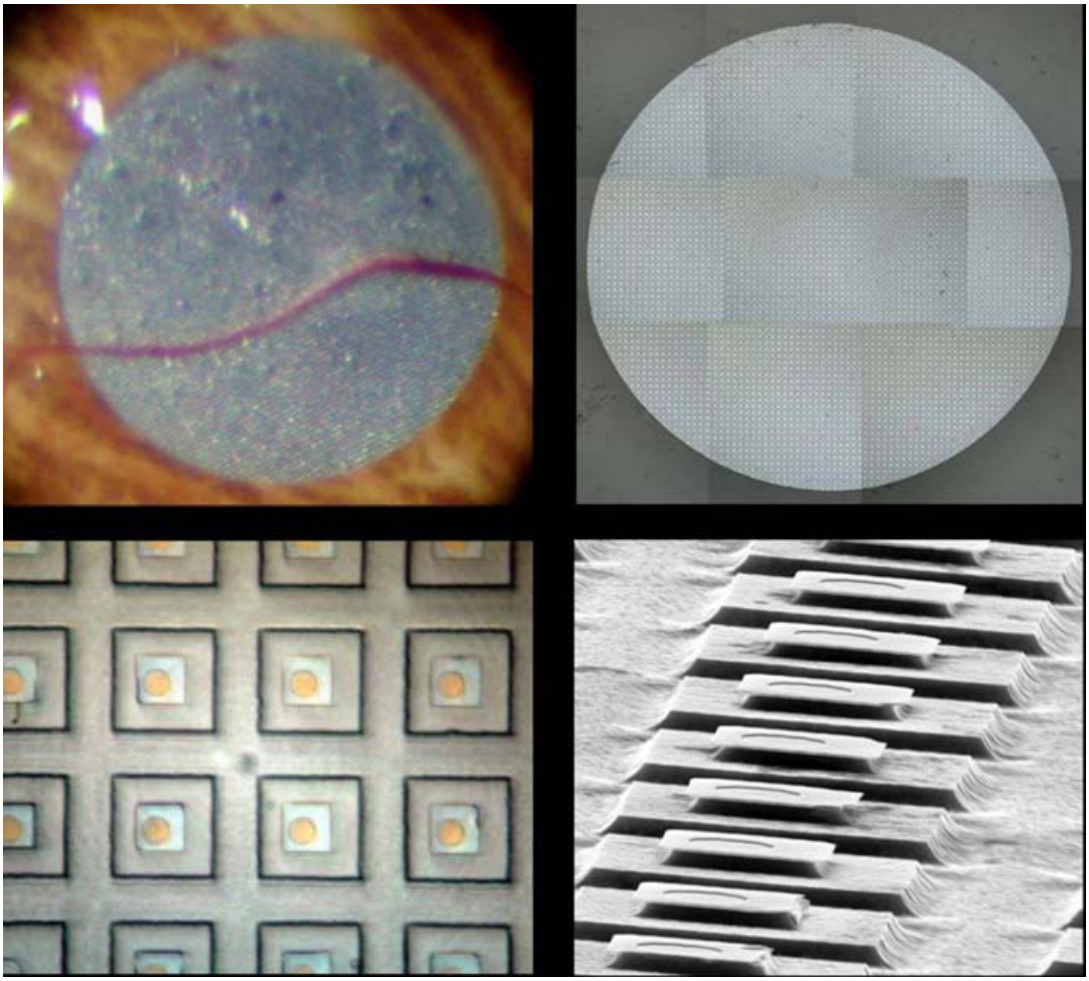

Figure 1.13: Montage of Artificial Silicon Retina (ASR) with different magnifications. Fundus photograph of ASR in subretinal space (top left, 23X), explanted ASR device (top right, 25X), light micrograph of individual ASR pixels (bottom left, 500X), high-angle SEM of pixels (bottom right, 1650X) (Image from (Chow et al., 2010)).

The first human clinical trial was carried out between 2000 and 2001 on 6 patients legally blind from retinitis pigmentosa. While the implants had good safety profile with no reported adverse event for up to 18 months in all the 6 patients , the visual outcome and the proposed beneficial effects were more controversial. Three out of the 6 patients showed an

improvement in visual acuity as measured by the EDTRS chart, but only one patient had an improvement in the automated visual field test. There were also unexpected areas of visual improvement distant to the implant site. The authors attributed this observation to the protective or rescue effects of the neurotrophic factors released by the retina as a result of electric stimulation from the implant, a hypothesis that is supported by evidence from a study performed on Royal College of Surgeons rats (Pardue et al., 2006). However, it has subsequently been shown that photovoltaic energy from microphotodiodes alone was insufficient to activate the dystrophic retinal cells in humans to transmit useful visual information (Zrenner et al., 1999). Nevertheless, further implantations of the ASR were carried out in human subjects in 2010 to study the neurotrophic effect and the long term outcomes of the device .

d) Alpha-IMS, Retina Implant AG

Unlike the epiretinal prostheses described above which receive visual input from an external video-camera system, the alpha-IMS implant (and similarly in ASR) receives visual input directly. By strategically placing a light-sensitive, photovoltaic micro-photodiode array (MPDA) subretinally (preferably at the macula), the micro-photodiodes convert electromagnetic light waves directly into electrical energy, thereby directly replacing the function of photoreceptors. In terms of image generation, the alpha–IMS makes use of the patient's own optical system within the eye, which naturally focuses light onto the retina as images.

However, one serious limitation of using a photodiode based system was already shown in ASR (Chow et al., 2005; 2003). These photodiodes were not as efficient as natural photoreceptors at converting electromagnetic light waves into electric impulses, and as such could not generate adequate electrical charges to elicit action potentials to stimulate the remaining visual system. To overcome this problem in the design of their prototype, Zrenner et al. at Retina Implant AG supplied each photodiode with an external electrical power connection, so that the signals generated by the photovoltaic micro-photodiode array could be amplified at the individual photodiode level (Zrenner et al., 2011; 1999).

The first generation of Retinal Implant AG devices were temporarily implanted in 11 subjects in 2005 in a clinical trial (clinicaltrials.gov identifier: NCT00515814) (Wilke et al., 2011). The device consisted of a 16 electrode-array for direct electrical stimulation of the retina, as well as the photovoltaic microphotodiode array (MPDA). The implant was placed subretinally and powered externally by a percutaneous wire, which exited in the retro-auricular region of the subject as a connection plug (Besch et al., 2008). Out of the 11 subjects, 3 subjects did not report any visual perception with electrical stimulation. This was due to local non-perfusion of the retina in 2 subjects, and device failure in 1 subject. For the remaining 8 subjects, 5 subjects could discern simple patterns such as lines and letters, and 4 of whom could detect direction of motion. Two subjects could also read large letters (Wilke et al., 2011). Although visual function improvement was demonstrated, the implant was removed from all the subjects after a few weeks as per protocol (except in one subject who declined removal) and no long-term durability data is available from this trial (Besch et al., 2008; Nakauchi et al., 2006).

Subsequently, a second-generation device featuring some design improvement, termed the alpha-IMS, has been developed. The alpha-IMS consists of an internal and an external unit. The internal unit has 3 components (see Figure 1.13):

a) a subretinal portion (ideally placed subfoveally),

b) an extraocular portion (through the episclera and lateral orbital wall);

c) a subcutaneous portion (from the lateral orbit to retroauricular region).

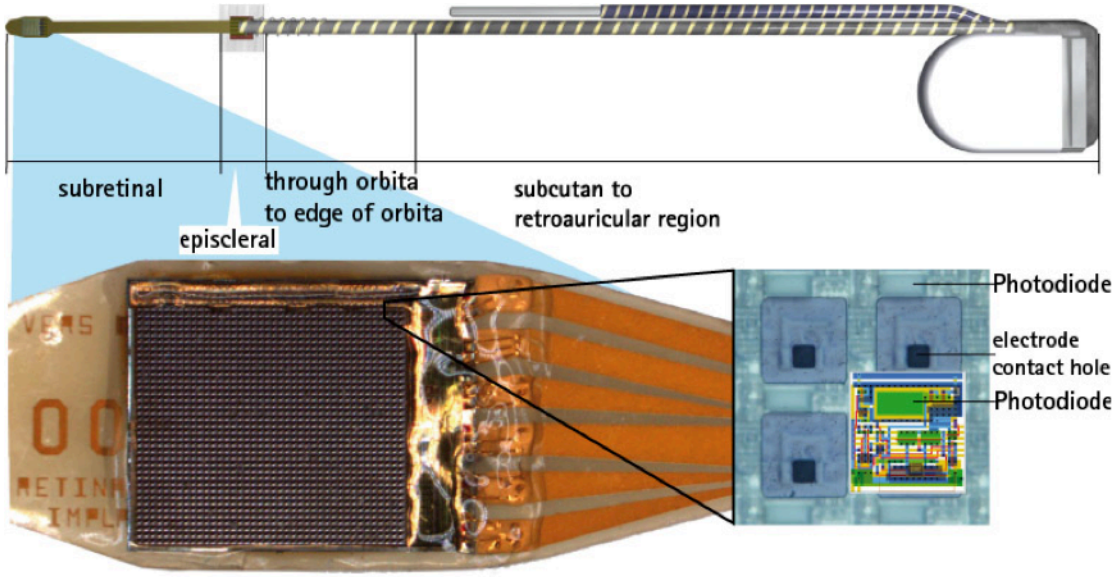

Figure 1.14: Illustration showing the internal unit of the alpha-IMS implant. It consists of a 3×3 mm microchip (magnified in bottom image). Within the microchip, there are 1,500 microphotodiodes (further magnified view in bottom right), each of which is connected to an electrode for signal amplification. (Image modified from (Stingl et al., 2013c))

The subretinal portion of the device is composed of 1500 MPDA each connected to an amplifier and its own Titanium nitride electrode. Each microphotodiode functions independently from its neighbours like a pixel, and the amplification is determined by the intensity of the light received by the microphotodiode. Ideally, the 3x3 mm microchip implant would be placed subfoveally or as close to fovea as possible to allow optimal stimulation of the MPDA by the incoming light, giving a visual field of 11°x 11°.

The extraocular portion of the device consists of a silicone cable connecting the MPDA to the internal coil, and has a rather tortuous course. It first leaves the eye transchoroidally to reach the lateral orbital rim, before tunnelling underneath the temporalis muscle (the subcutaneous portion) in the subperiosteal space to reach the retro-auricular space where it ends as an internal coil buried subdermally (see Figure 1.14).

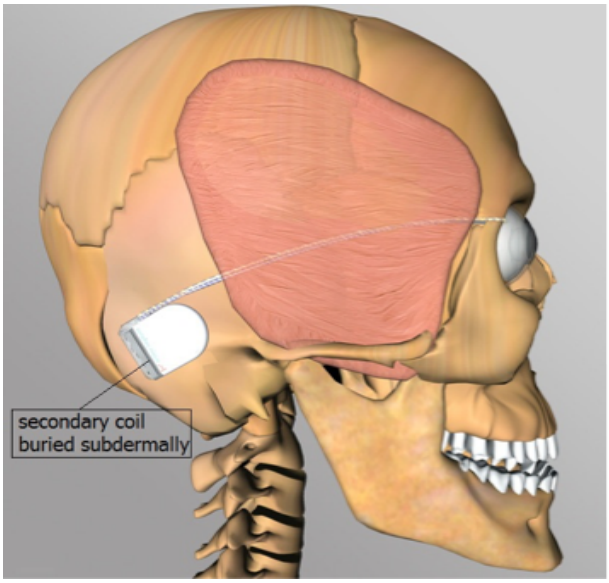

Figure 1.15: Schematic drawing of the course of the extraocular and subcutaneous portion of the Alpha-IMS implant. (Imaged modified from (Stingl et al., 2013c))

The secondary coil acts as a bridge of connection between the internal unit and the external unit. The external unit of the alpha-IMS device essentially consists of an external power source which terminates in a primary coil (see Figure 1.15).

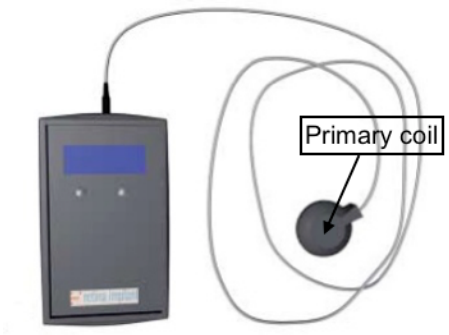

Figure 1.16: The external unit of alpha-IMS retinal implant. It consists of an external power supply, which terminates as the primary coil. (Image from ("alpha-IMS of Retina Implant AG," n.d.))

By holding the primary coil to the retroauricular region, it becomes magnetically attached to and held in place by the internal coil. The external power supply is then transmitted across the primary coil to the secondary coil by electromagnetic induction. This induced electric energy in turn amplifies the MPDA and activates the retina (see Figure 1.16).

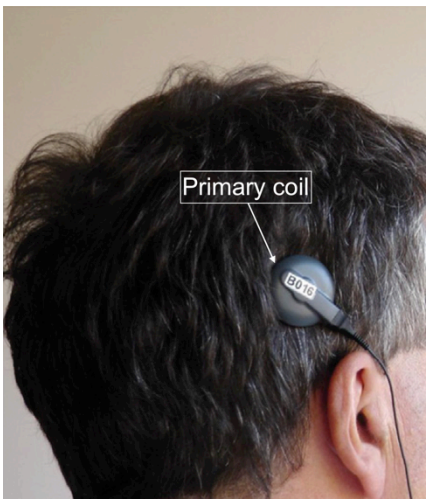

Figure 1.17: Photograph showing the primary coil of the alpha-IMS retinal prosthesis being held in place magetically by the subdemral secondary coil in the retro-auricular region. External electrical power is transfered from the primary coil to the secondary coil by electromagnetic induction to amplify the electric signals generated by the microphotodiode array.

A multi-centre phase II clinical trial with alpha-IMS started in May 2010 (ClinicalTrials Identifier: NCT01024803), with the ophthalmology department of the John Radcliffe Hospital at Oxford and King's College Hospital in London amongst the trial centres. The first patient in the UK received the implant in March 2012. A preliminary report of the first 10 patients showed favourable results. One patient had irrevocable functional loss due to damage to the inner retina. Of the remaining 9 patients, 7 could localise light and 5 could detect motion (with angular speed of up to 35 degrees/s). Six subjects had measurable gratings acuity (up to 3.3 cycles / degree), while 2 had measurable visual acuity with Landolt C-ring (equivalent to Snellen visual acuity of 20/546 or 1.43 logMAR). In addition, 4 subjects showed statistically significant improvement in the recognition and localisation of objects ($p < 0.05$). Three of the subjects were also able to read large letters in an alternative-force-choice test (Stingl et al., 2013c; Zrenner et al., 2011).

A further 12-month interim report on 29 patients showed that 21 patients had improvement in performing activities of daily living and in mobility. There were also initial significant improvement ($p < 0.05$, Wilcoxon test) in detection, localisation and recognition of geometric shapes with the device switched on versus off at 3 months post-operative visit. Unfortunately, this improvement was not sustained and the difference in

performance no longer achieves statistical significant ($p > 0.05$) at the 6 months post-operative visit. Four of the patients could not perceive the light with the subretinal implant due to reasons including: intra-operative optic nerve trauma, post-operative retinal oedema, retinal ischaemia over the area of the MPDA and technical failure of the device. On the other hand, 4 patients were able to perform standardised visual acuity testing using contrast reversal Landolt C- rings, and achieved equivalent acuities of 20/2000, 20/2000, 20/606 and 20/546 at the 3 months post-operative visit (Stingl et al., 2015). The alpha-IMS received its CE marking in July 2013.

A summary of all the various visual prostheses currently available for clinical use or undergoing human clinical trials is shown in Table 1.1. A comparison of all the above-mentioned retinal prostheses in terms of their stimulation approach (epiretinal versus subretinal), clinical trial outcomes, visual function assessment and long-term biocompatibility in human clinical trials is shown in Table 1.2.

Visual Prostheses	Retinal Prostheses				Optic Nerve Head Prostheses	Cortical Prostheses
	Argus® II	**Alpha-IMS**	**IRIS® II**	**Epi-ret 3 ("wireless" implant)**		
Image Capture	Extrinsic video-camera	Intrinsic optical system	Extrinsic video-camera	Extrinsic video-camera	Extrinsic video-camera	Extrinsic video-camera
Number of Electrodes	60	1500 micro-photodiodes, each connected to an amplifier and electrode	150	25	MiVip: 4 contact electrode AV-DONE: 3	Dobelle eye: 64 Utah Electrode Array (UEA): 100
Field of Vision	Up to 20°	11° x 11°	Not available (up to 40˚ on previous models with 61 electrodes)	Not available	14° x 41 °	Not available
Site of Stimuli	Inner retina with epiretinal electrodes	Outer retina with subretinal electrodes	Inner retina with epiretinal electrodes	Inner retina with epiretinal electrodes	Optic nerve head	Primary visual cortex
Status	Commercially available in Europe (CE mark in March 2011) and the USA (FDA approval February 2013). Clinical Trials Identifier: NCT01490827.	Commercially available in Europe (CE mark in July 2013). Clinical Trials Identifier: NCT01024803.	Phase II clinical trial commenced January 2016. Clinical Trials Identifier: NCT02670980	Completed acute clinical study. Awaiting further development and approval for chronic study.	Experiments performed on human volunteer subjects.	Experiments performed on human volunteer subjects.

Table 1.1: Summary of various visual prostheses currently available or undergoing human clinical trials. (Table modified from (Luo and daCruz, 2014)

	Epiretinal Implant			Subretinal Implant	
	Argus® II	**IRIS® II**	**Epi-ret 3**	**Alpha-IMS**	**Artificial Silicon Retina**
Clinical Trial Outcomes	FDA approved Europe CE mark 30 humans in trial; 9SAEs	Europe CE mark Phase II clinical trial closed to recruitment – awaiting outcome	Phase I trial (28 days) completed 6 humans in trial; no SAEs reported	Europe CE mark; 2 SAEs	6 humans in Phase I trial; no SAEs reported 42 humans in Phase II trial; ceased operations
Visual Function	Visual testing: VA/ object / motion / mobility Best VA: 20/1262	N/A	Electric stimulation: phosphenes reported	Visual testing: VA/ object/ motion/ localisation Best VA: 20/546	Visual testing: VA/ object/ mobility Increased area of phosphehes and possible neuro-protective effect reported
Long-term biocompatibility	Trans-scleral cables may increase infection. Complications: hypotony, conjunctival erosion, dehiscence, endophthalmitis, retinal detachments reported.	N/A	Fully intraocular. Complications: loose tacks, epiretinal gliosis, increased IOP reported.	Intraocular image capture Complications: decreased retinal perfusion, intra-operative optic nerve trauma, haemorrhage, raised IOP reported.	Fully intraocular (subretinal). No complications reported, specifically no retinal detachment, implant displacement or chronic inflammation.

Table 1.2: Comparison of epiretinal versus subretinal prostheses in human clinical trials.

1.3 Future Development & Other Treatment Modalities

Prosthetic vision is a rapidly expanding field with multiple groups of researchers worldwide developing new devices to improve the quality of vision, as well as improving the safety and efficacy of data transmission in long-term use. Moreover, different ways of neurotransmission (other than electric stimulation) have also been explored. In the following sections, we will look at a few prominent research groups whose devices are likely to impact the field in the near future, as well as groups developing other treatment strategies for the treatment of end-stage retinal degeneration.

1.3.1 Bionic Vision Australia Group

The Bionic Vision Australia is a consortium of researchers formed in March 2010 after receiving a $42 million grant from the Australian Research Council in December 2009. Led by Professor Anthony Burkitt, the consortium brings together a multidisciplinary team with the aim to develop two different types of retinal prostheses:

a) Wide-View device;
b) High-Acuity device.

a) The Wide-View Device

The aim with Wide-View device was to improve the mobility and navigational function of the patients by improving their field of vision ("Wide-View device - Bionic Vision Australia," n.d.). The ultimate goal is to produce a 98-channel electrode array, with the electrodes arranged in a unique hexagonal mosaic pattern. Each hexagonal unit is a "stimulating unit" composed of 7 electrodes: a central stimulating electrode surrounded by 6 guarding electrodes. The main function of the guarding electrodes is to contain the charge spread of the central stimulating electrode, therefore reduce inference between stimulating units. Any of the seven electrodes in one hexagon can be serially employed as a stimulating electrode and all other surrounding electrodes form the new guarding electrodes. This hexagonal stimulation technique has been

shown to produce discrete, localised retinal activation as recorded at the visual cortex of cat retina (Wong et al., 2007). Encouraged by the results from the Seoul National University group (see section 1.3.2), the Bionic Vision Australia researchers have chosen to place their implants supra-choroidally (Wong et al., 2008).

On 3rd September 2012, the first prototype (consisting of 24 electrodes) of this device was successfully activated in the first patient, who received surgical implantation of the device a month prior. The clinical trial completed recruitment in October 2014, with a total of 3 patients. During the 2-year study, the supra-choroidal implants were reported to be stable with no clinical sign of movement or migration, as well as being safe with no unexpected device-related serious adverse events. The group also reported improvement in the patients' ability to see light and shapes, as well as navigation. Further psychophysical testing and analysis performed on these patients will allow improvement of the design and processing algorithm ("Bionic Vision Australia successfully completes clinical trial of retinal implant in retinitis pigmentosa : Bionic Vision Australia," n.d.).

b) The High-Acuity Device

In contrast, the High-Acuity device aims to provide functional central vision to assist with tasks such as face recognition and reading large print. It is composed of a 1024 electrode array made of diamond material and is to be inserted epiretinally ("High-Acuity device - Bionic Vision Australia," n.d.).

As of 31st December 2016, Bionic Vision Australia has ceased operations, and the technologies developed thus far by the group are being commercialised by Bionic Vision Technologies Pty Ltd (BVT) (see www.bionicvis.com).

1.3.2 Suprachoroidal Implant – Seoul National University Group

The Seoul National University researchers first developed a pillar shaped 108-channel electrode array which are 40μm in height with a mushroom-shaped heads (Kim et al., 2008).These electrode arrays were implanted

suprachoroidally in rabbit eyes and successfully stimulated rabbit retina to show proof of concept. More recently, they have developed a 7-channel polyimide electrode system for long term implantation to assess safety and biocompatibility and have established polyimide is safe for long term implantation (Zhou et al., 2008). The main advantage of a suprachroidally placed device is the theoretical superior safety profile for electrical stimulation, as no neural tissue is in direct contract with the electrodes. As a result, the safe electrical stimulation charge for a suprachoroidal device is deemed to be 3 times that of a retinal device (Nakauchi et al., 2006).

1.3.3 Photosensitive Suprachoroidal Implant – NIDEK Co. Ltd & Osaka University

The Japanese ophthalmic equipment company teamed up with the University of Osaka and the Nara Institute of Science and Technology to develop a suprachoroidal transretinal stimulation device in 2001.

The implant technology employs several chips, each with 9 electrodes mounted onto a flexible polyimide substrate. A 576-channel electrode array would entail 64 chips mounted onto a flexible polyimide substrate (Ohta et al., 2007). A more recent improvement on the device involves incorporation of a light-sensing circuit within the chips, to guide the stimulus properties, comparable to the use of multiphotodiode array in Retina Implant AG company's alpha-IMS implants. In vivo experiments in rabbits have been carried out and showed feasibility of transretinal stimulation to elicit visual responses. However, further development in encapsulation and long-term stability of the device have to be established before clinical application (Tokuda et al., 2009)

1.3.4 Biohybrid Implant

Apart from various advances in developing ever-increasing number of electrodes to improve the visual resolution of the prostheses, the Institute of Physical and Chemical Research (RIKEN) in Nagoya, Japan, has developed a biohybrid implant, in which the nerve cells were cultured directly onto a silicon chip. The nerve cells were treated with growth factors and the chip was then implanted either epiretinal or subretinally in animal models. The nerve cells were encouraged to grow towards the CNS and form synaptic connections with

the adjacent retinal layers, interfaced with an electro-conductive polymer as electrodes. As of 2009, the RIKEN team are working towards improving the conductivity of the polymers and biocompatibility tests and no long term data is yet available (Yagi, 2009).

1.3.5 OUReP™ (Okayama University-type Retinal Prosthesis)

Developed by the Okayama University in Japan, the dye-coupling photo-electric subretinal prosthesis involves incorporation of the 2-[2-[4-(dibutylamino)phenyl]ethenyl]-3-carboxymethylbenzothiazolium bromide dye on a polyethylene film, and this has been shown to produce adequate electrical charge to evoke neural responses in the retinal cells of chick embryos from light waves, compared with photodiodes alone (Dobelle, 2000; 1998; Dobelle et al., 1979; Henderson et al., 1979; Uji et al., 2005; 2006). Preliminary results of subretinal implantation into rats have shown that tissue reactions like apoptosis were negligible with only slight glial response after 1 month. Subsequent subretinal implantation into Royal College of Surgeons rats showed reduction of retinal cell apoptosis at 5 months after implantation, and maintenance of visual behaviour in these rats at 2 months after implantation, compared with controls (Alamusi et al., 2015). The dye itself was also shown to have neuroprotective effects, preventing retinal cell apoptosis in RCS rats with intravitreal injections (Liu et al., 2017).

1.3.6 Thalamus (Lateral Geniculate Nucleus) Implant

As the first major relay station of the visual pathway where the majority of the ganglion cell nerve fibres synapse, the lateral geniculate nucleus (LGN) offers an attractive site for electrical stimulation. It has the advantage of having a large surface area whereby neurones from the macular regions congregate and have a high retinal area to thalamus area ratio, allowing for placement of large number of electrodes to optimise visual resolution. The magnocellular and parvocellular pathways are also segregated in the LGN, allowing for separate stimulation of the different pathways for extraction and processing of different visual information. However, as the LGN is situated behind the optic chiasm in the visual pathway, relaying of visual images are separated along the vertical midline, with each LGN receiving visual information from the contralateral

vertical hemi-field from both eyes. A functioning LGN-stimulating prosthesis would therefore require bilateral stimulation to achieve a holistic visual presentation. There are 2 major groups currently carrying out research in this field: the Massachusetts General Hospital group lead by John Pezaris, and the Neurocomputing and Neurorobotics Reasearch Group at the Complutense University of Madrid in Spain.

Pezaris et al. have shown in macaque monkeys that LGN stimulation can give rise to reproducible phosphenes localised in space, as exhibited by the consistent saccades made by the monkeys in response to electrical stimuli, using surgical implantation techniques similar to deep brain stimulation (DBS) implants in the treatment of patients with Parkinson's disease (Pezaris and Eskandar, 2009; Pezaris and Reid, 2007). Panetsos et al. carried out further investigations mapping LGN stimulation to cortical responses at the visual cortex (V1) of rats and rabbits(Panetsos et al., 2009; 2011).

Future development in containing the charge spread of electrodes within the LGN to improve visual resolution and establishing safety for bilateral implantation and stimulation of the thalamus are some of the hurdles to overcome before clinical trials on human subjects could be carried out.

1.3.7 Optogenetic Retinal Prosthesis

Researchers have genetically modified the remaining undamaged retinal cells (e.g. bipolar cells and ganglion cells layers) from *rd1* mice by transfecting them with lentivirus carrying genes expressing photosensitive proteins (e.g. a microbial opsin channelrhodopsin ChR2), thereby rendering the remainder retina photosensitive (Deisseroth, 2011). This technique, known as optogenetic technology, is a rapidly expanding field, with more opsins becoming available. The first experiments showed non-specific transfection, with both ON-and OFF-bipolar and ganglion cell systems expressing ChR2 equally. Such non-specific expression could not give rise to useful visual information.

Nirenberg et al. recently published a study whereby the visual images captured by video camera were first processed by applying a neural code through an encoder, to generate signals that would be recognisable to the brain. These signals were then transformed into laser light pulses to activate the

optogentically treated, ChR2-expressing *rd1* mice retina (Nirenberg and Pandarinath, 2012). Promising results showed that once the visual images were processed with the neural code, the visual behaviours (i.e. optomotor tracking) of the *rd1* mice improved, implying that optogenetic retina was capable of accurately transmitting the processed image signals to the brain. Apart from establishing the optogenetic technique as a viable method of retinal activation and signal transmission, the paper also illustrated the importance of a robust, accurate **neural code** to process the visual images for accurate visual interpretation, which will be discussed further in **chapter 8**.

1.3.8 Gene Therapy & Stem Cell Therapy

With the advent of cell biotechnology and increasing understanding of the disease pathogenesis, gene therapy and stem cell therapy have made substantial progress over the past 2 decades (MacLaren et al., 2016). In gene therapy, the aim is to transfer genes encoding therapeutic proteins into the affected tissues by means of viral transfection. Stem cell therapy, on the other hand, offers replacement of lost or damaged tissues with new cells or tissues generated from stem cells.

In patients with some forms of RP and other retinal degenerative diseases such as choroideremia and Leber's congenital amaurosis, whereby the causative genetic defects are known, targeted gene therapy appears to be a reasonable approach. Indeed clinical trial for *RPE65*-associated Leber's congenital amaurosis commenced in 2007, and showed robust safety as well as functional improvement (Jacobson et al., 2012). More recently, clinical trials of gene therapy for choroideremia (MacLaren et al., 2014) and *MerTK*-associated RP (Ghazi et al., 2016) are also under the way and preliminary results showed good safety profiles.

While gene therapy offers an attractive treatment option early on in the disease to prevent photoreceptor and hence visual loss, it is unsuitable in patients with advanced disease where substantial atrophy of photoreceptors, RPE and choriocapillaries has already occurred. In these patients, stem cell therapy offers the potential to replace the lost tissue and to some extent, function. At present, research into stem cell-derived RPE transplantation and clinical trials in this area have gained the most ground. The first stem cell-derived RPE

transplantation clinical trial involved injection of embryonic stem cell-derived RPE into subretinal space in patients with Stargardt disease (*ABCA4* mutation) and atrophic AMD (Schwartz et al., 2012; 2015). More recently, a clinical trial involving subretinal implantation of embryonic stem cell-derived RPE patch has begun in Moorfields Eye Hospital, in partnership with Pfizer Inc. ("New trial for wet AMD," n.d.). Lately, a Japanese research group has reported success with transplanting a sheet of RPE generated from induced pluripotent stem cell (iPSC), in to a patient with wet AMD. The iPSC was derived from the patient's own skin fibroblast. Although the vision of the patient did not improve, it remained stable and the transplanted RPE sheets remained intact at 1 year (Mandai et al., 2017). Success in tissue transplantation using iPSC opens up an exciting arena in transplantation medicine, by reducing issues such as immune rejection, tissue supply and ethical concerns using embryonic-derived stem cells.

Given the pluripotent nature of stem cells, with increasing understanding and further research in the field, transplantation of other retinal cells such as photoreceptors or even the entire retina, may be feasible in the foreseeable future.

1.4 Aims of the thesis

The commencement of this PhD coincided with the granting of regulatory approval for Argus® II retinal prosthesis to be used as a humanitarian device. This approval was firstly obtained in the European Economics Areas (CE mark in March 2011), and later on in the USA (FDA approval in February 2013). With increasing numbers of patients receiving the implant worldwide, data on long-term clinical and functional outcomes become of paramount importance for clinicians to understand the impact of the device and advise potential patients.

The aims of this thesis are:

1. To examine the long-term clinical and functional outcomes in an early cohort of subjects implanted with the Argus® II system, from the original feasibility study (Clinical Trials Identifier: NCT01490827).
2. To elucidate the characteristics of the artificial vision that is perceived and its long-term repeatability and reproducibility in individual subjects.

3. To report on the safety of performing MRI brain scans in patients fitted with the Argus® II retinal prosthesis system.
4. To explore the feasibility of real-time neuroimaging using functional near infra-red spectroscopy (fNIRS), to monitor visual cortex activities with retinal stimulation in this early cohort of Argus® II subjects.

1.5 Overview of the thesis

Following on from this introduction, **Chapter 2** provides the background to Argus® II retinal prosthesis system by reviewing the literature on its proof of concept, development, design, case selection, surgical implantation and safety profile.

Chapter 3 describes a prospective study of 11 Argus® II subjects, which looked at their ability to identify 2D geometric shapes presented in high contrast (i.e. white shapes against black screen) with the use of the device. A further prospective study from a subset of 7 subjects was then performed to investigate whether this 2D shape identification could be translated into identification of 3D objects.

Previously published data showed that Argus® II subjects were able to locate and point to white squares (against a black background) presented on touch screens more accurately with the prosthetic system switched on versus off (Ahuja et al., 2011). Following on from this 2D target localisation study, **Chapter 4** describes a prospective study of 5 Argus® II subjects, looking at whether the Argus® II device could also facilitate localisation and prehension of an object in 3D, using a 3D motion tracking system.

As a wide range of performance levels was observed amongst this early cohort of Argus® II subjects, particularly for form recognition tasks (i.e. shapes and objects recognition), further investigation into the nature of prosthetic vision as perceived by individual subjects was warranted. **Chapter 5** describes a prospective study of 6 Argus® II subjects, whereby the phosphenes elicited by fixed stimulating parameters were depicted by individual subjects, and their characteristics were analysed and compared for shapes, sizes, consistency and reproducibility. Inter-stimuli intervals ranging from 20 minutes apart, down to 1 second were tested in each subject to investigate temporal resolution of the

phosphenes.

Chapter 6 describes a retrospective study of 3 Argus® II subjects who underwent MRI brain scan (for unrelated medical reasons). Implant stability and function before and after the scan were compared to assess the safety and effect of MRI brain scan on the Argus® II subjects.

Due to concerns with interference of signals from radiofrequency telemetry in the Argus® II system, functional MRI was deemed unsuitable for investigating cortical activities in Argus® II patients, despite initial demonstration of good safety with performing MRI brain scans in these patients in **chapter 6**. We therefore looked into the feasibility of capturing real-time primary visual cortex activities with retinal stimulation in these patients using a novel technique, functional near-infrared spectroscopy (fNIRS) in **Chapter 7**. We investigated the patterns of cortical activation in 6 subjects under 3 different stimulation conditions. We concluded that fNIRS is a useful neuroimaging tool in these patients, which could open up the arena of future neuroscience research into cross-modal plasticity in visual prostheses.

The findings described in **Chapters 3 to 7** and their significances are then brought together in the final concluding **Chapter 8**.

Chapter 2

Background

2.1 Introduction to Argus® II Retinal Prosthesis

The Argus® II Retinal Prosthesis system (Second Sight Medical Products Inc., Sylmar, California, USA) is a commercially available device that restores a very low level of vision to patients with profound vision loss from outer retinal dystrophies. It has become the most widely used and most successful retinal prosthesis currently available in terms of regulatory approval. Since obtaining the CE mark in 2011 and FDA approval as a humanitarian device in 2013, commercial implantation has begun in many countries worldwide. Use of the device has been predominantly for patients with profound vision loss from retinitis pigmentosa and to a lesser extent, choroideremia as well as a planned cohort with extensive geographic atrophy from age-related macular degeneration (ClinicalTrails.gov Identifier: NCT02227498).

The cost of the Argus® II retinal prosthesis system is approximately $150,000 US dollars, with additional cost in surgical implantation and training with the use of the device ("The Argus II Retinal Prosthesis ('Bionic Eye') Receives Medicare Approval - VisionAware Blog - VisionAware," n.d.). Based on a multi-state transition Markov model, the cost effectiveness of the Argus® II system has been estimated to have a incremental cost effectiveness ratio (ICER) of €14,603 Euros/QALY (Vaidya et al., 2014). This falls below the published societal willingness to pay of EuroZone countries, and hence is deemed a cost-effective intervention compared to current standard of care of RP patients. To date, more than 200 devices have been implanted in 40 centres worldwide and the number is likely to increase. The content of this chapter has been published as a review article (Luo and daCruz, 2016).

2.2 Components of the Argus® II Retinal Prosthesis

Although termed a *retinal* prosthesis and popularly known as the '*bionic eye'*, devices such as the Argus® II are effectively photoreceptor replacements. As such, they are limited in their ability to replace retinal function in totality. The success of a retinal prosthesis depends on how well it is able to replace the functions of the degenerated or absent photoreceptors, namely: a) efficient capture of visual images in the form of light from the outside world; b) transduction of the captured light into meaningful neurological signals; and c)

subsequent activation of the residual inner retina (bipolar cells and RGCs), from where visual information can be relayed by the optic nerve to the visual cortex.

To achieve these goals, the Argus® II retinal prosthesis system employed 3 external components and 3 internal components. The 3 external components are: (see Figure 2.1)

1. A glasses mounted video-camera – for real-time image capture.
2. A portable computer (the Visual Processing Unit, VPU) – for processing of the captured scenes and translation into electrical stimulating parameters conveying spatial-temporal information.
3. An external coil (built into the side arm of the glasses) – for wireless transmission of the processed data from the VPU and electrical power to the internal components using RF telemetry.

Figure 2.1: Photograph of a patient fitted with the Argus® II retinal prosthesis system. The external components consisted of a spectacle-mounted video-camera, a portable computer (the Video Processing Unit, VPU), and an external coil. The VPU enables real-time processing of the captured scenes and translation into electrical stimulating parameters conveying spatial-temporal information. The external coil allows for wireless transmission of the processed data from the VPU and electrical power to the internal components using radiofrequency (RF) telemetry. (Image from (Luo and daCruz, 2016))

The 3 internal components are: (see Figure 2.2)

1. An internal coil – as a wireless receiver of RF telemetry, converting radio waves back to electromagnetic waves to recover both data and electrical power.
2. An inbuilt Application-Specific-Internal-Circuit (ASIC) – for generating appropriate electrical pulses in accordance with the stimulating parameter data recovered from the internal coil, which are then relayed to the multi-electrode array.

3. A 60-channel microelectrode (6 x 10) epiretinal array – consisting of 60 platinum electrodes (diameter = 200µm) spaced 200µm apart, embedded in a thin film of polyimide. Each microelectrode is connected to the ASIC in a parallel circuit via a metallised polymer connecting cable, such that each electrode can be activated independently according to the stimulating parameters. The array comes into direct contact with the retinal surface, allowing injection of electrical charges locally to stimulate the underlying retinal tissues (see Figure 2.3).

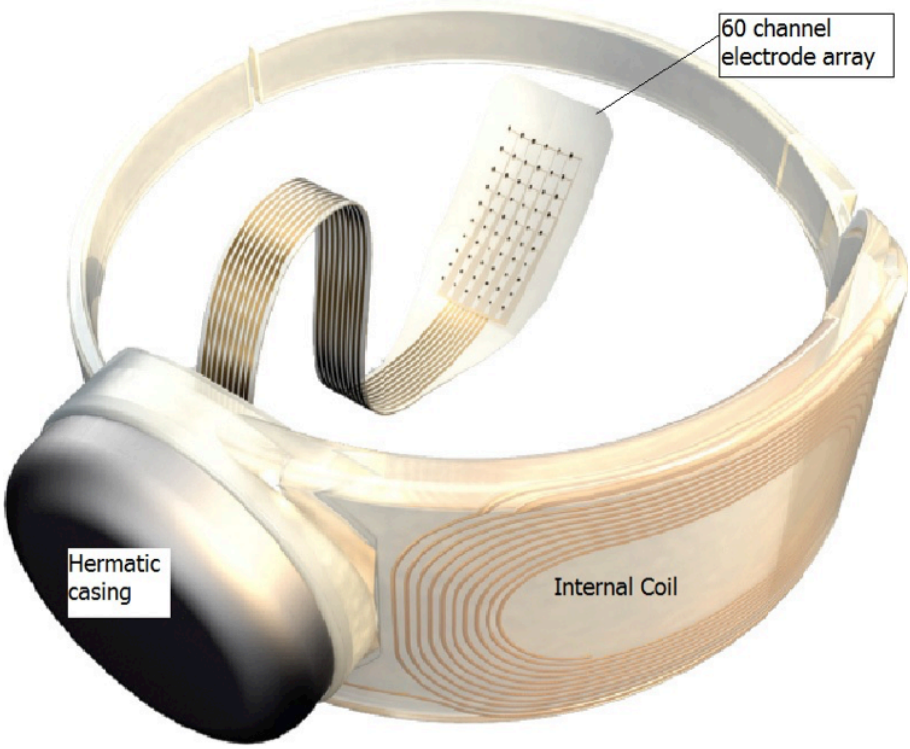

Figure 2.2: An illustration of the internal components of the Argus® II retinal prosthesis system. These are: an internal coil, an inbuilt Application-Specific-Internal-Circuit (ASIC) housed in the hermatic casing, and a 60-channel stimulating electrode array (all labelled). The internal coil acts as a wireless receiver of RF telemetry, converting radio waves back to electromagnetic waves to recover both data and electrical power. The ASIC generates the appropriate electrical pulses according to the data received, which are then relayed to the electrode array where direct stimulation of the retinal surface takes place. (Reproduced with permission from Second Sight Medical Products Inc. and from (Luo and daCruz, 2016))

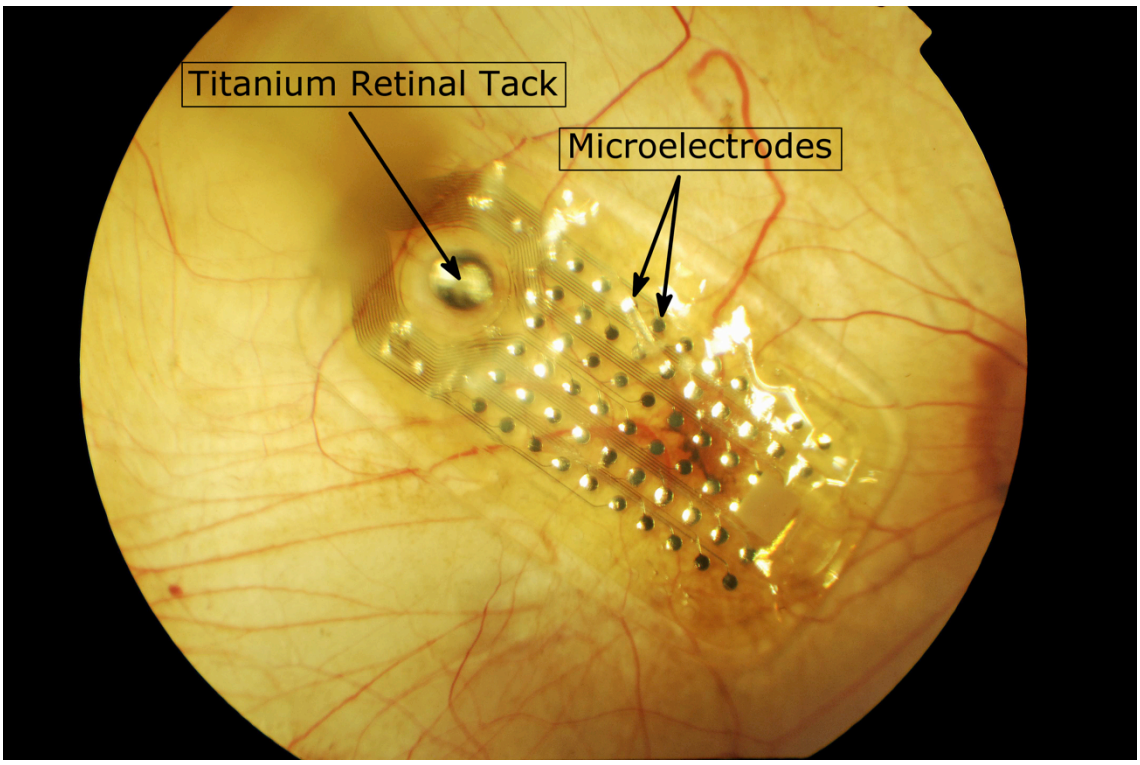

Figure 2.3: Colour fundus photograph of the microeletrode array with 60 platinum electrodes, implanted in a patient with choroideremia. The array rests on the retinal surface in direct contact with the retina, to allow efficient stimulation of the underlying retinal tissues. The array is held in place with a spring adjusted titanium tack that passes through retina, choroid and the sclera. (Image from (Luo and daCruz, 2016; Milam et al., 1998))

2.3 Choice of Candidates for Implantation

All current retinal prostheses (including the Argus® II Retinal Prosthesis) work by electrically eliciting patterned focal responses in the residual inner retina. Ideal candidates for treatment would therefore have conditions where the outer retina (i.e. photoreceptors and / or retinal pigment epithelium) has been destroyed by any mechanism, while the inner retina (e.g. bipolar cells, RGCs, horizontal cells and amacrine cells) remains relatively intact. The largest single group of disorders that manifests this combination of outer retinal loss with relative inner retina preservation is RP (Hartong et al., 2006; Milam et al., 1998).

RP denotes a group of hereditary outer retinal dystrophies, affecting around 1 in 3000 live births and more than a million people worldwide (Grover et al., 1999; Hartong et al., 2006). Affected individuals suffer from progressive visual loss which can be profound (0.5% with no light perception and 25% with ≤ 20/200 vision in both eyes) (Grover et al., 1999; Santos, 1997; Stone, 1992). Post

mortem histological studies of eyes of patients with moderate to severe RP have shown that even though all cellular layers of the retina underwent degeneration and cell loss with disease progression, the bipolar cell layer and the RGC layer remained relatively unaffected, with 78% and 30% preservation respectively, even in cases of severe RP (Guadagni et al., 2015; Santos, 1997; Stone, 1992). Treatment options for RP, other than for the associated cataract, epiretinal membrane and macular oedema, are limited (Guadagni et al., 2015; Humayun et al., 2012). As such, they represent a currently untreatable group of patients who may benefit from retinal prosthesis treatment.

Owing to the exploratory nature of the study, the recruitment criteria for entry into the Argus® II phase I / II clinical trial was RP patients with logMAR 2.9 (bare light perception) vision or worse (Humayun et al., 2012; Machemer et al., 1971; 1972). If visual loss in the eyes was asymmetrical, the worse-seeing eye was chosen as the study eye to minimise potential harm to the patient.

2.4 Surgical Implantation

Surgical implantation of the Argus® II Retinal Prosthesis involves the standard vitreoretinal surgery techniques of pars plana vitrectomy (Friedman, 1958; Machemer et al., 1972; 1971; Schepens and Okamura, 1957) and scleral buckling procedures (Friedman, 1958; Luo and daCruz, 2016; Schepens and Okamura, 1957). If the patient is phakic, lensectomy is usually performed from the outset, as subsequent cataract formation would render clinical monitoring difficult.

A standard 3-port pars plana vitrectomy is first performed, with removal of the posterior hyaloid face to prevent future development of an epiretinal membrane. Any pre-existing epiretinal membrane is removed at the time of surgery in order to optimise electrical contact between the microelectrodes and the retinal surface. A 360˚ conjunctival peritomy is performed to allow isolation of all 4 recti muscles in preparation for placing the encircling band carrying the extraocular portion of the device.

The internal coil and ASIC are sealed in protective hermetic cases, which have a concave under surface, conforming to the curvature of the globe. These are placed flush on bare sclera surface and sutured onto the sclera, usually in the

supero-temporal quadrant of the globe, at a pre-determined distance from the limbus (approximately 5mm) depending on the axial length of the globe (see Figure 2.4). A 5mm pars plana sclerotomy in the supero-temporal quadrant allows introduction of the microelectrode array into the vitreous cavity (see Figure 2.5) – this is the only intraocular portion of the device. With appropriate scleral placement of the extraocular part of the device, the microelectrode array would rest naturally on the retinal surface at the posterior pole with minimal tension. Gentle manipulation of the array position is possible to optimise placement in the macular region. Once the array position is satisfactory, a spring-tensioned, titanium retinal tack is inserted at the heel of the array, to ensure close apposition of the array and the retinal surface (see Figure 2.6). The sclerotomy is then sutured close around the traversing cable connecting the array to the ASIC to avoid scleral leakage and hypotony.

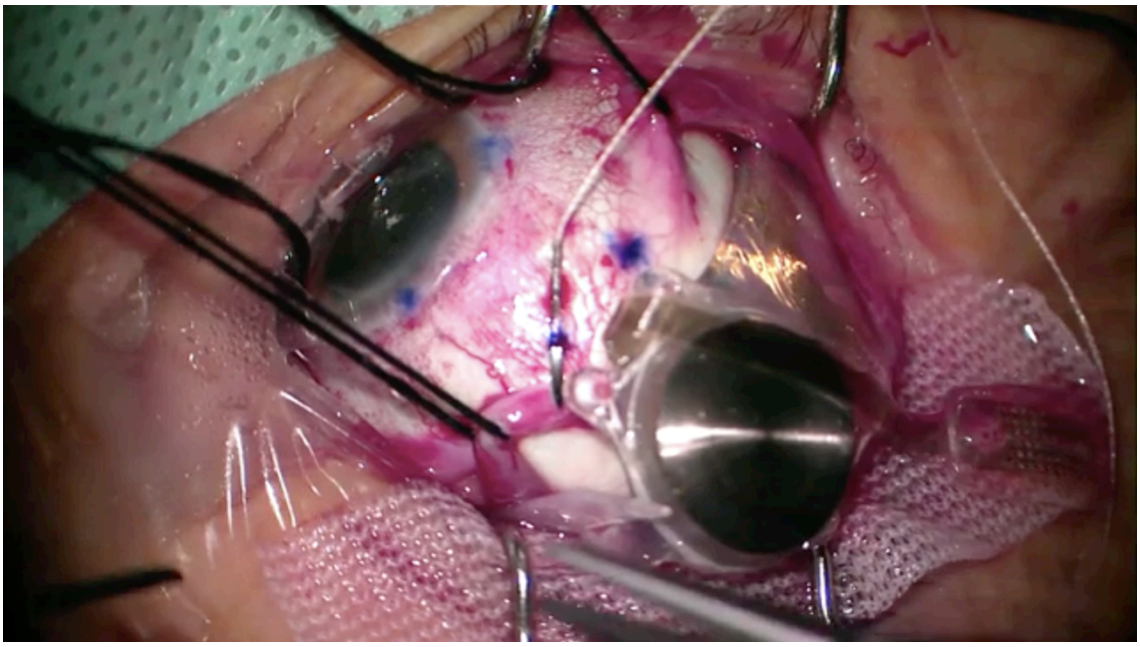

Figure 2.4: Intra-operative photograph of the ASIC in a hermetic casing being sutured onto the sclera 5mm from the limbus. (Still image captured from surgical video, courtesy of Stanislao Rizzo with permission and from (Luo and daCruz, 2016))

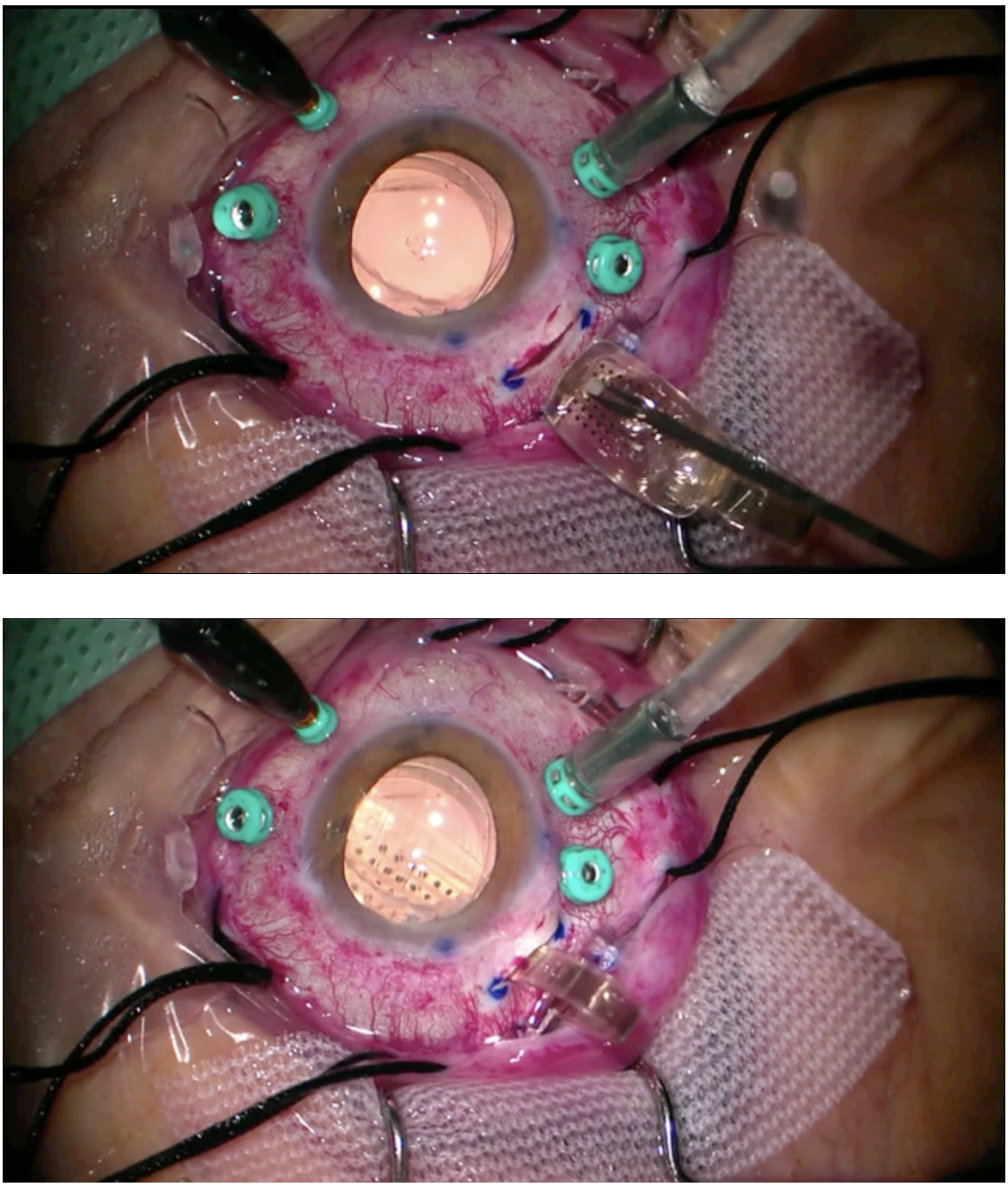

Figure 2.5: Intra-operative photographs showing the insertion of the microelectrode array into the vitreous cavity via a 5mm pars plana sclerotomy. (Still image captured from surgical video, courtesy of Stanislao Rizzo with permission, and from (Luo and daCruz, 2016))

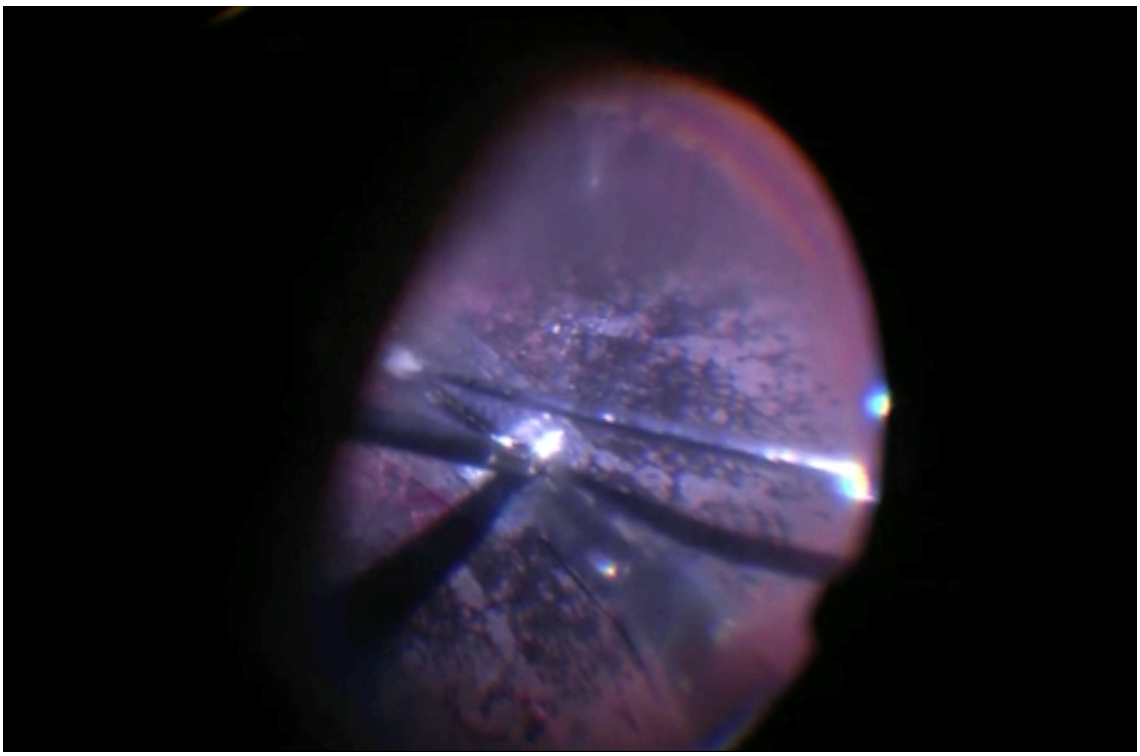

Figure 2.6: Intra-operative photographs showing the Titanium tack being passed through the heel of the microelectrode array and then through the retina choroid and sclera, thereby fixing the array to the retinal surface. (Still image captured from surgical video, courtesy of Stanislao Rizzo with permission, and from (Luo and daCruz, 2016; S. Rizzo et al., 2014))

The internal coil and ASIC cases on the sclera are further stabilised by a silicone encircling band, which passes under each of the 4 recti muscles around the globe before being gently tightened and held with a Watzke's sleeve. Finally, an allograft (e.g. Tutoplast®) or autologous fascia-lata patch is sutured over the hermetic cases before the conjunctival closure over the device. Surgical time generally falls between 1.5 – 4 hours, as reported in a single centre post-marketing study (Humayun et al., 2012; S. Rizzo et al., 2014). This is remarkably shorter than the initial surgical time reported during the phase I feasibility trial, whereby the median surgical time was 4 hours and 4 minutes (range from 1 hour 53 minutes to 8 hours 32 minutes)(Humayun et al., 2012). In this interim report, it was explained that there was a single case with very prolonged surgical time. It was due to the fact that the subject had previously undergone multiple surgeries on the implanted eye, resulting in extensive fibrosis of conjunctiva and reinsertion of the previously disinserted lateral retus muscle was also required intra-operatively. In summary, surgical implantation of Argus® II retinal prosthesis can be performed within reasonable time frame by surgeons with standard vitreoretinal surgical skills.

2.5 Safety Profile

Given that the aim of the Argus® II programme was to develop a commercially available retinal prosthesis, the safety of chronic implantation was central to the early clinical studies. The interim report of a 6-month to 2.7-year follow-up of the first 30 Argus® II patients showed a good initial safety profile, with 21 patients (70%) manifesting no severe adverse events (SAEs) during this period (Humayun et al., 2012). Of the 9 patients who experienced SAEs, the commonest complication was conjunctival erosion or dehiscence (5 patients). All except one of them were satisfactorily treated with re-suturing. This patient suffered from recurrent conjunctival erosion, hypotony with 360˚ choroidal effusions and retinal detachment, resulting in subsequent explantation of the device. The retinal detachment was successfully treated post-explantation with silicone oil tamponade and the patient's intraocular pressure returned to normal without further sequelae. Other SAEs included: 2 cases of retinal detachment (including the above-mentioned patient), 2 cases of hypotony with choroidal effusions (including the above-mentioned patient), 3 cases of culture-negative presumed endophthalmitis and 2 cases of retinal tack dislocation requiring re-tacking. Except for the one patient who underwent eventual explantation, all of the other patients' SAEs were treated successfully either surgically or medically (e.g. intravitreal antibiotics for endophthalmitis), and they retained good functional use of their device during the follow-up period. Most of the SAEs (82%) occurred within the first 6 months, with 70% occurring within the first 3 months. After some protocol adjustment halfway through the trial including device design improvement, surgical modifications, and the addition of a prophylactic intra-vitreal antibiotic injection at the end of surgical implantation, the rate of SAEs reduced significantly, and there were no further cases of endophthalmitis in the second half of the study (i.e. the last 15 cases) (Humayun et al., 2012; S. Rizzo et al., 2014).

More recently, a report of the 12-month follow-up outcome of 6 patients who received the implant in a single centre performed by a single surgeon was published (Humayun et al., 1994; S. Rizzo et al., 2014). There were no SAEs such as wound dehiscence, endophthalmitis or retinal detachment that required further surgery. There was one patient with post-operative elevation of

intraocular pressure that was managed medically, and one patient with moderate choroidal detachment, which resolved spontaneously. These outcomes are markedly better than the safety profile observed during the clinical trial phase of the Argus® II Retinal Prosthesis.

2.6 History of Development

Research into the possibility of retinal prosthetic vision began in the early 1990s with Mark Humayun, Robert Greenberg and Eugene de Juan at Johns Hopkins University. They first demonstrated that focal electrical stimulation with a platinum electrode could elicit localised retinal responses in isolated animal retinas (Humayun et al., 1994; 2005; 2003; Yanai et al., 2003) (discussed in detail in section 2.7.1). The group subsequently moved to the University of Southern California (USC), and started a collaboration with the Second Sight company that would eventually lead to the development of the Argus I and Argus® II retinal prostheses.

2.6.1 Argus I System

The prototype retinal prosthesis, the Argus I, began its phase I clinical trial involving 6 patients in 2002 (Horsager et al., 2009; Humayun et al., 2005; 2003; Yanai et al., 2003). The main differences between the first generation device and the Argus® II device are:

1. The stimulating array of Argus I consisted of 16 microelectrodes (4 x 4 configuration), of either 260μm or 520μm in diameter, or both sizes alternating in a checkerboard pattern, with a centre-to-centre inter-electrode separation of 800μm (see Figure 2.7 inset) (Horsager et al., 2009; Zrenner et al., 2011).
2. In the Argus I system, the hermetic casing containing the internal coil and ASIC was placed subcutaneously in the temporal bone recess, with the connecting cable leaving the periorbital space via a lateral canthotomy and tunnelled along the temporal bone subcutaneously to reach the temporal recess (see Figure 2.7). This approach was similar to that of the cochlear implant and the alpha-IMS subretinal implant (Brummer and Turner, 1977; Brummer et al., 1983; Zrenner et al., 2011), and required dissection of the temporal region with the assistance of maxillofacial /

otolaryngology expertise and extended surgical time. As such, this approach has been revised in the subsequent Argus® II design to simplify the implantation.

3. In the Argus I system the external coil is situated over the temporal bone, held magnetically to the subcutaneous internal coil.

Initial results from this clinical trial with a follow-up period of up to 33 months supported safety and long term functioning of the device. A wide range of electrode thresholds were observed both within and across the subjects, but many electrodes were able to elicit visual percepts within the safety charge density limit (Brummer and Turner, 1977; Brummer et al., 1983; Caspi et al., 2009).

Variability in the performances across the subjects was also noted, but was generally encouraging with the subjects being able to enumerate and localise high contrast objects with greater accuracy than by chance. Two subjects were also able to orientate shape (in the form of letter ‘L’) and identify 3 common objects (i.e. plate, cup and knife) with greater accuracy than by chance. Furthermore, using high contrast square wave gratings, one subject was able to differentiate the orientation of the gratings in 4 directions (vertical, horizontal, diagonal to right, diagonal to left) significantly better than by chance. The best level of resolution achievable was equivalent to logMAR 2.21 vision, in keeping with the theoretical resolution possible with the 4 x 4 array (Caspi et al., 2009; Horsager et al., 2009). The ability to carry out these tasks supported the notion that the subjects are capable of interpreting patterned electrical stimulation. Based on these results, the next generation retinal prosthesis – the Argus® II – with 60 microelectrodes, was developed.

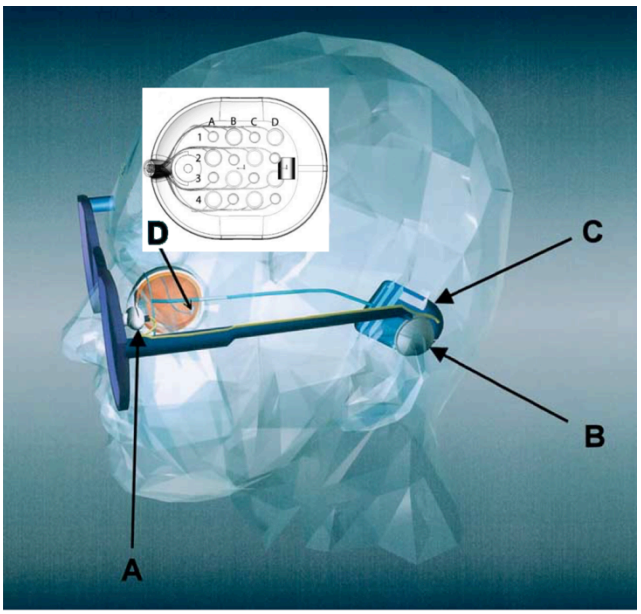

Figure 2.7: An illustration of the Argus I retinal implant in situ showing: (A) a video-camera mounted in glasses frame; (B) the external coil for wireless RF telemetry transmission held magnetically to the underlying subcutaneous internal coil; (C) the hermetic casing containing the internal coil and ASIC embedded subcutaneously in the temporal bone recess, with the connecting cable leaving the periorbital space via a lateral cantotomy and tunnelled along the temporal bone subcutanelously to reach the temporal recess; (D) multi-electrode array implanted intraocularly on the epiretinal surface. The inset shows the multi-electrode array consisting of 16 electrodes (4 x 4 configuration). The electrodes are alternating 260μm and 520μm in diameter in a checkerboard pattern. The centre-to-centre inter-electrode separation is 800μm. (Modified and reproduced with permission from (Horsager et al., 2009; Humayun et al., 2003) and (Humayun et al., 2003; Luo and daCruz, 2016; Sekirnjak et al., 2009), and from (Humayun et al., 1994; Luo and daCruz, 2016; 2014; Rose and Robblee, 1990))

2.7 Proof of Concept

The development of the Argus® II Retinal Prosthesis, as with all retinal prostheses, was based on the following assumptions:

1. The inner retina (RGCs with / without bipolar cells) of end-stage RP patients remains functionally intact allowing transmission of information along the visual pathway to the visual cortex.
2. The residual inner retina can be activated focally with localised electrical stimulation to elicit discrete phosphenes without causing damage or toxicity to the retina.
3. Retinotopy is relatively preserved in the residual inner retina and along the visual pathway, such that simultaneous multi-focal stimulations would

form geometric patterns of phosphenes in accordance with retinotopic locations.

4. The elicited geometric patterns of phosphenes can be relayed in a spatio-temporally correct manner along the visual pathway and interpreted by the primary visual cortex as recognisable visual patterns.
5. Limited pixels can still provide useful visual function.

The evidence for the first premise has already been discussed in section 2.3. The rest of this section will therefore focus on animal and human studies that support the remaining concepts.

2.7.1 Focal Retinal Stimulation

Animal Studies

Safety of Retinal Stimulation

To establish whether focal electrical stimulation of the inner retina could be achieved using microelectrodes and stimulating parameters within the established safety density charge limits (Humayun et al., 1994; Jensen et al., 2003a; Rose and Robblee, 1990) carried out a series of experiments: on the retinas of bullfrogs in an eye cup preparation; on a normal retina from an intact rabbit eye under terminal anaesthesia; and on rabbit eyes with the outer retinal function abolished by intravenous sodium iodate infusion. Using a pair of epiretinal platinum electrodes of 200μm in diameter separated by 200μm (the same diameter as that of the final Argus® II device) the authors demonstrated that the thresholds for activating these 3 retinal preparations were: 2.98μC/cm^2, 8.92μC/cm^2 and 11.0μC/cm^2 for bullfrog, normal rabbit retina and rabbit retina with abolished outer retinal function respectively. Even though stimulation of the retinal tissue with outer retinal dysfunction required higher stimulating charge density, all of them were within the predetermined safety limit for long term retina stimulation with platinum electrodes (limit = 50 - 150μC/cm^2) (Jensen et al., 2003b; Rose and Robblee, 1990). Similar responses have also been achieved by electrically stimulating transgenic P23H-1 rats' retinas, which had lost responses to light stimuli secondary to photoreceptor degeneration (Lilly et al., 1955; Sekirnjak et al., 2009).

Localisation of Retinal Responses

Humayun et al. (1994) demonstrated that the retinal responses elicited were localised to the area of electrical stimulation, as the recording electrode only detected activity when it was placed in between the stimulating electrode and the optic disc, but not when it was distal to the stimulating electrode-optic disc path (e.g. when it was placed nasal to the optic disc while the stimulating electrode was placed in the temporal retina). This indicated that the RGC responses elicited by electrical stimulation are only recordable from axons close to the point of stimulation, but not from axons of cells residing far away from the electrical stimuli. However, this study did not examine axons from distal cells that passed through the area of stimulation. Overall it at least showed probable gross retinotopic localisation of retinal responses, allowing for the possibility of simultaneous multi-focal stimulation to form geometric patterns, which could then potentially give rise to pixelated vision.

The issue of the inadvertent activation of bypassing axons from RGCs distal to the point of stimulation remains one of concern for creating discrete phosphenes. This potential problem exists due to the layering of axons in the macula region and the arcuate displacement of nerve fibres away from the fovea to minimise the visual obstruction of light falling on the central high-density photoreceptors. Stimulation of the RGC axon fibres, instead of the cell body (soma), would theoretically convey the perception of peripheral retinal activation, rather than a retinotopically correct pattern of photoreceptor activation. This may be more problematic with epiretinal electrodes, which are anatomically closer to the nerve fibre layer (hence the axon fibres), than the RGC soma. Furthermore, with a diameter of 200μm, each electrode encompasses the equivalent area of hundreds of photoreceptors (see Figure 2.8), further reducing the achievable resolution.

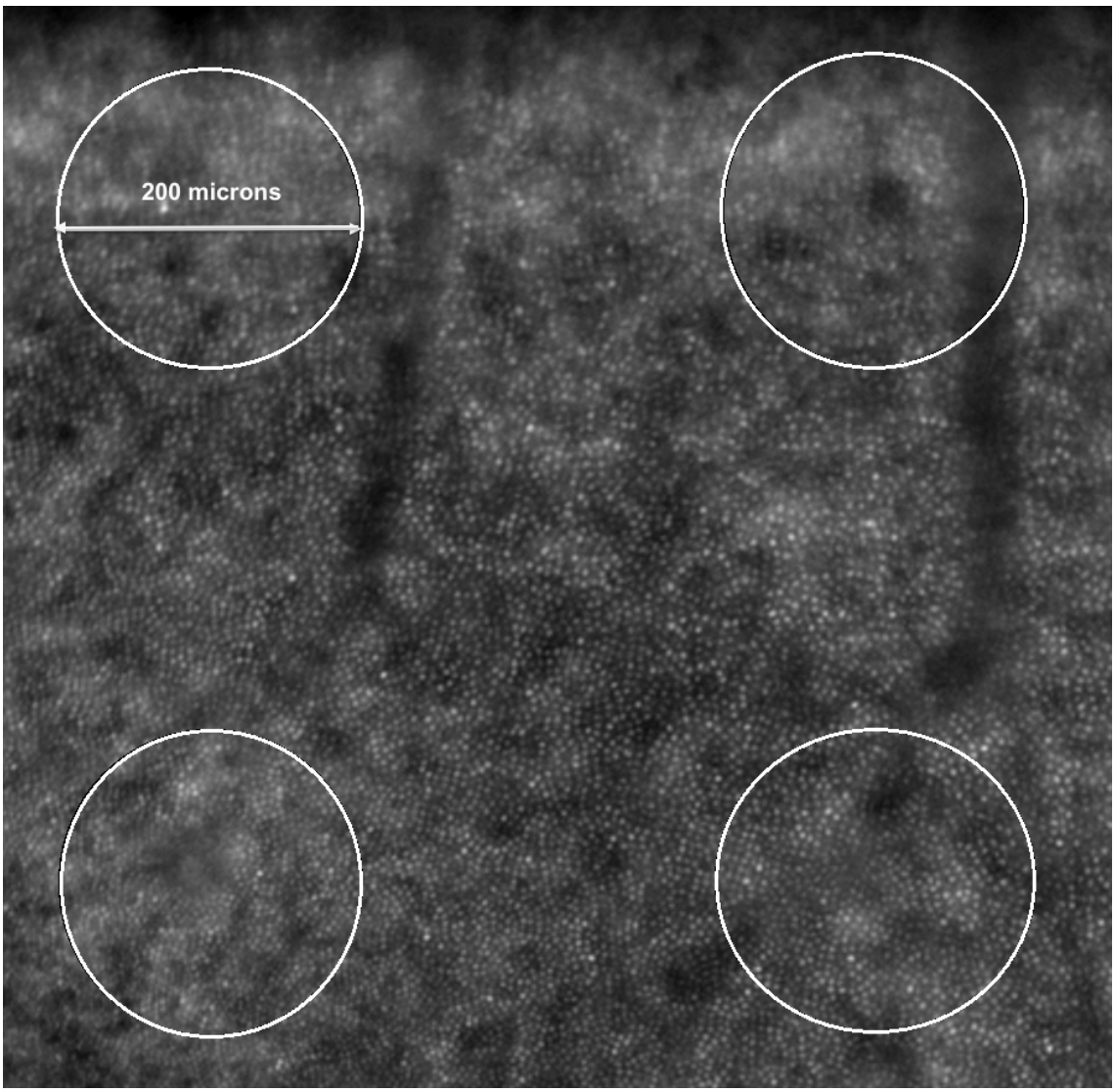

Figure 2.8: Adaptive optics (Imagine Eyes – rtx1™) retinal image of a healthy subject, taken at 3 degrees temporal to fixation. Individual cone photoreceptors can be seen as discrete dots. Within this macular region, the ratio of photoreceptors: bipolar cells: retinal ganglion cells approaches 1:1:1, allowing maximal visual resolution. In comparison, the 4 white circles are representative of the retinal surface areas covered by the Argus® II retinal prosthesis microelectrodes, with a diameter of 200μm each, drawn to scale. Activation of one microelectrode would therefore result in equivalent simultaneous activation of hundreds of photoreceptors. The resolution achievable is thus limited. (Reproduced with permission from (Greenberg et al., 1999; Luo and daCruz, 2014))

With the assumption that selective activation of localised RGCs will lead to production of discrete phosphenes, further work has been carried out to determine the nature of retinal activation with epiretinal electrodes, and to explore methods of focal retinal stimulation (e.g. by varying stimulating parameters and / or reducing the stimulating electrode size). Using isolated rabbit retinas and ultra fine electrodes (2μm), (Jensen et al., 2003a; Nanduri,

2011) set out to investigate the differences in the thresholds of stimulating RGC axons versus cell bodies. They discovered that the electrical threshold of activation was lowest with mono-polar cathode stimulation applied directly over the RGC soma (assuming the soma is located within its light receptive field), and that the threshold increased as the stimulation moved further away from the soma. With cathode stimulation, the RGC soma threshold was about half of that of the axon. However, this difference was not observed when anode stimulation was applied, which showed similar thresholds for both RGC soma and axon activation. In addition, application of cadmium chloride, a synaptic blocker, did not abolish the retinal responses, suggesting that the responses may originate in the RGC, rather than from bipolar cells.

In a separate study by the same group using mono-polar cathode stimulation, the authors found that with smaller electrode sizes (5μm in diameter), and shorter stimulating durations (0.1ms pulses), the threshold for directly activating RGC was much lower (37 times lower) than that required to activate the RGC indirectly via synaptic transmission. Even with a 125μm electrode and 2ms stimulating pulse, the average threshold for direct RGC activation was still half of that of trans-synaptic RGC activation (Jensen et al., 2003b; Sekirnjak, 2006; Sekirnjak et al., 2008). While the results from Jensen et al.'s group pointed towards a potential way of selective RGC soma activation, the conical configuration of the needle-shaped stimulating electrode and the mono-polar cathode stimulation were very different from the intended multi-electrode array design (which has a disciform planar configuration), and the safer charge-balanced biphasic stimulation (which reduces the Faradaic reaction at the electrode-tissue interface, hence minimising tissue damage) (Abramian et al., 2010; 2011; Lilly et al., 1955; Lovell et al., 2005; Sekirnjak et al., 2008). However, despite the fact that both Jensen et al. and (Behrend et al., 2011; Greenberg et al., 1999; Jepson et al., 2013) computer modelling demonstrated lower thresholds for RGC soma compared with the axons, other evidence suggests that the RGC axons appear to be the preferred site of activation (Horsager et al., 2009; Nanduri, 2011; Twyford et al., 2014). As such, whether it is the RGC soma or axon that is preferentially stimulated by the Argus® II device *in vivo*, remains ambiguous.

Multielectrode Array Stimulation

To expand the study on other animal retinas and test out settings and configurations which were similar to the intended retinal prosthesis design, Sekirnjak et al. (2008) carried out experiments on the retinas of rats, guinea pigs and later, macaque monkeys (which bear close resemblance to human retinas). They used multi-electrode arrays with micro-electrodes of 6μm – 25μm in diameter and charge-balanced biphasic stimulations to investigate retinal responses (Addi et al., 2008; Guo et al., 2014; Sekirnjak, 2006; Sekirnjak et al., 2008). The threshold charge densities from their experiments were typically 100μC/cm^2, which were within the established safety limit. Addition of various synaptic blockers did not abolish the retinal responses, again indicating that the responses were of RGC origin.

Focal Retinal Stimulation

In a subset of macaque monkey RGCs, the parasol cells (both ON and OFF) were further stimulated with 9 – 15μm electrodes (comparable to the size of individual RGC somas) (Palanker et al., 2004; Sekirnjak et al., 2008). It was shown that these parasol cells responded to a single electrical pulse with a single evoked response at sub-millisecond latency (~ 0.2ms), and that the response was confined within the activated cell, without spreading to its neighbours (i.e. spatially specific).

Further work on other ganglion cell types of macaque monkeys' retinas were carried out by (Jepson et al., 2013; Mathieson et al., 2012), including ON and OFF midget cells and small bi-stratified ganglion cells as well as the ON and OFF parasol cells. All these ganglion cells could also be independently activated with sub-millisecond latency within established safety limits. Given that the parasol cells form a significant part of the magnocellular pathway, while midget cells form the parvocellular pathway, the authors postulated that epiretinal electrical stimulation has the potential to elicit signals of high temporal and spatial resolution in primate retinas using high-density multi-electrode arrays. Selective activation of ON and OFF RGCs has also been demonstrated in isolated rabbit retinas by (Humayun et al., 1999; Twyford et al., 2014), using a conical epiretinal electrode with a base diameter of 15μm (comparable to the surface area of a 40μm disc electrode), and high frequency electrical

stimulations (HFS) of 2kHz. They have shown that within the low magnitude range (20 – 60μA) of HFS, modulation of the amplitude elicited opposing spiking responses in ON and OFF RGCs, lending to the prospect of developing a retinal prosthesis capable of cell-type specific, selective activation in the future (Guo et al., 2014; Humayun et al., 1999).

More recently, an Australian research group at the University of New South Wales has proposed the use of a complex epiretinal stimulating unit, whereby a central stimulating electrode is surrounded by 6 hexagonally-arranged return electrodes, which collectively return the delivered current (Abramian et al., 2010; 2011; Lovell et al., 2005; Weiland et al., 1999). Electrical charge spread from single electrode stimulation has previously been demonstrated both by computer modelling and later experimentally in rabbit as well as salamander retinas (Behrend et al., 2011; J. F. Rizzo et al., 2003a; 2003b). This could be responsible for the clinical observation that some Argus I subjects reported phosphene sizes that were more than twice the physical size of the single stimulating electrode (Horsager et al., 2009; J. F. Rizzo et al., 2003a). The presence of electric currents in the return electrodes supported the notion of charge spread from the stimulating electrode. The hypothesis behind this arrangement of stimulating and return electrodes was that it might isolate a particular stimulating electrode from neighbouring active stimulating electrodes. This isolation of the stimulating electrode would theoretically minimise the effect of ‘cross-talking’ from charge leakages (Addi et al., 2008; Beebe and Rose, 1988), improving the ‘focus’ of retinal stimulation. In this stimulating unit, each electrode was 50μm in diameter and could act both as a stimulating or returning electrode. In a multi-electrode array (with centre-to-centre electrode distance of 200μm), this configuration allowed great flexibility in the stimulating pattern. Other methods of improving focal retinal stimulation have also been described, including minimising the distance between the stimulating element and the target cells (Palanker et al., 2004; Weiland et al., 2002), and the design of a bipolar stimulating / return pixel to minimise charge spread (Mathieson et al., 2012; J. F. Rizzo et al., 2003b).

Human Studies

Focal Epiretinal Stimulation

Following experiments in vertebrate retinas, (Humayun et al., 1999; Nadig, 1999; Walter and Heimann, 2000) carried out experiments in 5 blind volunteers (3 with RP; one with an unknown retinal degeneration since birth; and one with extensive AMD) to investigate the effect of focal epiretinal stimulation. Using handheld probes of bipolar platinum electrodes of 200μm in diameter, the authors performed intra-operative stimulations with the patients awake under local anaesthesia. With a focal stimulation, all 5 patients reported perception of a transient phosphene, ranging from “pin” to “pea” in size. The location of each of the perceived phosphenes in space corresponded broadly to that predicted retinotopically by the position of retinal stimulation within the 4 quadrants of the macula, except in the patient who was blind since birth. This may have been due to the lack of development of retinotopic organisation at the visual cortex level from sensory deprivation. Simultaneous stimulation of 2 sites separated < 1mm apart produced the perception of 2 separate phosphenes in one patient, while stimulation with an elongated piece of platinum wire gave rise to an elongated percept (“a pencil held at arm’s length”). These findings strongly supported the notion that focal electrical stimulations could elicit discrete phosphenes in a retinotopic manner in a diseased human retina with outer retinal degeneration.

Formation of Pixelated Vision

To explore whether multiple discrete phosphenes could be elicited simultaneously to form recognisable geometric patterns, further experiments were carried out by the same group of researchers using platinum multi-electrode arrays of 3 x 3 and 5 x 5 configurations on 2 different blind RP patients (Chen et al., 2006; Güven et al., 2005; Humayun et al., 1999). Each electrode was 400μm in diameter with an inter-electrode separation of 200μm, and was embedded in a silicone matrix. The first patient with the 5 x 5 array perceived a horizontal line when a row of electrodes was activated, and a vertical line when a column of electrodes was activated. The phosphenes appeared to merge together such that a continuous line (rather than discrete linear dots) was seen. When the electrodes in 2 columns and 1 row in the form

of a “U” shape were stimulated, the patient reported an “H” shaped percept. In the second patient with the 3 x 3 array, when the 8 electrodes forming the perimeter of the array were activated, a “box” with an empty centre was described. Both patients reported visual percepts which appeared to correspond to the pattern of multi-electrode stimulation, indicating that visual percepts could be modified by the stimulation pattern to give rise to form vision.

Stimulation Threshold and Associated Phosphenes

To further elucidate the effect of outer retinal loss on electrically elicited visual percepts, (Walter et al., 2005; Weiland et al., 1999) carried out an experiment on 2 patients with normal retinas, prior to their eye exenteration for orbital cancer. Krypton and argon laser retinal ablations (each about 1 disc diameter in size) were applied to the infero-temporal macula and supero-temporal macula respectively. Krypton red destroyed photoreceptors, while argon green destroyed both the outer and inner retinal layers, leaving only RGC nuclei and axons. Charge balanced, biphasic stimulations with a platinum wire electrode (125μm in diameter) were applied to areas of normal retina as well as the krypton and argon laser-ablated areas. Supra-threshold stimuli applied to a normal retinal area elicited a large, dark percept, while stimulation of the krypton-ablated area elicited a discrete, small white dot and stimulation of the argon-ablated area elicited a linear, thread-like percept that was somewhat fainter. Both patients reported similar visual percepts when the same retinal areas were stimulated and these visual percepts were repeatable.

(Humayun et al., 1996; J. F. Rizzo et al., 2003b; 2003a) from the Boston Retinal Implant Group also explored the feasibility of multi-focal epiretinal stimulation using iridium oxide electrodes, to give visual percepts of recognisable geometric shapes. Using arrays of variable electrode sizes (50μm, 100μm and 400μm in diameter), epiretinal stimulations were performed in 5 blind RP patients and 1 patient with a normal healthy retina who was awaiting an exenteration procedure for orbital cancer. They (Greenberg et al., 1999; J. F. Rizzo et al., 2003a) observed that in general, the stimulation thresholds were much lower in the normal retina compared to diseased RP retinas. For the 50μm electrodes, the threshold to produce phosphenes exceeded that of the established charge density limit (quoted from established literature to be 1mC/cm^2 with cathodic

stimulation) (Beebe and Rose, 1988; Dagnelie and Stronks, 2014; Humayun et al., 2003; Stronks et al., 2013). Even with the 100μm and 400μm electrodes, only the normal retina thresholds were below the established charge density limit. Severely damaged retinas from RP appeared to have 4 – 19 times higher thresholds than normal retinas, which raised the concern for long-term electrical stimulation in severe RP patients. However in a later study, the iridium oxide safety charge limit was found to be higher than previously estimated, measuring up to 4mC/cm^2 with a 0.2 ms stimulating pulse (Stronks et al., 2013; Weiland et al., 2002), suggesting that safe chronic stimulation was possible.

In a follow-on study, contrary to Humayun et al. and Weiland et al.'s findings, (Brindley and Lewin, 1968; J. F. Rizzo et al., 2003b) showed that out of the 5 blind RP patients, only 3 patients experienced perception of a single discrete phosphene with single electrode stimulation. Single electrode stimulations were carried out by either 100μm or 400μm electrodes. Of the 185 visual percepts elicited in the 3 patients, only 6 %, 35% and 85% of these phosphenes were perceived as small single dots. Other phosphenes were more complex in nature, such as a "line", or a "cluster of 2 or 3 images". Even in the patient with a normal retina, only 57% of single electrode stimulations yielded single discrete phosphenes. When simple geometric patterns of electrodes were stimulated (e.g. a line or letter 'L" or "T"), out of 84 stimulations, the proportion of phosphenes matching the expected retinotopic representation was 55%, 21% and 29% respectively in the 3 RP patients, and 43% in the normal retina patient.

When the same stimulating parameters were applied to the same electrodes at different times to test the reproducibility of phosphenes, the results were variable between the patients. One RP patient reported similar phosphenes in 2 out of 2 trials, while the other 2 patients reported similar phosphenes in 19/23 trials and 9/12 trials respectively. The patient with normal retina reported reproducibility in 9/11 trials. Notably in one RP patient, when 2 electrodes spaced 1860μm apart were stimulated simultaneously, one phosphene was reported 5 out of 6 times while two phosphenes were observed once. Subsequent sequential stimulation of one followed by 2 electrodes for comparison yielded a single brighter percept twice, a brighter and larger percept once, a larger percept once, and the sensation of "motion" once.

J. Rizzo et al. confirmed that single discrete phosphenes could be achieved with single electrode stimulations in some patients, but noted that there was considerable variability amongst the patients (later borne out in the chronic implantation and stimulation studies, see **Chapters 3 – 5).** The patterns of the phosphenes elicited were often not predictable from the patterns of electrode array stimulation.

2.7.2 Cortical Responses from Electrically Stimulating Diseased Retina

A further requirement of a functional retinal prosthesis is the successful relay of the elicited electrical signals from the retina to the visual cortex. Several research groups have looked into the cortical responses to epiretinal electrical stimulation, using electrophysiology measurements in both animals and humans.

Animal Studies

Cortical activities from epiretinal stimulation were first demonstrated in rabbit retinas, using subcutaneously implanted / extradural electrodes over the visual cortex (Cha et al., 1992b; Nadig, 1999; Walter and Heimann, 2000). The cortical electrically-evoked potentials (EEPs) were comparable to that of visually-evoked potentials (VEPs) in both wave forms and in responses to changes in stimulus strength and frequency, suggesting that EEPs also originated from focal retinal activation.

Further demonstration of eliciting EEPs by focal electrical stimulation has been made in normal and *rd1* mice, and normal and RCD1 dogs (Chen et al., 2006; Güven et al., 2005; Sommerhalder et al., 2006). These two animal studies showed that EEP elicitation was also achievable in animal models of outer retinal degeneration. There was a distinct early response (latency < 10ms) and late response (latency > 50ms). Synaptic blockade using cadmium chloride ($CaCl_2$) abolished the late responses, but not the early responses, indicating that the early responses were from direct activation of RGC. Epiretinal electrical stimulation thus elicited cortical responses both via direct activation of RGC and via trans-synaptic signal transmission.

With the aim of visualising neuronal activity changes in the visual cortex, (Sterling and ACM, 1971; Walter et al., 2005) performed direct optical imaging of the cortical surface following epiretinal stimulation in rabbits. With neuronal activation visualised as darkening of the cortical area, topographical changes in the area of activation could be seen to follow sequential pairs of epiretinal electrodes being activated. The cortical activation was temporally matched and appeared to follow the visuotopic organisation of the cortex. This confirmed that retinotopic stimulation gives rise to focal, visuotopically preserved patterns of cortical activation.

Human Studies

Apart from working on *rd1* mice and RCD1 dogs, Chen et al. also performed measurements of EEP in one human with RP, using gold disc scalp electrodes over the occipital cortex. The epiretinal stimulation was carried out by an implantable epiretinal electrode array. Eight epiretinal electrodes were activated simultaneously, using supra-threshold currents. EEPs were recordable from the human RP patient on 2 separate occasions 3 weeks apart. On both occasions, EEPs were recorded with a latency of > 50ms. This was unexpected as previous works from (Dagnelie et al., 2007; Humayun et al., 1996) and computer modelling from (Greenberg et al., 1999; Wang et al., 2008) suggested RGC as the main site of electrical activation. The authors have commented that this may be due to the lack of sensitivity of scalp electrodes in detecting the early signal response.

More recently, EEPs have been recorded in both Argus I and Argus® II patients (Dagnelie and Stronks, 2014; Humayun et al., 2003; Stronks et al., 2013; Terasawa et al., 2002). (Humayun, 2001; Stronks et al., 2013) reported EEP recordings from 4 Argus® II retinal implant patients. Despite using all available electrodes for stimulation for each patient to maximise the cortical response, the signal-noise ratios were still low, thus requiring prolonged recording time and more substantial signal processing than standard VEPs. Nevertheless, the authors were able to identify characteristic features in the waveform. In particular the second peak, P2, was identified as the most reproducible outcome measure as it correlated well with the patients' subjective report of the phosphene elicited by the supra-threshold stimulus. However, although the

patients reported a decline in their perceived phosphene brightness over time with continuous stimulation, this was not reflected in the P2 recordings.

Despite numerous animal and human studies providing objective evidence of cortical activation in response to epiretinal stimulation, little is understood about how these cortical activities reflect image processing and / or interpretation along the visual pathway and at the cortical level. Neither is the correlation between EEPs and visual function well understood.

2.8 Simulation of Potential Visual Outcomes with Retinal Prosthesis

While physically replacing millions of photoreceptors with microelectrodes is not technically feasible, the actual number of microelectrodes required to restore functioning vision may be far lower. With the cortical implant, (Brindley and Lewin, 1968; Hayes et al., 2003; Humayun, 2001) first demonstrated the feasibility of partially restoring vision by the means of pixelated scenes – visual patterns made up of punctate spots of light (phosphenes). With this in mind, researchers set out to estimate the number of pixels (hence the number of functioning microelectrodes for focal retinal stimulation) theoretically required to provide useful function, using a combination of psychophysical experiments and computer simulations. For the purpose of practical application in Argus® II subjects, simulations were performed to establish the number of pixels required for 3 levels of visual tasks: navigational vision, facial and object recognition, and reading vision.

2.8.1 Navigational Vision

(Cha et al., 1992b; Thompson, 2003) used a monochromic monitor mounted on a pair of goggles for projecting scenes. The monitor was further covered by a perforated mask to create pixelated images. Seven normally sighted volunteers were asked to wear the goggles and navigate through a maze. The obstacles and the configuration of the maze were altered randomly for each trial in order to prevent route learning by the participants. They found that the field of view and the number of pixels were the two strongest determinants of navigational ability, and collectively accounted for 83.7% of the variance in walking speed.

Training and practice improved the performance of maze navigation (i.e. walking speed and number of contact with obstacles), and each subject required about 40 trials for the performance to be stabilised. The authors estimated that a minimum of 25 x 25 (625 in total) pixels projected centrally to the fovea, with a field of view of 30˚, was required for normal walking speed to navigate through the maze. (Brindley, 1964; Brindley and Lewin, 1968; Sommerhalder et al., 2006) also reported a very similar estimation of pixel requirements for navigation, recommending a visual field of 23˚ x 33˚ and a minimum of 500 pixels, while earlier work by (Sterling and ACM, 1971) indicated that a much lower number of 200 pixels might be adequate for recognition of small obstacles.

To allow comparisons of several more feasible designs of electrode arrays in navigation and mobility performances, (Cha et al., 1992a; Dagnelie et al., 2007) looked at the differences in navigational performance with 3 different densities of simulated pixelated vision: 4 x 4, 6 x 10 and 16 x 16 pixels. The authors used a combination of real mobility navigation – whereby the normal sighted participants wore a prosthetic vision simulator to walk through a maze; and a virtual reality navigation – whereby the participants navigated through a virtual maze with a game controller, again only watching a simulated pixelated vision display. The authors found that with adequate practice, an experienced user could navigate with the same efficiency using 6 x 10 pixelated vision, as with 16 x 16 vision. To further emulate the effect of phosphene “drop-outs” as encountered in the real-life use of the Argus® II Retinal Prosthesis System (due to poor electrode-retinal contact and / or unresponsiveness of the underlying retinal tissue to electrical stimulation within the safety charge density limit), the same group of researchers evaluated the effect of introducing random removal of pixels, and addition of background noise (i.e. random sparks, to mimic the spontaneous background photopsia experienced by many end-stage RP patients) in a virtual maze navigation (Hayes et al., 2003; Wang et al., 2008). The simulated prosthetic vision display was also “gaze-locked”, such that the presented scene did not vary with eye movement, to emulate the fact that the same area of retina was always stimulated by the electrode array, irrespective of eye movement. The authors concluded that a phosphene drop-out rate of 30% significantly extended the time required to perform the virtual maze

navigation (by 40%), while addition of background noise and variation in luminance contrast did not significantly affect navigation.

2.8.2 Object & Facial Recognition

Object and facial recognition form an important aspect of visual function as well as playing a significant role in social interaction. Apart from the number of pixels as discussed previously, a second important factor in the rendition of prosthetic vision is the ability to perceive differences in image grey levels (i.e. luminance contrast). By varying the stimulating parameters (e.g. amplitude and frequency), the luminance contrast of different pixels can be adjusted, giving the perception of different grey levels. The greater the range of grey levels perceivable, the better the scene recognition (Dagnelie et al., 2006; Terasawa et al., 2002).

(Humayun, 2001; Sommerhalder et al., 2003) set out to determine the pixel number and grey levels required for facial recognition. Using a head-mounted, customised Low Vision Enhancement System (LVES) display, simulated pixelated facial images were projected over the entire macular region of 8 normally sighted volunteers. The dot size, spacing, drop-out rates, grid size (visual field) and number of grey levels were varied in the simulation, to emulate the 3 different array designs: 4 x 4 (covering a 7.3˚ x 7.3˚ visual angle), 6 x 10 (covering a 11.3˚ x 19.3˚ visual angle) and 16 x16 array. While unsurprisingly the best performance was seen in the 25 x 25 array with 6 grey levels (over 75% accuracy), reasonable facial recognition could be achieved with the 16 x 16 array with a minimum visual field of 10˚, drop-out rate of less than 30% and 4 grey levels. Recognition of common daily objects (e.g. cup, spoon, plate and pen) was only achievable with the 16 x 16 array, while the 6 x 10 array allowed description of the object shape, but not accurate identification (Hayes et al., 2003; Humayun, 2001; Sommerhalder et al., 2004).

(daCruz et al., 2013; Humayun et al., 2012; Thompson, 2003) tested a range of 16 different simulation conditions with varying combinations of the following parameters: dot size, drop-out rate, gap width (i.e. inter-dot distance), grid (array) size, grey levels and image contrast. The performance with each condition was compared with that of a standard condition to assess the effect of varying these parameters. The standard condition settings were: 16 x 16 array, 31.5 arc-min dot size, 4.5 arc-min gap size, 30% dot drop-out rate, and 6 grey

levels. While each of the parameters was shown to affect the recognition speed, image contrast in particular, had a great impact on performance. For high contrast images (i.e. darkest grey level = 0% luminance; brightest grey level = 100% luminance), good facial recognition was achievable except when the simulated image was reduced to 70% random dot drop-out rate and 2 grey levels. For low contrast images (i.e. darkest grey level = 44% luminance; brightest grey level = 56% luminance), reasonable facial recognition was also possible with up to 70% dot drop-out rate, but a minimum of 4 grey levels and at least 17% of target image size was required. With more difficult images, the performance of the participants was shown to improve with practice.

2.8.3 Reading vision

As early as 1964, Brindley et al. estimated that 50 channels would permit recognition of one “printed or typed letter”, and that 600 channels would suffice for normal reading speed with the aid of automatic scanning (Brindley, 1964; Brindley and Lewin, 1968; Sommerhalder et al., 2004; 2003). This was supported by (J. F. Rizzo et al., 2003b; Sterling and ACM, 1971) and later on by (Cha et al., 1992a; Nanduri et al., 2011; 2012; 2008) who also looked into the factors affecting reading in phosphene-based pixelated vision. Using a phosphene simulator similar to that described in section 2.2.1, they estimated that 625 points (25 x 25 array, covering a 10˚ visual field) implanted within 1cm^2 of the area representing the fovea in the visual cortex would provide 20/30 vision.

While the earlier works were aimed at estimating reading vision provided by cortical implants, researchers at Johns Hopkins University set out to investigate the potential vision of 3 different retinal prosthesis arrays, namely 4 x 4, 6 x 10, and 16 x 16, using a head-mounted prosthetic vision simulator (as described in section 2.2.1) (Hayes et al., 2003; Pérez Fornos et al., 2012). They estimated that the potential visual acuity achievable with each of these arrays were 20/1810, 20/1330, and 20/420 respectively. Reading was achievable in all 8 participants with the 16 x 16 array and 36-point fonts, with 2 of them able to read 27-point fonts (equivalent of 20/450 reading acuity). With the 6 x 10 array, 2 participants were able to read 72-point fonts with an average reading speed of 1.02 words per minute. The reading speed could be vastly improved with good

text scanning technique, achieving a reading speed of 30 – 60 words per minute using the 16 x 16 array (Dagnelie et al., 2006). (Sommerhalder et al., 2003) also estimated that as few as 300 pixels would be adequate for close to perfect reading of 4-letter words (>90% correctly read words) when presented within the central 10˚ of visual field, while 600 pixels distributed over a retinal surface of 3mm x 2mm would be required for reading of a full-page text (Sommerhalder et al., 2004).

In summary, the above studies have shown theoretically that while more than 600 pixels would allow near normal functioning such as reading and navigation, reasonable visual function could be achieved with far fewer pixels (16 x 16 array, 4 grey levels and drop-out rate of less than 30%). The current Argus® II Retinal Prosthesis with 6 x 10 pixels would be predicted to provide reasonable navigational and some reading vision – as borne out by around 20% of patients from the Argus® II phase I / II clinical trials (daCruz et al., 2013; Humayun et al., 2012). There is also evidence that training and practice by way of visual rehabilitation improve the performance of visual tasks (Sommerhalder et al., 2004; 2003). However, there is still a substantial discrepancy between the predicted performance and the actual functional capability in all the Argus® II patients. This is in part due to the fact that these pixelated vision simulations were based on the assumption that each phosphene was perceived as uniform, discrete dots, which appear and disappear in accordance with the duration of electrical stimuli. In reality, although many percepts were indeed reported as white / yellow dots, the shapes, forms and persistence of many phosphenes elicited from epiretinal electrical stimulation are much more complex and vary greatly within subjects. This will be discussed in detail in **Chapter 5**.

As previously discussed, (J. F. Rizzo et al., 2003b) have observed that frequently, more than one phosphene of indiscriminate shape was described by subjects following single electrode stimulation. Furthermore, the same percept was not always described by the subject despite using identical stimulating parameters. This finding was also reported by (Nanduri et al., 2012; 2011; 2008), who further demonstrated changes in phosphene shape, size and brightness with varying stimulating frequency and amplitude. Additionally, phosphene perception has been found to have poor temporal correlation with the duration of the electrical stimuli. They were frequently reported to last less

than 2 seconds, despite persistent electrical stimulation. There is also a wide inter-subject variability (Pérez Fornos et al., 2012). Due to the number of factors involved and the variability in perception within and between subjects, the actual number of pixels required to produce useful vision has remained difficult to predict.

2.9 Conclusions

In summary, early animal and human studies have demonstrated the ability of focal retinal stimulation to elicit discrete phosphenes using epiretinal electrodes. Experiments with prosthetic vision simulators showed that reasonable navigational and reading (of 72-points font letters) vision could potentially be achieved with a 6 x 10 epiretinal electrode array, such as one employed by the Argus® II retinal prosthesis system.

Since the commencement of the phase I/II clinical trial in 2006, the Argus® II system has succeeded in being well tolerated with acceptable safety profile, resulting in the granting of the CE mark and FDA approval. However, the true impact of the system in the subjects' lives remains unknown.

In the following chapters (**chapters 3 and 4**), we set out to investigate the real-life performance of target recognition and localisation in a cohort of chronically implanted subjects. To explain the variation in the visual performance observed amongst the subjects, we further explored the fundamental difference in the prosthetic vision as perceived by each subject in **chapter 5**.

As a commercial device, clinical safety of not only the device implantation itself, but also the compatibility with other common clinical investigative procedures is an important aspect of clinical outcome. As such, in **chapter 6**, we reported on the safety of Magnetic Resonance Imaging (MRI) brain scans in 3 Argus® II subjects who underwent the scans.

Collectively, we aim to give a report on selected aspects of long-term clinical and functional outcomes in real-life settings in Argus® II retinal prosthesis subjects in this thesis.

Chapter 3

Form Vision

(Shapes & Objects Recognition)

3.1 Introduction

Despite a plethora of theoretical predictions and extensive animal testing, confirmation of successful stimulation of the inner retina with matching perceptions by the patients has only become possible since the commencement of long-term human trials of retinal prostheses. The Argus I trial began in 2002 and the international multi-centre phase II clinical trial of the Argus® II began in 2007 (clinicaltrials.gov identifier: NCT00407602).

As a result of the regulatory trials, the Argus® II retinal prosthesis system has been shown to function safely and reliably over long periods of time (Humayun et al., 2012; Zhou et al., 2013). The visual performance, however, has been variable among the subjects, ranging from reading of large letters in high-performing subjects (daCruz et al., 2013), to reliable perception of light only in others. Out of the 30 subjects enrolled in the phase II trial, 50.0% were able to identify direction of motion significantly better with device switched on versus off at 5 years after implantation; while 38.1% also had measurable gratings acuity of logMAR 2.9 or better {daCruz:2016kx}.

The ability to differentiate visual forms with the view to recognising objects and elements in real-life relies on 2 assumptions:

a) patterned electrode stimulations are able to reproducibly elicit distinguishable, discrete phosphenes; and
b) the phosphenes are represented in a retinotopic manner to convey spatial form.

In this study we set out to investigate the feasibility of using the Argus® II implant to enable subjects to differentiate form, firstly by assessing their recognition of two-dimensional (2D) geometric shapes presented on a LCD screen, followed by recognition of three-dimensional (3D) objects from real-life. We hypothesised that the use of Argus® II retinal prosthesis would improve the subject's ability to identify a range of geometric shapes than without the device. We also hypothesised that the performance in 2D shapes recognition could be translated into 3D objects recognition.

The experiments were performed in 2 parts and discussed under the following 2 headings:

1. Two-Dimensional screen-based Shapes Recognition Study; and
2. Three-Dimensional Objects Recognition Study.

3.2 Patients & Methods

Eleven subjects with RP implanted with the Argus® II retinal prosthesis system as part of the Second Sight phase I/II feasibility study (clinicaltrials.gov identifier: NCT00407602) were recruited from 4 centres in Europe. This study was approved by the institutional review board or ethics committee of each of the centres involved, and followed the tenets of the Declaration of Helsinki. Informed consent was obtained from all the subjects.

The Shapes Recognition Study was performed in 11 subjects who were available for regular training and psychophysical testing in the 4 European centres, namely London and Manchester in the UK, Paris, and Geneva. The subsequent Objects Recognition Study was performed in a subset of 7 of these 11 subjects based in the 2 UK centres. The subjects from the centres in Europe were not included due to difficulties in the logistics of patient accessibility and distance. Of the 8 UK-based subjects, only 7 subjects participated in the Objects Recognition Study, as one subject (Subject ID: 52-002) has since immigrated outside of the UK. All of the subjects received appropriate training with the general use of the Argus® II device as well as training specific to the tasks prior to testing.

3.2.1 Shapes Recognition Study (2D)

3.2.1.1 Materials

Test I: Solid Shapes

Eight geometrically distinct solid shapes were selected for this testing, namely: circle, semi-circle, triangle, square, cross, rectangle, pentagon and hexagon (see Figure 3.1). The shape optotypes were created using PowerPoint (Microsoft®, Redmond, Washington, USA) for presentation on a 15-inch flat LCD screen with the screen resolution set to 1024×768 pixels, against a black

background.

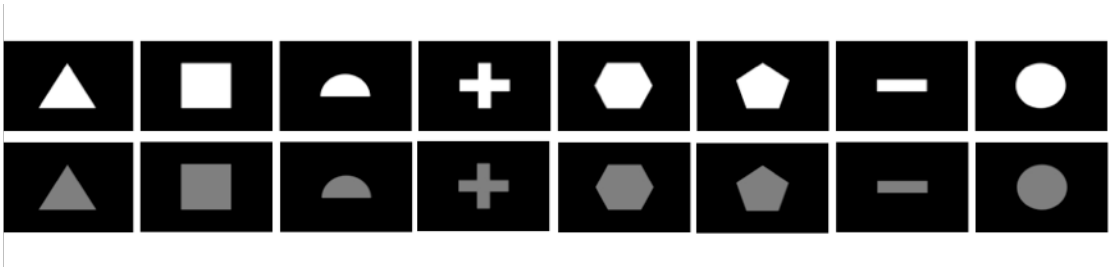

Figure 3.1: Eight geometric Solid Shapes chosen for the Shapes Recognition Study. During the Solid Shapes testing, each subject was presented with each of the 8 white solid shapes (top panel) in 5 different sizes (see Figure 3.2) in random order. Each image was presented once during the testing (i.e. 40 presentations per testing). This was then repeated with presentation of grey solid shapes (bottom panel), also in 5 different sizes. The subject was allowed up to 1 minute to identify each presented shape. The testing was performed with the Argus® II device switched on and then repeated with the device off. (Image modified from (Luo and daCruz, 2016))

Two shades (white or grey) in 5 different sizes (XL = 22.6 cm, L = 14.3 cm, M = 9.0 cm, S = 5.6 cm, XS = 3.6 cm; see Figure 3.2) were created for each optotype.

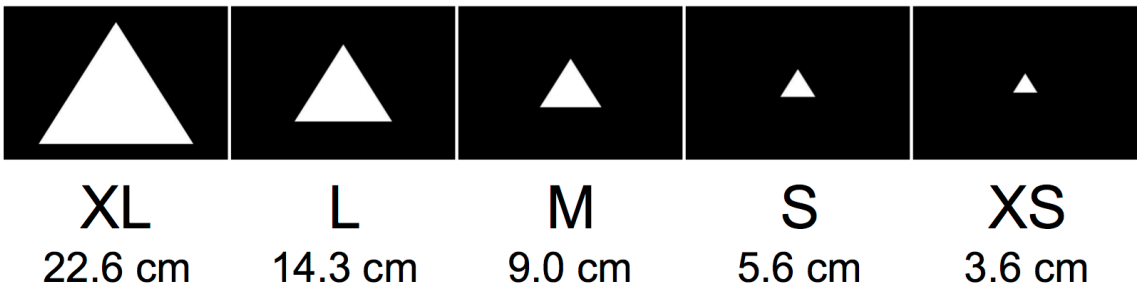

Figure 3.2: The five different sizes of each geometric shape created for the Shapes Recognition Study. The white solid triangles are shown here in XL (22.6cm), L (14.3cm), M (9.0cm), S (5.6cm) and XS (3.6cm) sizes. During the testing, the subjects were presented with each of the 8 chosen geometric shapes in the any of these sizes in random order.

The use of white and grey shades allowed us to determine the effect of contrast on performance. By varying the optotype size presented, we prevented the use of size (rather than shape) as a discriminator for optotype recognition.

Test II: Outlined Shapes

The outlined forms of these 8 geometric shapes (see Figure 3.3) were also created in both white and grey, and in 5 different sizes as above, for presentation against a black background on LCD screen.

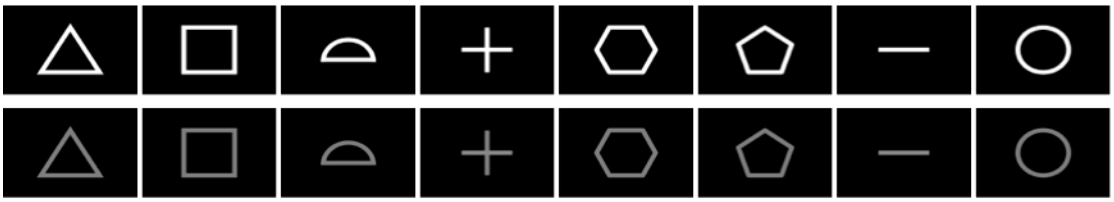

Figure 3.3: The eight Outlined Shapes chosen for the Shapes Recognition Study. During the Outlined Shapes testing, as with the Solid Shapes testing, each subject was presented with each of the 8 white outlined shapes (top panel) in 5 different sizes (see Figure 3.2) in random order. Each image was presented once during the testing (i.e. 40 presentations per testing). This was then repeated with presentation of grey outlined shapes (bottom panel), also in 5 different sizes. The subject was allowed up to 1 minute to identify each presented shape. The testing was performed with the Argus® II device switched on and then repeated with the device off. (Image modified from (Luo and daCruz, 2016))

3.2.1.2 Pre-test Training

A standardised pre-test training was carried out with the Argus® II retinal prosthetic device switched on. Each subject was presented with each of the 8 shapes in the largest size (XL = 22.6 cm) sequentially in a darkened room. During the training, with each presented image, the subject was first instructed to carry out “macro-scans” with the video-camera glasses across the entire screen to determine the overall size of the image. Once the size was determined, the subject was asked to carry out “micro-scans” to trace along the edge of the presented image to determine its geometric shape. If the shape of the image could not be identified, the subject was guided to trace along the edge of the image until one could identify the shape. A further 8 randomly chosen shapes of mixed sizes and shapes were then presented once to the subject, to allow familiarisation with shapes presented in different sizes. All of the shapes were presented in white against black background during the training.

3.2.1.3 Test Conditions & Controls

The experiment was performed in a darkened room, with the LCD screen set at eye level, 30 cm in front of seated subjects.

During the testing, the subjects were presented with each of the 8 geometric solid shapes in both white and grey shades and in all 5 sizes in random order.

Each image of the same shade was presented once during the testing (i.e. 40 presentations per testing). Randomisation was provided by the MatLab® program (MatLab®, Mathworks, Natick, Massachusetts, USA). The subject was given up to 1 minute to identify each presented shape. At the end of the minute, the image would disappear from the screen and a response was requested (forced choice). Subjects were expected to guess if they did not feel they could identify the shape. Standardised instructions were given to all the subjects at the beginning of each experiment. The experiment was performed with the Argus® II retinal prosthetic device switched on and then repeated with the device switched off, in order to act as an internal negative control.

The entire experiment was then repeated with the 8 outlined shapes under the same settings and conditions as described for the solid shapes.

3.2.2 Objects Recognition Study (3D)

3.2.2.1 Materials

Test I: Solid Objects

As part of designing this experiment, the 7 participating subjects were interviewed to establish the 8 objects they would most like to be able to identify in their daily environment. The chosen objects were: a teapot, a mug, a plate, a salt and pepper cruet set, a bunch of keys, a mobile phone, a remote control and a wallet (see Figure 3.4). These objects were chosen as they represented a group of objects likely to be found together in a home setting, e.g. on a coffee table. As such, visual discrimination would be helpful.

Figure 3.4: Eight objects from real-life chosen for the Objects Recognition Study. During the testing, the subjects were presented with each of the 8 solid white objects in random order, with each object presented twice (i.e. 16 presentations) per testing. The subject was allowed up to 30 seconds to identify the object. The testing was performed with the Argus® II device set to one of the following 3 conditions: device switched on, device switched on but with signals scrambled (i.e. scrambled mode) and device switched off. (Image modified from (Luo and daCruz, 2016))

Test II: Outlined Objects

In order to elucidate the effect of accentuating the outlines of the objects in their recognition, the body of each object was partially covered with cutout black cardboard to create an edge effect. These outlined objects were also presented for testing as the second part of the Objects Recognition Study (see Figure 3.5).

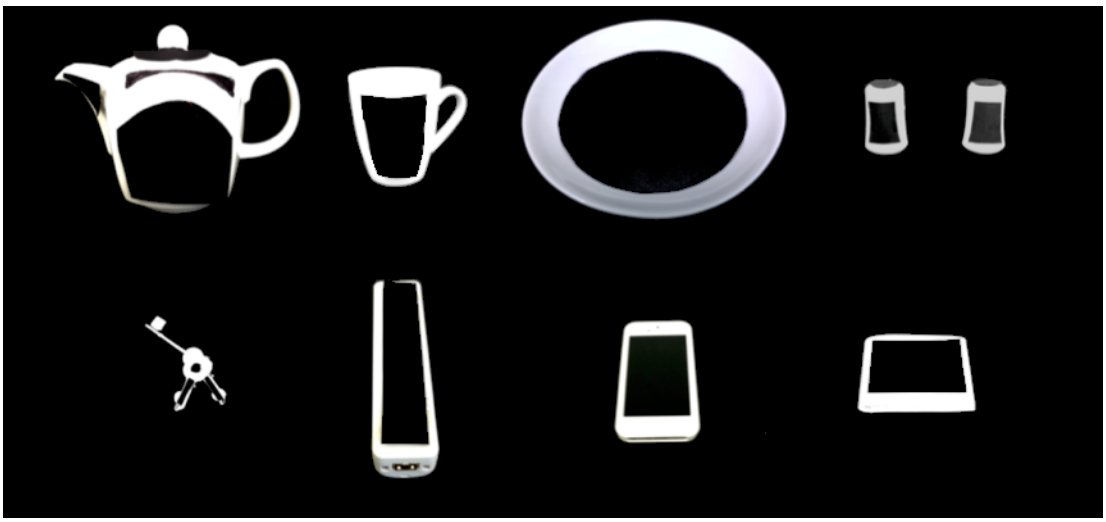

Figure 3.5: Eight objects from real-life covered with cutout black boards so as to accentuate their outlines in Objects Recognition Study. During the testing, as with the Solid Objects testing, the subjects were presented with each of the 8 outlined objects in random order, with each object presented twice (i.e. 16 presentations) per testing. The subject was allowed up to 30 seconds to identify the object. The testing was performed with the Argus® II device set to one of the following 3 conditions: device switched on, device switched on but with signals scrambled (i.e. scrambled mode) and device switched off. (Image modified from (Luo and daCruz, 2016))

3.2.2.2 Pre-test Training

A standardised pre-test training took place with the Argus® II retinal prosthetic device switched on, in a well-lit room to mimic real-life environment (see Test Conditions and Figure 3.6).

The subject was presented with each of the 8 objects sequentially. For each object, the subject was first instructed to perform “macro-scans” across the worktop to determine the object’s size and whether it had height. This was followed by “micro-scans” to identify and follow the outlines of the object. The subject was then asked to touch the object to match his visual perception to the tactile information of the object. The distinctive visual features for the different objects were summarised to the subjects as below:

- Small objects: mobile phone, remote control, wallet, set of keys
  - Small object with irregular shape: a set of keys
- Large objects: teapot, mug, plate
  - Large object without height: plate
  - Large object with height: teapot or cup
- Two separate objects: salt and pepper set.

3.2.2.3 Test Conditions & Controls

The experiment was performed in a well-lit room to simulate the real-life environment. The worktop was covered with a black felt cloth to serve as a dark background, against which objects of white or highly reflective hues were presented to maximise contrast. Two black armrests were placed on either side of the presented object, about 50 cm apart, so as to help the subject locate the presented object (see Figure 3.6). The subjects were seated with the worktop at their waist level, and instructed to place their arms on the two armrests on the worktop. They were informed that the object for identification would be placed in between the two armrests.

Figure 3.6: Two dark blocks (~50 cm apart) acting as armrests were placed on either side of the presented object during Objects Recognition Study. By placing their hands / arms on the armrests during the testing, the subjects could locate the presented object more easily.

During the testing, the 8 solid objects were presented sequentially in random order, with each object presented twice (i.e. 16 presentations) per testing. The subject was allowed up to 30 seconds to identify the object, upon which time the object would be removed from the field of view of the subject, and an answer was required (forced choice).

The experiments were performed with the Argus® II retinal prosthetic device set to one of the following 3 conditions:

1. Device on (standard mode);
2. Device in scrambled mode (internal positive control, see below); and
3. Device off (internal negative controls).

Signal-Scrambling Mode of Argus® II Retinal Prosthesis

Signal-scrambling mode (hereinafter referred to as scrambled mode) allows transmission of electrical impulses to the electrode array, but the pattern of array activation is systemically altered such that it no longer reflects spatial form, essentially turning the Argus® II into a light detection device (Caspi et al., 2009; daCruz et al., 2013). For example, if the subject were looking at a white line on a black background in standard mode, a line of electrodes would be activated. However, in scrambled mode, the same number of electrodes would be activated in random positions across the array without any resemblance of linearity (see Figure 3.7). If the subject were using the Argus® II as a light detection device and inferring form vision, then there would be no difference in outcome between standard and scrambled mode. Conversely, any difference in the performance with the device in standard mode versus scrambled mode would therefore reflect the degree of perception of spatial information originating from the device, rather than inference of form from head scanning.

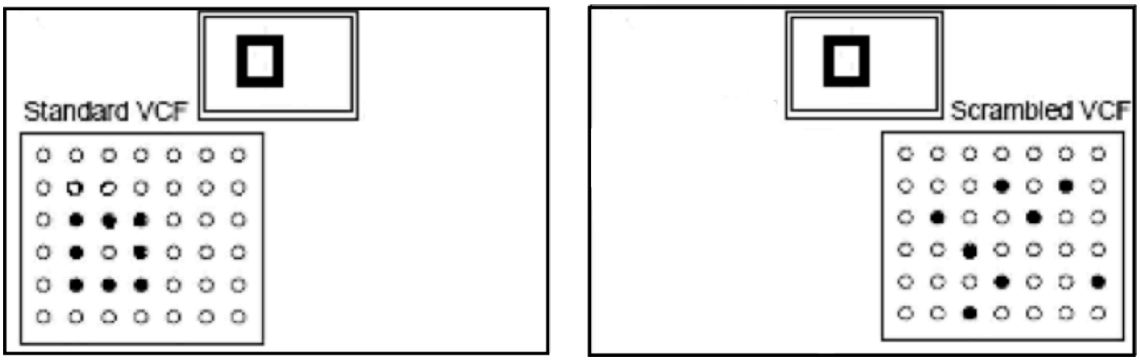

Figure 3.7: A diagrammatic illustration of the difference between the electrode array activation patterns under the standard and scrambled modes (as labelled) when the camera is viewing a square box. In scrambled mode, the spatial correspondence between a point's real position and the stimulation position on the array has been randomised. In this way, the patient does not receive spatial information but does receive non-spatial light detection information. (Image modified from (daCruz et al., 2013))

Two sets of experiments were performed with the Argus® II device under condition 1 and 2, while one set of experiment was performed under condition 3 for each subject. Both the order of objects presented and the conditions under

which the testing was performed were randomised using the random number sequence generated by the Research Randomizer website (https://www.randomizer.org). The subjects were masked to the device setting conditions.

The experiment was repeated with the 8 outlined objects under the same settings and conditions as described for the solid objects.

3.2.3 Statistical Analysis

All of the statistical analyses and graphical presentations were performed using SPSS program (IBM® SPSS® Statistics version 22). Non-parametric tests were chosen for the analysis, as normality of the distribution of the results could not be assumed given the small sample size.

3.3 Result

3.3.1 Subjects and Implant

Gender, age at diagnosis and implantation, and the number of electrodes activated and functioning at the time these tests were performed for each subject are as shown in Table 3.1. Some subjects have considerably less number of electrodes activated (namely 51-003, 52-002, 61-001 and 72-002) compared with other subjects. In these subjects, many of their microelectrodes were disabled at the first post-operative threshold testing, either because the threshold level to elicit visual percepts exceeded that of the safe density charge limit; or stimulation caused physical discomfort to the subject.

Subject ID	Sex	Age at Diagnosis (Years)	Age at Surgery (Years)	Number of Working Electrodes
51-003	M	19	72	28
51-005	M	7	55	60
51-006	M	46	66	56
51-007	M	28	63	56
51-009	F	11	45	60
52-001	M	30	50	60
52-002	M	16	65	29
52-003	M	25	60	37
61-001	M	3	53	11
61-003	M	34	57	51
72-002	M	15	60	29

Table 3.1: Demographics of the 11 Argus® II subjects who participated in Shapes Recognition Study. 51-003, 51-005, 51-006, 51-007, 51-009, 52-001 and 52-003 also participated in the Objects Recognition Study. M = Male, F = Female.

3.3.2 Shapes Recognition Study

Test I: Solid Shapes

The median (interquartile range) percentage of correct identification of white solid shapes was 22.5 (15.0 – 32.5)% with the Argus® II device on, and 12.5 (12.5 – 15.0)% with the device off (P = 0.033, Wilcoxon signed rank test).

For grey solid shapes, the median (interquartile range) percentage of correct identification was 17.5 (12.5 – 35.0)% with the device on, and 12.5 (10.0 – 15.0)% with the device off (P = 0.032, Wilcoxon signed rank test).

With the Argus® II device on, there is no statistically significant difference in the identification of white solid shapes compared to grey solid shapes (P = 0.65, Wilcoxon signed rank test).

Overall, the median (interquartile range) percentage of correct identification of all solid shapes was 20.0 (14.4 – 33.1)% with the Argus® II device on, and 12.5 (10.0 – 15.0)% with the device off (P = 0.002, Wilcoxon signed rank test, see Figure 3.8).

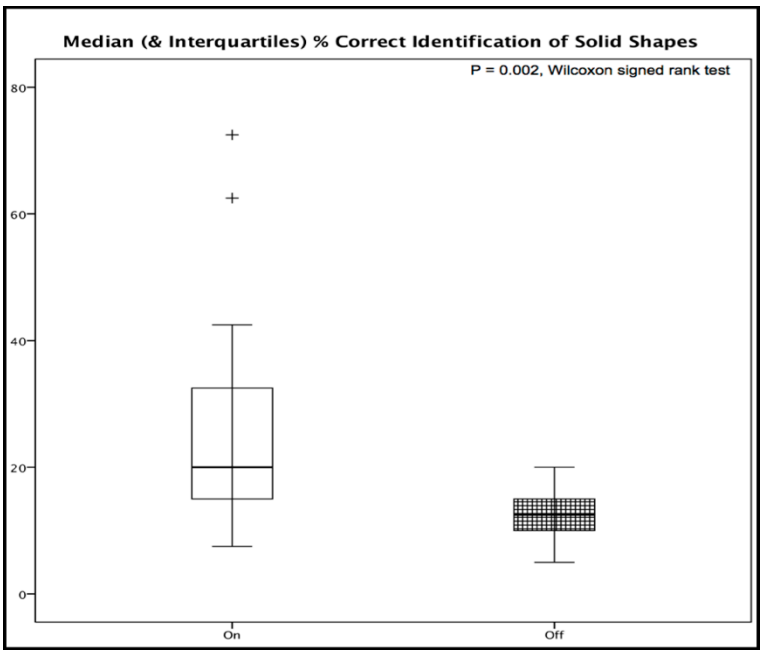

Figure 3.8: Box and Whisker plot showing the median and interquartile range of the mean % of correct identification of solid shapes with the Argus® II retinal prosthesis device switched on and off as labelled. (+ denotes the outliers)

Test II: Outlined Shapes

The median (interquartile range) percentage of correct identification of white outlined shapes was 33.8 (27.5 – 51.3)% with the Argus® II device on, and 13.8 (11.3 – 17.5)% with the device off (P = 0.003, Wilcoxon signed rank test).

For grey outlined shapes, the median (interquartile range) percentage of correct identification was 32.5 (18.8 – 38.8)% with the device on, and 13.8 (12.5 – 15.0)% with the device off (P = 0.006, Wilcoxon signed rank test).

With the Argus® II device on, the subjects were able to correctly identify white outlined shapes significantly better than grey outlined shapes (P = 0.018, Wilcoxon signed rank test).

Collectively for all outlined shapes, the median (interquartile range) percentage of correct identification was 33.1 (26.6 – 48.1)% with the device on, and 13.8 (12.2 – 15.3)% with the device off (P < 0.001, Wilcoxon signed rank test, see Figure 3.9).

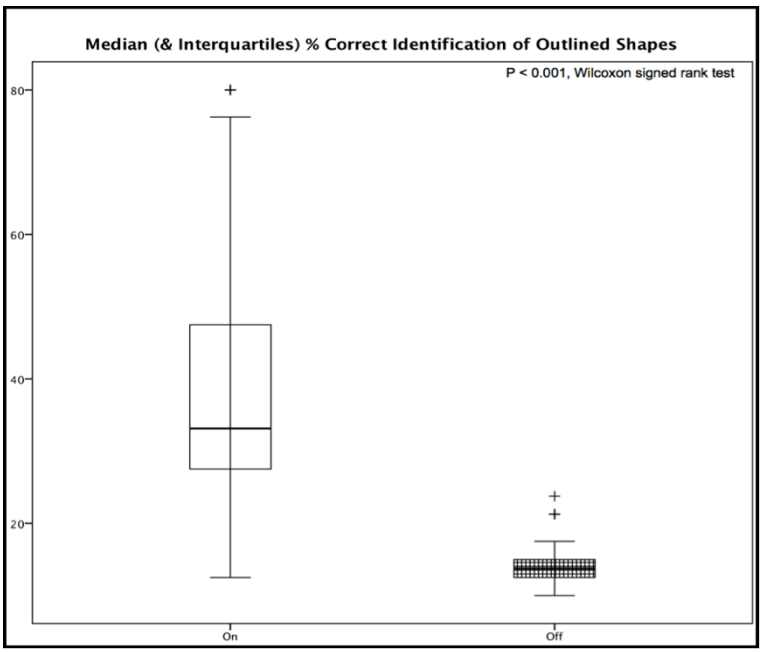

Figure 3.9: Box and Whisker plot showing the median and interquartile range of the mean % of correct identification of outlined shapes with the Argus® II retinal prosthesis device switched on and off as labelled. (+ denotes the outliers)

In addition, the greater accuracy of identifying outlined shapes (median 33.1%) versus solid shapes (median 20.0%) with the device on was statistically significant ($P < 0.001$, Wilcoxon signed rank test).

3.3.3 Objects Recognition Study

Test I: Solid Objects

The median (interquartile range) percentage of correct identification of solid objects was 31.25 (25.00 – 45.31)% with the device on, 25.00 (18.75 – 31.25)% with the device in scrambled mode, and 12.50 (6.25 – 18.75)% with the device off ($P = 0.016$, Friedman's test, see Figure 3.10). For identifying solid objects, while the subjects performed significantly better with the device on versus off ($P = 0.016$, Wilcoxon signed rank test), there is no statistical significance in the performance with the device on versus with the device in scrambled mode ($P = 0.193$, Wilcoxon signed rank test).

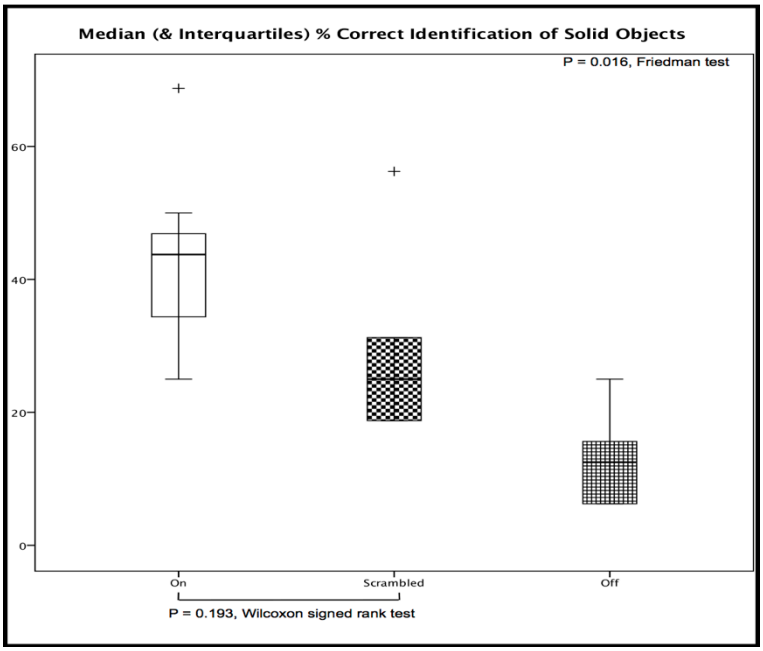

Figure 3.10: Box and Whisker plot showing the median and interquartile range of the mean % of correct identification of solid objects with the Argus® II retinal prosthesis device switched on, device on and in scrambled mode and off as labelled. (+ denotes outliers)

Test II: Outlined Objects

The median (interquartile range) percentage of correct identification of outlined objects was 43.75 (34.38 – 50.00)% with the device on, 18.75 (10.94 – 25.00)% with the device in scrambled mode, and 6.25 (0.00 – 12.5)% with the device off (*P* = 0.006, Friedman's test, Figure 3.11).

For identifying outlined objects, the difference in the performance with the device on versus with the device in scrambled mode, and with the device on versus device off are both statistically significant (*P* = 0.002, and 0.012 respectively, Wilcoxon signed rank test).

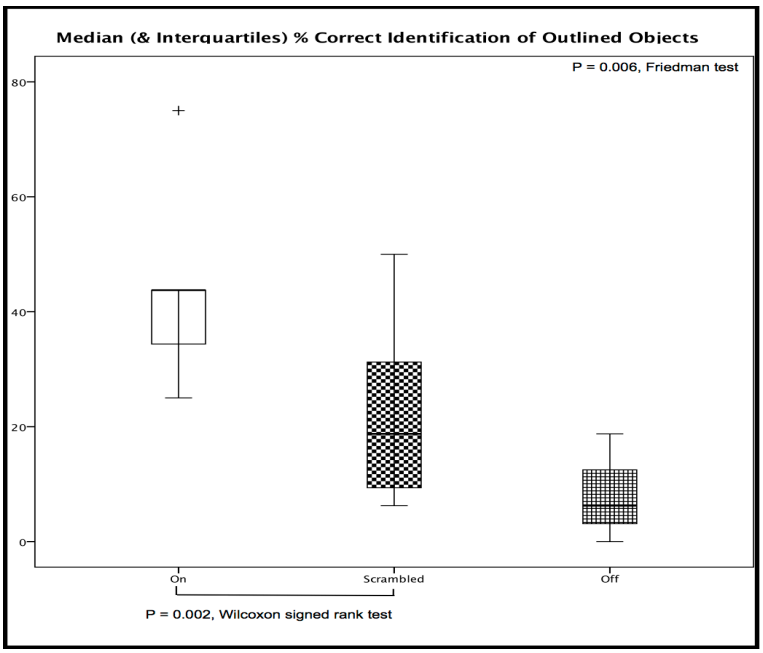

Figure 3.11: Box and Whisker plot showing the median and interquartile range of the mean % of correct identification of outlined objects with the Argus® II retinal prosthesis device switched on, switched on in scrambled mode and off as labelled. (+ denotes outliers)

The subjects were also able to identify outlined objects with greater accuracy (median 43.75%) than with solid objects (median 31.25%) with the device (*P* = 0.015, Wilcoxon signed rank test).

3.4 Discussion

The Argus® II retinal prosthesis system has allowed subjects who are blind due to RP to perform certain visual tasks not possible with their native vision. Despite published outcomes for improved motion detection (Dorn et al., 2013; Humayun et al., 2012; Zhou et al., 2013), spatial-motor co-ordination (Ahuja et al., 2011; daCruz et al., 2013), grating visual acuity (daCruz et al., 2016; Humayun et al., 2012) and large letter recognition (daCruz et al., 2013; Luo and daCruz, 2016), it remains unclear as to whether these abilities could be of assistance to the subjects' day-to-day living. In this study we endeavoured to look at aspects of form perception in both artificial (shapes recognition) and practical (objects recognition) ways with the artificial vision provided by the Argus® II retinal prosthesis, in order to begin to examine the use of artificial vision in real-life.

From our study, the Argus® II retinal prosthesis enabled the subjects to identify 2D geometric shapes on screen with greater accuracy (Figure 3.8) than with their native vision. This accuracy could be improved by presenting the shapes as schematic outlines instead of in solid forms (Figure 3.9, $P < 0.001$, Wilcoxon signed rank test). When presented with real-life objects, a similar phenomenon was observed. The subjects were able to identify a range of common objects better with the assistance of the retinal prosthesis (Figure 3.10), with greater accuracy achieved when objects with accentuated outlines were presented (Figure 3.11, $P = 0.015$, Wilcoxon signed rank test).

It is interesting to note that the change in contrast (i.e. white versus grey) did not affect the identification of solid shapes, but identification of outlined shapes was improved by greater contrast ($P = 0.018$, Wilcoxon signed rank test). Meanwhile, scrambling of the retinal prosthesis signals (i.e. scrambled mode) significantly reduced the accuracy of identifying outlined objects ($P = 0.015$, Wilcoxon signed rank test), while the effect on solid object identification was not significant. This discrepancy in performance could be due to the fact that when viewing a solid form (whether in 2D or in 3D), the homogenous surface gave rise to a large reflectance, which resulted in eliciting a visual percept of substantial size and intensity that reflect the overall surface area of the viewed shape / object, at the expense of spatial resolution. Under this circumstance, the Argus® II device effectively functioned as a reflectance detector instead of detecting form (as in scrambled mode), and factors such as the overall reflectance and size of the target played a major role in its identification, rather than its spatial form.

At present, most of the published data on the visual functions of Argus® II retinal prosthesis were based on simulated visual tasks displayed on screens, performed under controlled artificial settings (Barry et al., 2012; Caspi et al., 2009; daCruz et al., 2012; Dorn et al., 2013; Luo and daCruz, 2016). To determine if these screen-based outcomes could be predictive of performance in a more realistic setting, we looked at the correlation between the subjects' identification of white outlined shapes on screen and that of real-life outlined objects. As shown in Figure 3.12, there is a general positive trend, although the sample size is too small to determine the strength of this correlation.

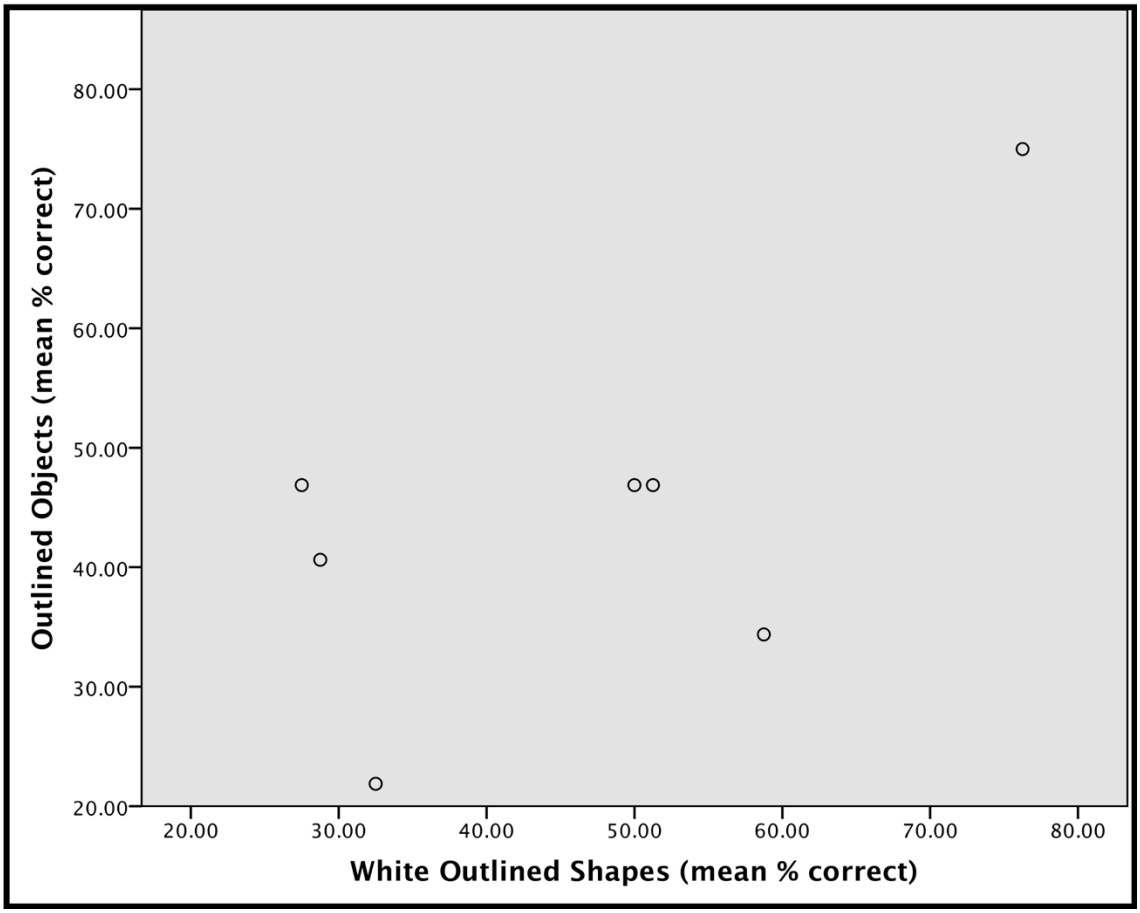

Figure 3.12: Scatter plot showing the correlation between the performance of white outlined shapes identification versus outlined objects identification in 7 subjects, using the Argus® II device. There is a general positive trend, however the sample size is too small to assess the strength of this correlation (Pearson's correlation, r = 0.65).

As seen in other Argus® II studies (Barry et al., 2012; Caspi et al., 2009; daCruz et al., 2012; Dorn et al., 2013; Luo and daCruz, 2016), there is considerable variation in the performance of the 11 subjects, as evident in the wide interquartile range of median percentages of correct identification of shapes / objects. Explanation for this have included age, duration of blindness, the type of genetic defect as well as variable retinal circuitry remodelling in degenerative diseases (Jones et al., 2012; Luo and daCruz, 2016; Marc et al., 2007; 2003). A further factor may be due to variations in the temporal profile of perception as detailed by Fornos et al. (Caspi et al., 2009; daCruz et al., 2013; Pérez Fornos et al., 2012). Despite this variability, overall there is a strong indication that highlighting the outlines of objects will enhance their identification, and will aid the patients in their home environment.

Owing to the small sample size, repeatability of the results could not be adequately addressed. Another limitation with this study is that the subjects were given up to 30 seconds in the Objects Recognition Study to identify the presented object. It therefore remains debatable whether visual identification within this time frame could be directly translated into daily use. To gain a more comprehensive and realistic view of integrating the device into daily life use, further assessment with the subjects in their own home environment would be useful.

With the current cohort of Argus® II subjects, we have observed a few high performing subjects, who could correctly identify up to 75% of the presented objects. In a similar study with letter / word reading in 21 Argus® II subjects, multiple regression analysis showed that the number of electrodes activated and the age of the subject at the time of implantation showed the greatest contribution to performance difference (daCruz et al., 2013), with the age at implantation being the only statistically significant factor. This may reflect the presence of healthier residual inner retina at the time of implantation.

With greater understanding of the factors affecting device performance (Ahuja and Behrend, 2013), and further investigations into the correlation between subject performance and genotype-phenotype, we would be able to formulate more stringent selection criteria for future patients to offer more accurate prediction of performance and maximise their benefits from the device.

In conclusion, the Argus® II retinal prosthesis system allowed subjects blind from outer retinal degeneration to better identify a range of shapes and common daily life objects in a controlled setting. The ability to do so varies greatly from subject to subject and we are currently unable to predict the outcome for individual subjects. Recognition of shapes and objects appeared to be improved by enhancing their schematic outlines, suggesting that the usefulness of the Argus® II may be enhanced in real-life situations by simple modification of the objects. Given the growing availability and use of the Argus® II devices worldwide, evidence of how the system could be used more effectively in real-life could help improve rehabilitation and training for the future.

Chapter 4

Target Localisation

4.1 Introduction

One of the main criticisms of the use of an external camera for image capture in a retinal prosthesis system is the dissociation between the visual scene captured by the camera (which is always directed straight ahead), and that of the subject's eye position. In a normally sighted person, the sense of an object's location within one's visual field is directly correlated with the position of the image on the retina and its displacement from the fovea relative to head position. The latter is communicated as part of the proprioceptive information that is co-ordinated by the vestibular and other sensory systems. As such, complex proprioceptive skills such as hand-eye co-ordination are often developed in relation to one's eye position. In an Argus® II subject, the image captured by the external camera is always projected onto a fixed area of the retina determined by the placement of the electrode array. Such misalignment between the camera position and the patient's eye could interfere with the patient's perception of spatial localisation, as has been previously suggested (Sabbah et al., 2014).

In terms of resolving the head and eye position, however, it has been shown that the Argus® II subjects in the clinical trials have developed an effective compensatory mechanism, whereby they keep their gaze (eye position) straight ahead at all times while using the device, and move their head (rather than eyes) to change the direction of gaze. With this technique, 96% of the 27 Argus® II subjects were able to localise and point to bright squares on a touch screen with higher accuracy than without the device (Ahuja et al., 2011).

Prehension, the act of reaching out and grasping a visually identified object, is an important milestone in our motor skills development during infancy (Halverson, 1943). It forms a basic way for us to explore and interact with our environment, and is a task we carry out many times a day in our daily life. Visual inputs are crucial in first directing the trajectory of the reaching hand, then allow for adaptive changes to be made to shape the reaching hand in accordance with the perceived characteristics of the target object (e.g. shape, texture, weight), to achieve a firm and stable grasp of the object (Halverson, 1943; Hohlstein, 1982).

In this study, we set out to explore if the aiming and pointing performance with the Argus® II device, as exemplified by the two-dimensional target localisation under laboratory setting (Ahuja et al., 2011), could be translated into real-life practical applications of object localisation and prehension in the three-dimensional space. Secondly, we wanted to examine whether enhanced visualisation of their fingers would improve the subjects' performance in prehension. We hypothesised that effective visualisation of one's reaching fingers in three-dimensional space would improve the proprioception of the subject, which would in turn aid in the accuracy of object prehension. The outcome of this study has been published (Luo et al., 2015).

4.2 Materials & Methods

This is a prospective, internally controlled, interventional case series from a single centre. The current study was approved by the local ethics committee as part of the Argus II phase I/II feasibility study and respected the tenets of the Declaration of Helsinki. Informed consent was obtained from all the subjects.

4.2.1 Patient Eligibility

Five (out of a total of 7) subjects who received the Argus® II retinal prosthesis system implant as part of the Second Sight phase I / II feasibility study at Moorfields Eye Hospital between 2008 – 2010 were recruited (clinicaltrials.gov identifier: NCT00407602). All subjects were blind (logMAR 2.9 bare light perception or worse in both eyes) from RP or choroideremia and their demographics are as shown in Table 4.1. Two subjects were excluded from this study as one of them was medically unwell and under treatment from an unrelated neoplastic condition at the time of the study, while the other one declined to participate in the study. All the subjects had received visual rehabilitation training provided by the Second Sight Inc. with the general use of the device prior to testing.

Subject ID	Sex	Age at Diagnosis (Years)	Age at Surgery (Years)	Number of Active Electrodes
51-003	M	19	72	28
51-005	M	7	55	60
51-006	M	46	66	56
51-007	M	28	63	53
51-009	F	11	45	60

Table 4.1: Demographics of the 5 Argus® II subjects who participated in the Object Localisation Study.

4.2.2 The ProReflex® Motion Capture System

The ProReflex® Motion Capture system (Qualisys, Sweden) (*qualisys.com*, n.d.) consists of specialised infrared (IR) motion detection cameras and the Qualisys Track Manager (QTM) software for motion data analysis. Each camera consists of a group of flashing IR light emitting diodes (LEDs) situated external to the camera lens, and an image sensor. During motion capture, IR retro-reflective markers are attached to the areas of interest. The IR light emitted by the camera LEDs is reflected back from the reflective markers and detected by the camera lens and image sensor. The QTM software calculates the central point and size of each marker signal in real-time, thus giving marker position and hence the movement trajectory of the marker over time.

4.2.3 The Flashing Beacon Finger Marker

All of the Argus® II subjects were able to reliably perceive flashes of light with the device. To enhance the visualisation of the subjects' own fingers in space, we devised a bright beacon consisting of 2 x 5-Watt LED lights of ~5mm in diameter, with adjustable brightness intensity and flashing frequency. The beacon was attached over the nail of the index finger of each subject's dominant hand used in the prehension task (see below), and both the intensity and frequency of the beacon were adjusted individually until the subject reported reliable and persistent visualisation of the flashing beacon with the Argus® II device. The pulsating nature of this beacon allowed the subjects to distinguish between this signal and signal from other non-pulsating objects (i.e. the LEGO® blocks used for the prehension task). None of the subjects reported visualisation of the flashing beacon without the use of the device.

4.2.4 Test Conditions & Setting

A 60 cm x 70 cm tabletop covered in black felt cloth in a uniformly illuminated room served as our worktop. A doorknob (also covered in black felt) was placed at middle of one border of the worktop, to act as a pre-determined starting point for the prehension task (described below). The target object for prehension was a white cuboid made of 2 x 2 LEGO® blocks (3.1cm x 3.1cm) x 6 layers in height (5.7 cm), giving a total volume of 54.78cm^3. White LEGO® blocks were chosen to maximise the contrast against the black worktop.

Three of the specialised ProReflex® infrared cameras were triangulated around the table at a height of approximately 1.5 meters above the table, to enable a 3 dimensional (3D) recording of all movements within the worktop area.

Three lightweight IR retro-reflective markers of approximately 7mm in diameter were placed on the subject's dominant hand, as determined using the Edinburgh handedness questionnaire,(Oldfield, 1971) for recording its movement in 3D. One marker was attached to the wrist using a Velcro strap and two were placed on the subject's opposing distal borders of the thumbnail and index fingernail. The target object was also marked with an IR retro-reflective marker. Movements of the IR retro-reflective markers were tracked by the ProReflex® Motion Capture system as described above and recorded directly by a personal computer based system (see Figure 4.1 and supplementary video).

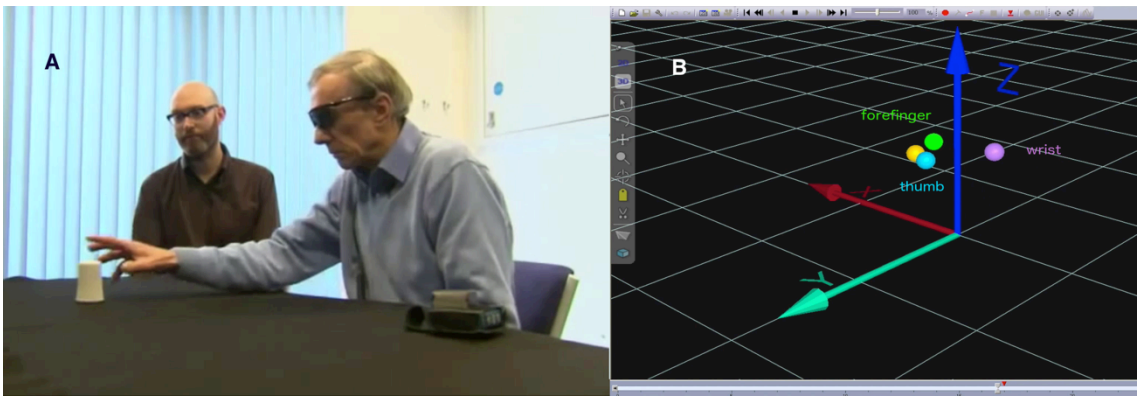

Figure 4.1: Prehension of objects in 3D space. (A) An Argus® II subject carrying out prehension tasks. (B) The time taken and the trajectory of the prehensile hand during prehension tasks were captured using ProReflex® Motion Capture system, Qualisys, Sweden. IR-reflective markers were attached to the wrist (lilac sphere), thumb (blue sphere) and forefinger (green sphere) of the subject, and to the target object (yellow sphere). During prehension, movements of these markers in 3D with time were captured by 3 IR cameras, which surveyed the scene. The accuracy of the prehension tasks could then be analysed.

4.2.5 Prehension Task

The subjects were seated during the task such that the worktop was at their waist level, and the doorknob was situated at their sagittal midline, along the table border closest to them.

At the beginning of the task, the subject's dominant hand (with IR retro-reflective markers and flashing beacon attached as described above) was positioned at the pre-determined start point (as designated by the doorknob). During each task, the subject was instructed to locate the target object (i.e. the white LEGO® cuboid) on the worktop, reach out and grasp the object with their dominant hand, place the object to one side before returning their hand to the start point. The subject had up to 30 seconds to complete each task, after which time, the motion recording would stop automatically and any further movement would not be captured and analysed. The placement of the target object was varied in an random order (as generated by a computerised randomiser) ("Research Randomizer: Free Random Sampling and Random Assignment," n.d.) in one of the following 4 locations with one repeat, resulting in a total of 8 trials per set of prehension task. The 4 locations were (see Figure 4.2):

- Location 1: near (~20cm away) and to the right of the sagittal midline;
- Location 2: near (~20cm away) and to the left of the sagittal midline;

- Location 3: far (~40cm away) and to the right of the sagittal midline;
- Location 4: far (~40 cm away) and to the left of the sagittal midline of the subject.

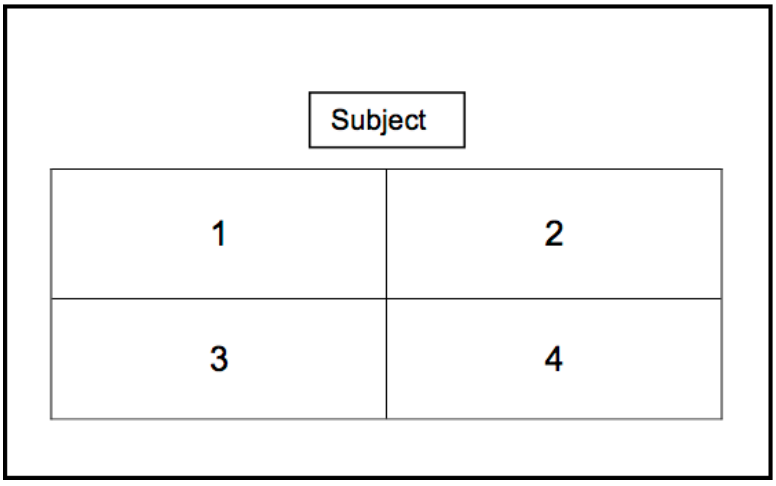

Figure 4.2: Schematic drawing of the prehension task setup showing the subject's position in relation to the worktop table. The target object (i.e. the white LEGO® cuboid) would be placed in one of the 4 locations in random order during the task. (Image from (Luo et al., 2015))

Each subject was asked to carry out the task under the following conditions:

- Argus® II device switched on, finger marker beacon switched on; 2 sets of tasks were performed (16 trials in total) per subject.
- Argus® II device switched on, finger marker beacon switched off; 2 sets of tasks were performed (16 trials in total) per subject.
- Argus® II device switched off, finger marker beacon switched on; 2 sets of tasks were performed (16 trials in total) per subject.
- Argus® II device switched off, finger marker beacon switched off; 1 set of tasks was performed (8 trials in total) per subject.

The subject was masked to the settings of the Argus® II retinal device and finger marker beacon, and the order in which the above conditions were carried out were also randomised.

4.2.6 Motion Data Analysis

Each IR retro-reflective marker (located on the target object as well as the subject's dominant hand) generated x, y, z co-ordinate outputs for each 30-

second recording. These data were analysed using a purpose written script (Matlab 8.0.0.783 R2012b, The Mathworks Inc, Massachusetts, U.S.A).

To analyse the accuracy of prehension, the First Hand Stop (FHS) was marked manually for each of the 30-second recordings by two independent observers. The FHS was defined as the hand position at which the trajectory of the subject's moving hand first showed a sudden change in velocity (i.e. a reduction in speed and / or a change in direction of movement). This would represent where the subject perceived the location of the target object to be, and reached out his / her hand accordingly.

4.2.7 Statistical Analysis

All of the statistical analysis and graphical representations were performed using SPSS program (IBM® SPSS® Statistics version 22). Non-parametric tests were chosen for the analysis, as normality of the distribution of the results could not be assumed given the small sample size.

4.3 Results

4.3.1 Success of Prehension

The percentage of successful prehension ± standard deviation was: 71.3 ± 27.1% with the Argus® II device switched on and the finger marker switched on; 77.5 ± 24.5% with the device on and the finger marker off; 0.0 ± 0.0% with the device off and finger marker on, and 0.00 ± 0.00% with the device off and finger marker off. The difference in performance between finger marker on and finger marker off is not significant, whether the prosthesis was switched on (P = 0.546) or switched off (P = 1; Wilcoxon signed rank test).

Since the finger marker beacon setting did not appear to affect the performance of prehension task, the data for all the performance with the Argus® II device switched on and switched off were amalgamated respectively for further analysis.

Collectively, the percentage of successful prehension ± standard deviation for all performances with the Argus® II device switched on was 74.4 ± 23.4% and 0.0 ± 0.0% with the device switched off (P = 0.04, Wilcoxon Signed Rank test).

The performance of successful prehension for each subject was shown in Table 4.2.

Subject	Prosthesis Setting					
	On			Off		
	Prehension initiated (%) (n = 32)	Successful prehension after initiation (%)	Mean ± S.D. FHS - Target Distance (mm)	Prehension initiated (%) (n = 16)	Successful prehension after initiation (%)	Mean ± S.D. FHS - Target Distance (mm)
51-003	21 (66%)	14/21 (66.7%)	140.0 ± 140.7	0 (0%)	NA	NA
51-005	29 (91%)	27/29 (93.1%)	67.9 ± 25.3	0 (0%)	NA	NA
51-006	19 (59%)	18/19 (94.7%)	57.3 ± 21.8	0 (0%)	NA	NA
51-007	32 (100%)	32/32 (100%)	52.4 ± 27.5	0 (0%)	NA	NA
51-009	31 (97%)	28/31 (90.3%)	145.2 ± 66.8	0 (0%)	NA	NA

Table 4.2: Percentage of prehension initiation and percentage of successful prehension with the retinal prosthesis switched on versus switched off for each subject. Where prehension was initiated, the mean ± standard deviation distance (mm) of First Hand Stop (FHS) to the target object for each subject's performance was shown. N = total number of trials. (Image from (Luo et al., 2015))

4.3.2 Accuracy of Prehension

The distribution of FHS relative to the target object for each prehension task is presented graphically for each subject in Figure 4.3. The location of the target object was assigned the co-ordinates of (0, 0), while the designated starting point was assigned the arbitrary co-ordinates of (2000, 2000). The relative displacement of the FHS in the x and y axis from the target object was calculated and plotted accordingly.

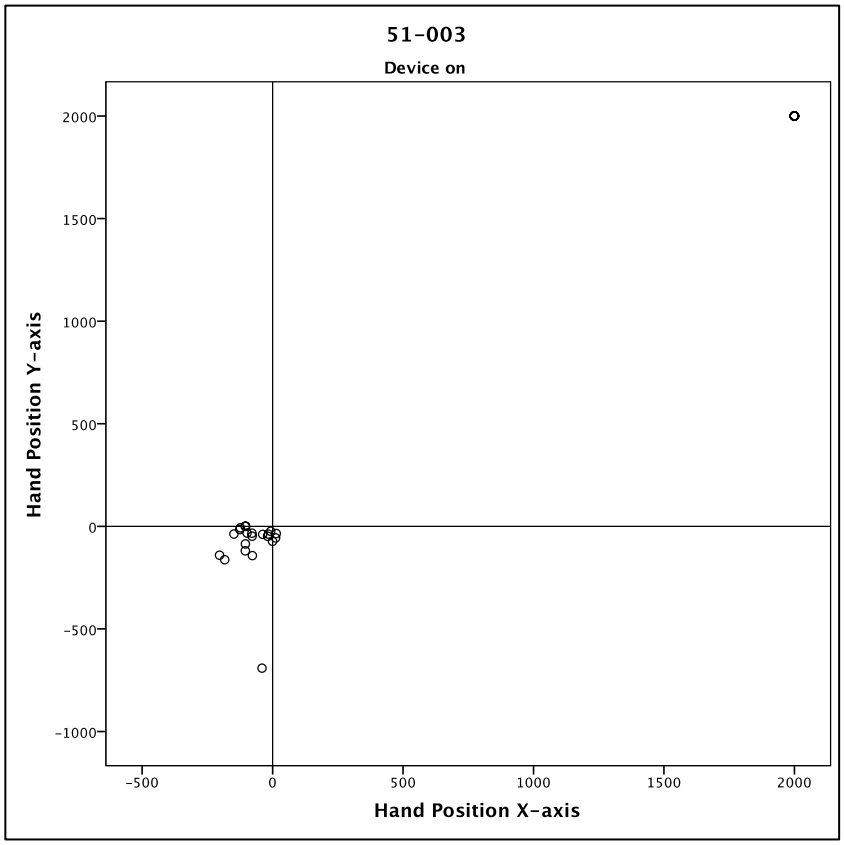

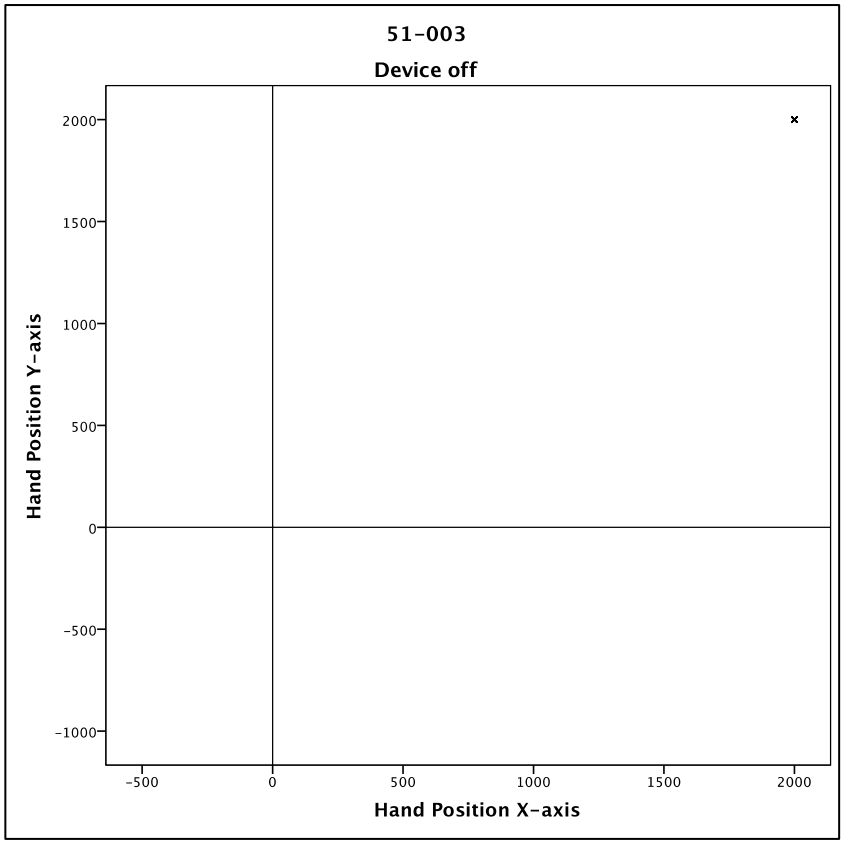

Scatter plots showing the relative (x, y) co-ordinates of the First Hand Stop (FHS) to the target object for the prehension tasks for 51-003. An open circle '**O**' denotes the FHS with prosthesis switched on; a cross '**X**' denotes the FHS with the prosthesis switched off.

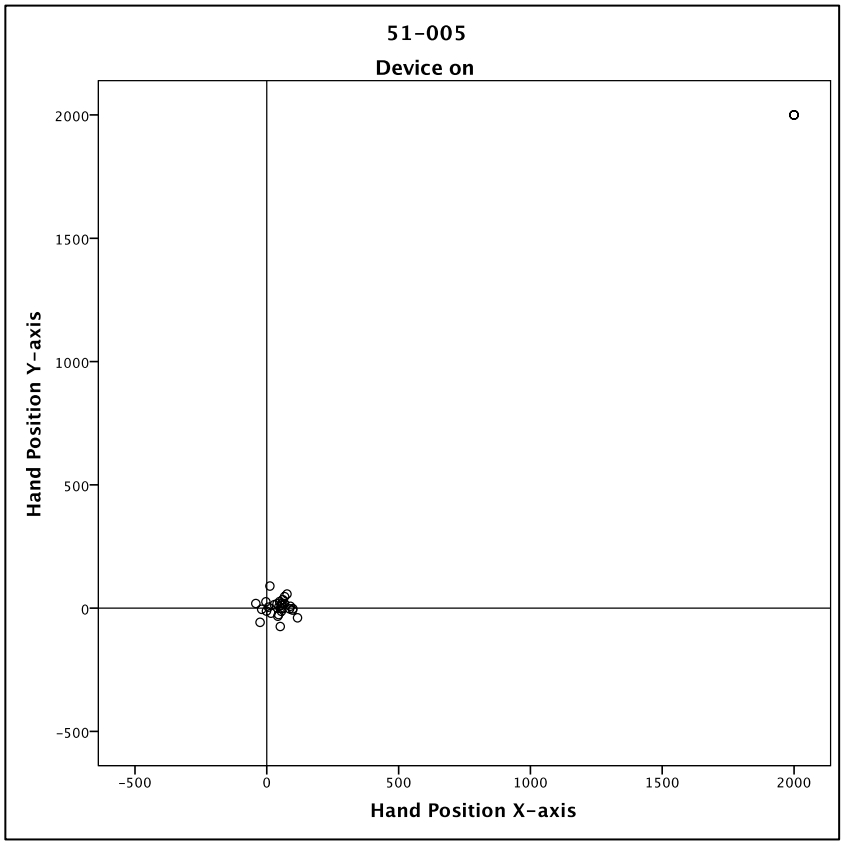

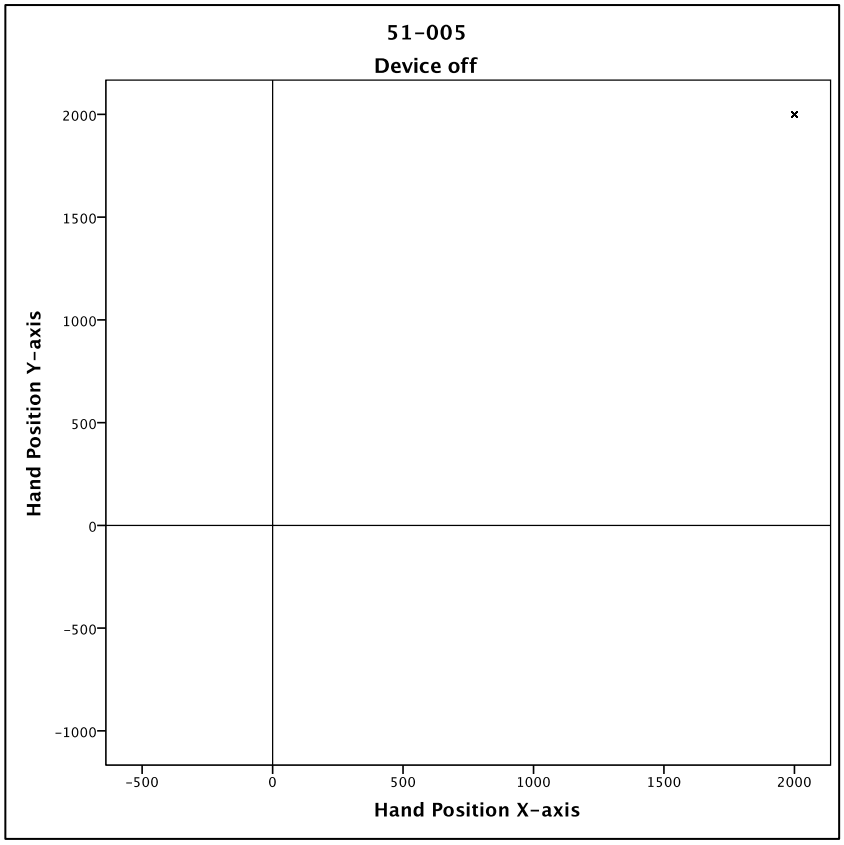

Scatter plots showing the relative (x, y) co-ordinates of the First Hand Stop (FHS) to the target object for the prehension tasks for 51-005. An open circle '**O**' denotes the FHS with prosthesis switched on; a cross '**X**' denotes the FHS with the prosthesis switched off.

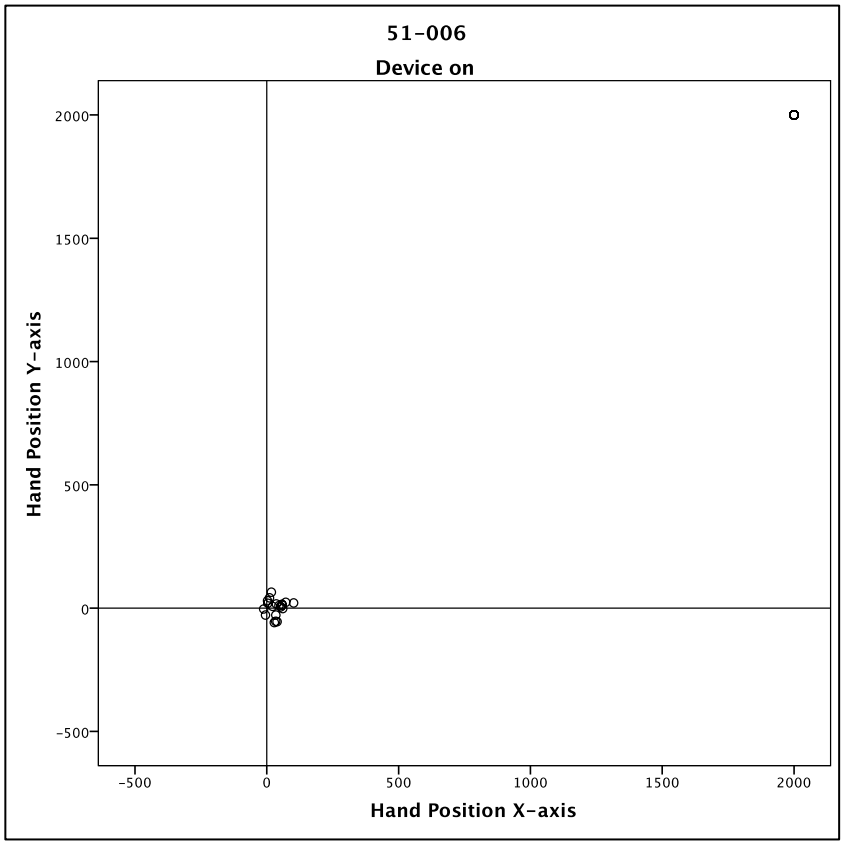

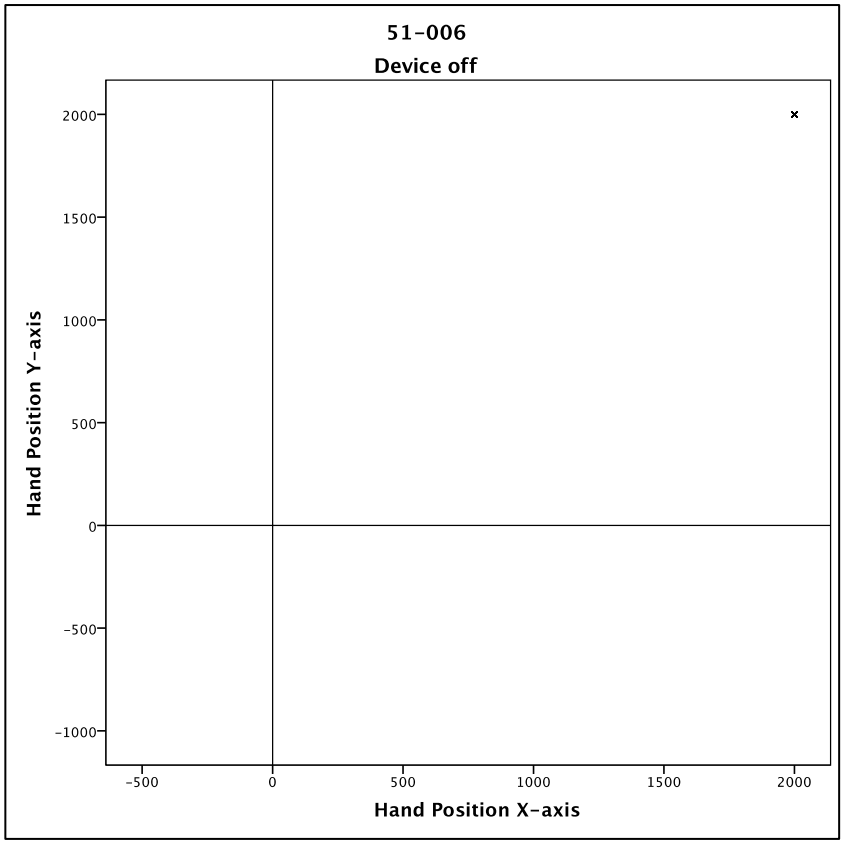

Scatter plots showing the relative (x, y) co-ordinates of the First Hand Stop (FHS) to the target object for the prehension tasks for 51-006. An open circle '**O**' denotes the FHS with prosthesis switched on; a cross '**X**' denotes the FHS with the prosthesis switched off.

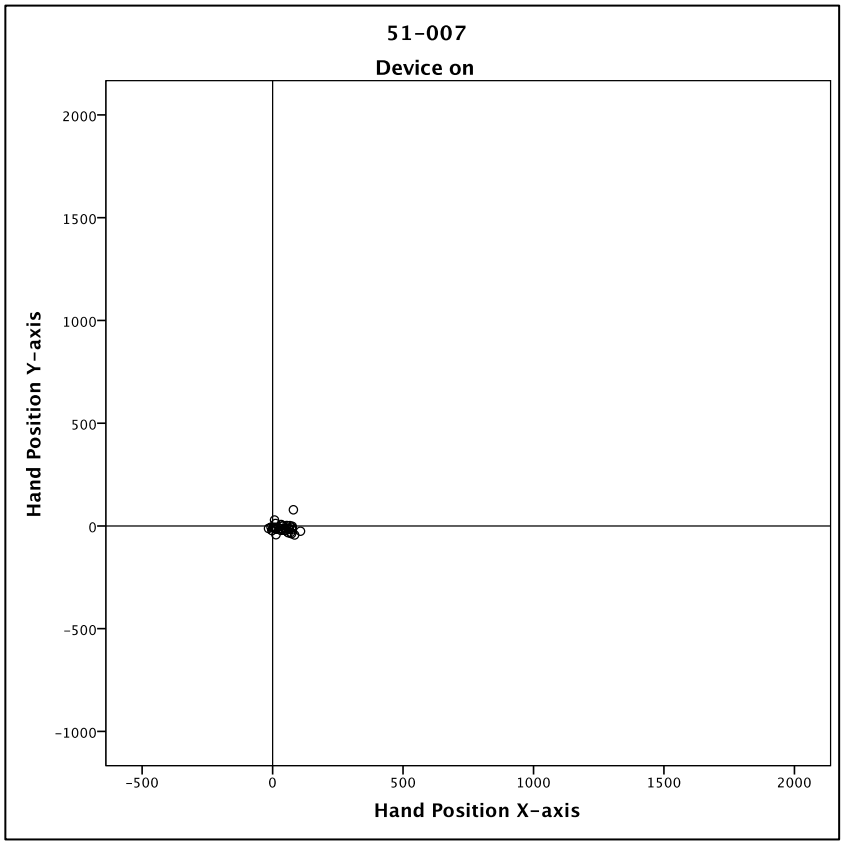

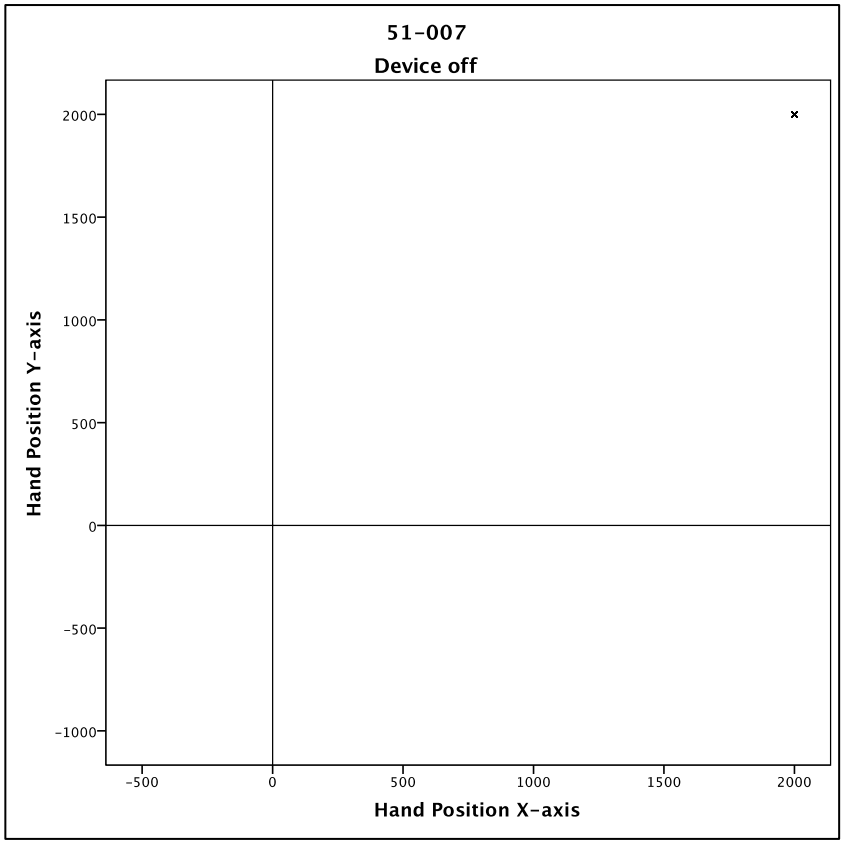

Scatter plots showing the relative (x, y) co-ordinates of the First Hand Stop (FHS) to the target object for the prehension tasks for 51-007. An open circle '**O**' denotes the FHS with prosthesis switched on; a cross '**X**' denotes the FHS with the prosthesis switched off.

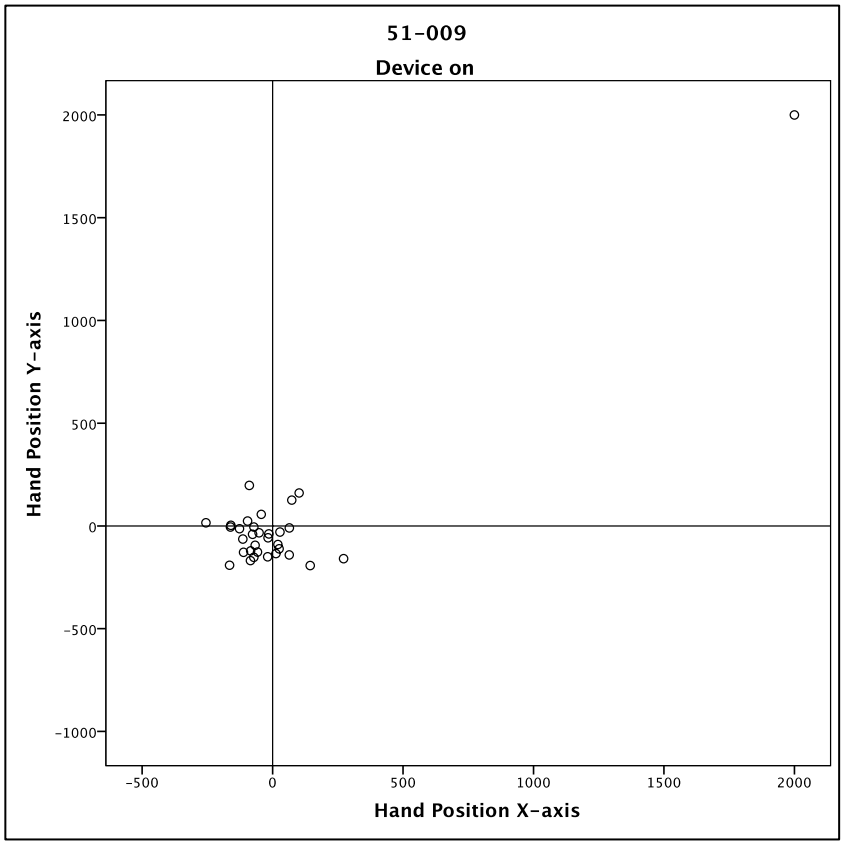

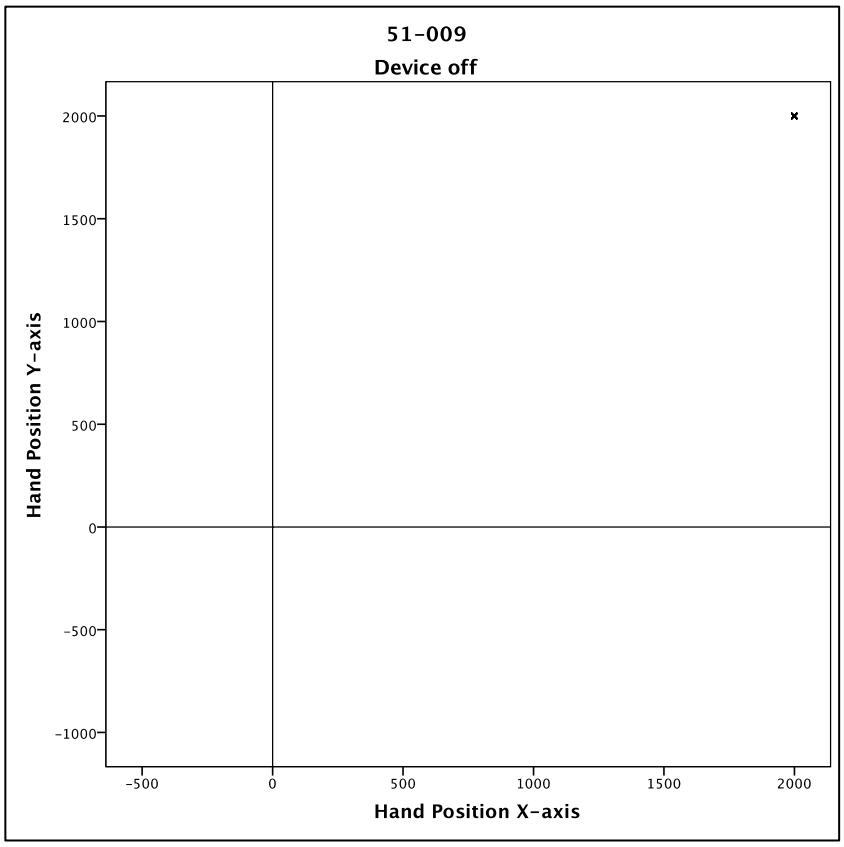

Scatter plots showing the relative (x, y) co-ordinates of the First Hand Stop (FHS) to the target object for the prehension tasks for 51-009. An open circle '**O**' denotes the FHS with prosthesis switched on; a cross '**X**' denotes the FHS with the prosthesis switched off.

Figure 4.3: Scatter plots showing the relative (x, y) co-ordinates of the First Hand Stop (FHS) to the target object for the prehension tasks for each subject. An open circle '**O**' denotes the FHS when the prehension was performed with the prosthesis switched on; a cross '**X**' denotes the FHS when the task was performed with the prosthesis switched off. The FHS was defined as the hand position at which the trajectory of the subject's moving hand first showed a sudden change in velocity (i.e. a sudden reduction in speed and / or a change in direction of movement). The FHS represented where the subject perceived the target object to be and placed his / her hand accordingly. The closer the FHS was to the target object location, the greater the accuracy of the spatial localisation. The location of the target object was assigned the co-ordinates of (0, 0), while the designated starting point (i.e. at the doorknob) was assigned the arbitrary co-ordinates of (2000, 2000). The relative displacement of the FHS in the x and y axis from the target object was calculated and plotted accordingly.

The closer the FHS was to the target object location, the greater the accuracy of the spatial and corresponding proprioceptive localization. When the subject failed to visually locate the target object during the allowed time, no attempt of prehension was initiated and the subject's hand remained at the designated start point (i.e. at the artificial doorknob).

When the Argus® II retinal prosthesis was switched off, none of the subjects were able to visually locate the target object. Their dominant hand therefore remained at the designated start point and the corresponding FHS – target object distance was therefore conceptually infinitely large. This is shown in Figure 4.3, where all the cross-points (denoting hand positions with prosthesis switched off) were seen at the (2000, 2000) co-ordinates, the assigned start point, for all the subjects.

With the prosthesis switched on, prehension was attempted (indicating visual localization of the target object by the subjects) on 82.5% (range 59 – 100%) of the trials. Once prehension was initiated, the subjects were able to successfully reach and grasp the object on 89.0% (range 66.7 – 100%) of the trials.

The mean ± standard deviation distance (mm) of FHS to the target object for all the attempted prehension was 92.2 ± 78.4 mm. The performance for each subject was as tabulated in Table 4.2. Graphically, most of the open-circle-points (denoting hand positions with the prosthesis switched on) were seen clustered around the target object location (0, 0).

4.4 Discussion

The precision of prehension evolves in a systematic manner, from primitive squeeze, hand and palm grasp, to the superior and precise digital grasp (Halverson, 1943). While our adult subjects would have acquired the fine motor skills of prehension in their childhood, decades of blindness have deprived them of the visual inputs required to perform this important functional task.

Visualisation of the target object was the first step in target object prehension. Our study has shown that the Argus® II retinal prosthesis enabled the subjects to visually locate the object, and subsequently achieve prehension otherwise not possible without the device (74.4 ± 23.4% versus 0.0%, $P = 0.043$, Wilcoxon signed rank test). Similar to the findings of Ahuja et al.(Ahuja et al., 2009), it appears that the Argus® II subjects were able to use the visual information they have received from the prosthesis with proprioceptive information to locate an object in 3D space with some degree of accuracy.

The use of a flashing beacon finger marker to improve direct visualisation of the subject's own finger did not contribute to any improvement in the performance of prehension. The successful completion of prehension without constant finger visualisation demonstrated that proprioceptive cues alone were adequate to achieve reaching and object contact (Clifton et al., 1993), and that the subjects retained good proprioception despite decades of blindness.

It is interesting to note that most of the patients performed well in this task, and the two high-performers in the form discrimination / recognition tasks (see **Chapter 3**) did not show superior performance. There was also no statistical difference in the performance of object prehension with the Argus® II system in standard mode versus scrambled mode (Kotecha et al., 2014), as would be expected from the nature of the task. These results indicate that it remains possible for Argus® II subjects to co-ordinate head / neck proprioception and image location on the retina relative to head position, to develop hand-camera co-ordination to complete accurate target localisation and prehension tasks.

Chapter 5

Phosphene Characterisation

5.1 Introduction

Despite its growing clinical use since entering the commercial market in Europe (2011) and worldwide (2013), data describing the features of artificial vision perceived by the users of the Argus® II retinal prosthesis remain scarce in the published literature (Humayun et al., 1996; 1999; 2003; Rizzo et al., 2003b). The idea of developing useful vision by epiretinal electrical stimulation hinges on the premise that stimulation with a single electrode gives rise to a discrete focal percept in a retinotopic manner. Simultaneous stimulation with multiple electrodes therefore theoretically leads to perception of a pattern in concordance with the pattern defined by the stimulating electrodes (Humayun et al., 1999).

However in earlier studies, as discussed in detail in **Chapter 2** (Section 2.7.1 *Human Studies)*, Rizzo et al. have called into question the consistency and reproducibility of phosphenes elicited by patterned epiretinal microelectrode stimulation (Rizzo et al., 2003b). In a study involving 5 end-stage RP patients and one patient with normal retina, only 48% of the single-electrode stimulations and 32% of the multi-electrode stimulations elicited visual percepts that matched the electrical stimulation patterns. Of the single-electrode stimulations, 3 subjects reported “a line” on some occasions, while “clusters of 2 or 3 images” were seen on other occasions. In particular, the authors reported that only 66% (out of 99 stimulations) of the elicited visual percepts were reproducible in 3 RP patients on 2 separate trials despite using the same stimulating parameters to activate the same electrodes. Such inconsistencies in the form and reproducibility of phosphenes would seriously undermine the formation of pixelated vision. Furthermore, as shown in **Chapter 3**, there is a wide variation in the performance level of form discrimination / recognition tasks by our cohort of chronically implanted Argus® II subjects. The reason for such performance variation is still poorly understood.

In this study, we set out to investigate the consistency and reproducibility of phosphenes elicited in the same cohort of subjects chronically implanted with the Argus® II system. All of the subjects described have had the device implanted and functioning for over 5 years at the time of the study. The outcome of this study has been published (Luo et al., 2016).

5.2 Method

5.2.1 Subject Inclusion / Exclusion Criteria

This is a single-centre prospective study. All but one of the 7 subjects from Moorfields Eye Hospital NHS Foundation Trust implanted with the Argus® II retinal prosthesis system as part of the phase I/II clinical trial (clinicaltrials.gov Identifier: NCT00407602) took part in the study (n = 6). The one subject was excluded as his device ceased to function after developing retinal detachment and a thick epiretinal membrane as a result of a fall. The participating subjects' demographic features and operation dates are shown in Table 5.1. The study was approved by the local ethics committee, and adhered to the tenets of the Declaration of Helsinki.

Subject ID	Diagnosis	Year of Operation	Age at Time of Operation (yrs)
51-001	Retinitis Pigmentosa	2008	70
51-003	Retinitis Pigmentosa	2008	72
51-005	Retinitis Pigmentosa	2009	55
51-006	Choroideremia	2009	66
51-007	Retinitis Pigmentosa	2009	63
51-009	Retinitis Pigmentosa	2009	45

Table 5.1: Demographics and operation dates of the Argus® II subjects who participated in the Phosphene characterisation Study. (Table from (Luo et al., 2016))

5.2.2 Selection of Stimulating Electrodes & Parameters

For each subject, a cluster of 4 electrodes (hereinafter referred to as a quad) closest to the fovea, which were functioning with thresholds within the safety charge density limit, was selected for stimulation, and the elicited phosphenes characterised for the purpose of this study (see Figure 5.1).

An estimated location of the fovea was made on the fundus photograph (taken at the outset of the study) and was used for each subject as a reference point, measuring 15.5 ± 1.1° from the centre of the optic disc horizontally, and -1.5 ± 0.9° vertically (Rohrschneider, 2004). The foveal position was estimated as there were no remaining classical anatomical or structural features of the normal fovea on colour photographs, fluorescein angiograms or OCT scans due to severe end-stage RP.

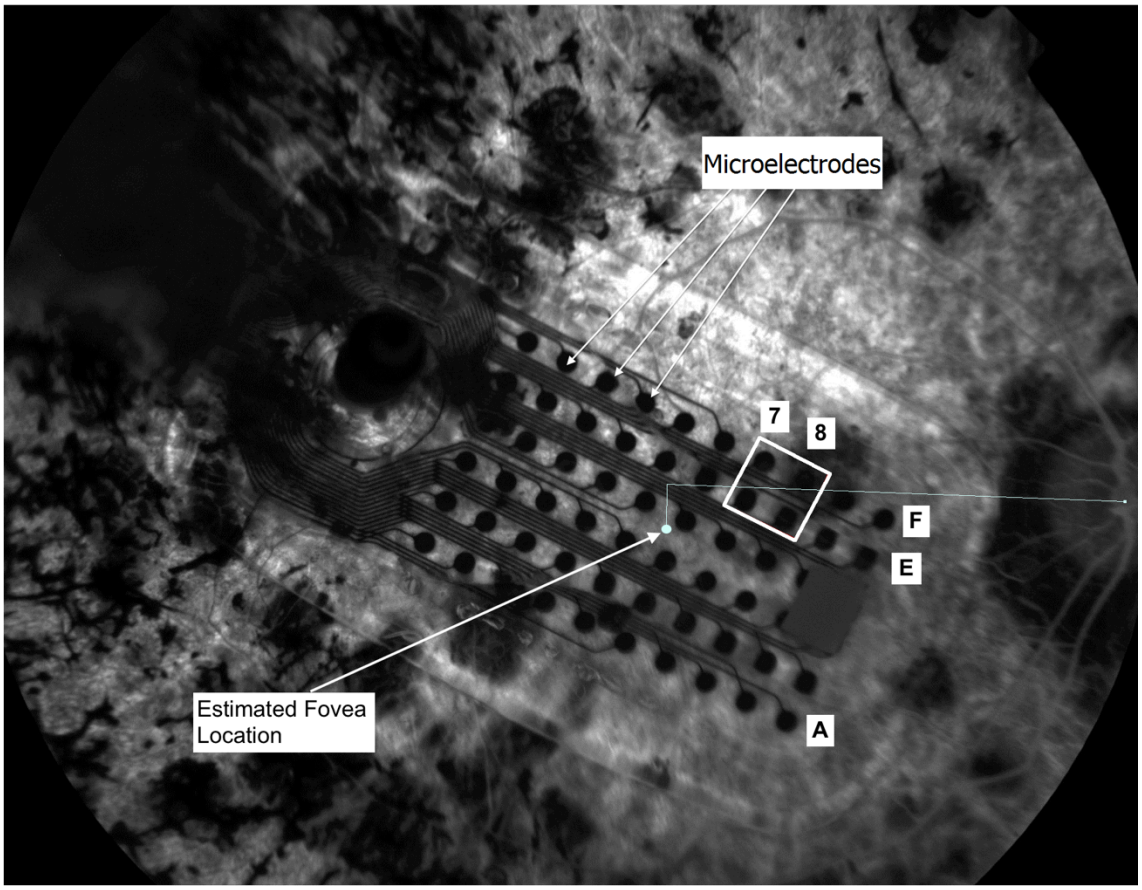

Figure 5.1: A redfree fundus photograph of one subject (ID: 51-007) with the Argus® II retinal implant in situ. The designated four electrodes (i.e. quad) for stimulation are indicated as those enclosed in the white square. The foveal location is estimated to be 15.5° temporal and 1.5° inferior to the centre of the optic disc. The quad-fovea relation is calculated from the estimated fovea location, to the centre of the stimulated quad. (Image from (Luo et al., 2016))

Once the designated quad was chosen, the stimulating current for each subject was arbitrarily set to be 100μA above the threshold (measured within the last 6 months) initially, and then adjusted according to the strength of response and comfort level reported by the subject. We aimed to elicit a clear, definite visual percept without causing any discomfort or physical “tingling” sensation for each subject. Default settings for the Argus® II retinal prosthesis system Clinical Fitting System (CFS) employed for device fitting and standard testing were likewise used for this study, which generate cathodic-first, charge-balanced biphasic square waves to avoid tissue damage from charge build up. These default waveform parameters were: phase width of 0.46ms, inter-phase duration of 0s, and total stimulation duration of 250ms at the frequency of 20Hz (“Argus® II Retinal Prosthesis System,” n.d.). Swept source OCT (DRI OCT-1 Atlantis, TOPCON®) imaging through the chosen quad for each subject was performed, to assess the contact between the stimulating electrodes and the retinal surface

(see Figure 5.2).

The position of each electrode in the 6 x 10 array is designated alphabetically by row (A to E), and numerically by column (1 to 10) as shown in Figure 5.1. The selected quad, quad-retina relation, quad threshold, and stimulating current for each subject were as shown in Table 5.2.

Subject ID	Quad	Quad-Retina Relation (on OCT)	Threshold (μA)	Stimulating Current (μA)	Phosphene Features	Phosphene Duration, t (s)
51-001	C07C08 D07D08	In contact *no significant ERM	137	277	White filled-in circle	0.5 < t < 1
51-003	A07A08 B07B08	In contact *no significant ERM	250	350	Electric blue filled-in circle	t < 0.5
51-005	E05E06 F05F06	In contact *no significant ERM	137	237	Bluish-grey vertical line, with fizzy vertical edges	t < 0.5
51-006	A07A08 B07B08	Quad-retina separation = 377 μm; no ERM visible	371	552	Yellow “7” shape	0.5 < t < 1
51-007	E07E08 F07F08	In contact *no significant ERM	24	124	Orange filled-in ring which ripples out	0.5 < t < 1
51-009	E07E08 F07F08	In contact *no significant ERM	97	124	Orange horizontal lines x 2, with fizzy brightness in between the lines	0.5 < t < 1

Table 5.2: Phosphene features described by each chronically implanted Argus® II retinal prosthesis subject, from stimulating the designated quad with the above parameters. (Table from (Luo et al., 2016))

* In images where the electrode array is in direct contact with the retinal surface, owing to the artefact caused by the acoustic shadow of the array, it is difficult to ascertain the presence, if any, of mild epiretinal membrane.

51-001

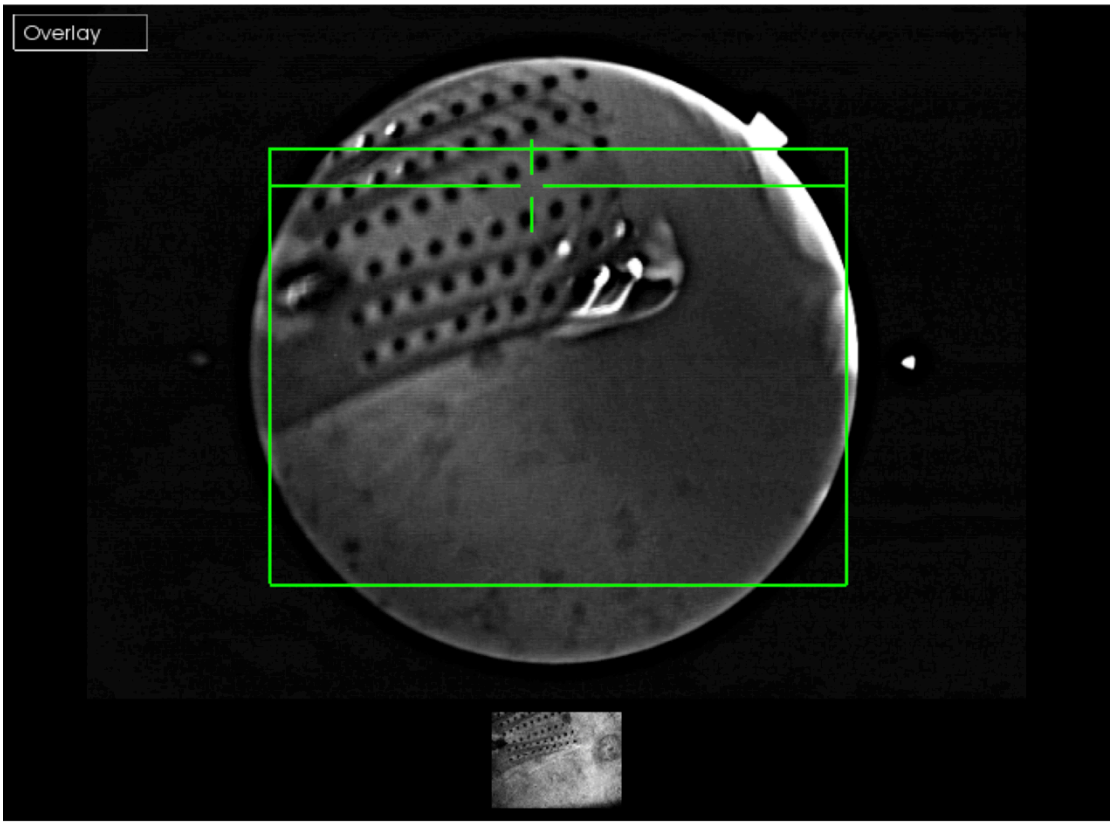

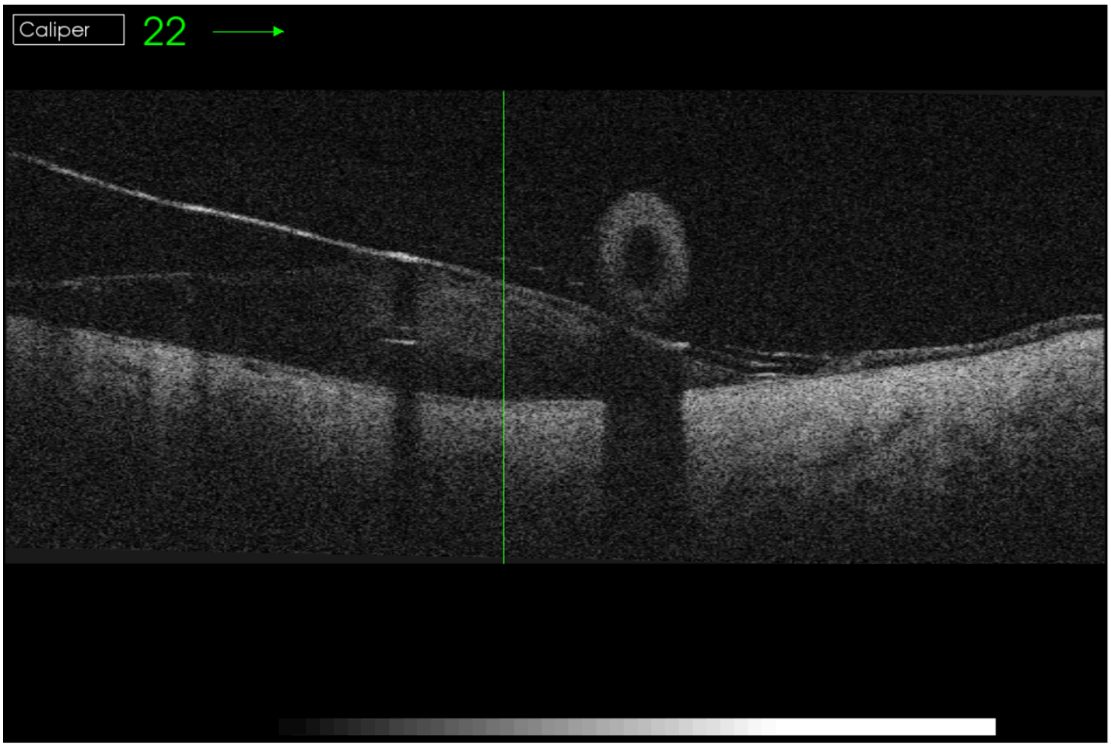

Swept source OCT (DRI OCT-1 Atlantis, TOPCON®) imaging through the chosen quad for 51-001.

51-003

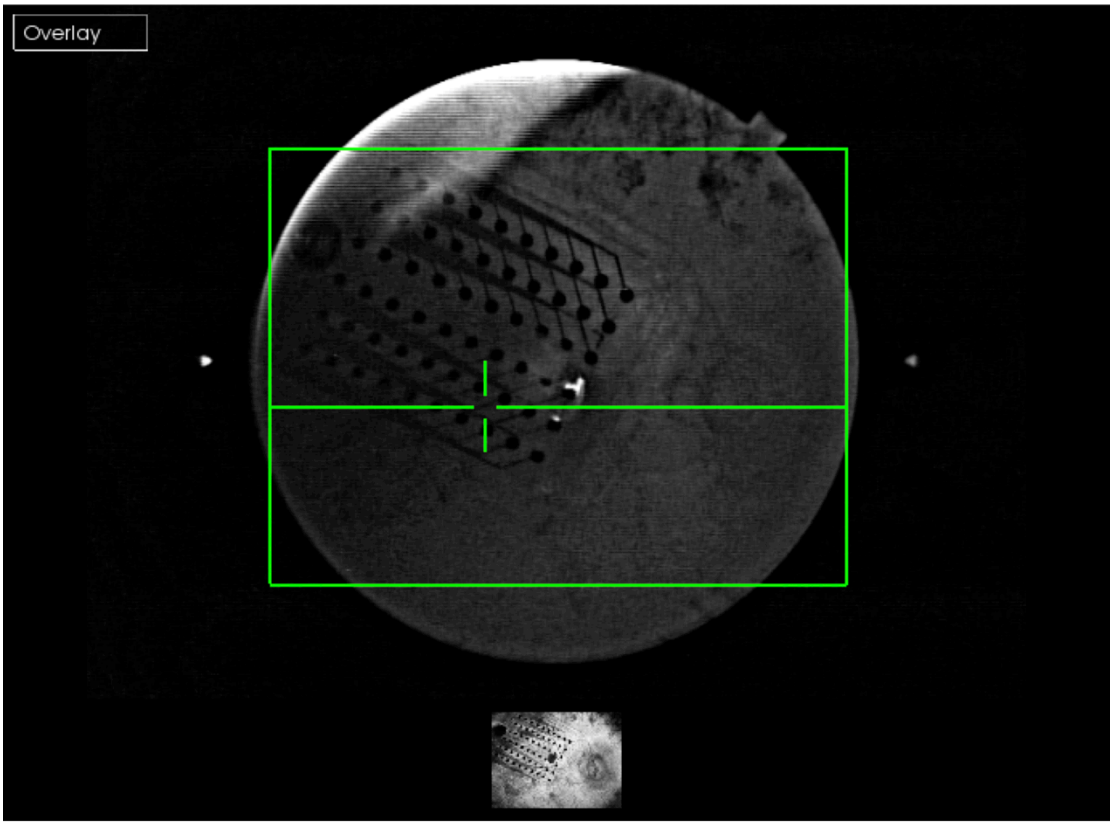

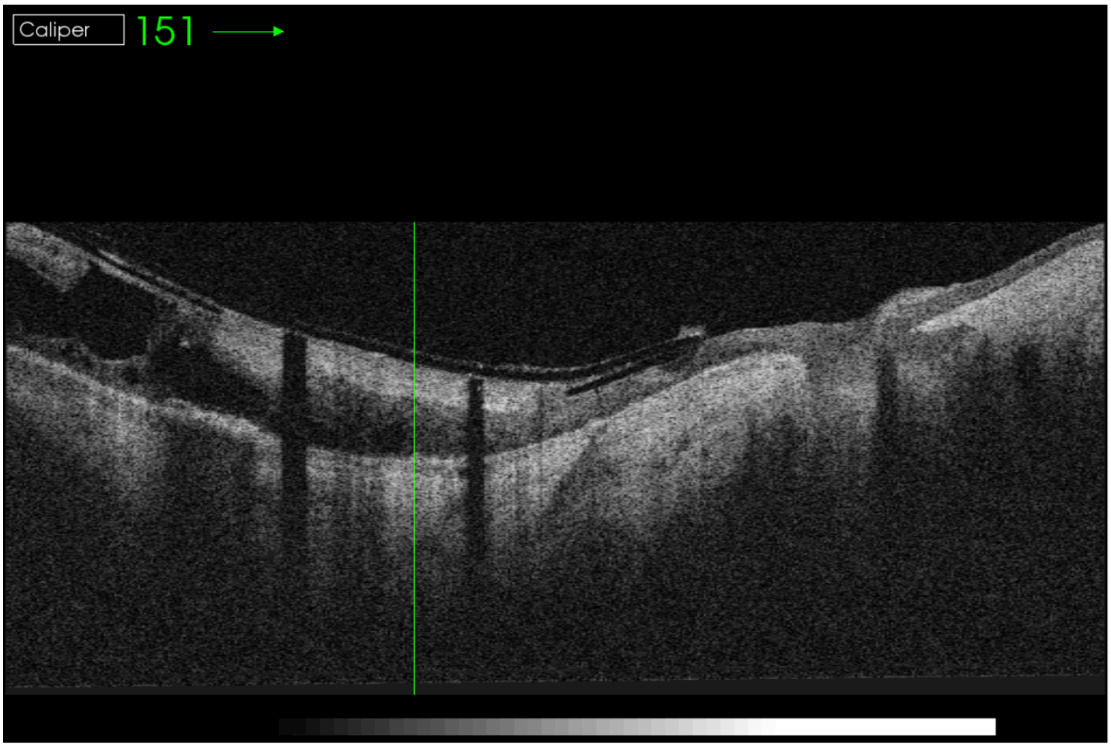

Swept source OCT (DRI OCT-1 Atlantis, TOPCON®) imaging through the chosen quad for 51-003.

51-005

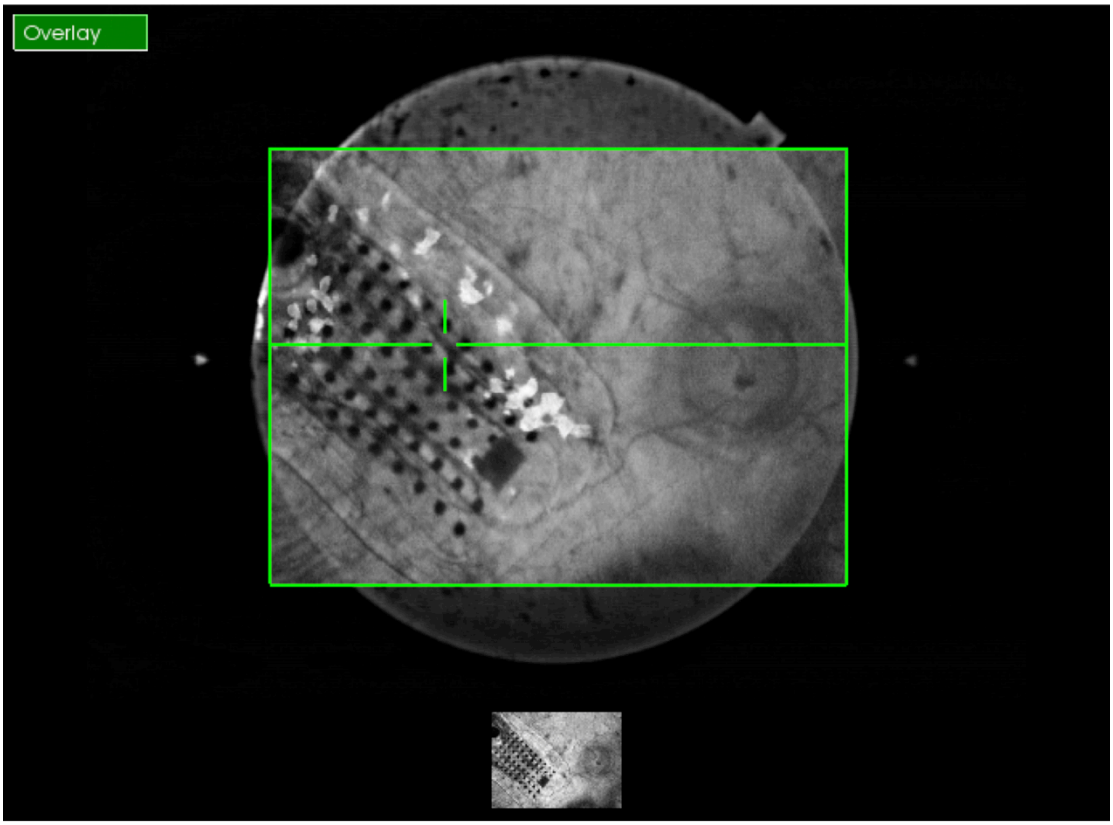

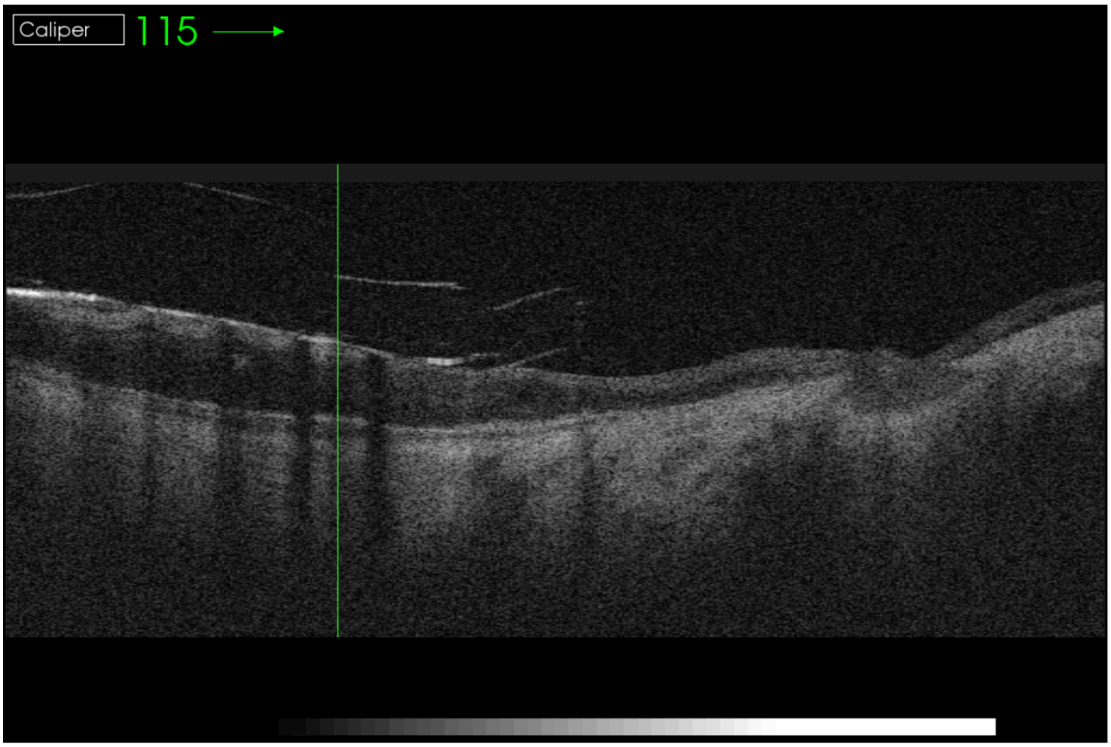

Swept source OCT (DRI OCT-1 Atlantis, TOPCON®) imaging through the chosen quad for 51-005.

51-006

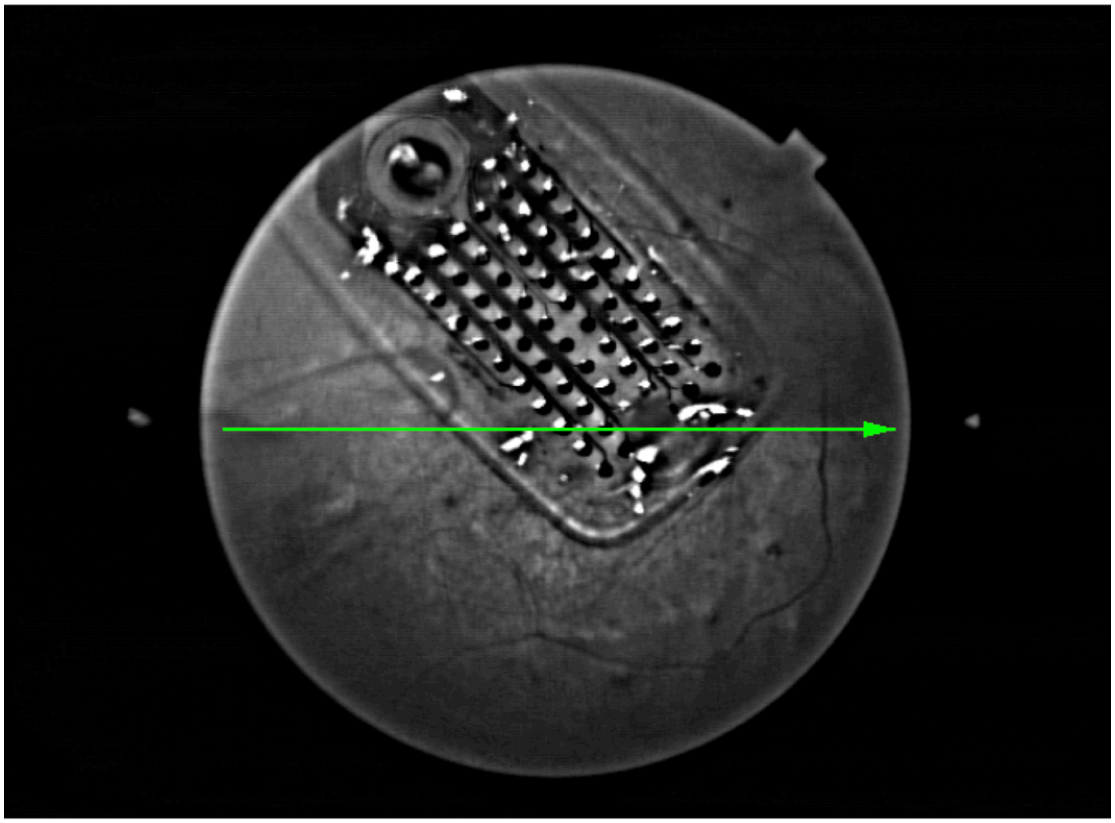

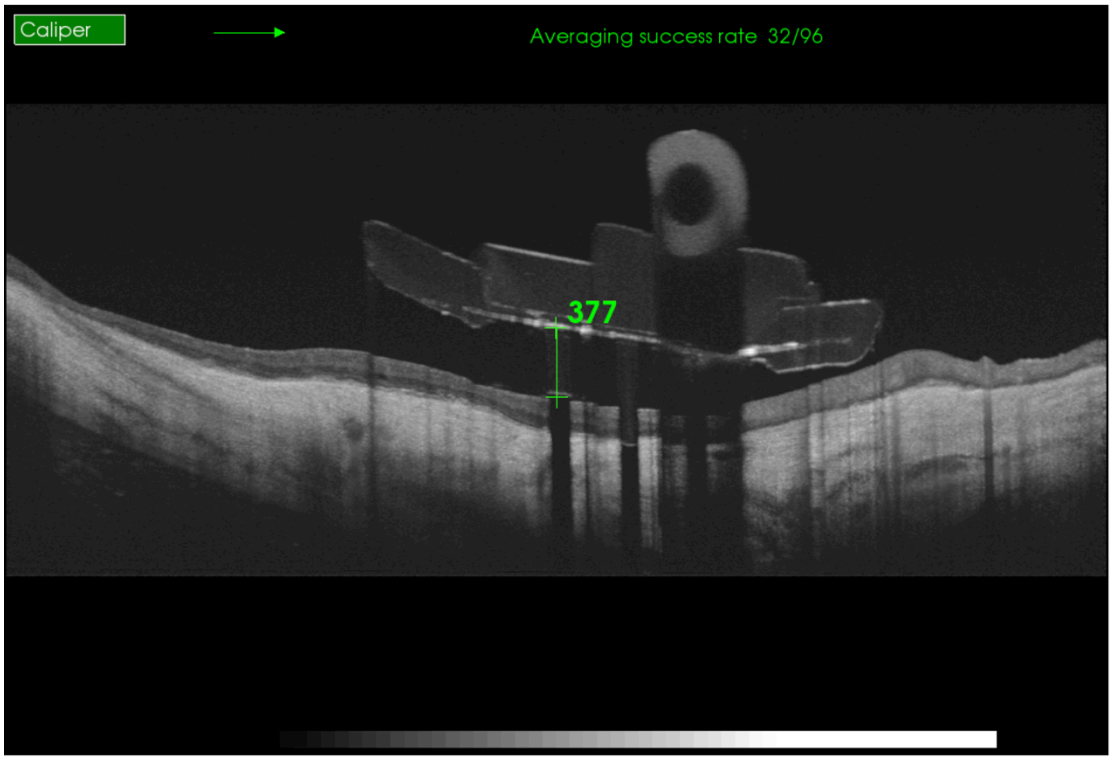

Swept source OCT (DRI OCT-1 Atlantis, TOPCON®) imaging through the chosen quad for 51-006.

51-007

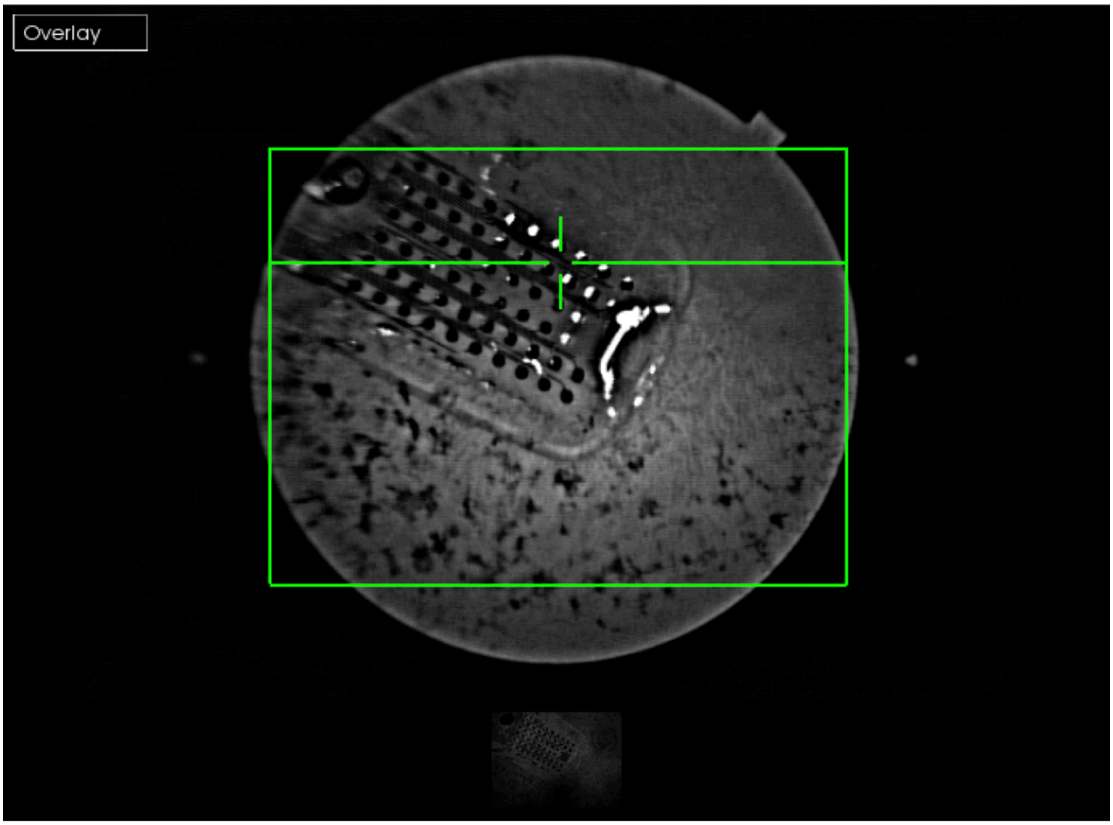

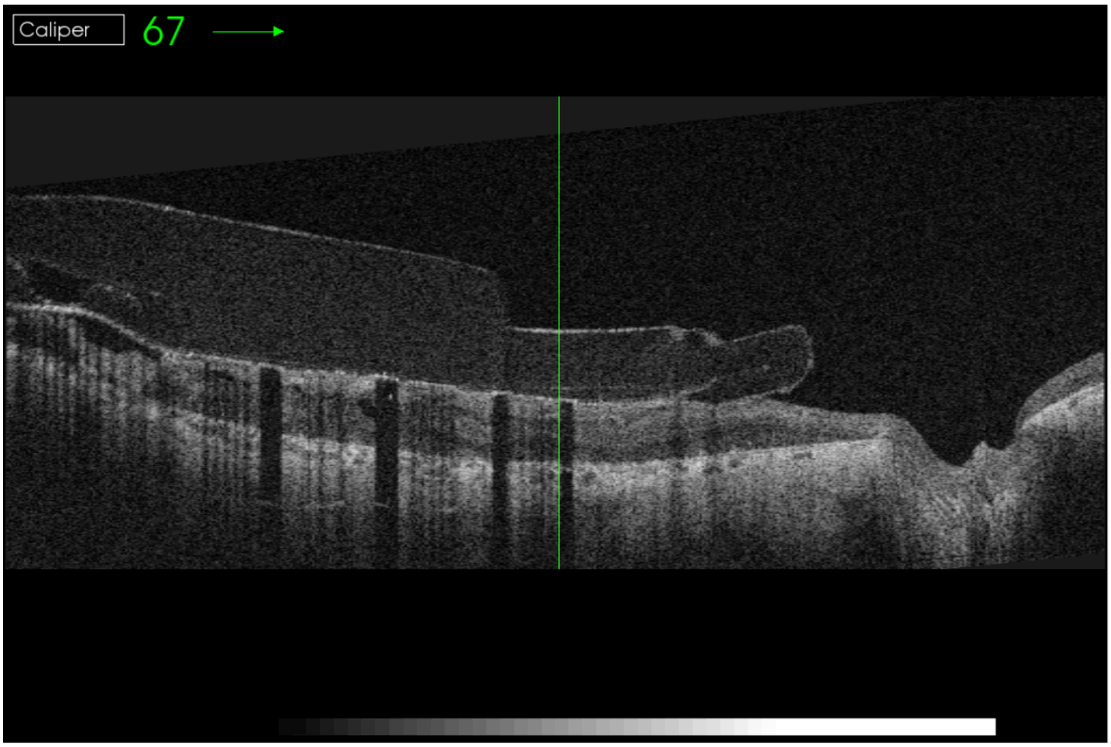

Swept source OCT (DRI OCT-1 Atlantis, TOPCON®) imaging through the chosen quad for 51-007.

51-009

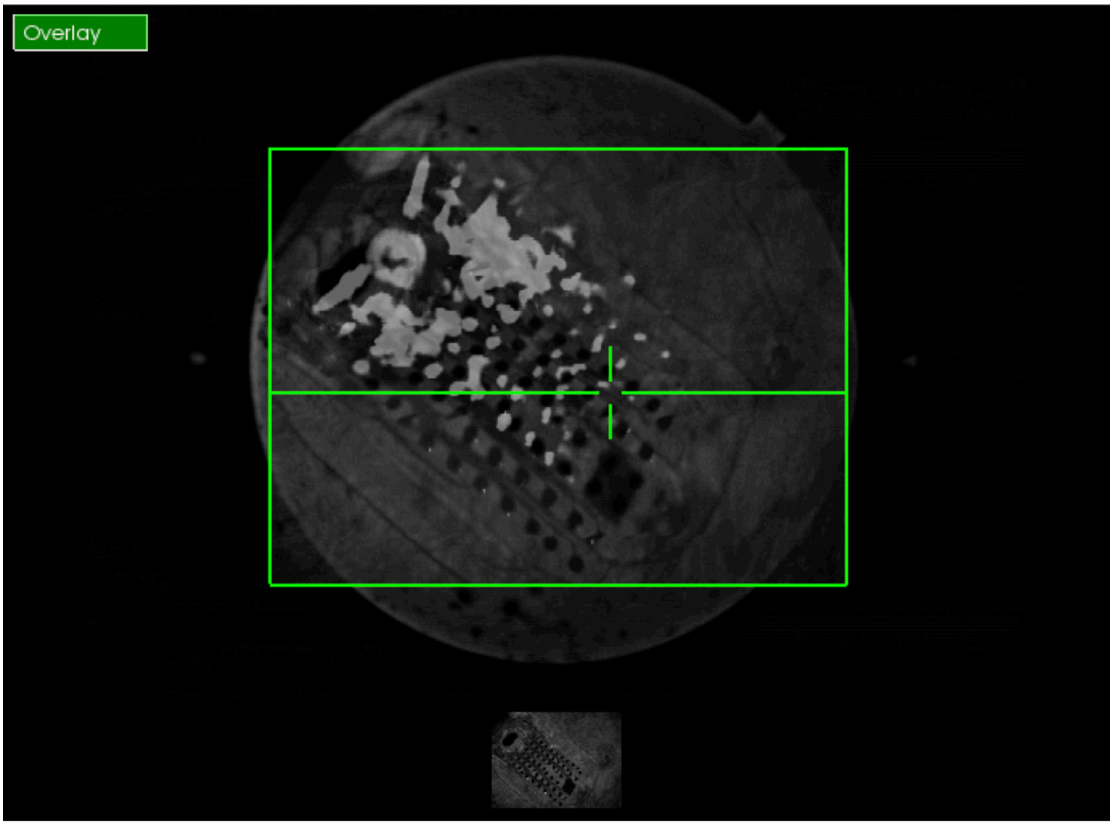

Swept source OCT (DRI OCT-1 Atlantis, TOPCON®) imaging through the chosen quad for 51-009.

Figure 5.2: Swept source OCT (DRI OCT-1 Atlantis, TOPCON®) imaging through the chosen quad for each Argus® II subject. This allows assessment of the contact between the stimulating quad electrodes and the retinal surface. The quad was in direct contact with the retinal surface in 5 subjects, while in subject 51-006, there was a 377μm separation.

5.2.3 Phosphenes Depiction

To record the phosphenes perceived by each subject, we constructed a wall covered with smooth-surface black mats. The subjects were first asked to stand up and stretch out both arms fully to touch the black wall, so that their shoulders were square facing the wall. The standing position of each subject was then adjusted so that the distance between the front of their eyes and the wall equalled to 30cm. Next, the subjects were asked to point with the index finger of both hands simultaneously on the black wall, to where they believed the centre of their visual field was, while keeping their head and eyes pointing straight ahead. A stack of white A4 sized papers (in landscape layout) was then placed underneath the index fingers of each subject and pinned to the wall, so that the index fingers were pointing at the centre of the top sheet of paper (i.e. the centre of the paper was approximating the proclaimed centre of each subject's visual field). A drawing pin with a protruding cylindrical head was then inserted at the point where their index fingers contacted with the wall, so as to mark the location of the proclaimed visual field centre.

During the experiment, the subjects were asked to position themselves according to the set up above, hold on to the pre-placed drawing pin head and adjust their head and eye position until they felt the centre of their visual field was in alignment with the drawing pin. With each quad stimulation, the subjects were instructed to keep their non-dominant hand on the drawing pin as a point of reference, while drawing on the paper the outline of the phosphene they perceived in relation to their visual field centre with a marker pen. A fresh sheet of paper was used for each phosphene depiction (see Figure 5.3).

Figure 5.3: Colour photograph showing an Argus® II subject depicting the phosphene he perceived from the selected quad stimulation. The subject was positioned with his shoulders square facing the wall and with the eye to wall distance of 30 cm. The protruding blue drawing pin was positioned at the visual field centre as indicated by the subject. Before commencing each quad stimulation, the subject was first asked to hold on to the drawing pin with his non-dominant hand, and adjust his head and eye position until he felt his visual field centre was in alignment with the drawing pin. When the quad was stimulated, he was instructed to keep his non-dominant hand on the drawing pin as a point of reference, while drawing on the paper the outline of the phosphene perceived in relation to the visual field centre with a marker pen. A fresh sheet of paper was used for each phosphene depiction. (Image from (Luo et al., 2016))

5.2.4 Experiment Design

We set out to test the consistency and reproducibility of phosphenes within each subject when the selected quad was stimulated using the same settings, but at different time intervals between the stimulations. The experiments were divided into those with long inter-stimuli intervals and short inter-stimuli intervals.

For the long intervals experiments, the subjects were asked to draw the perceived phosphenes at baseline, and then at subsequent time points whereby the inter-stimuli intervals were: 20 minutes, 10 minutes, 5 minutes, 2.5 minutes and 1 minute. For the short intervals experiments, the phosphenes were depicted at baseline, as well as at following stimulations with these inter-stimuli intervals: 30 seconds, 20 seconds, 10 seconds, 5 seconds, 2 seconds and 1 second. Due to built-in safety features in the Argus® II system proprietary

software and delay in the radio frequency link transmission between the external and internal coil of the device, we could not reduce the inter-stimuli interval below 1 second. Each set of long intervals experiments and short intervals experiments was repeated once on the same day (4 sets of experiments per visit). This was then repeated on a separate visit between 1 week and 1 month later. In total, each subject yielded 4 sets of data for the long intervals experiments, as well as 4 sets of data for the short intervals experiments, obtained over 2 separate visits. The aim of long inter-stimuli intervals experiments was to assess the reproducibility of the phosphenes over different time periods, while the short inter-stimuli intervals experiments allowed us to evaluate the temporal resolution of the phosphenes up to 1Hz stimulations.

5.2.5 Data Analysis

All the phosphene drawings were scanned in full size and stored as digital images for further computer processing and analysis.

To assess the consistency and reproducibility of the depictions, we compared the phosphene drawings for variability in: a) shape, b) size and c) location within each subject.

a) Shape Comparison

Adobe® Creative Suite® 5 Photoshop® was employed for the initial image processing. All the scanned phosphene drawings for each set of stimulations were imported as individual layers in the program, and superimposed at the point of subjective visual field centre (i.e. the point marked with the drawing pin). The colour of each phosphene drawing was altered to reflect the inter-stimuli interval of the stimulation that elicited the phosphene. Such superimposition allowed us to display and qualitatively compare the shapes of the drawings across different stimulation intervals, as well as across different sets of experiments simultaneously.

b) Size Comparison

To compare the variations in size of the phosphene drawings, we employed the “scale tool” in the GNU Image Manipulation Program (GIMP) software version

2.8. The “scale tool” automatically forms a closest-fit rectangle with the maximum horizontal and vertical dimension of any selected image. By selecting individual phosphene drawings, we were able to calculate and compare the changes in the diagonal length of the closest-fit rectangles across the different drawings, which indirectly reflected the changes in drawing size (see Figure 5.4).

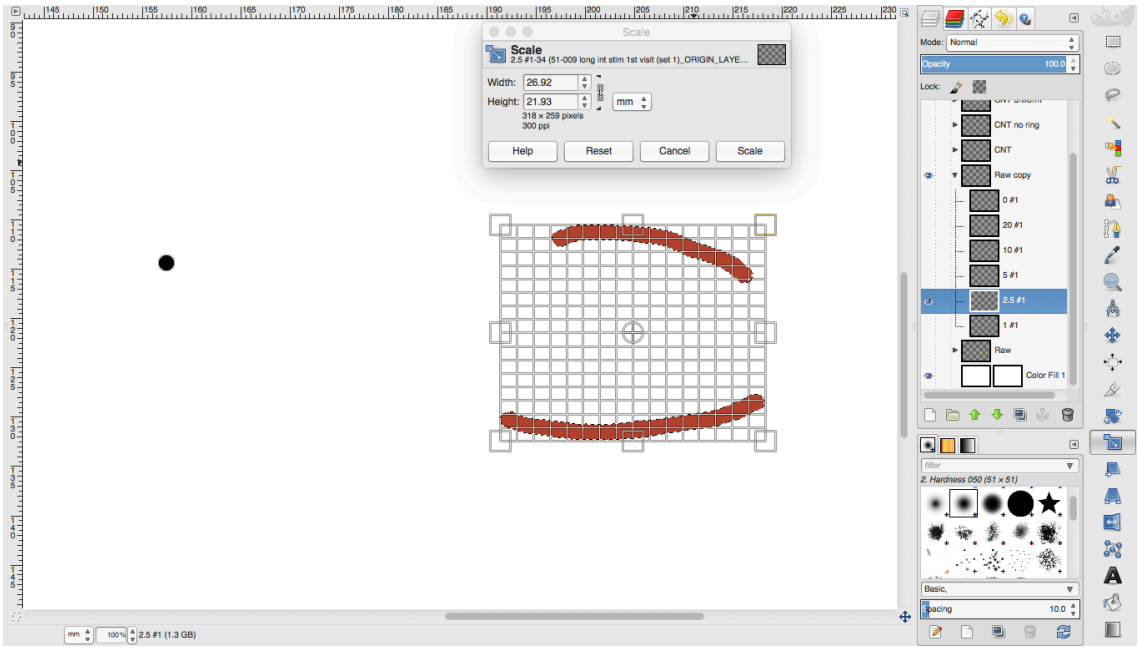

Figure 5.4: A screen shot showing the “scale tool” function of the GNU Image Manipulation Program (GIMP) software version 2.8. The “scale tool” automatically forms a closest-fit rectangle with the maximum horizontal and vertical dimension of any selected image, as exemplified by the closest-fit rectangle of a phosphene depicted by subject 51-009 after a long inter-stimuli interval stimulation. By selecting individual phosphene drawings, we were able to calculate and compare the changes in the diagonal length of the closest-fit rectangles across the different drawings, which indirectly reflected the changes in drawing size. The black dot denotes the subjective visual field centre.

c) Location Analysis & Comparison

Analyses on phosphene locations were performed in 2 ways. Firstly, we set out to show the variability of these locations within each set of experiments. Secondly, we were interested to find out whether the locations of depicted phosphenes matched the retinotopic orientation of the stimulated quad for each subject.

To facilitate location analyses, we calculated the centroid for each of the phosphene drawings using a Python plug-in in the GNU Image Manipulation

Program (GIMP) software version 2.8. ("Light and shadow centroids | GIMP Plugin Registry," n.d.) Within each set of experiments (containing phosphene drawings of different inter-stimuli interval stimulations), the centroid of all the phosphene centroid points was then calculated. This **set centroid** represented the average location of the perceived phosphenes for that set of stimulations (see Figure 5.5).

Figure 5.5: This composite image shows phosphenes depicted by subject 51-009 during an experiment of long inter-stimuli intervals stimulations. The colours of the drawings reflected the specific inter-stimuli intervals that elicited the phosphenes. The centroid of each phosphene drawing is shown as a solid circle of the same colour. The visual field centre is shown as the black dot. The **set centroid** (i.e. the average location of all the phosphene centroid points) is shown as a white circle and marked with an arrow. (Image (Luo et al., 2016))

To assess the variability in phosphene locations, the distance between each phosphene centroid and the set centroid point was measured for each set of experiments. These variations in the distances could then be compared across different sets of experiments within each subject as well as amongst different subjects. The location of all the 8 set centroid points for each subject relative to the subjective visual field centre could also be compared, to show intra-subject variability across the different sets of experiments.

To further simplify the analysis, a summary centroid location for all the 8 sets of experiment for each subject (hereinafter referred to as ‘final centroid’, later explained in Figure 5.7) was calculated. This final centroid location was used to compare with the expected phosphene location calculated from the quad-fovea relation of each subject’s the fundus photographs (see Figure 5.1), to assess retinotopic agreement.

5.3 Results

5.3.1 Shape Comparison

Each subject reported consistently seeing phosphenes of the same colour and shape irrespective of the inter-stimuli intervals. However, across the subjects, there is great variability in the shapes and sizes of the phosphenes perceived (see Figure 5.6). The features of the phosphenes as described by each subject are summarised in Table 5.2.

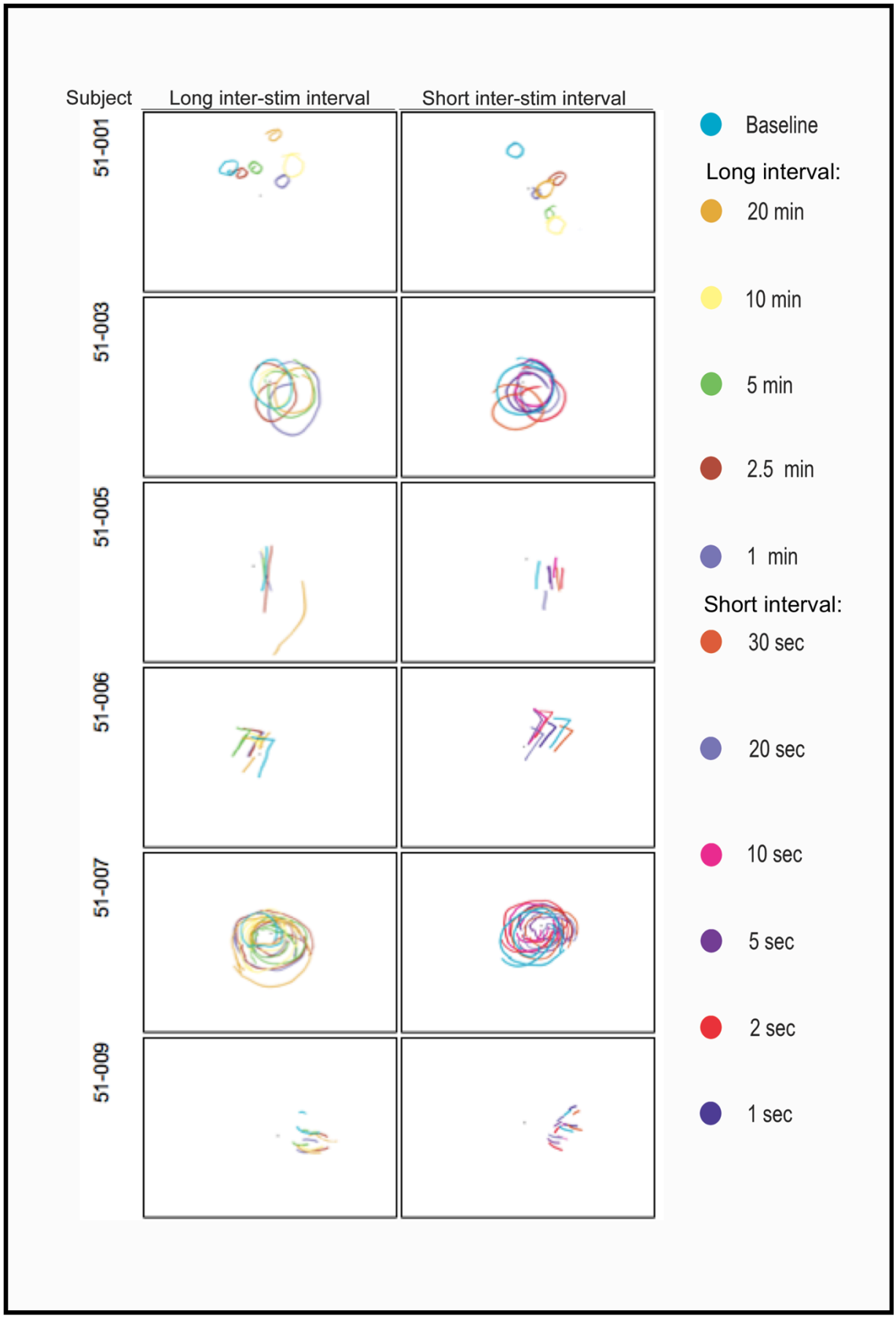

Figure 5.6: The phosphene drawings for the first set (out of 4 sets) of long inter-stimuli interval stimulations (left hand panels), and that of the short inter-stimuli interval stimulations (right hand panels), are displayed for each of the Argus® II subjects. The colour of each phosphene drawing reflects the inter-stimuli interval of the stimulation that elicited the depicted phosphene, rather than the actual colour perceived by the subject. (Image from (Luo et al., 2016))

5.3.2 Size Comparison

The mean ± standard deviation of the diagonal distance of the closest-fit rectangle for each set of phosphene drawings is shown in Table 5.3. Three subjects (51-005, 51-006 and 51-009) drew phosphenes of significantly different size during long inter-stimuli interval stimulations (P = 0.005, 0.005 and 0.01 respectively, Friedman's test), while one subject (51-007) drew phosphenes significantly different in size during short interval stimulations (P = 0.01). For the remaining 2 subjects, phosphene depictions for both long and short inter-stimuli interval stimulations were consistent with no statistically significant size variation. Independently of the drawings, all of the subjects reported that they perceived phosphenes of similar sizes with their given quad stimulations.

Subject ID	Diagonal Distance of Closest-fit Rectangle for Phosphene, mm					
	51-001	**51-003**	**51-005**	**51-006**	**51-007**	**51-009**
Long Interval1	27.98 ± 6.28	84.24 ± 14.94	58.53 ± 25.34	58.53 ± 25.34	102.20 ± 21.73	36.89 ± 9.11
Long Interval2	27.42 ± 5.90	93.73 ± 11.18	46.09 ± 11.03	46.09 ± 11.02	115.17 ± 15.85	28.62 ± 4.94
Long Interval3	25.90 ± 7.81	103.69 ± 5.51	29.92 ± 9.81	29.92 ± 9.81	105.47 ± 19.52	51.99 ± 13.10
Long Interval4	25.90 ± 7.81	102.88 ± 4.72	32.46 ± 5.02	32.46 ± 5.02	111.43 ± 18.80	29.72 ± 5.26
Friedman's Test, P =	0.18	0.22	*0.005	*0.005	0.71	*0.01
Short Interval1	21.16 ± 4.51	82.73 ± 7.80	26.88 ± 4.43	26.88 ± 4.43	93.97 ± 10.49	30.67 ± 3.09
Short Interval2	18.03 ± 7.70	84.12 ± 6.56	24.83 ± 4.60	24.83 ± 4.60	96.42 ± 9.41	26.81 ± 4.01
Short Interval3	25.67 ± 6.42	100.28 ± 11.99	20.86 ± 7.42	20.86 ± 7.42	90.93 ± 13.29	30.87 ± 4.22
Short Interval4	20.68 ± 3.66	84.95 ± 5.54	23.85 ± 4.06	23.85 ± 4.64	76.30 ± 12.58	30.49 ± 3.28
Friedman's Test, P =	0.48	0.17	0.74	0.07	*0.01	0.18

Table 5.3: A comparison of phosphene size variation depicted by Argus® II subjects. This table shows the mean ± standard deviation (in millimetres) of the diagonal distance of the closest-fit rectangle for each set of phosphene drawings. Friedman's analysis of variance showed statistically significant difference in the drawing size for long inter-stimuli interval stimulations in 3 subjects, and in short inter-stimuli interval stimulations in 1 subject (marked with asterisk, *). (Table from (Luo et al., 2016))

5.3.3 Location Analysis & Comparison

a) Location Variability

Variability in the phosphene locations was first evaluated in terms of changes in the mean ± standard deviation of the distance between the set centroid point and the individual phosphene centroids within the set (see Table 5.4).

Subject ID	Mean ± S.D. Phosphene Centroid-Set Centroid Distance mm					
	51-001	**51-003**	**51-005**	**51-006**	**51-007**	**51-009**
Long Interval1	30.7 ± 11.5	13.0 ± 3.43	19.1 ± 18.8	8.3 ± 5.9	6.4 ± 2.7	8.9 ± 3.9
Long Interval2	27.0 ± 20.6	9.0 ± 7.0	25.2 ± 17.4	9.4 ± 7.2	6.3 ± 2.1	14.2 ± 6.4
Long Interval3	27.5 ± 13.7	9.4 ± 5.6	20.5 ± 9.9	19.8 ± 9.24	6.0 ± 2.3	15.2 ± 6.3
Long Interval4	27.5 ± 6.4	8.3 ± 3.9	13.3 ± 5.1	10.2 ± 6.5	9.0 ± 1.5	12.6 ± 5.6
Short Interval1	22.7 ± 14.6	10.2 ± 7.3	12.3 ± 8.2	14.0 ± 5.8	8.1 ± 5.4	11.3 ± 5.0
Short Interval2	28.4 ± 17.4	8.6 ± 2.7	16.8 ± 5.9	12.7 ± 8.4	11.2 ± 6.8	10.5 ± 6.5
Short Interval3	36.1 ± 21.5	12.4 ± 6.2	18.1 ± 9.6	13.0 ± 9.4	7.9 ± 4.4	11.5 ± 6.3
Short Interval4	39.8 ± 15.5	10.5 ± 8.0	14.6 ± 7.3	14.8 ± 8.1	16.8 ± 7.5	11.6 ± 7.5

Table 5.4: Intra-subject variability of the phosphene locations (represented by phosphene centroids) depicted by each of the Argus® II subjects. The mean (± standard deviation) distance of the individual phosphene centroids to the set centroid for all sets of experiments are shown. (Table from (Luo et al., 2016))

The changes in the position of the phosphenes across different sets of experiments are shown as set centroid distribution relative to each subject's visual field centre (see Figure 5.7 and Table 5.5).

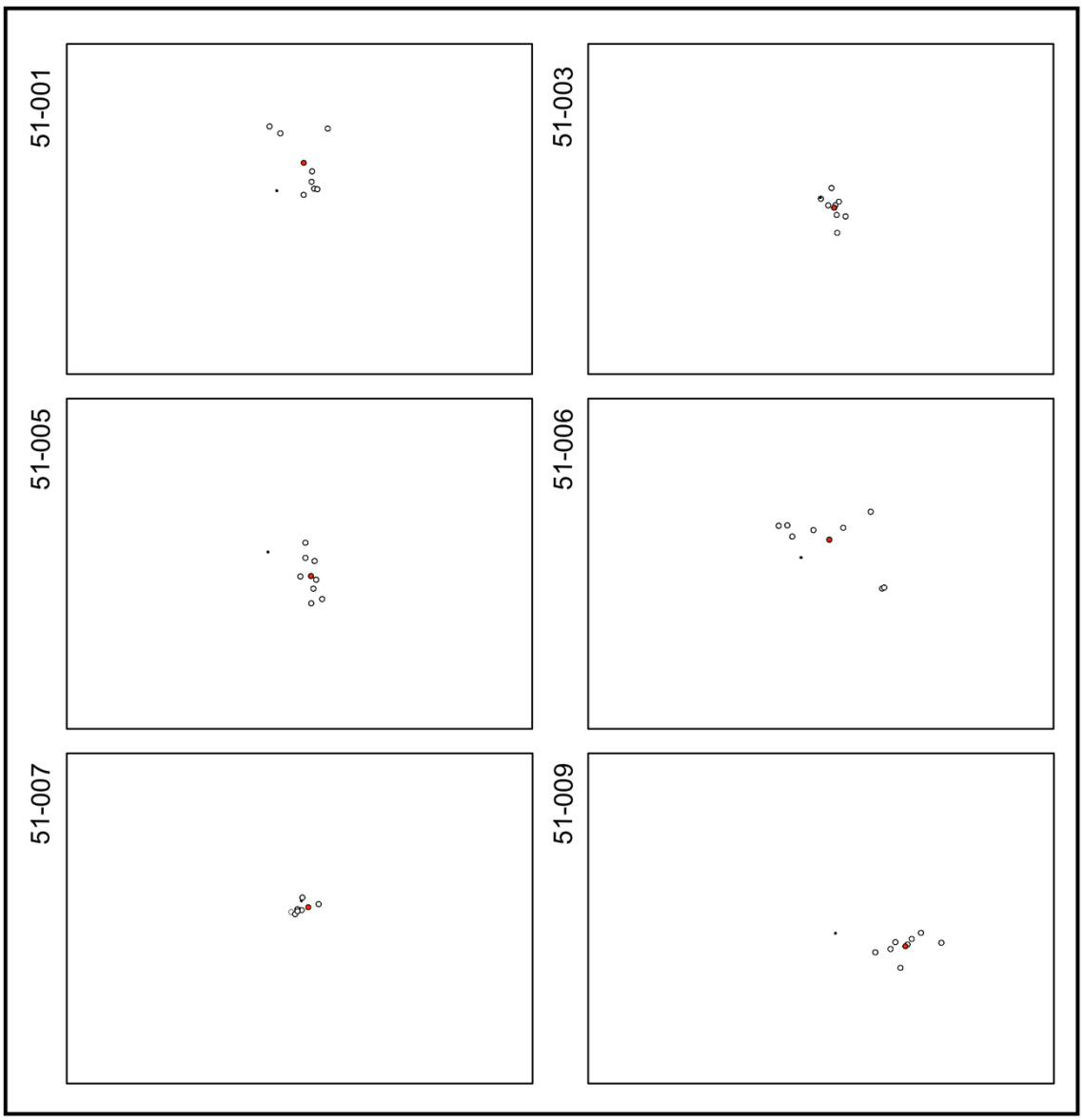

Figure 5.7: Diagrams showing the centroids of the phosphenes depicted by each of the chronically implanted Argus® II retinal prosthesis subjects. The set centroids (white circles) and the final centroid point (centroid of the set centroids, denoted as a red circle) are shown relative to each subject's visual field centre (black dot). (Image from (Luo et al., 2016))

Subject ID	51-001	51-003	51-005	51-006	51-007	51-009
Set Centroid: Long Interval1	36.6 mm S(T)	20.0 mm IT	25.9 mm IT	14.5 mm SN	9.3 mm IN	38.7 mm IT
Set Centroid: Long Interval2	17.7 mm (I)T	9.2 mm ST	42.9 mm IT	22.3 mm SN	7.0 mm IN	28.2 mm IT
Set Centroid: Long Interval3	25.7 mm ST	0.00 mm O	35.5 mm IT	19.3 mm ST	9.6 mm IN	68.0 mm (I)T
Set Centroid: Long Interval4	23.9 mm (S)T	6.9 mm IT	24.4 mm (I)T	24.6 mm SN	6.1 mm IN	36.6 mm IT
Set Centroid: Short Interval1	25.9 mm (S)T	15.1 mm IT	37.2 mm IT	33.0 mm ST	5.8 mm I	46.6 mm (I)T
Set Centroid: Short Interval2	22.9 mm ST	11.9 mm IT	46.0 mm IT	55.3 mm ST	11.2 mm IT	46.9 mm IT
Set Centroid: Short Interval3	41.2 mm S(N)	24.8 mm IT	30.3 mm IT	56.2 mm IT	2.0 mm ST	48.9 mm (I)T
Set Centroid: Short Interval4	51.4 mm ST	10.6 mm IT	24.8 mm ST	55.5 mm IT	36.2 mm T	54.5 mm T
Final Centroid	24.8 mm ST	10.9 mm IT	31.5 mm IT	21.4 mm ST	6.1 mm IT	45.4 mm IT

Table 5.5: This table shows the distance and relative location of the set centroid to Argus® II subject's visual field centre. ST = superotemporal to, IT = inferotemporal to, SN = superonasal to, IT = inferotemporal to, and O = the set centroid overlaps the visual field center. When the angle of deviation of the set centroid point is less than 10° from the horizontal or vertical line, the direction of deviation is bracketed. The **final centroid** was calculated to represent the summary position of all the set centroids for each subject. (Table from (Luo et al., 2016))

b) Retinotopic Agreement

The quad-fovea location and the expected phosphene location for each subject are as shown in Table 5.6. Out of the 6 subjects, 4 subjects' depicted phosphene locations fell in the same quadrant of the visual field as that of the expected phosphene location. Two subjects' (51-001 and 51-005) depicted phosphenes in the same hemi-field (temporal and inferior respectively) as the expected locations.

Subject ID	001	003	005	006	007	009
Quad	C07C08 D07D08	A07A08 B07B08	E05E06 F05F06	A07A08 B07B08	E07E08 F07F08	E07E08 F07F08
Quad-Fovea Distance	1100μm	1000μm	1200μm	1300μm	1100μm	2400μm
Quad Position Relative to Fovea	SN	SN	ST	IN	SN	SN
Expected Phosphene Location in VF	19.2 mm IT	17.5mm IT	21.0 mm IN	22.7 mm ST	19.2 mm IT	42.16 mm IT
Final Centroid Location in VF	24.8 mm ST	10.9 mm IT	31.5 mm IT	21.4 mm ST	6.1 mm IT	45.4 mm IT

Table 5.6: This table shows the quad position relative to the estimated fovea location from fundus photograph for each subject. The expected phosphene location and the final centroid location relative to each subject's visual field (VF) center are also shown. SN = superonasal; ST = superotemporal; IN = inferonasal; and IT = inferotemporal. (Table from (Luo et al., 2016))

5.4 Discussion

With the establishment of good long term safety profiles (Ho et al., 2015; Humayun et al., 2012) and advances in biotechnology promising larger number of pixels in the future (Stronks and Dagnelie, 2014), high resolution pixelated vision from electrical retinal stimulations may become an important avenue for vision restoration. Despite the encouraging outcomes showing improved visual performance with the use of the device(daCruz et al., 2012; Garcia et al., 2014; Humayun et al., 2012; Luo and daCruz, 2016), understanding of the interaction between the stimulating parameters and the individual subjects' visual percepts remains poor. Clearly the ability to produce consistent, controllable and retinotopically-defined phosphenes will remain central to improving prosthetic vision in the future.

We chose the parafoveal quad as our focus for evaluation as physiologically, the photoreceptor: bipolar cells: ganglion cells ratio in this region approaches 1: 1: 1. Direct electrical stimulation at this area would therefore theoretically be most predictable, giving rise to focal, dot-like phosphenes, whether the bipolar

cells and / or ganglion cells were the main target of electrical stimulation. Greater density of ganglion cells found in this region also allowed for lower stimulating currents to be used to elicit distinctive phosphenes reliably (i.e. lower threshold). Quad stimulation, rather than single electrode, was chosen as only 2 out of the 6 subjects had functioning single electrodes in the parafoveal region at the time of the study.

Interestingly, our study has shown that irrespective of the variability in size and location of the drawn phosphenes, all our subjects reported perceiving phosphenes of the same shapes and similar sizes when using the same stimulating parameters. This consistency was seen across different inter-stimuli intervals (with temporal resolution down to 1 second) and was reproducible on separate occasions ranging from 1 week to 1 month apart. However, in spite of the good intra-subject consistency, each of the 6 subjects experienced phosphenes of totally different shapes and sizes. It is likely that the inter-subject variations reflect the variety of genetic diseases, the duration the degeneration has been present, the different proportions of surviving bipolar and ganglion cell types, and the variability in reconnections and remodelling within these severely diseased retinas.

The wide variation in phosphene shape and size may in part explain the wide range of inter-subject performance levels observed when they performed tasks involving visual form differentiation, e.g. letter recognition, shapes and objects recognition (daCruz et al., 2012; Luo and daCruz, 2016). Indeed one subject (51-009) who consistently out-performed other subjects in all the vision form recognition tasks, depicted phosphene shapes closest to the stimulation pattern (i.e. 2 horizontal lines with filled in centre, simulating a box shape from the quad stimulation). It is also interesting to note that despite the inter-subject variability in perceived phosphenes, Argus® II subjects still performed statistically significantly better in visual form differentiation tasks with the device on than without. This may be attributable to the intra-subject consistency and reproducibility of the phosphenes elicited. Such consistency and reproducibility may allow each subject to learn and adapt to the prosthetic visual information (albeit crude and unlike natural vision), and use it to make consistent, simple decisions about form. This learning is evident in the improvement of

psychophysical and other visual tasks performance with training (Chader et al., 2009; Stronks and Dagnelie, 2014).

Sabbah et al. reported that the perceived position of the phosphene is dependent on the direction of gaze (i.e. the eye position) of the Argus® II subject, and that misalignment of head and eye position occurred in all the subjects in their study (Sabbah et al., 2014). This would explain the variations in the location of the phosphene drawings in our study, even though the subjects were instructed to keep their head and eyes pointing straight ahead during the task. The largest deviation of the phosphene centroid location from the set centroid location was 39.8 ± 15.5 mm, indicating a disparity distance of about 5 cm, viewed at 30 cm away (≈ 9.5˚). One subject (51-007) showed greater localisation consistency than the others (see Figure 5.7), and this is consistent with his superior performance in carrying out object prehension tasks (see **Chapter 4**) (Luo et al., 2015). This is also in keeping with Sabbah et al.'s conclusion that the Argus® II subjects are able to develop strategies to minimize the impact of head-eye misalignment. Our study also showed that 4 out of the 6 subjects had phosphene locations in the expected visual field quadrant, as indicated by the relative quad-fovea location. These subjects may be better at keeping their head-eye alignment, such that their subjective visual field centre was in alignment with the estimated fovea location.

In general, our study showed that stimulation of the same quad with the same stimulating parameters gave rise to consistently reproducible phosphenes for a given subject in a cohort of chronically implanted subjects more than 5 years after the initial surgery. This consistency is an encouraging basis for the construction of more complicated pixelated images. Given the vastly different shapes and sizes of the phosphenes perceived by individual subjects, future work into determining the suitable stimulating parameters for each electrode / quad stimulation may be required for each subject, to achieve the construction of useful pixelated prosthesis based vision.

Chapter 6

MRI Brain Scan Safety

6.1 Introduction

Magnetic resonance imaging (MRI) is a frequently used investigative tool. Of the 30 million MRIs performed annually in the USA(OECD, 2012), 22% are brain scans ("Market Research MRI products," n.d.). With the increasing clinical use of the Argus® II retinal prosthesis following CE mark (March 2011) and FDA approval (February 2013), safety information on the use of MRI with the device will be useful.

Weiland et al. (Weiland et al., 2012) addressed the safety aspects of performing MRI in Argus® II patients based on in-vitro experimental findings with phantoms. They concluded that MRI performed at 1.5 or 3-Tesla field strength (highest spatial gradient magnetic field of 720 gauss/cm) in the absence of the external components, would not be detrimental to the patient and the device.

In this study, we reported 3 subjects chronically implanted with the Argus® II retinal prosthesis system, who underwent MRI brain scans for medical indications independent of the trial. To our knowledge, what is reported here represents the first experience of in-vivo MRI examinations performed with the Argus® II retinal implants in-situ. Some of the data from this study has been published (Luo et al., 2013).

6.2 Materials & Methods

This is a single-centre, retrospective case series. Three subjects chronically implanted with the Argus® II retinal prosthesis in the initial phase I/II feasibility study who underwent MRI brain scans for unrelated medical conditions were included. Argus® II device stability before and after the MRI brain scan was assessed both anatomically and functionally. The effect of the in situ Argus® II retinal implant on the diagnostic quality of the MRI brain scan image would also be evaluated.

6.2.1 Anatomical Assessment

As previously described in **Chapter 2** (section 2.2, Figures 2.2 and 2.3), the internal components of the Argus® II retina consists of an internal coil, an ASIC enclosed in a hermetically sealed case and a 60-channel microelectrode (6 x

10) array which rests on the retinal surface and is held in place with a custom-made, spring-tension, metallic tack (Second Sight Medical Products. Inc.). After surgical implantation, the only portion of the device that is directly visible is the epiretinal microelectrode array on the retinal surface.

To assess the anatomical stability, 4 modalities of assessment were applied:

a) Colour fundus photograghy

b) Optical coherence tomography (Topcon 3D-OCT 2000)

c) Electrode impedance measurements

d) Clinical examination with slit lamp biomicroscopy

The colour fundus photographs of the posterior pole were acquired before and after the MRI brain scan for en face comparison for each subject. OCT (Topcon 3D-OCT 2000) scans of the epiretinal microelectrode array was also performed before and after the MRI brain scan to assess any axial movement of the epiretinal microelectrode array. Further more, the electrical contact of the microelectrode array with the retinal surface could be reflected in the individual electrode impedance measurements. These measurements before and after the MRI brain scan were also compared. Slit lamp biomicroscopy examinations were performed after the MRI brain scan to look for any extraocular sign of implant movement or extrusion through conjunctiva.

6.2.2 Functional Assessment

The function of the Argus® II device was assessed by monitoring changes in the thresholds of the microelectrode array after the MRI brain scan for each subject. It has been observed that in all chronically implanted Argus® II subjects, there is a range of intra-subject inter-testing variability. As such, the thresholds of the 60 electrodes were tested at two stimulating current levels, 233μA and 677μA, and separated into 3 levels: a) low threshold (≤233μA), b) moderate threshold (≥233μA but ≤ 677μA), and c) high threshold (≥677μA). This allows comparison of proportional changes in threshold levels distribution with time within each subject. Any electrode that caused discomfort with stimulation was disabled during the testing.

6.3 Result

The demographics of the participating subjects are as shown in Table 6.1. The study was approved by the local ethics committee for our centre and respected the tenets of the Declaration of Helsinki.

Subject ID	Diagnosis	Year of Operation	Age at Time of Operation (yrs)	Date of MRI Brain Scan
51-007	Retinitis Pigmentosa	2009	63	September 2011
51-001	Retinitis Pigmentosa	2008	70	September 2012
51-003	Retinitis Pigmentosa	2008	72	February 2013

Table 6.1: Demographics and MRI brain scan dates of the 3 Argus® II subjects who underwent MRI brain scans for unrelated medical conditions.

6.3.1 Intraocular Implant Position & Function

6.3.1.1 Case 1 (Subject 51-007)

This Caucasian male received the Argus® II retinal prosthesis implant in 2009. He underwent 1.5- Tesla MRI brain scan in September 2011 for investigation of tinnitus. Colour fundus photographs of the posterior pole 3 months prior to and 8 months after the MRI brain scan did not show gross rotational or other topographical change in implant position (see Figure 6.1).

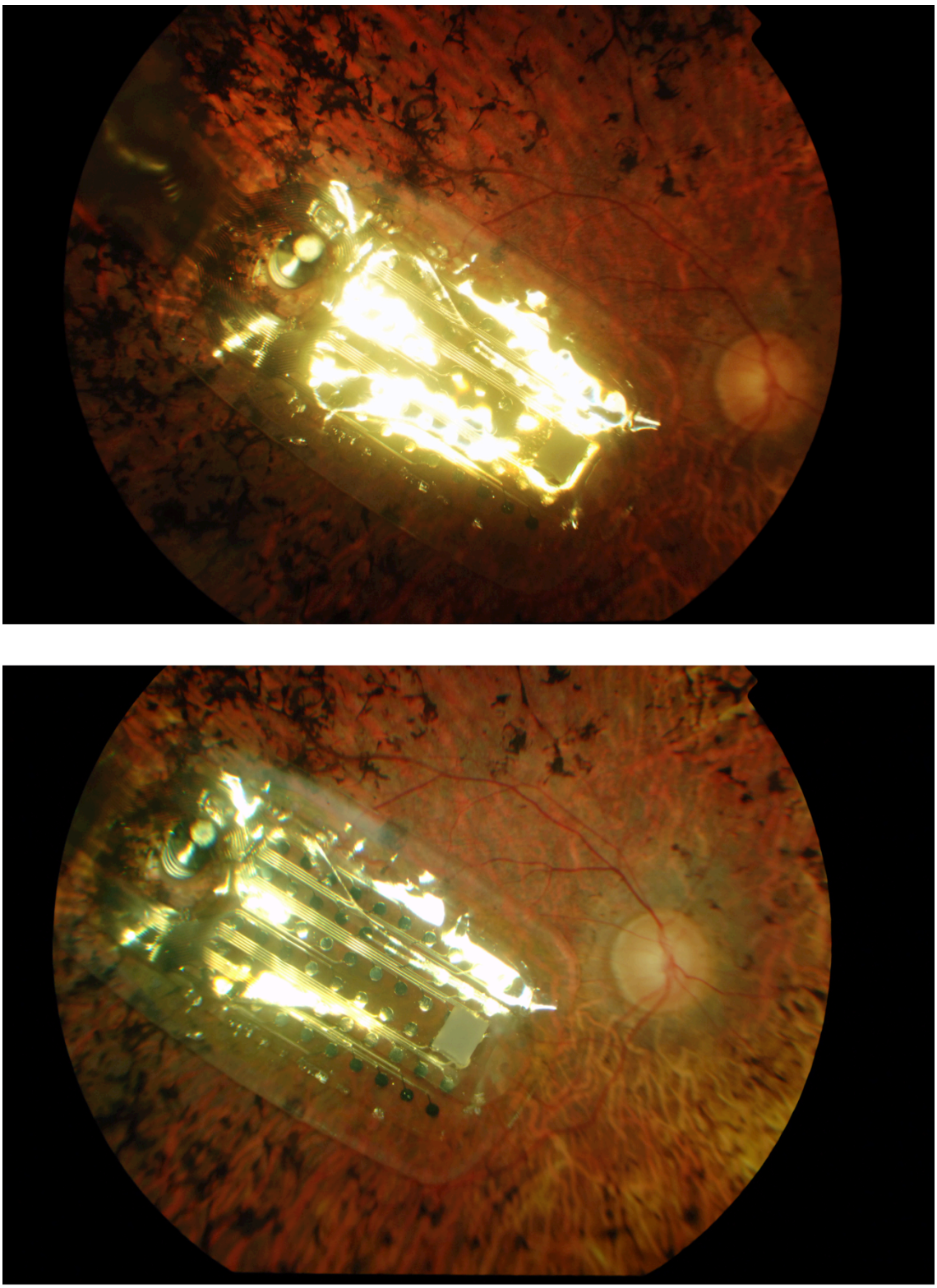

Figure 6.1: A colour fundus photographs of the right eye of subject 51-007 who received Argus® II retinal prosthesis implant in 2009. In the pre-MRI scan fundus photo (top image), the microelectrode array covers the majority of the macula region and is fixed to the retinal surface by the retinal tack to achieve retinal apposition. The post-MRI scan photo (bottom image) was taken 8 months after the scan. The microelectrode array remains fixed by the retinal tack to the retinal surface, covering the same area of the macula as before.

There is no evidence of implant dislocation, rotation, or retinal detachment. (Image modified from (Luo et al., 2013))

OCT scan of the microelectrode array 3 months before and 8 months after the MRI brain scan also did not show any change in axial position, with the implant remaining in direct contact with the retinal surface both before and after the MRI brain scan (see Figure 6.2). There are no associated complications of implant dislocation or retinal detachment to date. The distribution of electrode impedance was comparable before and after the scan, suggesting no change in retinal contacts (see Figure 6.3).

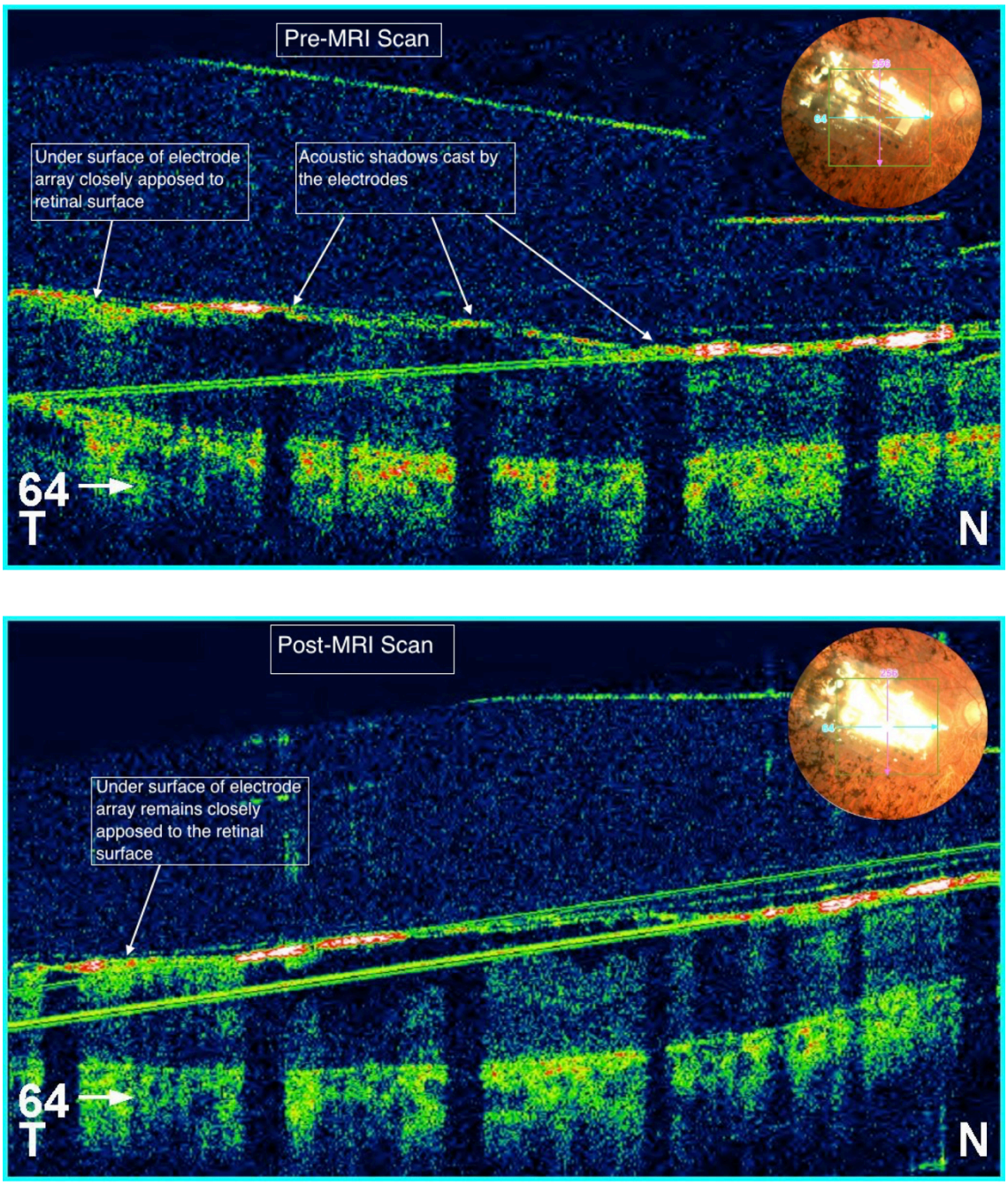

Figure 6.2: OCT image (Topcon 3D-OCT 2000) of Argus® II implant in the right eye of subject 51-007 at 3 months before the MRI brain scan (top image), and at 8 months after the scan (bottom image). In the pre-MRI OCT, the under surface of the retinal implant is closely apposed to the retinal surface. The upper surface of the Argus II implant is seen as the upper-most bright reflective layer. The electrodes of the implant are seen casting vertical acoustic shadows over the retina. In the post-MRI OCT, the under surface of the electrode array remains closely apposed to the retinal surface. (Image from (Luo et al., 2013))

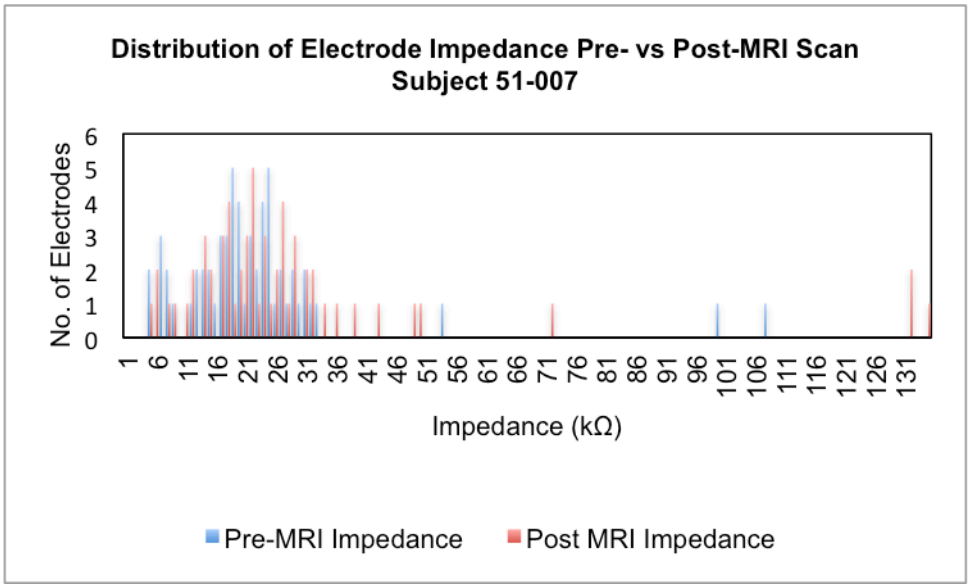

Figure 6.3: Histogram of electrode impedance distribution for subject 51-007 before and after MRI brain scan. (Image from (Luo et al., 2013))

With regards to implant function, serial threshold testing pre-MRI scan showed that there is a general trend of threshold increase with time, but there is no substantial change in the thresholds after the MRI scan in subject 51-007 (see Figure 6.4). This trend of gradual threshold increase with time has also been observed in the other 4 Argus® II subjects (51-003, 51-005, 51-006 and 51-009) from our unit who did not undergo MRI brain scan (controls).

MRI Brain Scan Subjects

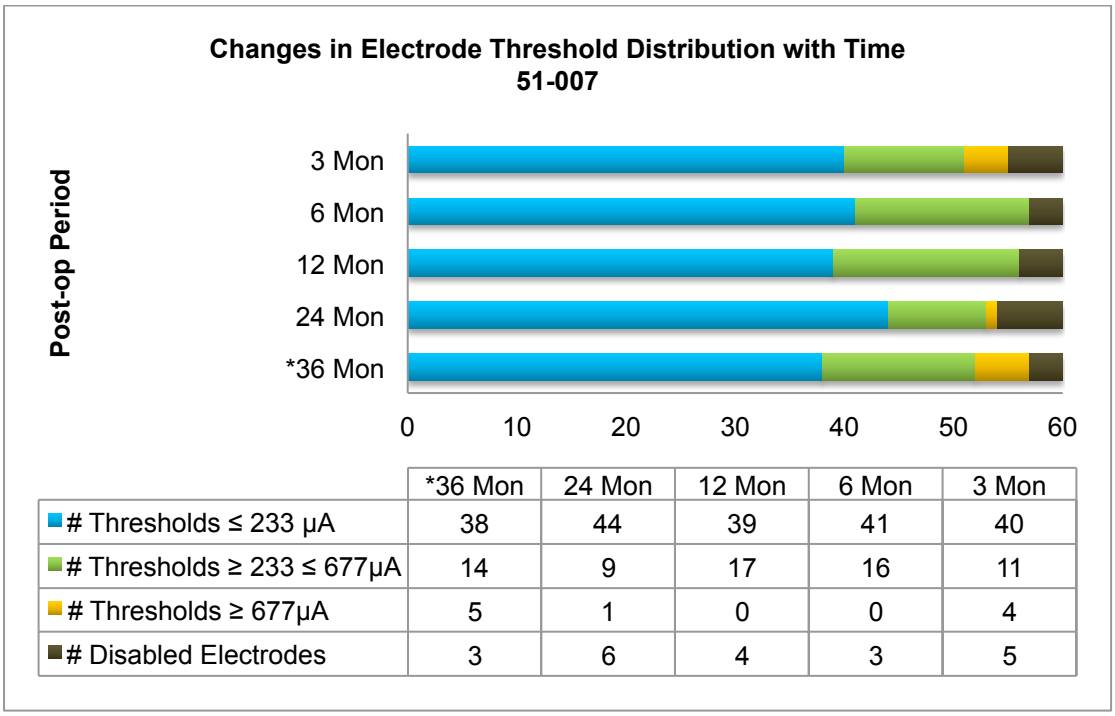

	*36 Mon	24 Mon	12 Mon	6 Mon	3 Mon
# Thresholds ≤ 233 µA	38	44	39	41	40
# Thresholds ≥ 233 ≤ 677µA	14	9	17	16	11
# Thresholds ≥ 677µA	5	1	0	0	4
# Disabled Electrodes	3	6	4	3	5

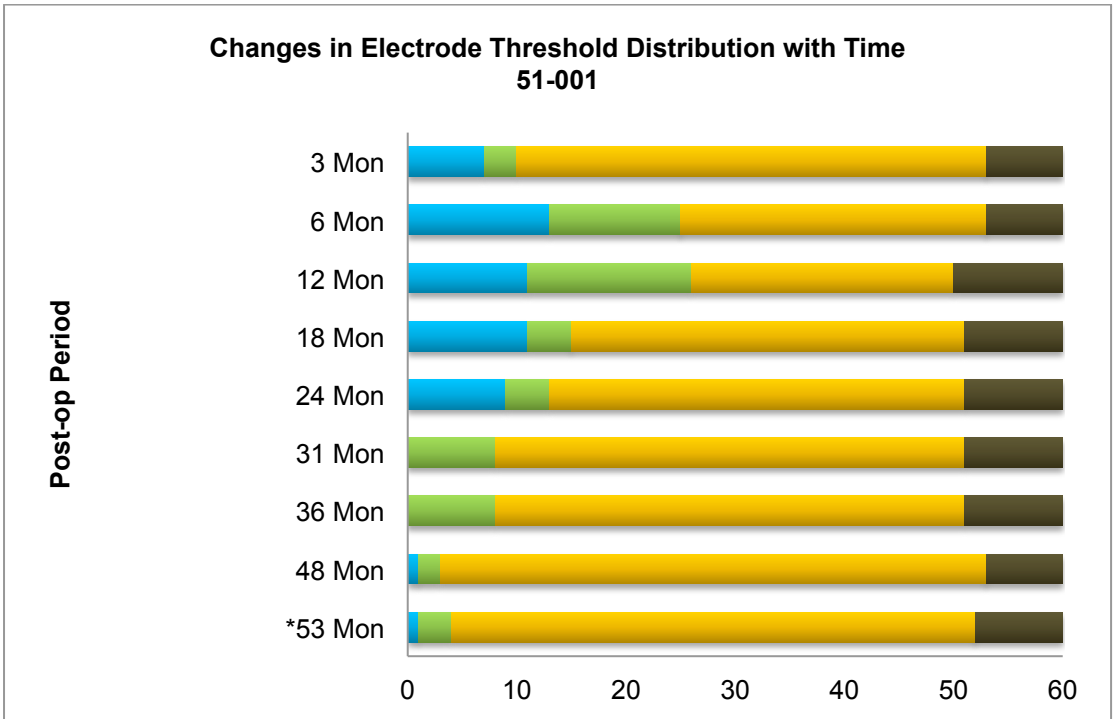

	*53 Mon	48 Mon	36 Mon	31 Mon	24 Mon	18 Mon	12 Mon	6 Mon	3 Mon
# Thresholds ≤ 233 µA	1	1	0	0	9	11	11	13	7
# Thresholds ≥ 233 ≤ 677µA	3	2	8	8	4	4	15	12	3
# Thresholds ≥ 677µA	48	50	43	43	38	36	24	28	43
# Disabled Electrodes	8	7	9	9	9	9	10	7	7

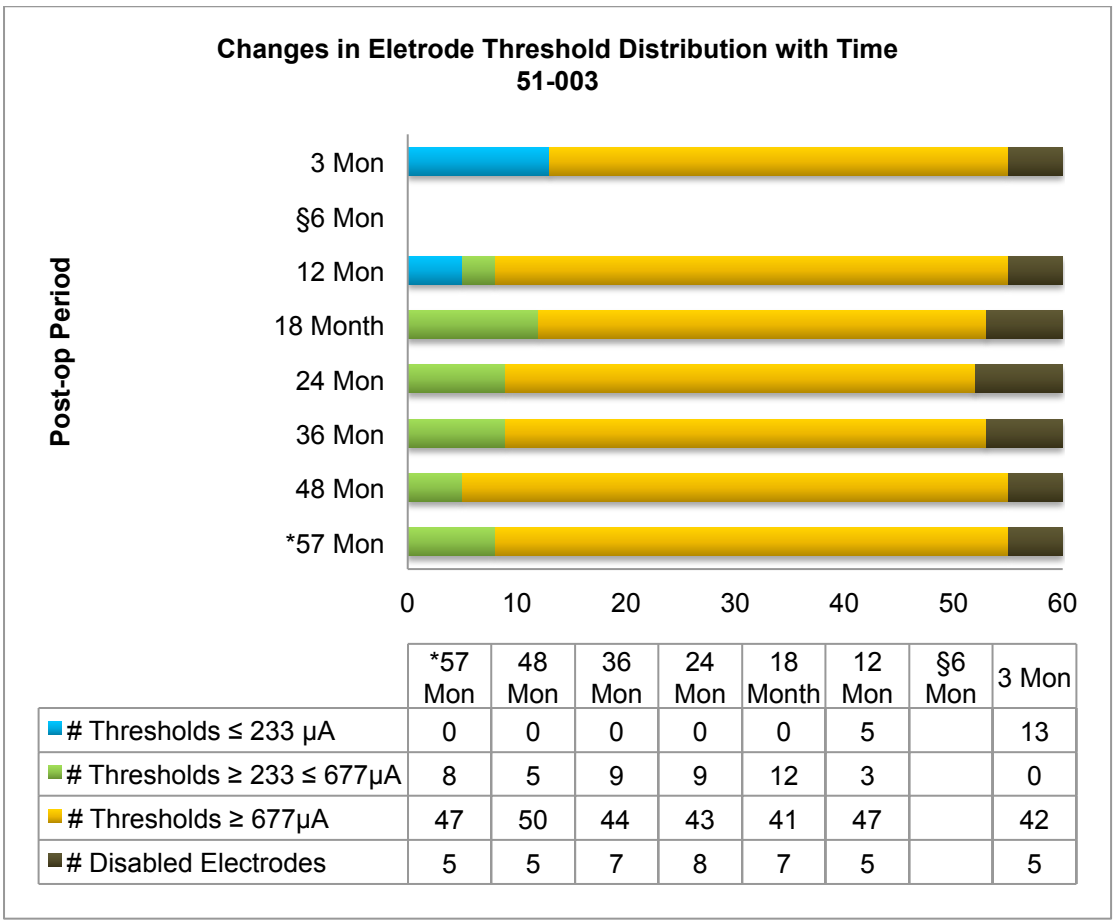

	*57 Mon	48 Mon	36 Mon	24 Mon	18 Month	12 Mon	§6 Mon	3 Mon
# Thresholds ≤ 233 µA	0	0	0	0	0	5		13
# Thresholds ≥ 233 ≤ 677µA	8	5	9	9	12	3		0
# Thresholds ≥ 677µA	47	50	44	43	41	47		42
# Disabled Electrodes	5	5	7	8	7	5		5

Controls

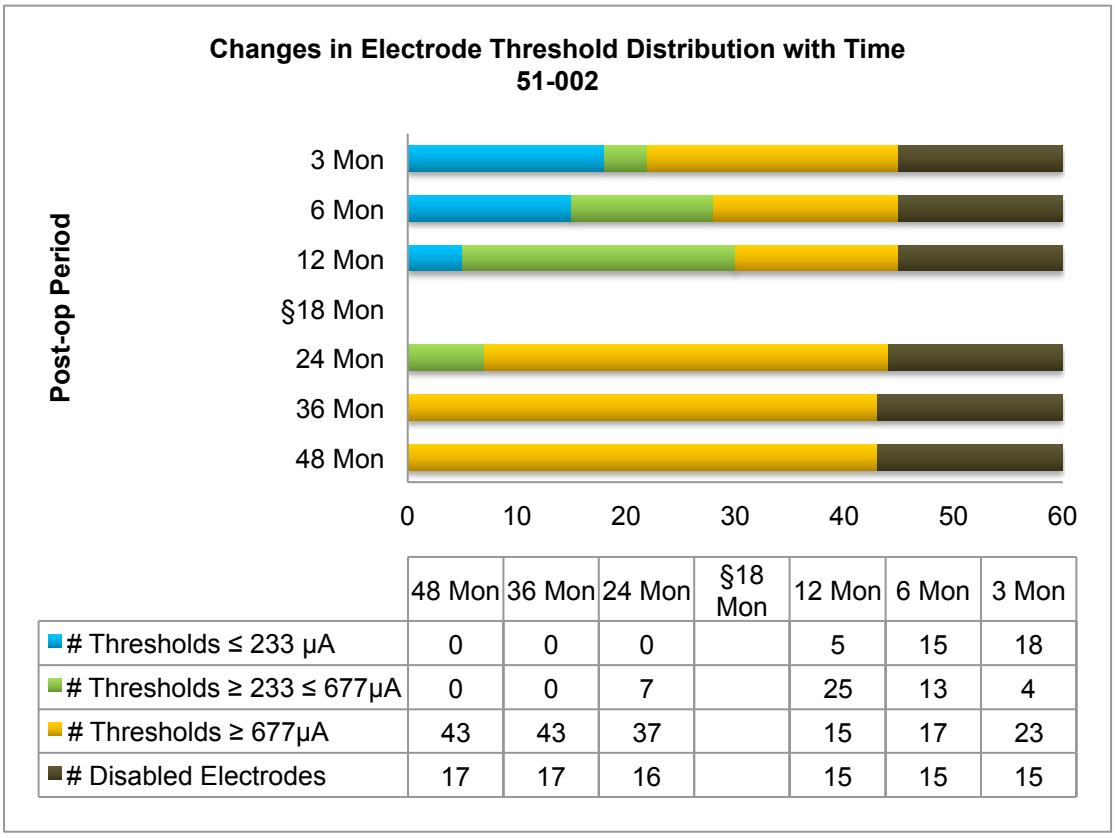

	48 Mon	36 Mon	24 Mon	§18 Mon	12 Mon	6 Mon	3 Mon
# Thresholds ≤ 233 µA	0	0	0		5	15	18
# Thresholds ≥ 233 ≤ 677µA	0	0	7		25	13	4
# Thresholds ≥ 677µA	43	43	37		15	17	23
# Disabled Electrodes	17	17	16		15	15	15

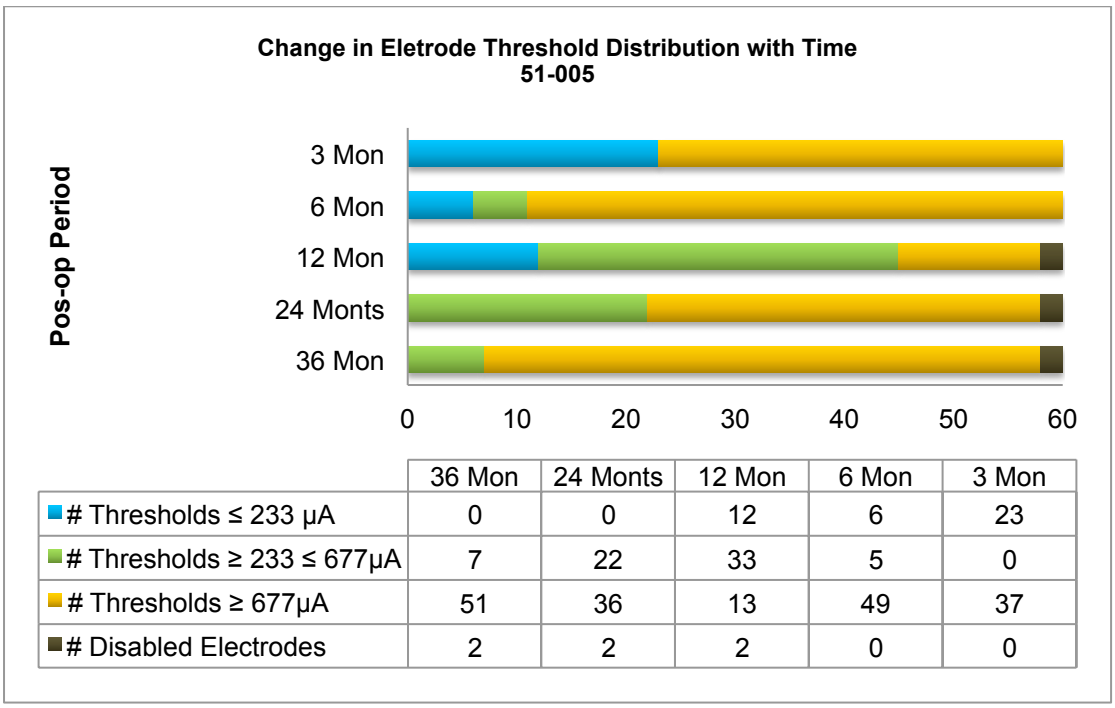

	36 Mon	24 Monts	12 Mon	6 Mon	3 Mon
# Thresholds ≤ 233 µA	0	0	12	6	23
# Thresholds ≥ 233 ≤ 677µA	7	22	33	5	0
# Thresholds ≥ 677µA	51	36	13	49	37
# Disabled Electrodes	2	2	2	0	0

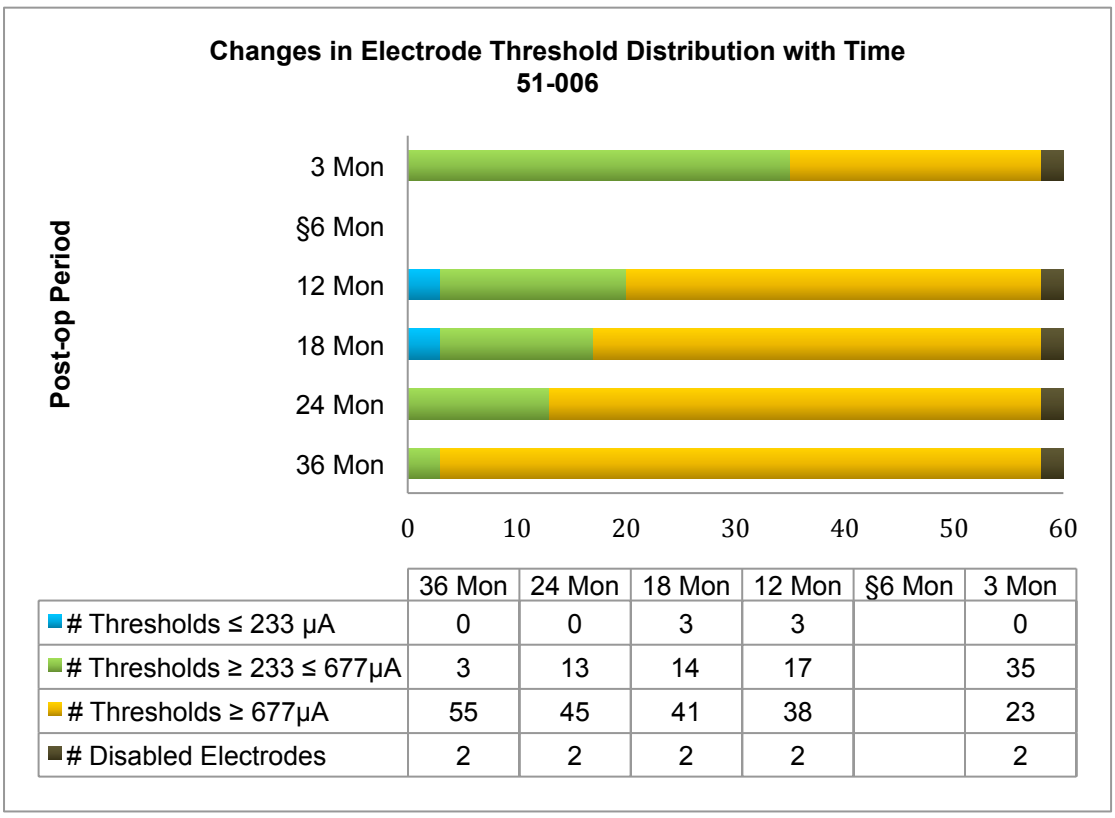

	36 Mon	24 Mon	18 Mon	12 Mon	§6 Mon	3 Mon
# Thresholds ≤ 233 µA	0	0	3	3		0
# Thresholds ≥ 233 ≤ 677µA	3	13	14	17		35
# Thresholds ≥ 677µA	55	45	41	38		23
# Disabled Electrodes	2	2	2	2		2

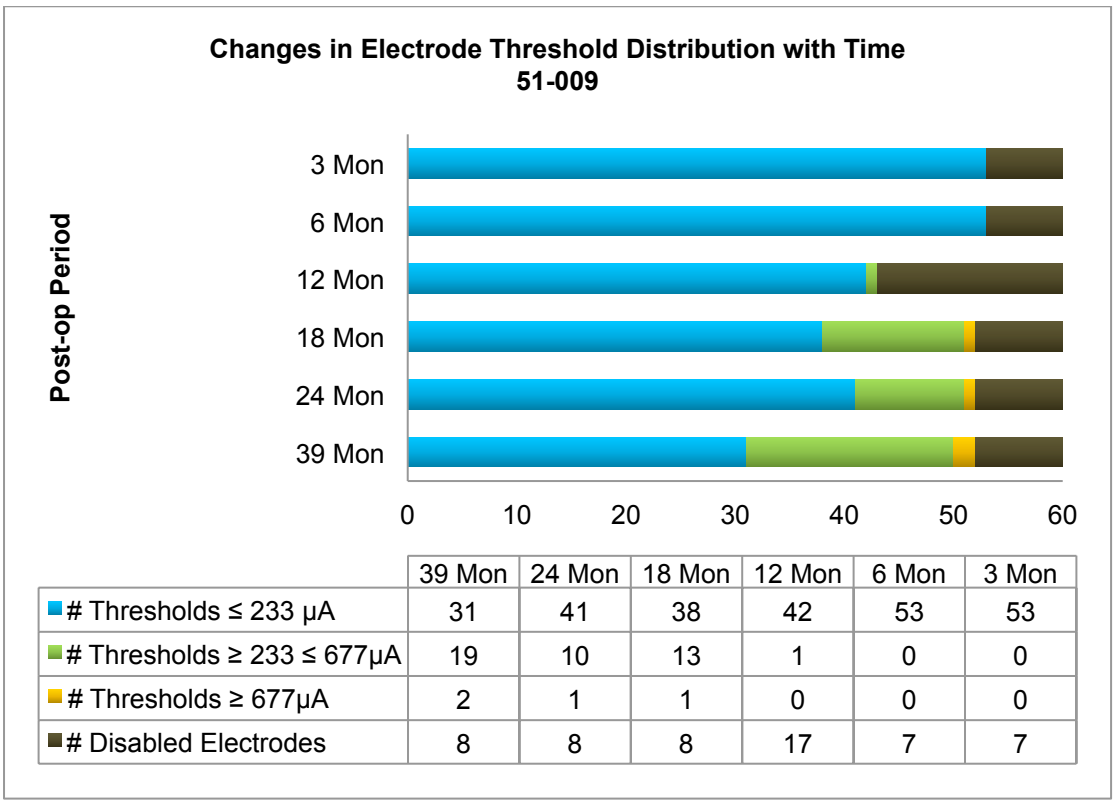

	39 Mon	24 Mon	18 Mon	12 Mon	6 Mon	3 Mon
# Thresholds ≤ 233 μA	31	41	38	42	53	53
# Thresholds ≥ 233 ≤ 677μA	19	10	13	1	0	0
# Thresholds ≥ 677μA	2	1	1	0	0	0
# Disabled Electrodes	8	8	8	17	7	7

Figure 6.4: Bar chart showing the proportional changes in electrode threshold distribution with time. The thresholds of the 60 electrodes were tested at two stimulating current levels, 233μA and 677μA, and separated into 3 levels: a) low threshold (≤233μA), b) moderate threshold (≥233μA but ≤ 677μA), and c) high threshold (≥677μA). During the testing, electrodes which caused discomfort with stimulation were disabled. The first 3 subjects (51-007, 51-001 and 51-003) underwent MRI brain scan. Their threshold testing performed after MRI brain scan is marked with asterisk (*), which took place 8 months after the scan for 51-007 (36 months post-op), and at 1 month after the scan for both 51-001 (53 months post-op) and 51-003 (57 months post-op). A similar trend of gradual increase in electrode threshold over time has been observed in all the subjects including the controls (51-002, 51-005, 51-006 and 51-009).§ Denotes episodes when the subject did not undertake electrode threshold measurement as it was optional on the protocol for those time points. (Image modified from (Luo et al., 2013))

6.3.1.2 Case 2 (Subject 51-001)

This Caucasian male underwent Argus® II retinal prosthesis implantation in 2008 and had a MRI brain scan in September 2012 at 1.5T for investigation of a base of tongue tumour. Fundus photographs, OCT and electrode measurements were performed 6 months prior to and at 1 month after the MRI brain scan. Topographically, there appears to be no change in the implant position, and no associated complications such as retinal detachment on the colour fundus photograph (see Figure 6.5).

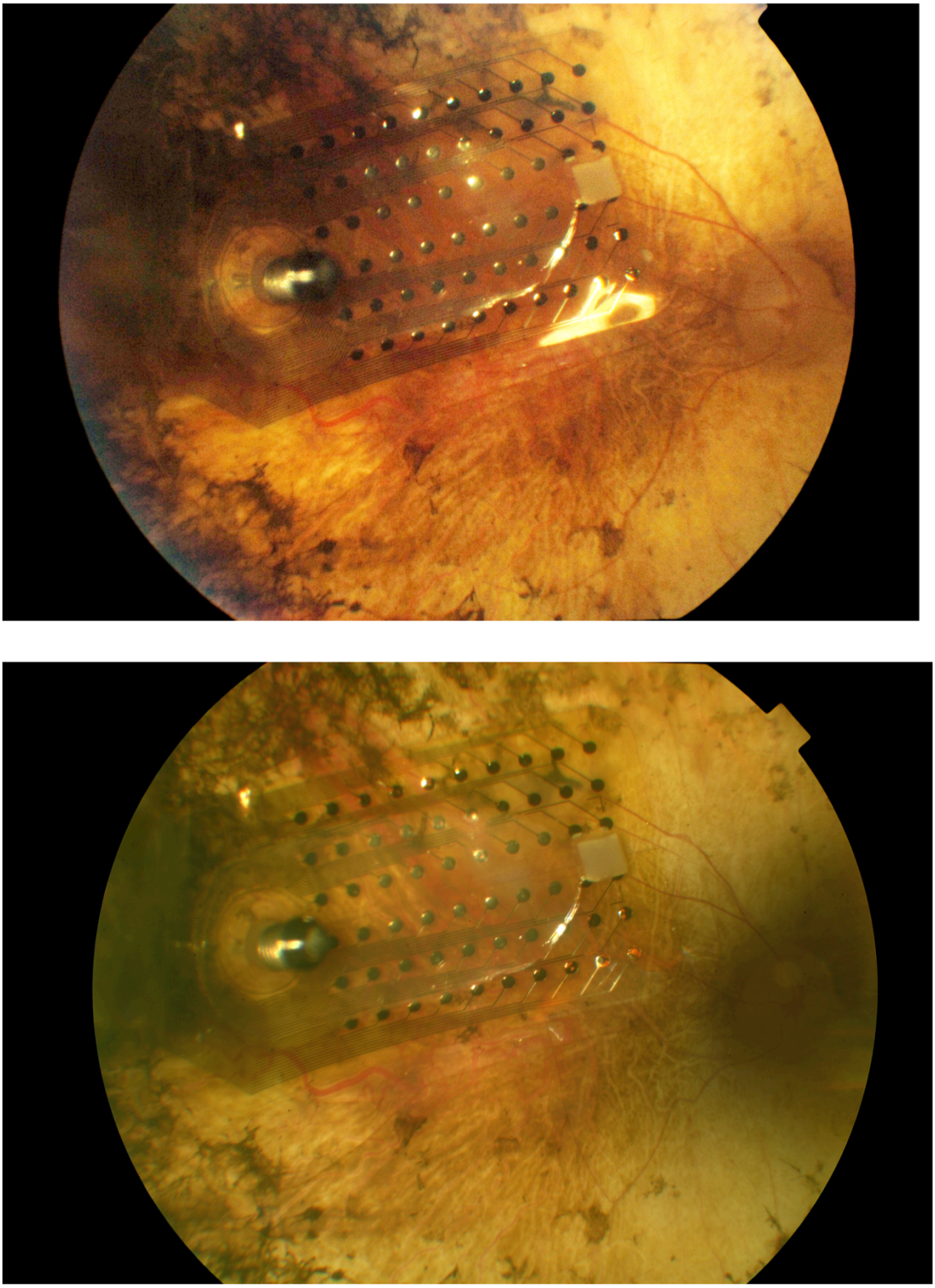

Figure 6.5: Colour fundus photographs of the right eye of subject 51-001 who received Argus® II retinal prosthesis implant in 2008. In the pre-MRI scan fundus photo (top image), the microelectrode array covers the superotemporal part of the macula. The post-MRI scan photo (bottom image) was taken 1 month after the scan, with the microelectrode array covering the same area of the macula as before. (Image modified from (Luo et al., 2013))

OCT scans showed an area of non-contact between the implant and the retinal surface, which pre-dates the MRI brain scan. This separation measured at a determined location (electrode D2) was 759μm before MRI brain scan, and remained stable post-scan, measuring 755μm (see Figure 6.6). This finding is supported by the similar distribution of the electrode impedance measurements (see Figure 6.7).

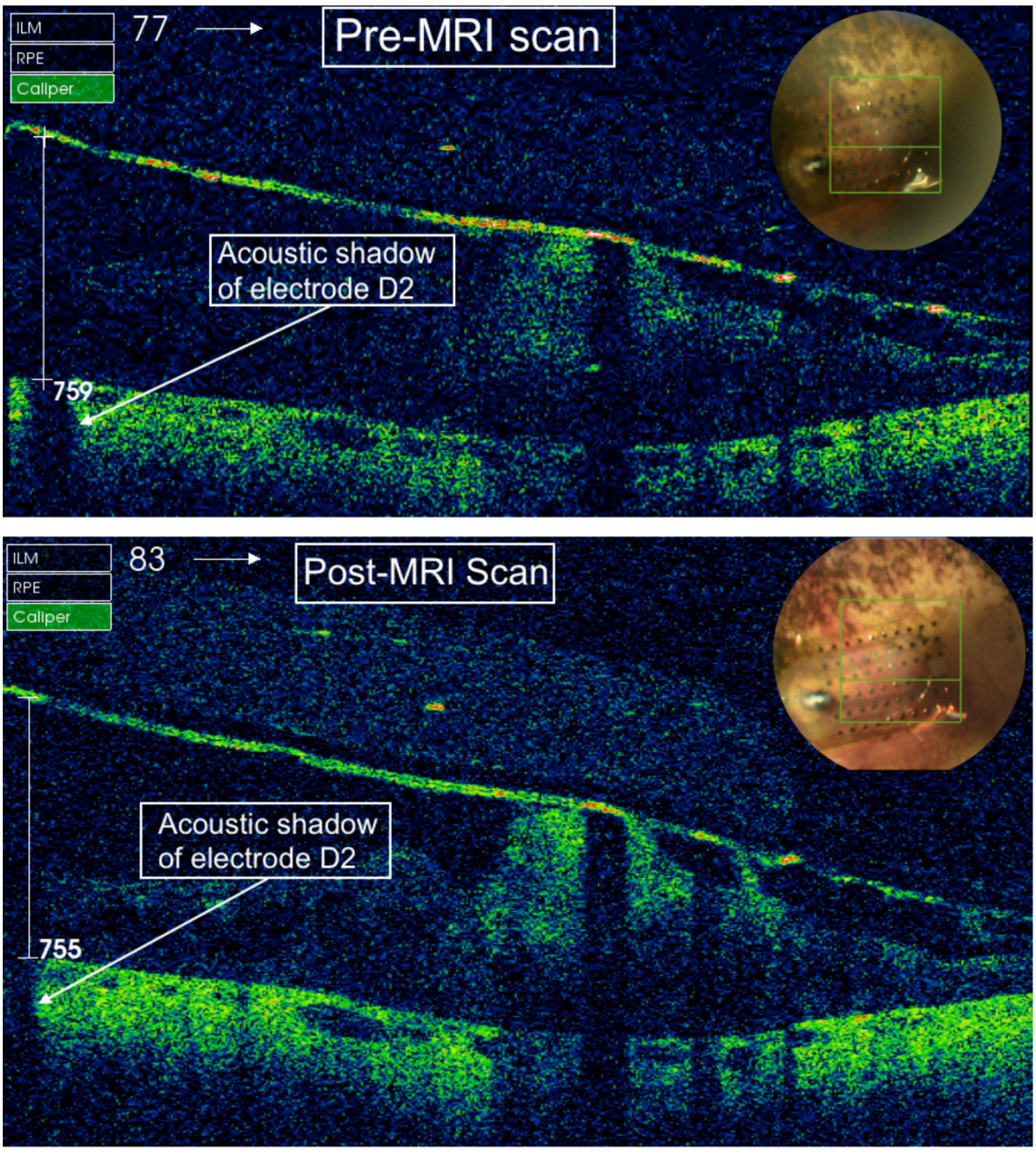

Figure 6.6: OCT image (Topcon 3D-OCT 2000) of Argus® II implant in the right eye of subject 51-001 at 6 months before the MRI brain scan (top image), and at 1 months after the scan (bottom image). In the pre-MRI OCT, the under surface of the retinal implant at electrode position D2 (second electrode of third row) was separated from the retinal surface by 759 microns. In the post-MRI OCT, the distance of retinal implant separation from the retinal surface under the electrode remained similar at 755 microns, indicating minimal change in axial position in relation to retinal surface. (Image from (Luo et al., 2013))

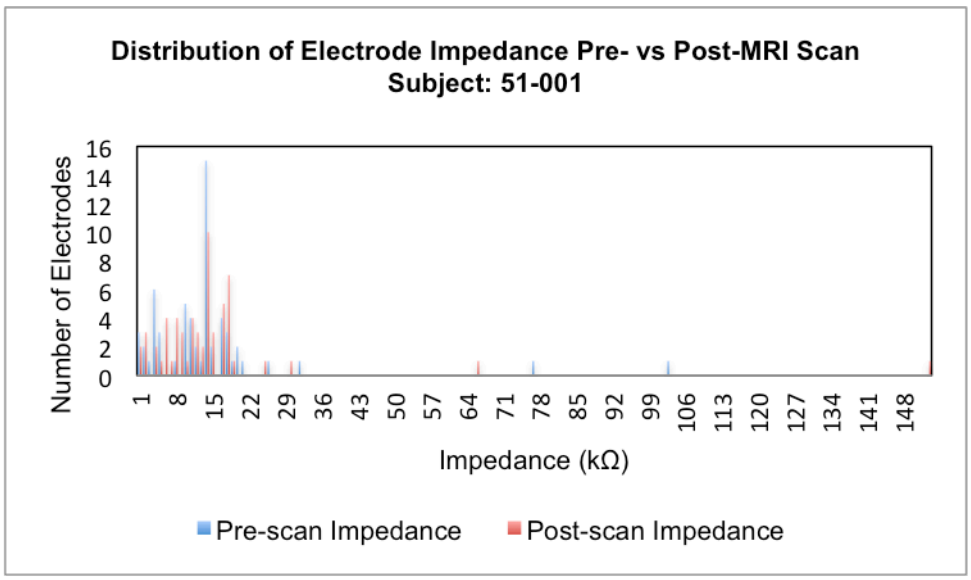

Figure 6.7: Histogram of electrode impedance distribution for subject 51-007 before and after MRI brain scan. (Image from (Luo et al., 2013))

Functionally, the electrode thresholds were also comparable before and after MRI scan, whilst exhibiting the general trend of chronological threshold increase as seen in controls (see Figures 6.4).

6.3.1.3 Case 3 (51-003)

This Caucasian male received Argus® II retinal prosthesis implantation in 2008 and underwent a MRI brain scan in September 2013 at 1.5T for investigation of a suspected cerebral vascular accident (CVA).

Fundus photographs, OCT and electrode measurements were performed 6 months prior to and at 1 month after the MRI brain scan. Similarly, there is no gross topographical change in the implant position as shown on the fundus photograph (see Figure 6.8).

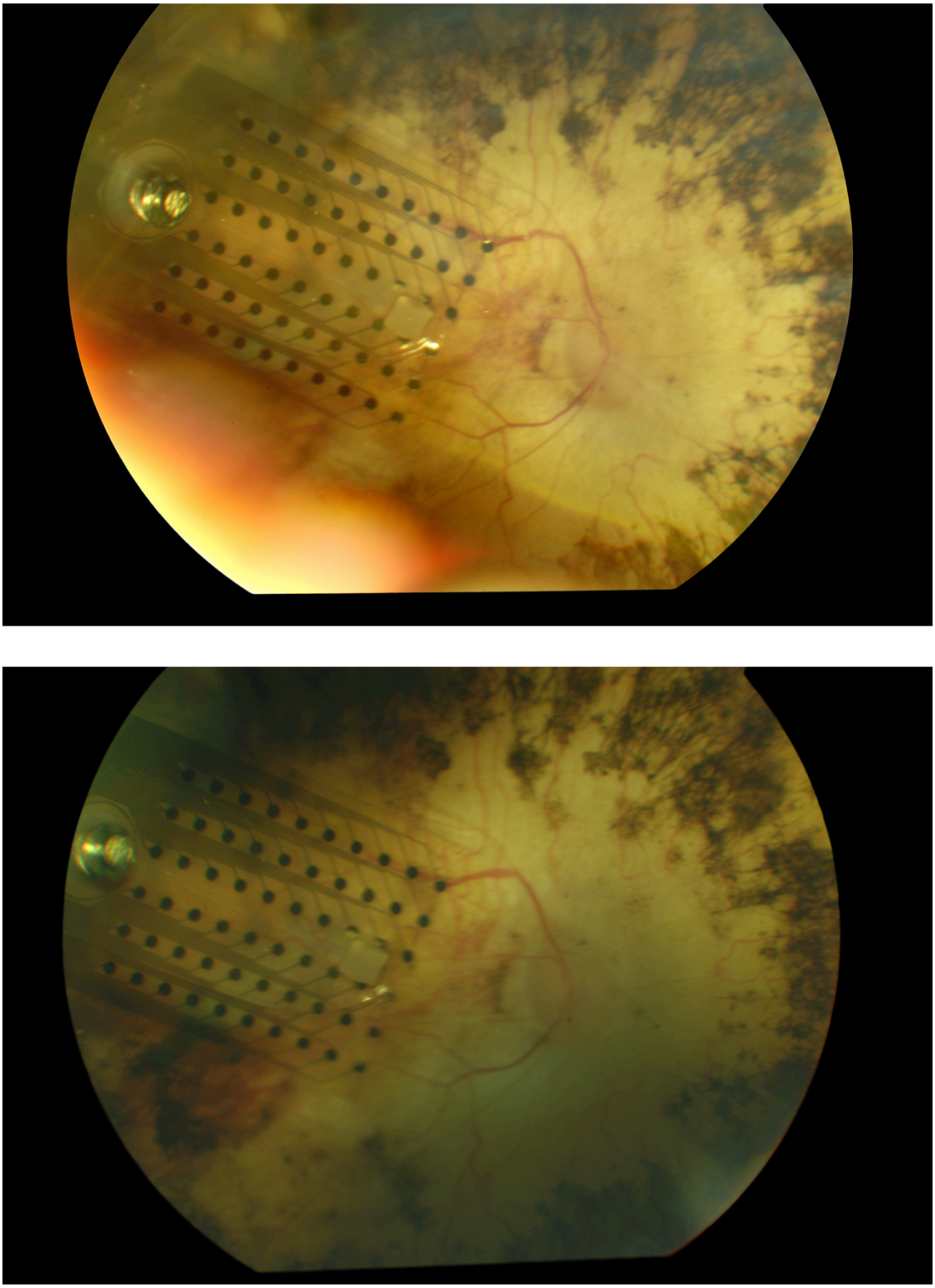

Figure 6.8: Colour fundus photographs of the right eye of subject 51-003 who received Argus® II retinal prosthesis implant in 2008. In the pre-MRI scan fundus photo (top image), the microelectrode array covers the superotemporal part of the macula. The post-MRI scan photo (bottom image) was taken 1 month after the scan, with the microelectrode array covering the same area of the macula as before.

OCT scan of the microelectrode array 6 months before and 1 month after the MRI brain scan also did not show any change in axial position, with the implant remaining in direct contact with the retinal surface both before and after the MRI brain scan (see Figure 6.9).

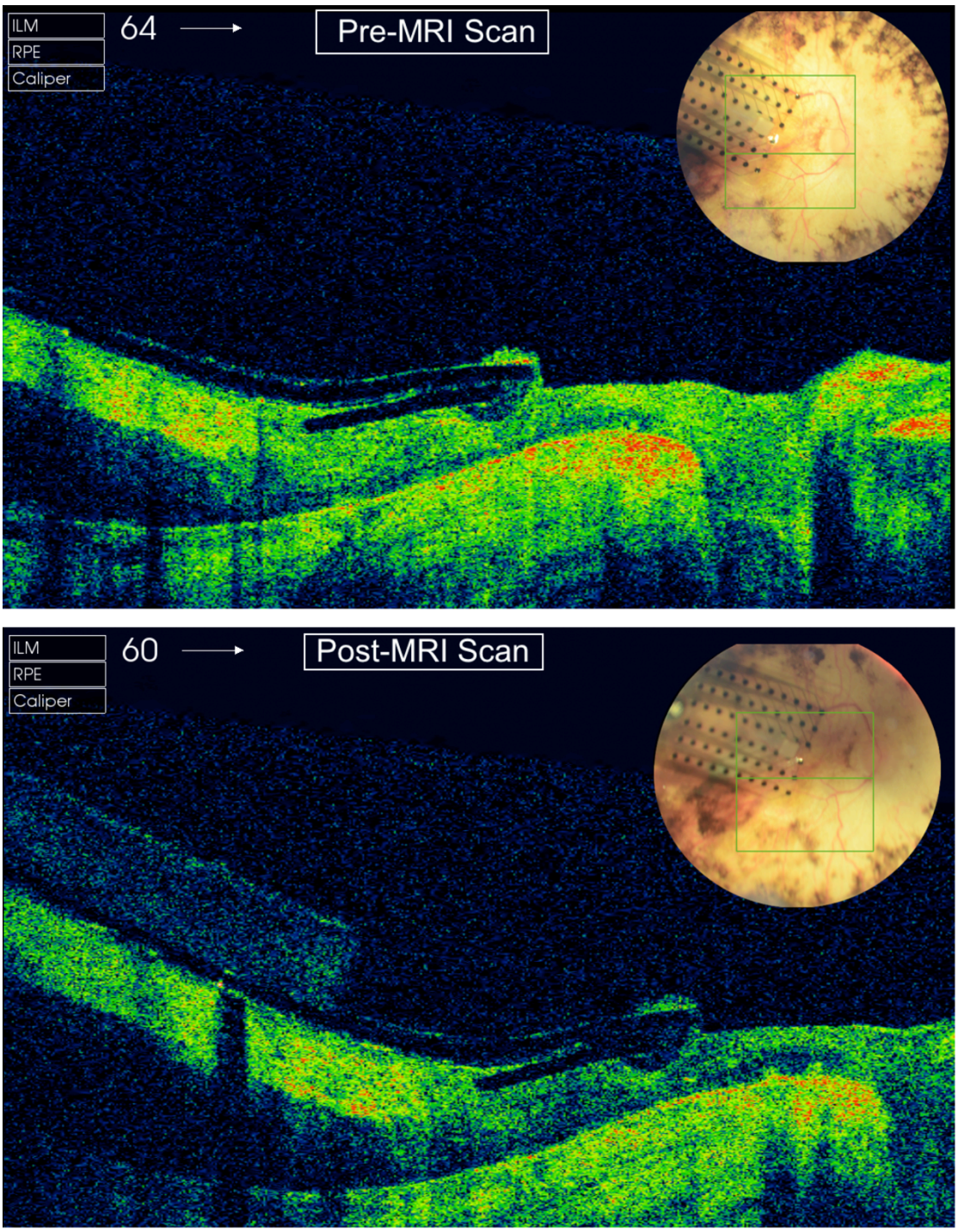

Figure 6.9: OCT image (Topcon 3D-OCT 2000) of Argus® II implant in the right eye of subject 51-003 at 6 months before the MRI brain scan (top image), and at 1 months after the scan (bottom image). In the pre-MRI OCT, the under surface of the retinal implant is closely apposed to the retinal surface, which remains so in the post-MRI OCT.

Electrode impedance measurements before and after the MRI brain scan showed a similar distribution, again indicating similar array-retina contact before and after the scan (see Figure 6.10).

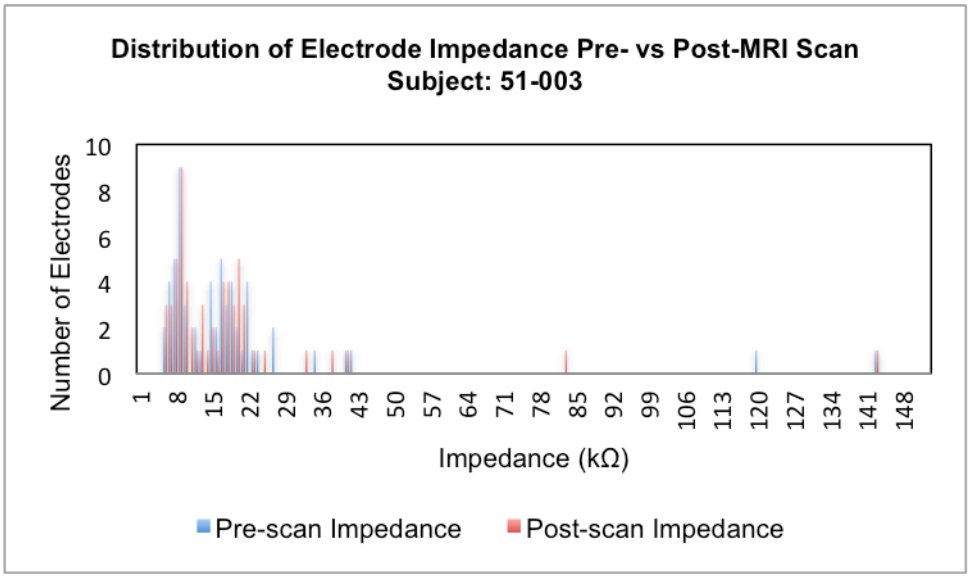

Figure 6.10: Histogram of electrode impedance distribution for subject 51-003 before and after MRI brain scan.

Functionally, as seen in the previous 2 subjects, the electrode thresholds were comparable before and after MRI scan, whilst exhibiting the general trend of chronological threshold increase as seen in controls (see Figures 6.4).

Extraocular Implant Assessment and Subjective Reports

Extraocular implant position and stability was assessed by slit lamp bimicroscopy clinical examination. There was no evidence of implant movement or extrusion through the conjunctiva in any of the 3 patients. The hermetically sealed case housing the receiving coil electronics remained unchanged in position under the subconjunctival fibrous capsule.

All 3 patients were able to carry out visual rehabilitation tasks as before the MRI scan, and did not report any subjective change in device functionality after the scan.

6.3.2 Effect of Argus® II Retinal Prosthesis on MRI

The MRI examinations were retrospectively evaluated by a consultant neuro-radiologist to assess the diagnostic quality of the imaging and related paramagnetic artifact generated from the prosthesis. The Argus® II implant produced local moderate paramagnetic artifacts at 1.5 Tesla field-strength measured maximally at 29mm x 37mm x 40mm (AP x TR x SI) (Weiland et al., 2012). This precluded clear visualisation of intra-orbital contents immediately

adjacent to the implant causing loss of signal return and anatomical distortion, but interpretation of other orbital and retro-orbital structures outside of this area was unaffected and diagnostic (see Figure 6.11).

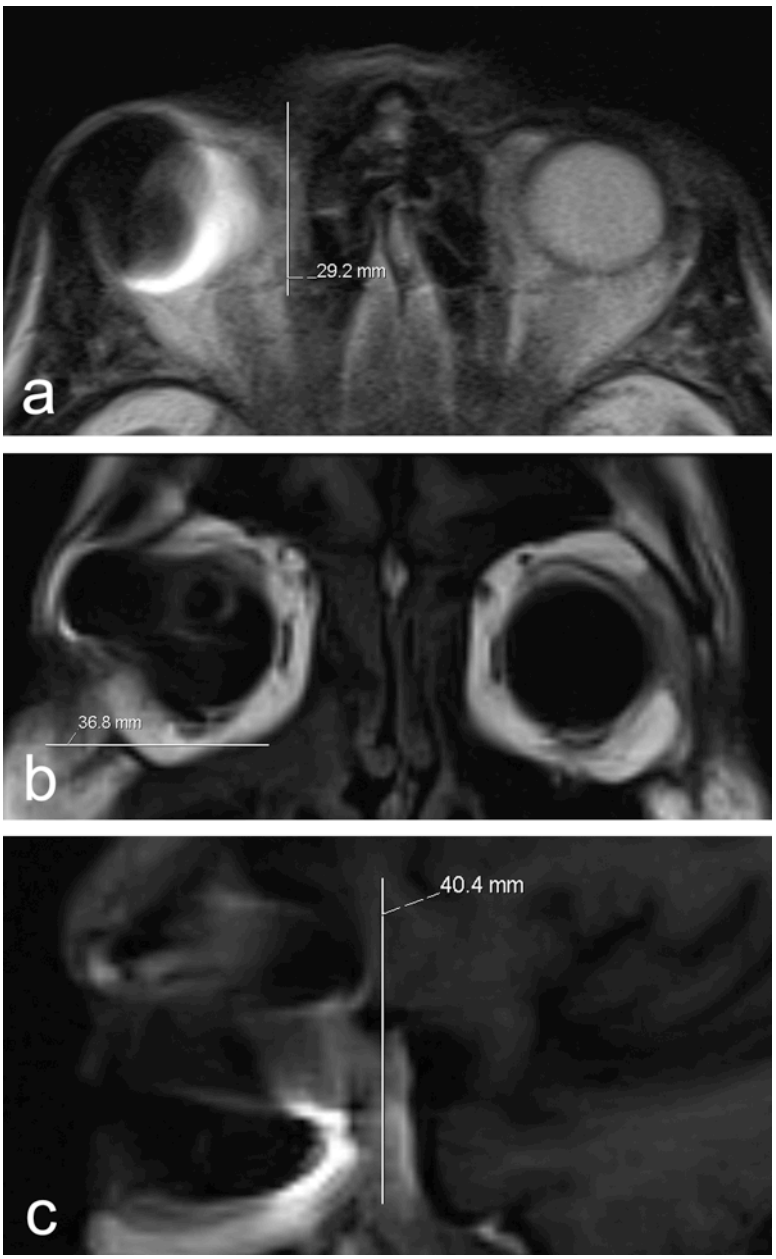

Figure 6.11: Magnetic Resonance Imaging at 1.5-Tesla with the Argus® II retinal implants in the right eye of a patient, on a) axial T2-weighted, b) coronal T1-weighted and c) sagittal T1-weigthed acquisitions. The measurements are the maximal dimensions of the artifact (in millimeters) in the anterior-posterior (AP), transverse (TR) and superior-inferior (SI) planes. (Image from (Luo et al., 2013))

6.4 Conclusion

In this study, we reported on 3 patients who underwent MRI brain scan at 1.5T with Argus® II retinal prosthesis in-situ. There appears to be no detrimental effect to the patients and their implant function with the scan. The implant position remained stable in all 3 patients after the MRI brain scan, as assessed topographically by colour fundus photography, axially by OCT scan, and

electrically by electrode impedance measurements. The device function also remained robust after the MRI brain scan, as shown objectively with the electrode threshold measurement, as well as from the patients' subjective reports.

The Argus® II implant produces an artifact of around 50mm x 50mm in size which would prevent visualisation of structures within the orbit, but visualisation of surrounding tissues outside these areas are unaffected. Further investigations into other safety issues such as the potential of generating electrical outputs to the retina during MRI scanning, with a greater number of samples would be required to fully determine the safety of MRI brain scan in Argus® II patients.

Chapter 7

Functional Near Infra-red Spectroscopy (fNIRS) Imaging of Primary Visual Cortical Activation

7.1 Introduction

In the previous chapters, we have demonstrated that the Argus® II retinal prosthesis system is capable of improving the visual function in extremely low vision patients who suffered from end stage outer retina diseases. However this visual improvement, particularly in terms of form vision(daCruz et al., 2013; Luo and daCruz, 2016) (see **chapter 3**), is highly variable amongst the subjects. This could in part be due to the variability in the specific phosphene characteristics experienced by individual subjects (Luo et al., 2016) (see **chapter 5**), as well as the unpredictable phosphene persistence in relation to stimulation duration (Pérez Fornos et al., 2012).

As discussed earlier in **chapter 5**, one possible explanation for these phosphene variances could be secondary to retinal remodelling and aberrant nerve regeneration within the severely diseased retina (Marc et al., 2007; 2003) (Jones et al., 2012; Jones and Marc, 2005). Furthermore, due to the prolonged period of blindness (all the subjects in our study have been blind for many years if not decades prior to receiving the retinal implant), it is likely that some form of cortical neural remodelling, or indeed colonisation of the primary visual cortex by other sensory modalities, may have occurred (Bavelier and Neville, 2002). It has been shown with cochlear implants that in deaf individuals with extensive cross-modal plasticity of the auditory cortex, the benefit of the implant is limited (Chen et al., 2016; Lee et al., 2001). As such, characterisation of the integrity of the primary visual cortex in blind patients, as well as demonstration of continual neural recruitment in the multimodal association areas (of the parietal cortex) in response to retinal stimulation, could be important predictive indicators of functional outcome in future retinal or other visual prosthetic implants.

To achieve this ambition, the pre-requisite is to identify a reliable way of measuring real-time activation of the primary visual cortex in response to retinal stimulation. Following demonstration of the safety of performing MRI brain scans in **chapter 6** (Luo et al., 2013), functional MRI would seem the imaging modality of choice for this study. However, safety of MRI brain scans in Argus® has only been demonstrated with the Argus® II device switched off during the scan, excluding the external image-capture and stimulating components. Secondly, on further discussion with our medical physicist collaborators from

University College London (UCL), there are concerns that the radiofrequency waves of the Argus® II system telemetry may be in the same wavelength spectrum as that of the radiofrequency pulse generating MRI scan signals, resulting in interference. As such, alternative method of measuring real-time cortical activation was sought.

In this study, we set out to explore the feasibility of using functional near infra-red spectroscopy (fNIRS) imaging as a mean of monitoring primary visual cortex activity, in response to direct retinal stimulation with the Argus® II retinal prosthesis.

7.2 Methods

7.2.1 Subject Inclusion / Exclusion Criteria

This is a single-centre prospective study. All 6 subjects who took part in the phosphene characterisation study (Luo et al., 2016) in **chapter 6** also took part in this study. These included all but one of the 7 subjects from Moorfields Eye Hospital NHS Foundation Trust implanted with the Argus® II retinal prosthesis system as part of the phase I/II clinical trial (clinicaltrials.gov Identifier: NCT00407602). One subject was excluded as his device ceased to function after developing retinal detachment and a thick epiretinal membrane as a result of a fall. The participating subjects' demographic features and operation dates are as previously shown in Table 5.1 in **chapter 5**, and are presented here in Table 7.1 below. All but one subject (51-003) are right-handed according to the Edinburgh Handedness Inventory (Oldfield, 1971). The study was approved by the local ethics committee, and adhered to the tenets of the Declaration of Helsinki.

Subject ID	Diagnosis	Year of Operation	Age at Time of Operation (yrs)	Hand dominance
51-001	Retinitis Pigmentosa	2008	70	Right-handed
51-003	Retinitis Pigmentosa	2008	72	Left-handed
51-005	Retinitis Pigmentosa	2009	55	Right-handed
51-006	Choroideremia	2009	66	Right-handed
51-007	Retinitis Pigmentosa	2009	63	Right-handed
51-009	Retinitis Pigmentosa	2009	45	Right-handed

Table 7.1: Demographics and operation dates of the Argus® II subjects who participated in the fNIRS Study.

7.2.2 Functional Near Infra-red Spectroscopy (fNIRS) Imaging

In functional near infra-red spectroscopy (fNIRS), the relative transparency of human brain tissues to light in the near infra-red (NIR) spectrum (650 – 1000nm) (Jobsis, 1977) is exploited to allow real-time measurement of changes in the concentration of oxygenated haemoglobin (O_2Hb) and deoxygenated haemoglobin (HHb) in blood as it passes through small vessels (<1mm in diameter) in the brain (Ferrari and Quaresima, 2012; Scholkmann et al., 2014). Typically, light sources emitting two NIR wavelengths are utilised: one wavelength is selected to have high absorbance by oxygenated haemoglobin, while the other is preferentially absorbed by deoxygenated haemoglobin. By placing NIR detectors at pre-determined distances from the NIR light sources, the local concentration of O_2Hb and HHb of the medium (in this case human brain tissues) can be calculated from the modified Beer-Lambert Law (Delpy et al., 1988):

$$A = -\log\left(\frac{I}{I_0}\right) = (c \times \varepsilon_\lambda \times l \times DPF) + G$$

where A is the absorbance of the NIR by the medium; I_0 is the initial intensity of the incident light (i.e. NIR emitted by the light sources), I is the intensity of the transmitted light after it leaves the medium (as measured by the NIR detectors); c is the density of the medium; ε is the molar extinction coefficient characteristic of the medium for a light of wavelength λ; l is the distance that the light travels in the medium (which corresponds to the light source-detector distance); DPF is

the differential pathlength factor that accounts for the non-linear trajectory of light in biological media; and G is the scatter (Gervain et al., 2011).

There are 3 main techniques in performing fNIRS: a) continuous-wave (CW) modality; b) frequency-domain (FD) modality; and c) time-domain (TD) modality. The CW modality consists of a constant illuminating light source, and the light attenuation through brain tissues is measured. This technique, though relatively straightforward to perform, does not measure DPF and G, and as such cannot provide absolute values of O_2Hb and HHb concentrations. Instead, changes in the O_2Hb and HHb concentrations relative to a baseline resting levels are measured. In FD modality, the intensity of the light is varied at a certain frequency and the resultant phase difference and intensity attention as the light travels through the brain tissues can be analysed to calculate the DPF and G. The TD modality on the other hand, employs single light pulses and the DPF is calculated from the average time-of-flight of photons as individual photons travel through the brain tissues. Both FD and TD techniques therefore provide absolute value measurements of O_2Hb and HHb concentrations in the medium as DPF and G values can be obtained. However, as both FD and TD techniques require much lower sampling rate, longer acquisition time and higher cost than CW modality, and for the purpose of research, relatively changes in O_2Hb and HHb concentrations provide adequate information on cortical activation, CW modality has become the most widely employed technique in research studies with well-established data (Ferrari and Quaresima, 2012). The following study is performed with the CW technique, and FD and TD modality will not be discussed further.

With the CW technique, the relative changes in the concentration of O_2Hb and HHb (rather than absolute values) are calculated using:

$$\Delta A = ((\Delta c_{oxy} \times \varepsilon_{\lambda_{oxy}}) + (\Delta c_{deoxy} \times \varepsilon_{\lambda_{deoxy}})) \times l \times DPF$$

whereby Δc_{oxy} and Δc_{deoxy} are changes in the concentration of oxygenated and deoxygenated haemoglobin respectively. By performing measurements using two wavelengths, thereby yielding two equations, the values of c_{oxy} and c_{deoxy} can be calculated from the change in absorbance (ΔA).

The penetrance of NIR light through tissue is calculated to be approximately between a quarter to three-quarters of the light source-detector distance (Gratton et al., 1994). The recommended source-detector distance is therefore between 2 – 3cm, so as to offer a good balance between topographical spatial resolution and tissue penetrance.

During activation of a cortical area, due to the physiological neurovascular coupling (NVC) response (Obrig et al., 2000; Sandman et al., 1984), there is an initial rise in oxygenated haemoglobin level (from increased influx of oxygenated haemoglobin to the area), which then falls with time. This is mirrored by an opposite but smaller change in deoxygenated haemoglobin level (see Figure 7.1). By placing an array of alternating source and detector optodes over the scalp of the occipital lobe, one can measure the underlying NVC response, hence cortical activation, of the primary visual cortex (see Figure 7.2).

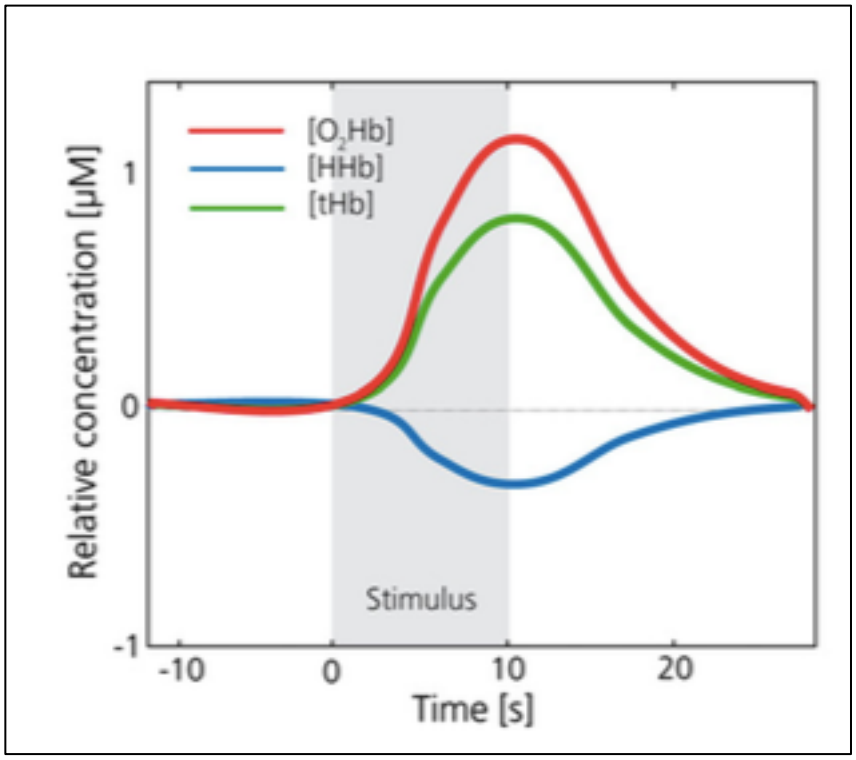

Figure 7.1: A sketch of an optode channel showing typical haemodynamic response in cortical activation. There is a statistically significant increase in the O2Hb level, matched by a statistically significant decrease in the HHb level following stimulation, before returning to baseline. (Image from (Scholkmann et al., 2014))

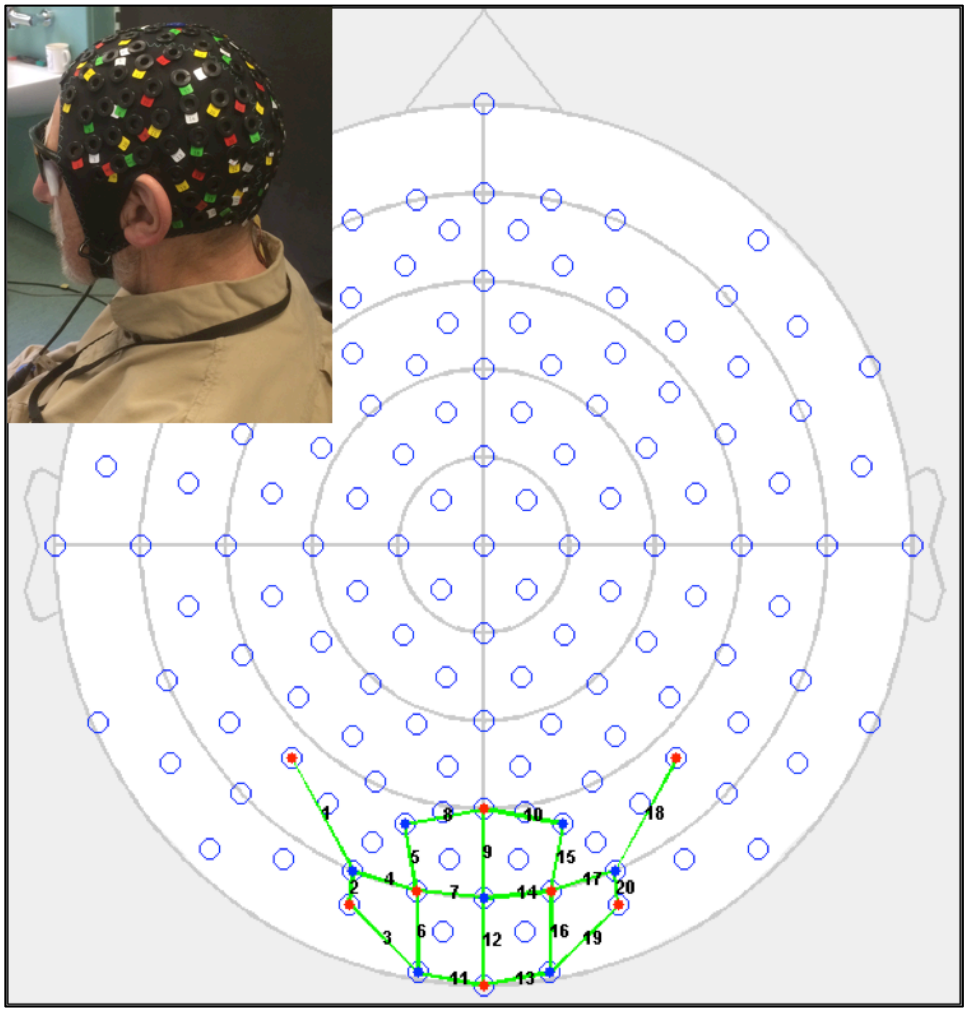

Figure 7.2: A schematic drawing based on the international electroencephalography (EEG) 10-5 system cap (Jurcak et al., 2007) showing optode arrangements for measuring visual cortex activity using the NIRScout system. The red dots denote the locations of NIR light sources; the blue dots denote the locations of the NIR detectors. The green lines represent optode channels between a specific light source and detector whereby local changes in O_2Hb and HHb concentrations can be measured. The channels are numbered as shown for data collection. The source-detector distance is 3 cm. A total of 20 optode channels are present in this arrangement. Photograph of a subject wearing the optode retaining cap is shown in the top left inset.

All the fNIRS measurements were performed using the NIRScout imaging system (NIRx® Medical Technologies, LLC, New York, USA) with 8 sources and 7 detectors at a sampling rate of 7.81Hz. The LED sources emitted fixed NIR wavelengths of 760nm and 850nm. During each experiment, the Argus® II retinal prosthesis stimulations were programmed using a purpose written script (Matlab 8.6.0.267246, R2015b, The Mathworks Inc, Massachusetts, U.S.A) and routed through the NIRScout system to be read by the data acquisition program

(NIRStar 12.4), to ensure the timing of prosthesis stimulation was recorded accurately for data analysis.

With the aid of a retaining cap akin to an electroencephalography (EEG) 10-5 system cap, all the light sources and detectors (optodes) were arranged to overlie the occipital region as shown in Figure 7.2 and Figure 7.3, for recording of fNIRS signals of the primary visual cortex. The source-detector distance is 3 cm. A total of 20 optode channels are available for data collection and analysis in this arrangement.

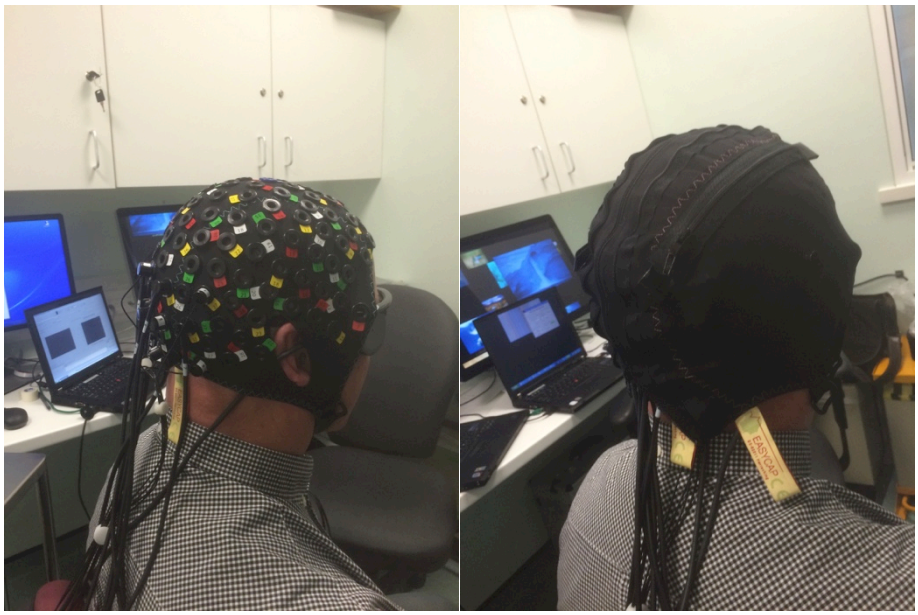

Figure 7.3: Colour photographs showing an Argus® II subject undertaking fNIRS imaging of his primary visual cortex. The retaining cap akin to an EEG cap was worn over the Argus® II retinal prosthesis system. The optodes were placed into the appropriate optode holders as shown in Figure 7.2 (left image). An over cap was then placed over the EEG cap to ensure good optode contact with the scalp and reduce light pollution during the study (right image).

7.2.3 Experiment Design

To assess the feasibility of fNIRS as a tool of capturing visual cortex activation in response to retinal stimulation with Argus® II retinal prosthesis, we employed the classical block design (Gervain et al., 2011) to evaluate the fNIRS response under 3 different stimulation conditions (see Section 7.2.4). Each block consists of a stimulation followed by a rest period of no stimulation, to allow the haemodynamic response function (HRF) to return to the baseline level. For each experiment, 10 blocks of stimulation were repeated, and the average

NIRS response across the blocks were analysed to reduce the background noise and increase the strength and reliability of the signals (see Figure 7.4).

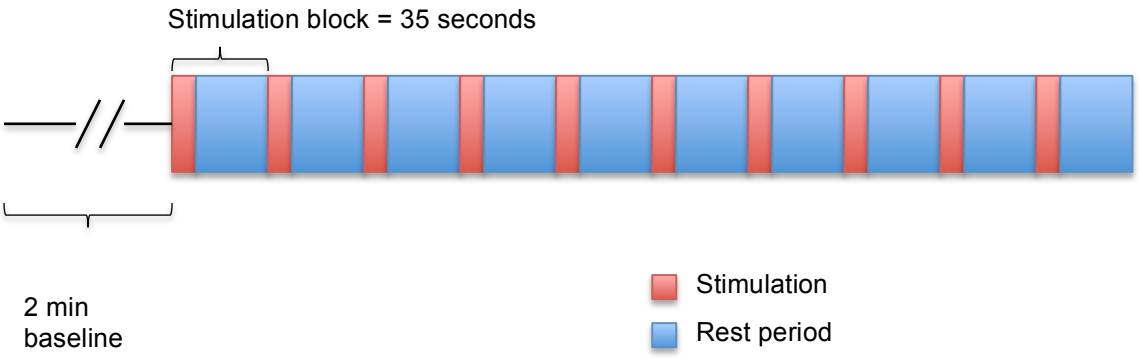

Figure 7.4: Schematic drawing of the experiment design. Each experiment started with recording 2 minutes of fNIRS response without any stimulation to establish the baseline O_2Hb and HHb concentrations, before leading on to 10 repeat stimulation blocks. Each stimulation block consisted of a specified stimulation followed by 35 seconds of rest period during which the haemodynamic response returned to baseline, before ensuing the next stimulation block. The fNIRS responses across the 10 stimulation blocks were then averaged during data analysis, to reduce the background noise and strengthen the signal reliability in each experiment.

Given the relatively short pulse stimulation duration with the Argus® II system electrodes set by the proprietary software (250ms at the frequency of 20Hz), and the small delay in haemodynamic response (typically around 5 seconds) to visual stimulation previously established in normal sighted humans (Colier et al., 2001; Kato et al., 1993; Wenzel et al., 1996), we set the stimulation block to 35 seconds. At the beginning of each experiment, we also recorded the fNIRS response for 2 minutes without any stimulation, to establish the resting period (baseline) O_2Hb and HHb concentrations, from which the relative change in the concentrations can be recorded and calculated.

7.2.4. Stimulation Conditions

Three stimulation conditions were employed in each subject, to explore if there is any variation in the fNIRS signals with varying degrees of retinal stimulation by the Argus® II retinal prosthesis.

The position of each electrode in the 6 x 10 Argus® II array is designated alphabetically by row (A to E), and numerically by column (1 to 10) as shown below in Figure 7.4 (also see **chapter** 5, Figure 5.1).

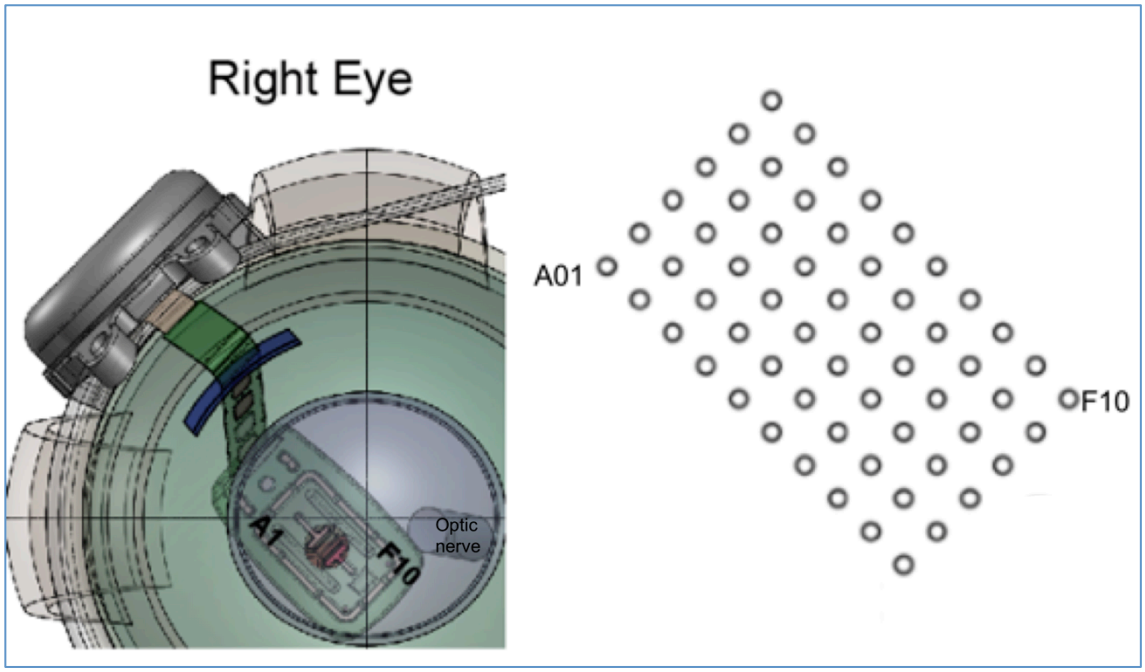

Figure 7.5: Schematic drawing of an Argus® II retinal prosthesis microelectrode array on the retinal surface, with a magnified view of the electrode array on the right. The position of each electrode is designated alphabetically by row (A to E) and numerically by coloum (1 to 10). The position of electrode A01 and F10 are as labelled.

Condition 1

In the first stimulation condition, we chose a cluster of 4 electrodes (hereinafter referred to as a quad) closest to the fovea for stimulation in each subject. This area is chosen as the fovea is represented by a large region of the primary visual cortex near the occipital pole, so much so that around 20cm^2 of surface area in each hemisphere of the occipital lobe is allocated to just the central 2˚ of visual field (Dougherty et al., 2003). The stimulating quad electrodes and parameters that elicited clear and consistent visual precepts closest to the fovea (i.e. foveal quad) in each subject were previously established (see **chapter 5**, table 5.2) (Luo et al., 2016) and are shown here in table 7.2.

Subject ID	Foveal Quad	Threshold (μA)	Stimulating Current (μA)	Phosphene Features	Phosphene Duration, t (s)
51-001	C07C08 D07D08	137	277	White filled-in circle	0.5 < t < 1
51-003	A07A08 B07B08	250	350	Electric blue filled-in circle	t < 0.5
51-005	E05E06 F05F06	137	237	Bluish-grey vertical line, with fizzy vertical edges	t < 0.5
51-006	A07A08 B07B08	371	552	Yellow “7” shape	0.5 < t < 1
51-007	E07E08 F07F08	24	124	Orange filled-in ring which ripples out	0.5 < t < 1
51-009	E07E08 F07F08	97	124	Orange horizontal lines x 2, with fizzy brightness in between the lines	0.5 < t < 1

Table 7.2: The chosen quad electrodes (closest to the estimated fovea location) and the stimulating parameters for each subject in Condition 1 (Table modified from (Luo et al., 2016)). The phosphene features were as reported verbally by each subject, and remained consistent throughout the study.

Condition 2

To investigate how increasing the area of retina stimulated would be reflected in the fNIRS signals at the primary visual cortex, we stimulated a total of up to 6 quads simultaneously in each subject. This included the initial foveal quad in Condition 1, as well as 5 other quads surrounding the foveal quad. Due to the constraint by the safety charge density limit of the electrode array (to prevent tissue damage), the stimulating current we applied for each quad when they were stimulated simultaneously was much lower than when each quad was stimulated separately.

The chosen quads for simultaneous stimulation and their stimulating parameters for each subject were as shown in Table 7.3.

Subject ID	6 Quads Stimulated in Condition 2 & 3	Stimulating Current per quad for Condition 2 (μA)	Stimulating Current per quad for Condition 3 (μA)
51-001	A08B07B08* C05C06D06* C07C08D07D08 E07E08F07F08 ***	155	360 360 320 335 N/A
51-003	A06B05B06* A07A08B07B08 A09A10B09B10 C05C06D05D06 C07C08D07D08 C09C10**	80	350
51-005	03D03D04* C05D05C06D06 C07C08D08* E03F03E04F04 E05F05E06F06 E07F07E08F08	50	237
51-006	A05B06** A07B07A08B08 A09B09A10B10 C05D05C06* C07D07C08D08 C09D09C10D10	110	552
51-007	C05C06D05* C07C08D07D08 C09C10D09D10 E06F05F06* E07E08F08* E09E10F09F10	45	124
51-009	C05C06D06* C07C08D07D08 C09C10D09D10 E06F06** E07E08F07F08 E09E10F09F10	30	124

Table 7.3: This table shows the chosen group of 6 quads stimulated simultaneously (in Condition 2) or sequentially (in Condition 3) for each subject during the study. The stimulating parameters for each Condition are also shown. When all the quads were stimulated at the same current under the condition, only one figure is shown. When the individual quads were stimulated at different currents, the stimulating current for each quad was shown (subject 51-001 Condition 3).

* denotes an electrode within the selected quad has been disabled as its threshold exceeded the safety density charge, and/ or its supra-threshold stimulation caused discomfort in the subject.

** signifies that 2 electrodes within the selected quad have been disabled for the above mentioned reasons.

*** only 4 quads were stimulated in subject 51-001 as the remaining quads of his Argus® II system were not functioning.

Condition 3

The same chosen group of 6 quads were also stimulated sequentially (foveal quad first, followed by the 5 surrounding quads in clock-wise manner) in Condition 3, to evaluate the fNIRS signals in response to moving retinal stimulations. Even though the stimulation duration of each pulse lasts only 250ms (as set by the Argus® II system proprietary software), due to built-in safety features and delay in the radio frequency link transmission between the external and internal coil of the device, the inter-stimuli interval was around 1 second. The stimulation duration in each block therefore lasted around 6 seconds, leaving 29 seconds for HRF recovery. The stimulating parameters in Condition 3 for each subject were as shown in Table 7.3.

7.2.5 Data Analysis

All data were exported from NIRScout as raw data of O_2Hb and HHb concentration levels and loaded into Matlab (version 8.6.0.267246, R2015b, The Mathworks Inc, Massachusetts, U.S.A) for further processing and analysis. A 3rd order low pass Butterworth digital filter was first applied, with the cut off frequency at 0.08 Hz, to suppress background and other high frequency noise such as heartbeats. The filtered signals were then decimated from the original sampling rate of 7.81Hz to 1Hz and detrended to remove the slow drift.

The fNIRS responses from the 10 stimulation blocks were averaged to get a mean change in the concentrations of both O_2Hb and HHb with time within the averaged block. From the averaged block, we selected the last 10 seconds (before the next stimulation) as the resting window. The resting (baseline) O_2Hb and HHb concentration levels were calculated as the mean of the respective values over the resting window. We then selected the 10 seconds after the initial 5 seconds delay (i.e. time frame of 5s to 15s after stimulation) as the active window. The values of the activated O_2Hb and HHb concentration levels were calculated as the mean of the respective values over the active window.

A positive fNIRS response in an optode channel is defined as a statistically significant difference (either an increase or decrease) between the mean baseline and the mean activated O_2Hb and HHb levels (paired T-test, $p < 0.05$) (Gervain et al., 2011). A Matlab script (version 8.6.0.267246, R2015b, The

Mathworks Inc, Massachusetts, U.S.A) was written to carry out the above analysis for each of the 20 optode channels in each experiment.

7.3 Results

7.3.1 Active Optode Channels per Subject

A graph of changes in O_2Hb and HHb concentration levels with time was automatically generated by Matlab when an optode channel showed a positive fNIRS response (as defined above). These active optode channels were mapped topographically on to a schematic drawing of the occipital lobe of the head to aid visualisation of the activated cortical region. The locations of the NIR sources were shown as red dots; the blue dots represented the locations of the detectors; and the active optode channels were shown as a green line labelled with the corresponding channel number. For each subject, the topographical map of optode channel activation and their respective O_2Hb and HHb concentration graphs were presented for all the 3 stimulation conditions.

51-001

Condition 1: Foveal Quad Stimulation

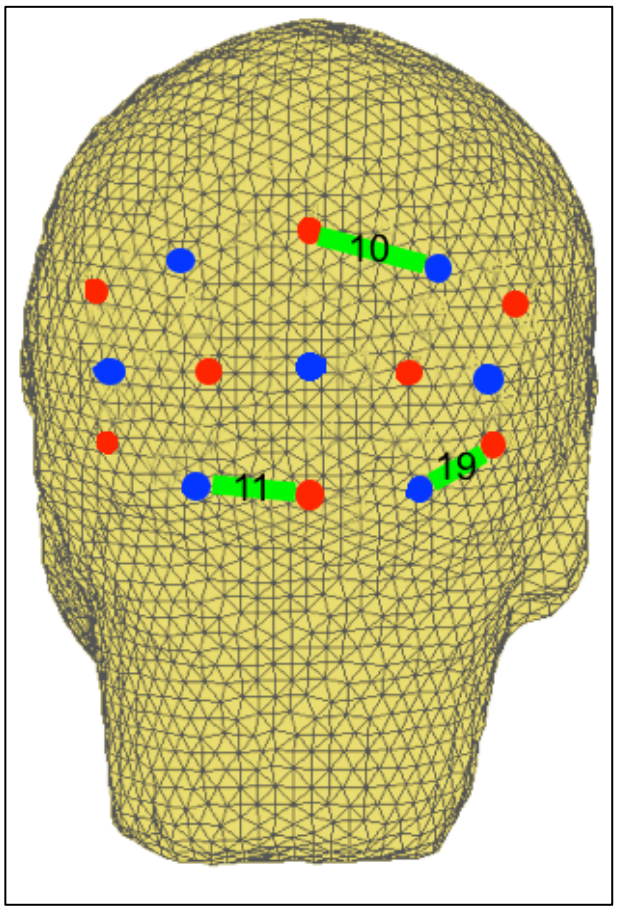

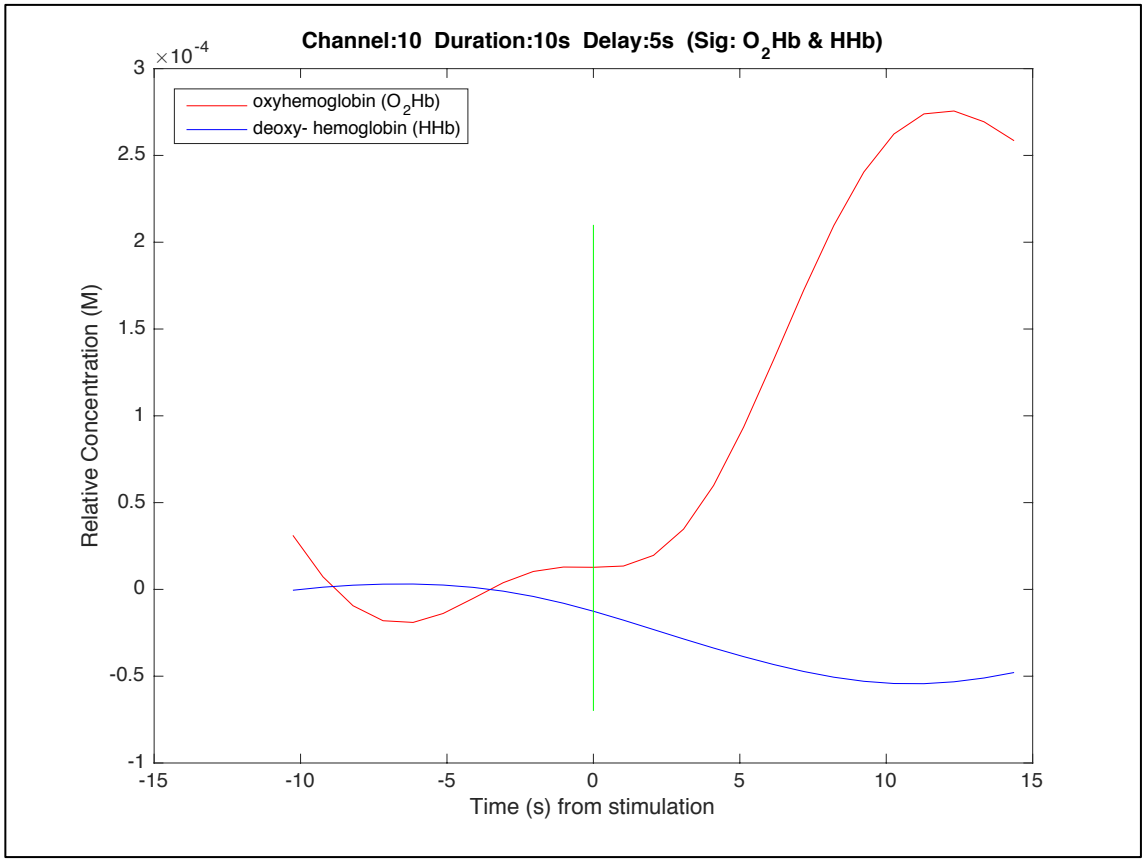

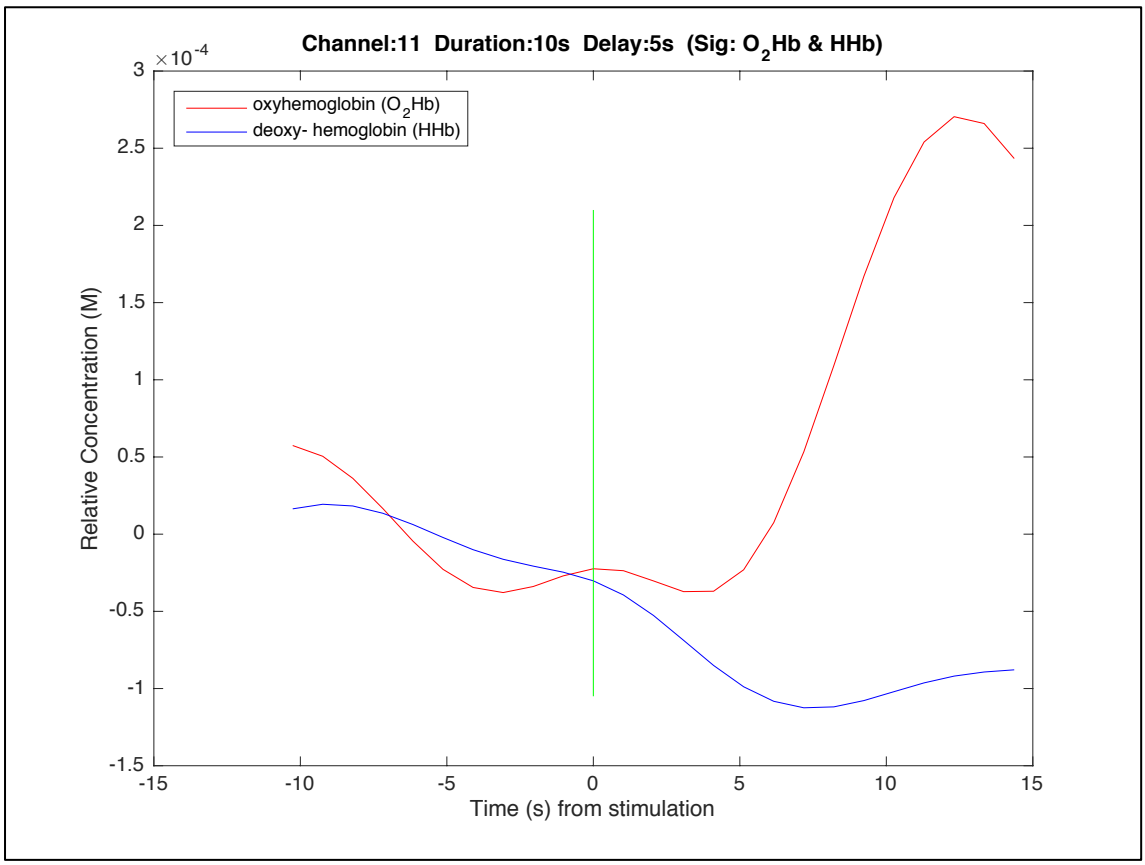
Channel:11 Duration:10s Delay:5s (Sig: O2Hb & HHb)
×10-4
oxyhemoglobin (O2Hb)
deoxy- hemoglobin (HHb)
Relative Concentration (M)
Time (s) from stimulation

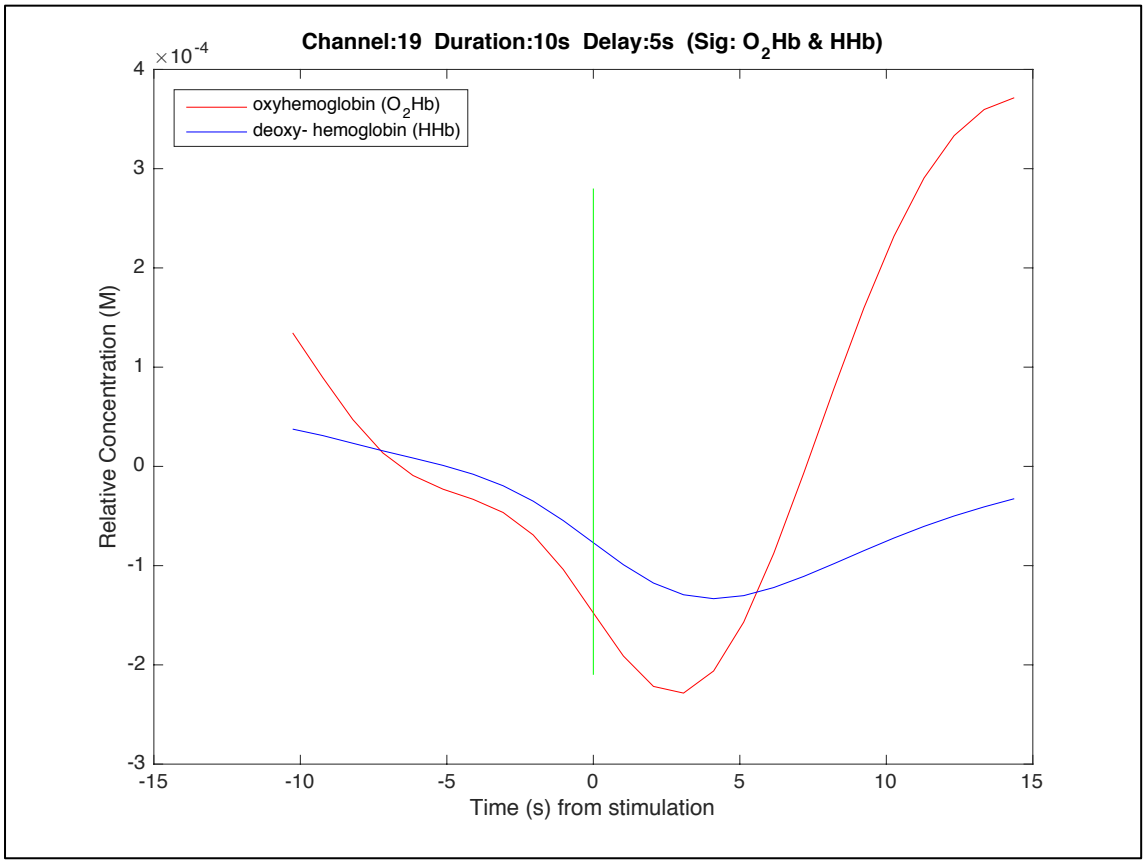
Channel:19 Duration:10s Delay:5s (Sig: O2Hb & HHb)
×10-4
oxyhemoglobin (O2Hb)
deoxy- hemoglobin (HHb)
Relative Concentration (M)
Time (s) from stimulation

Condition 2: Simultaneous Stimulation of 6 Quads

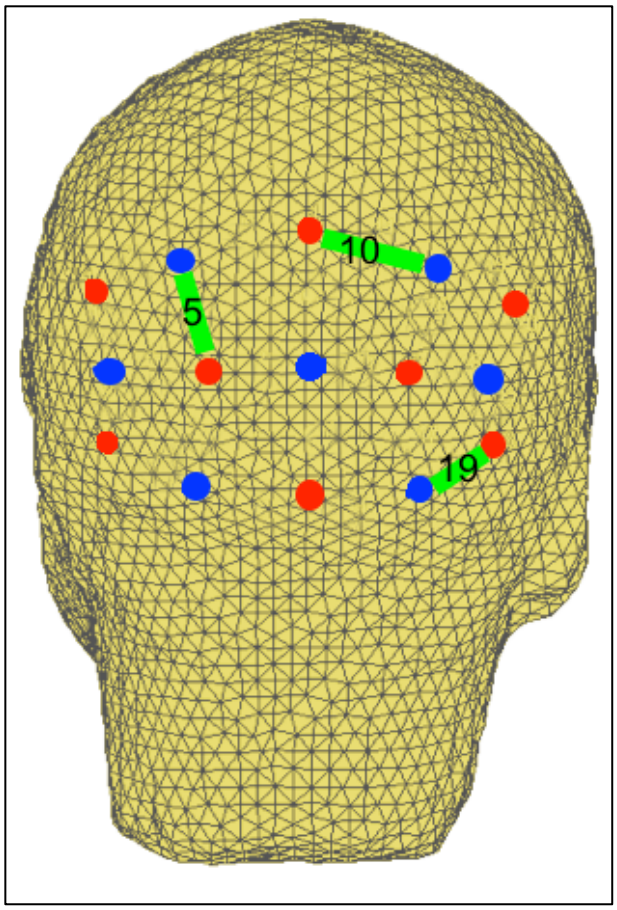

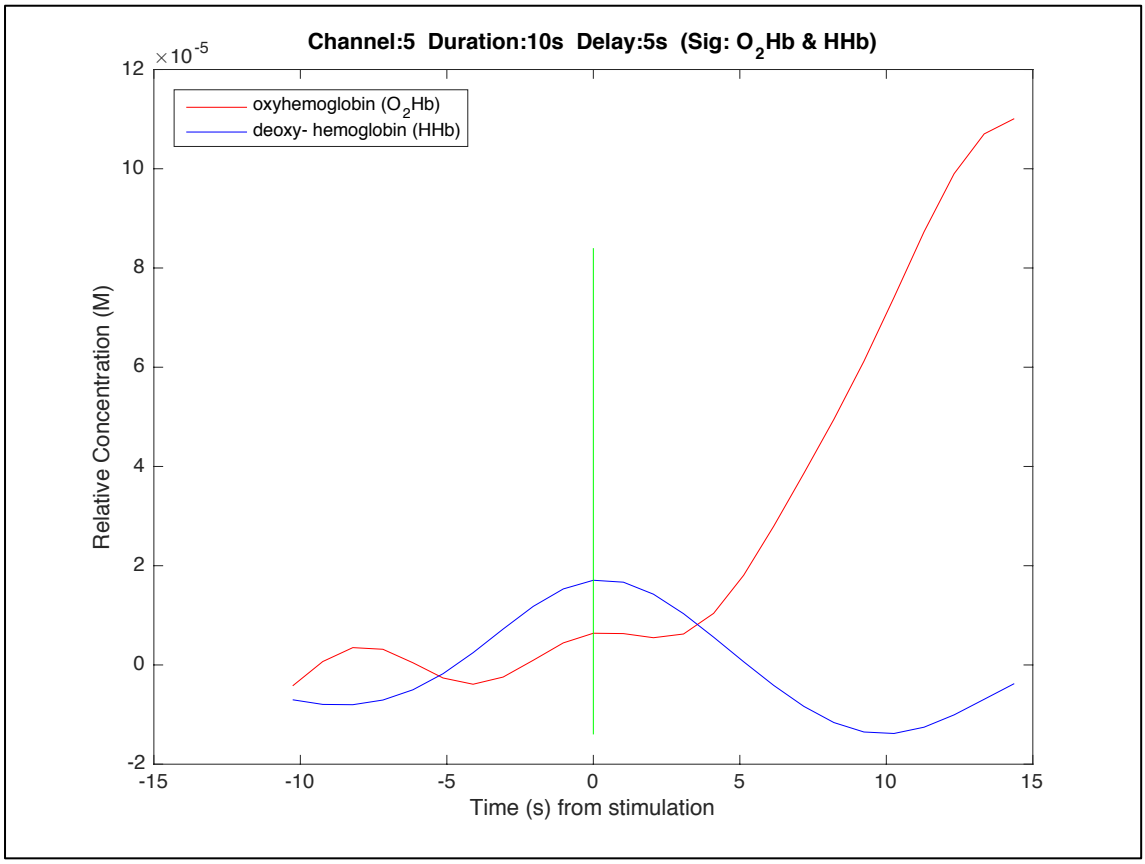

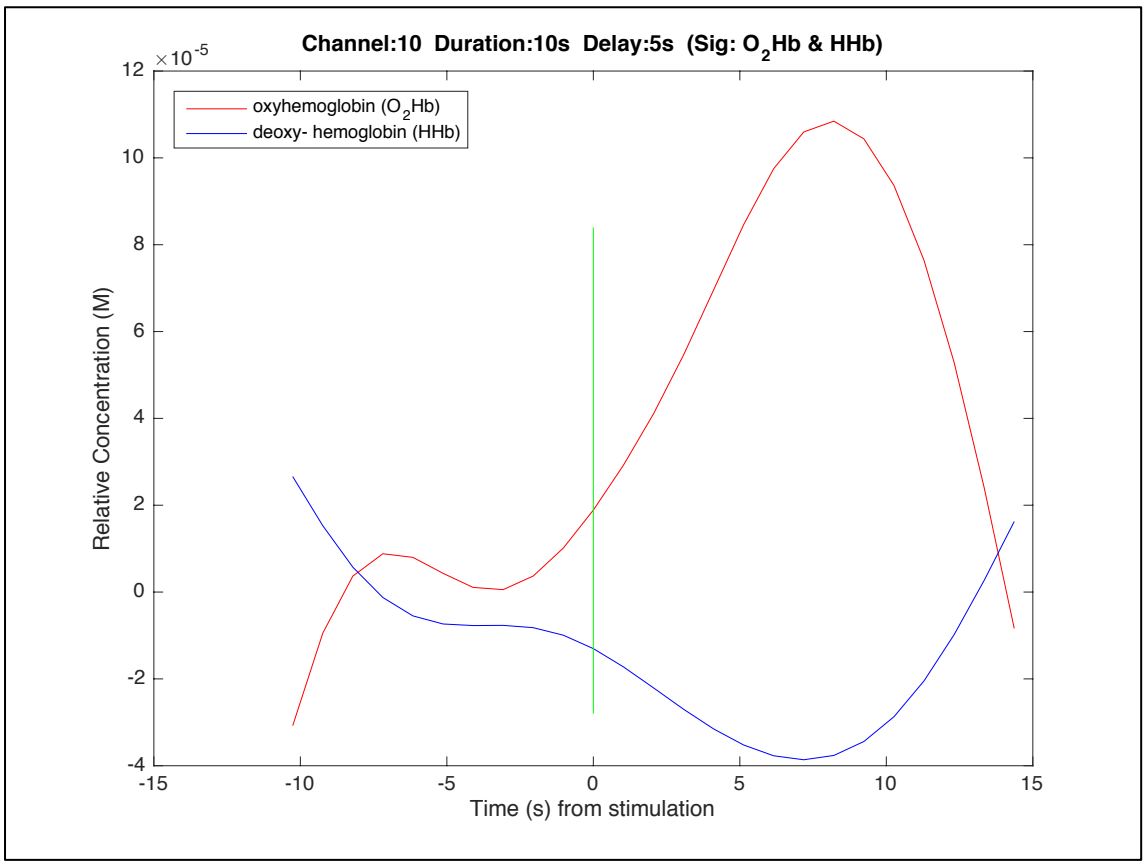
Channel:10 Duration:10s Delay:5s (Sig: O2Hb & HHb)
×10-5
oxyhemoglobin (O2Hb)
deoxy- hemoglobin (HHb)
Relative Concentration (M)
Time (s) from stimulation

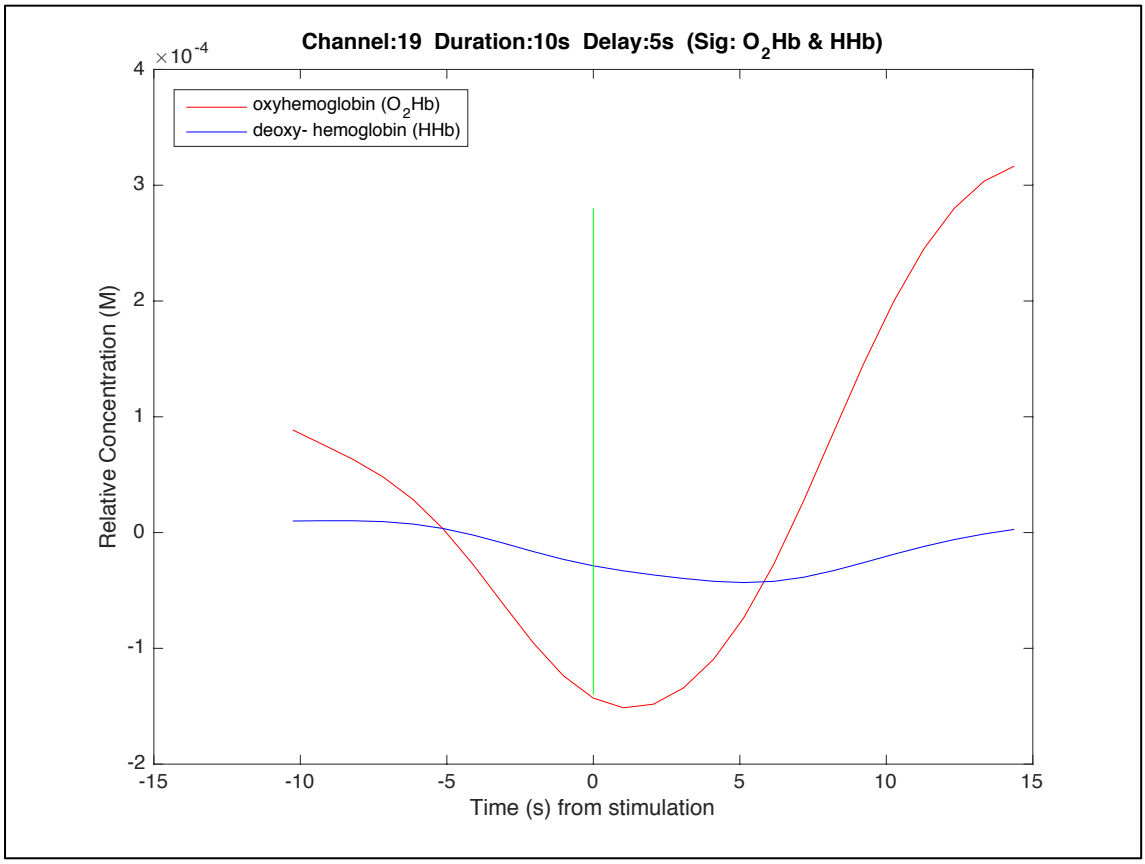
Channel:19 Duration:10s Delay:5s (Sig: O2Hb & HHb)
×10-4
oxyhemoglobin (O2Hb)
deoxy- hemoglobin (HHb)
Relative Concentration (M)
Time (s) from stimulation

Condition 3: Sequential Stimulation of 6 Quads

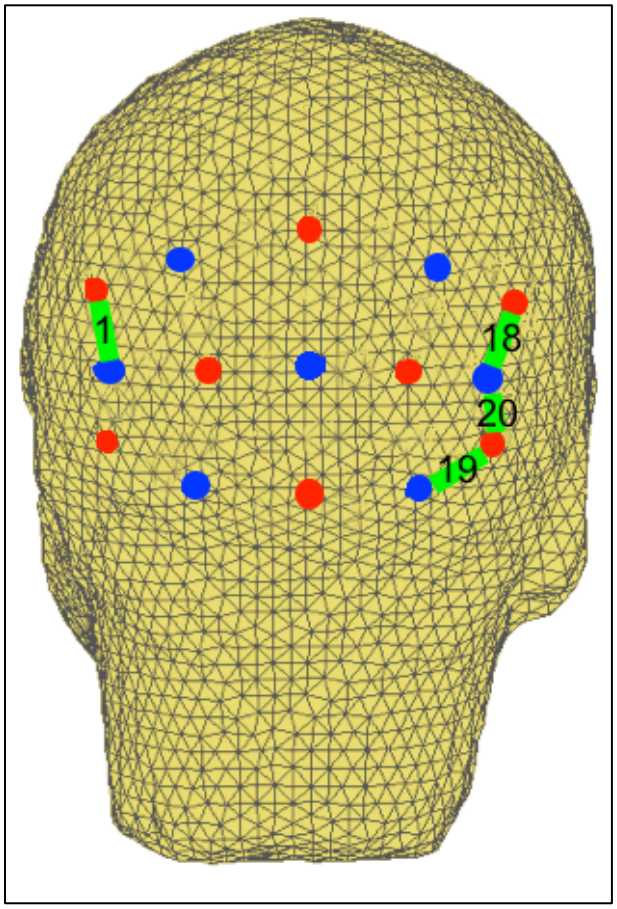

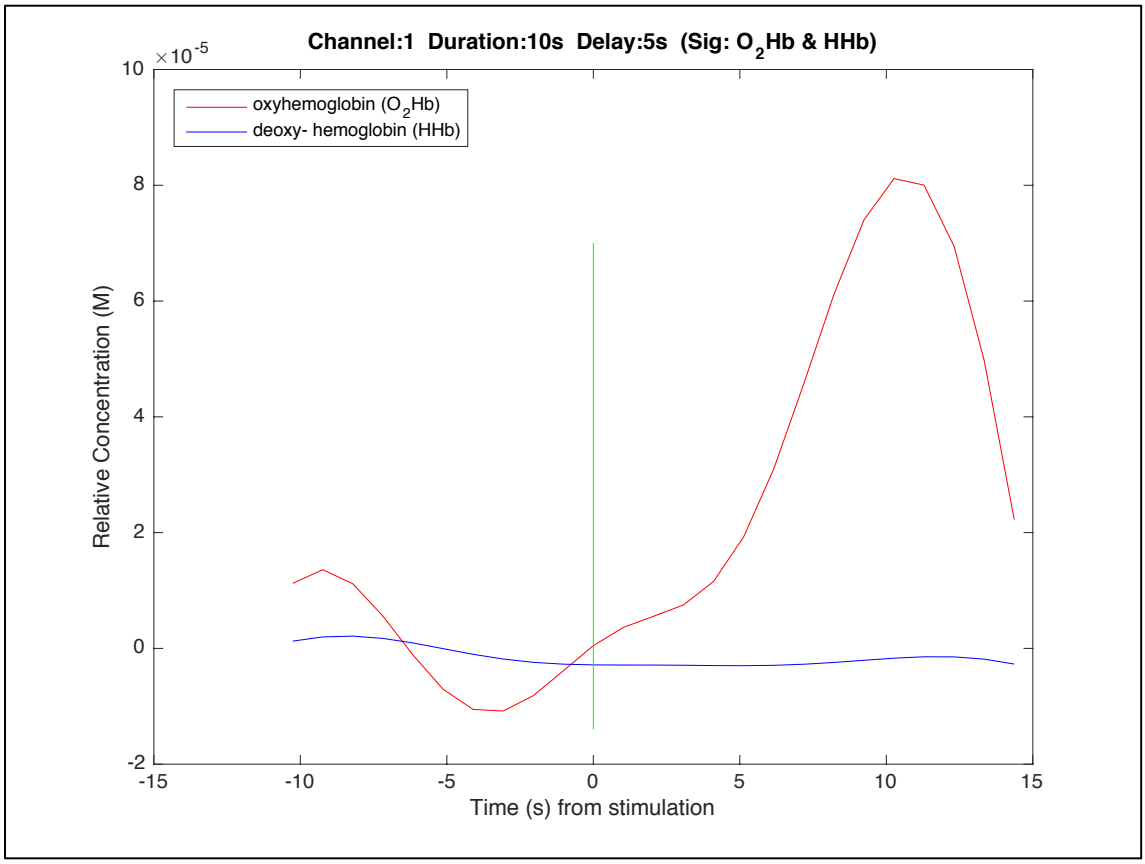

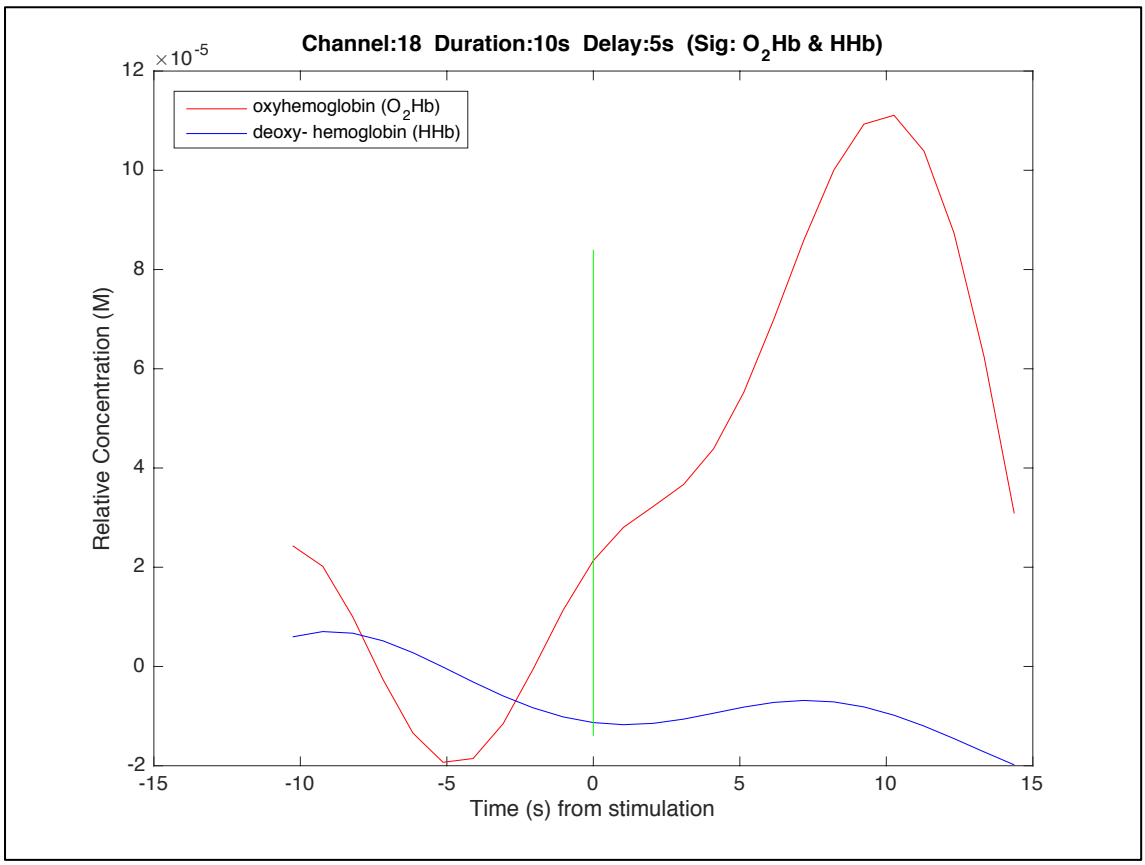
Channel:18 Duration:10s Delay:5s (Sig: O2Hb & HHb)
×10-5
oxyhemoglobin (O2Hb)
deoxy- hemoglobin (HHb)
Relative Concentration (M)
Time (s) from stimulation

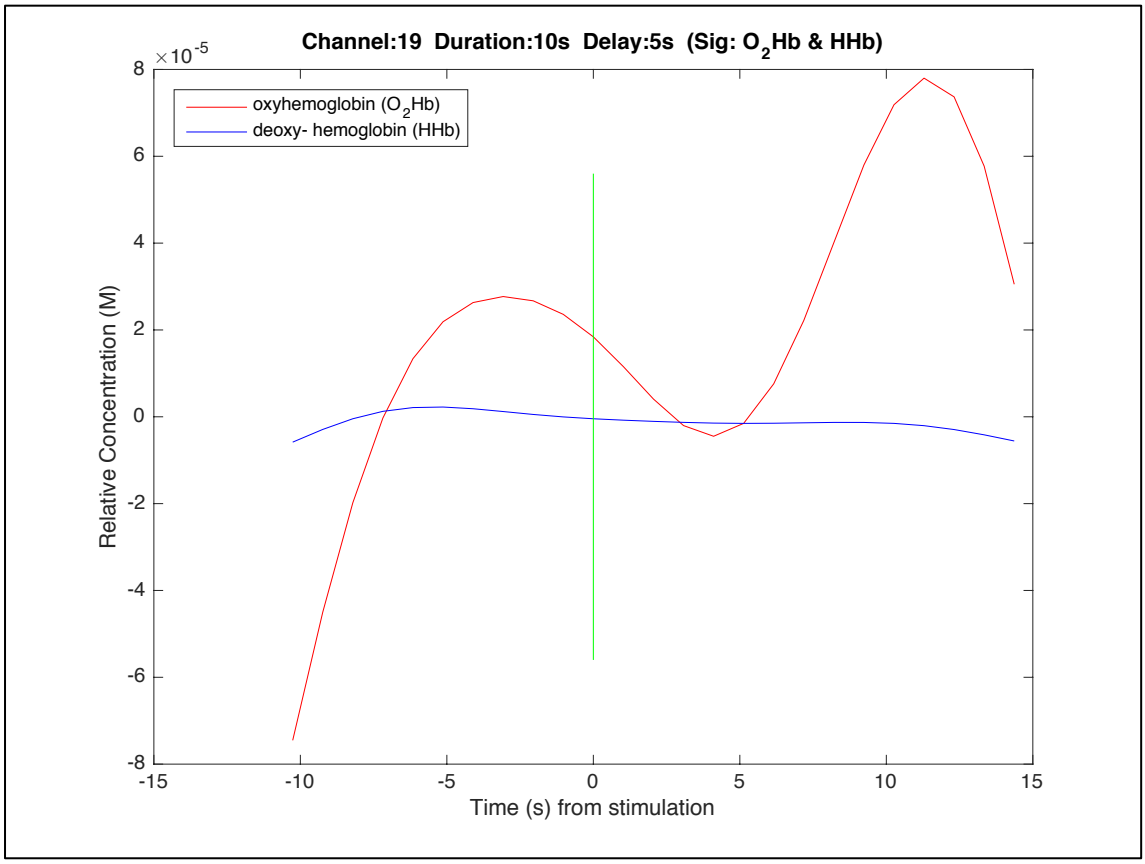
Channel:19 Duration:10s Delay:5s (Sig: O2Hb & HHb)
×10-5
oxyhemoglobin (O2Hb)
deoxy- hemoglobin (HHb)
Relative Concentration (M)
Time (s) from stimulation

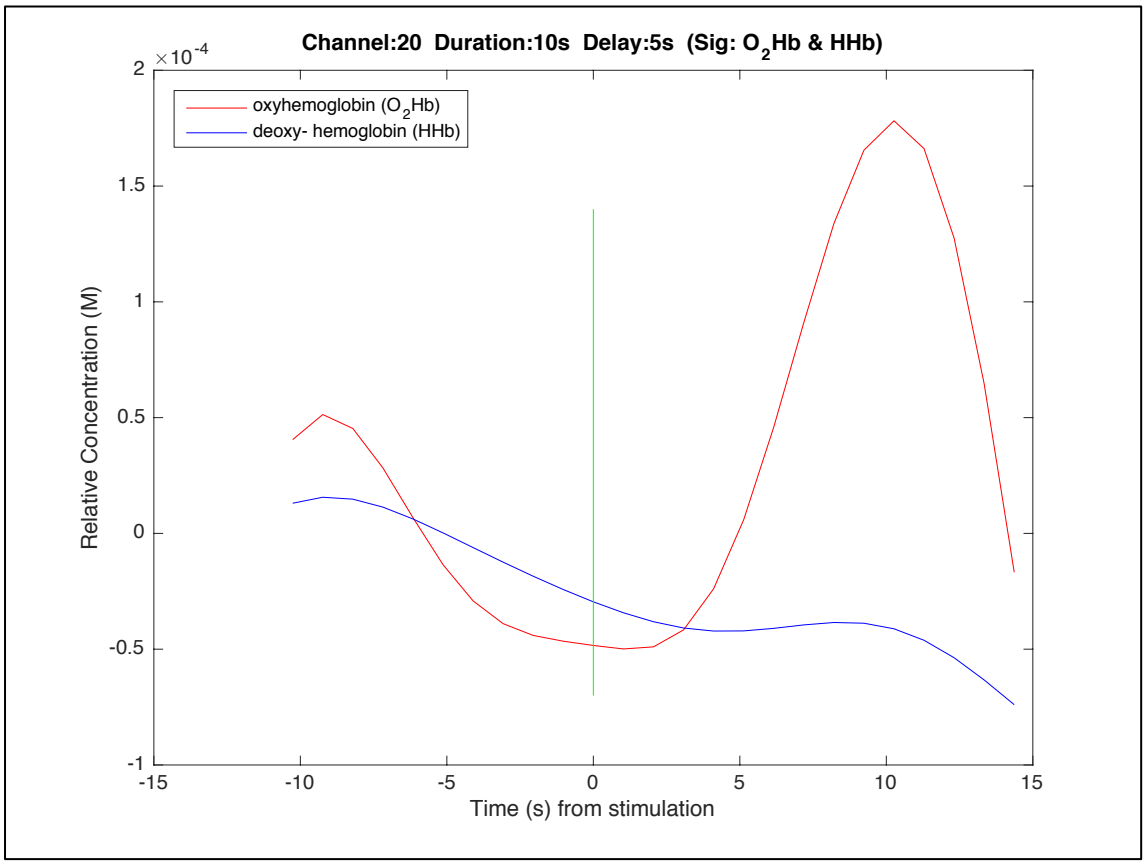
Channel:20 Duration:10s Delay:5s (Sig: O2Hb & HHb)
×10-4
2
1.5
1
0.5
0
-0.5
-1
oxyhemoglobin (O2Hb)
deoxy- hemoglobin (HHb)
Relative Concentration (M)
-15
-10
-5
0
5
10
15
Time (s) from stimulation

51-003

Condition 1: Foveal Quad Stimulation

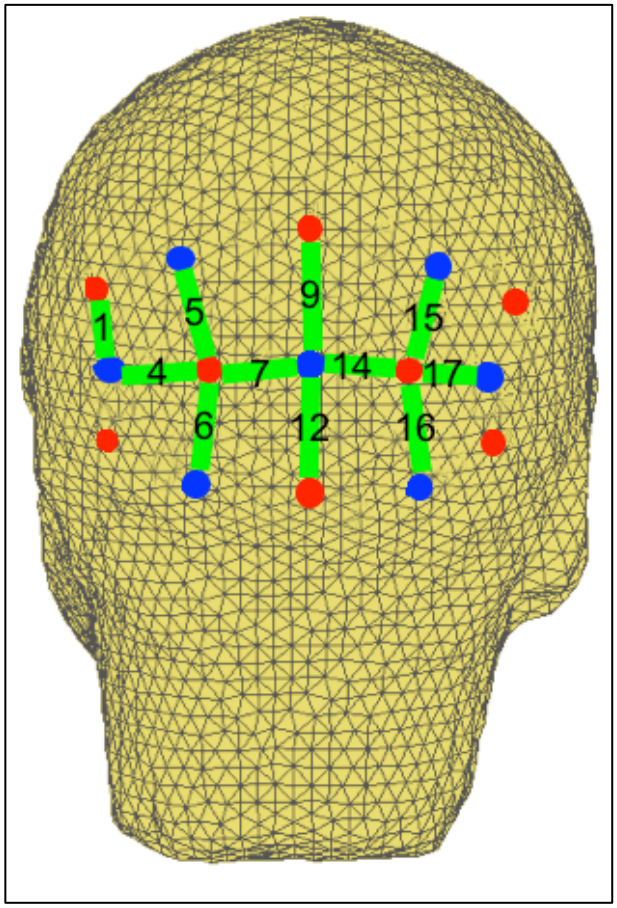

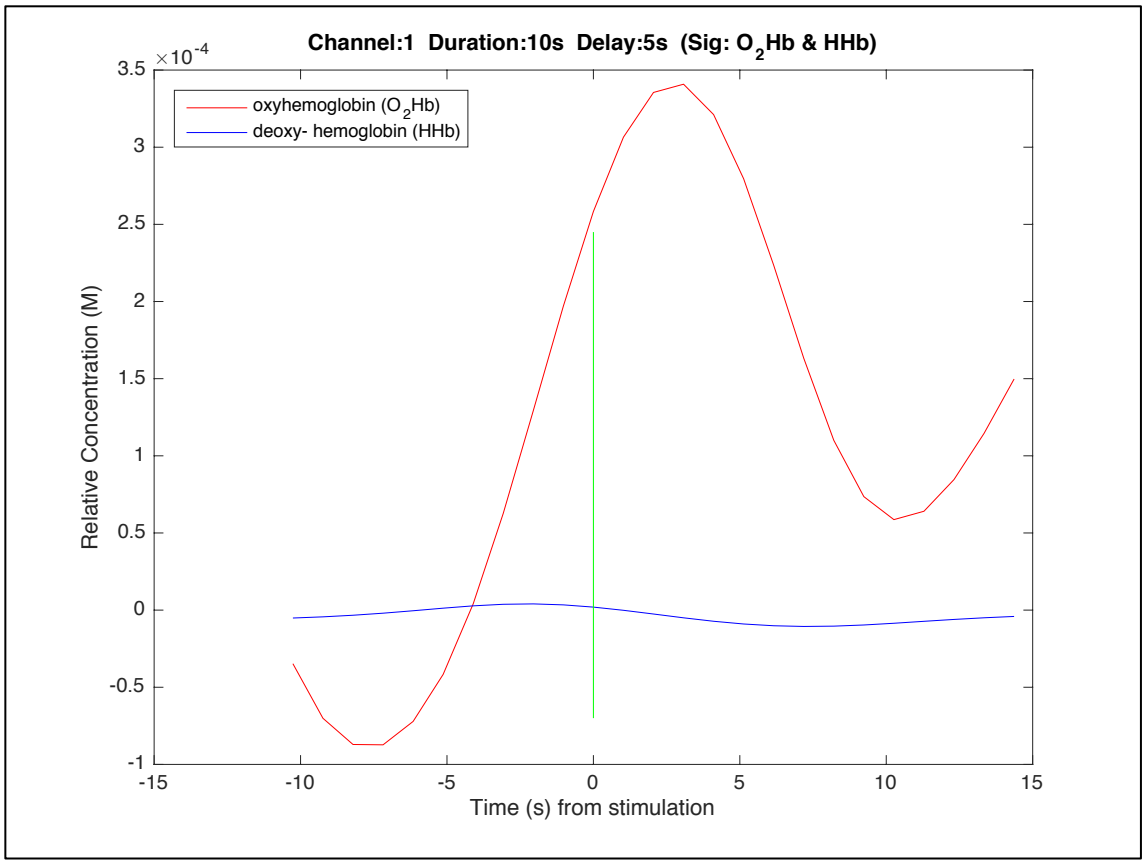

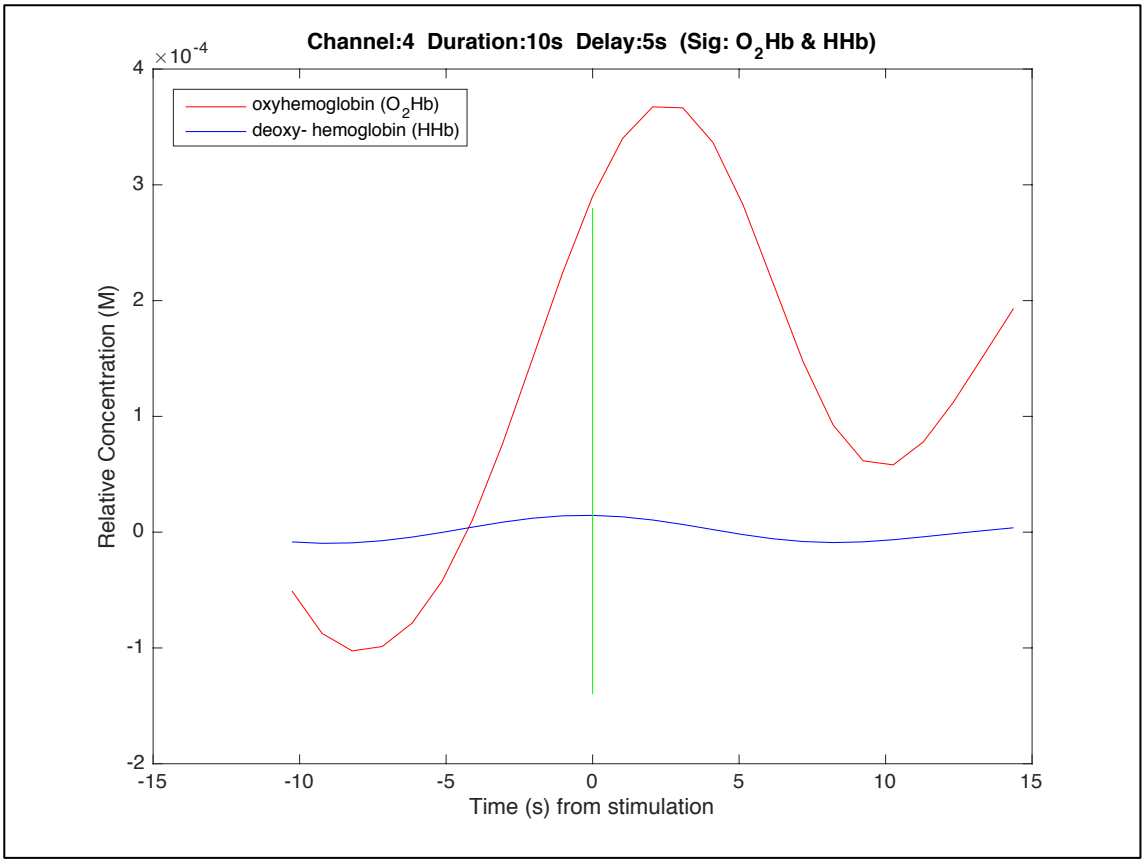
Channel:4 Duration:10s Delay:5s (Sig: O2Hb & HHb)
×10-4
oxyhemoglobin (O2Hb)
deoxy- hemoglobin (HHb)
Relative Concentration (M)
Time (s) from stimulation

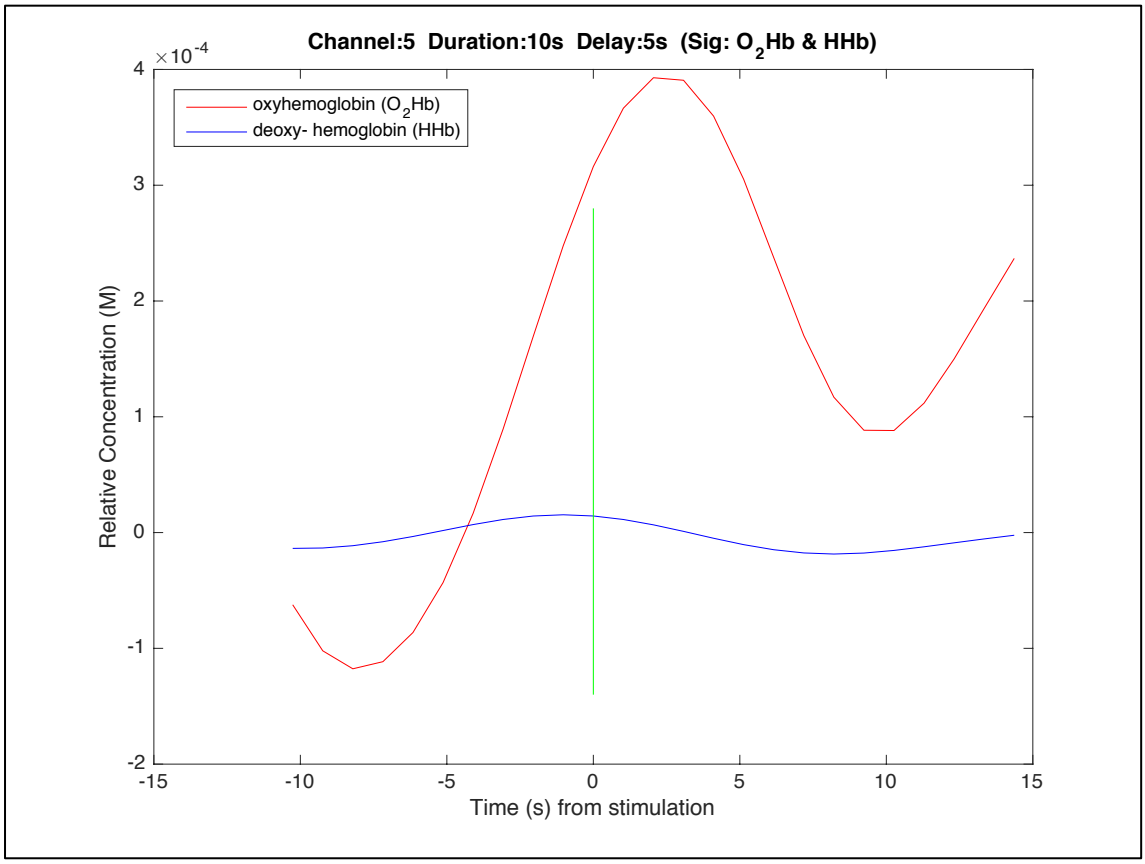
Channel:5 Duration:10s Delay:5s (Sig: O2Hb & HHb)
×10-4
oxyhemoglobin (O2Hb)
deoxy- hemoglobin (HHb)
Relative Concentration (M)
Time (s) from stimulation

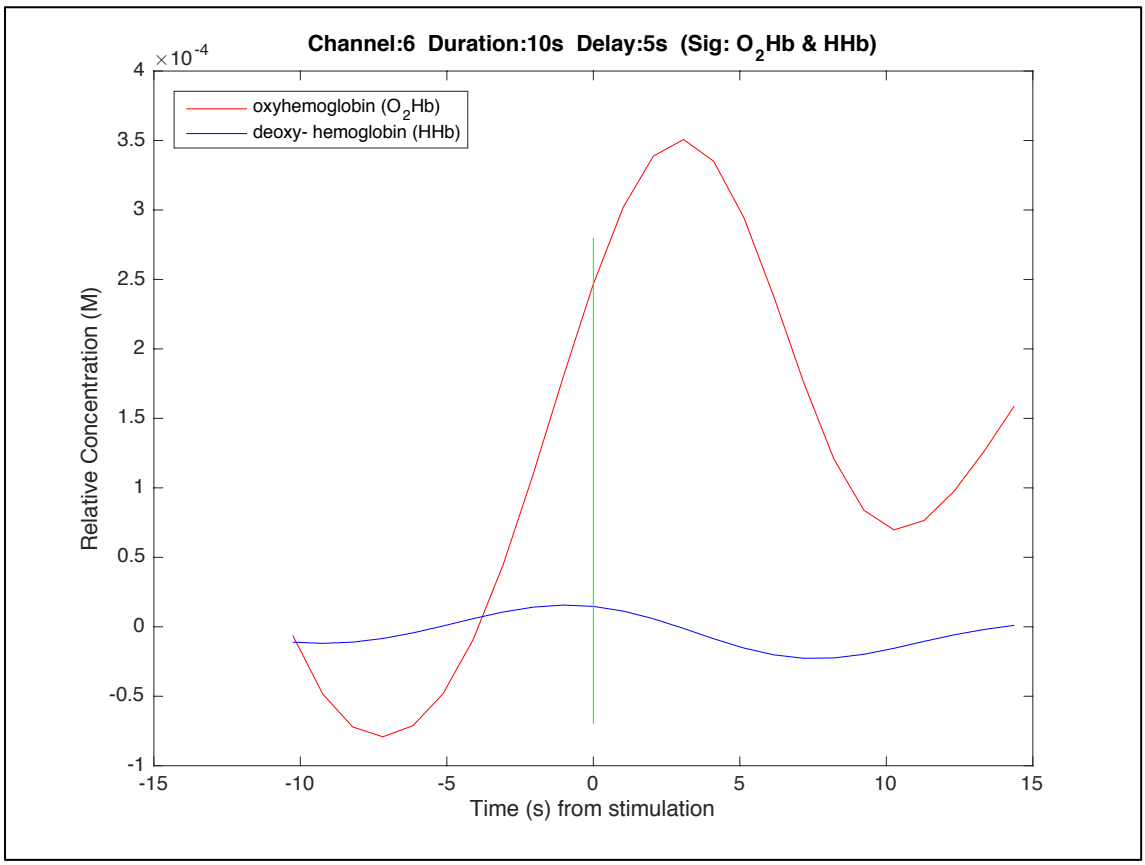
Channel:6 Duration:10s Delay:5s (Sig: O2Hb & HHb)
×10-4
oxyhemoglobin (O2Hb)
deoxy- hemoglobin (HHb)
Relative Concentration (M)
Time (s) from stimulation

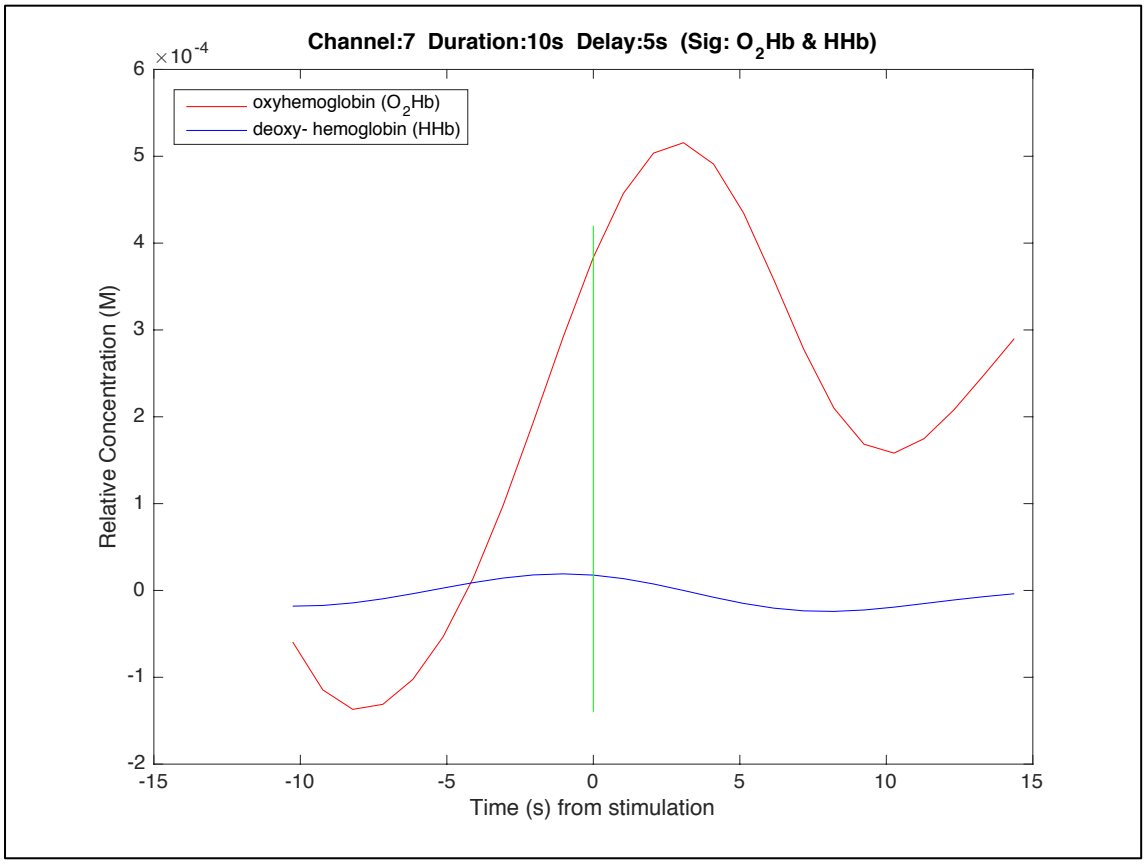
Channel:7 Duration:10s Delay:5s (Sig: O2Hb & HHb)
×10-4
oxyhemoglobin (O2Hb)
deoxy- hemoglobin (HHb)
Relative Concentration (M)
Time (s) from stimulation

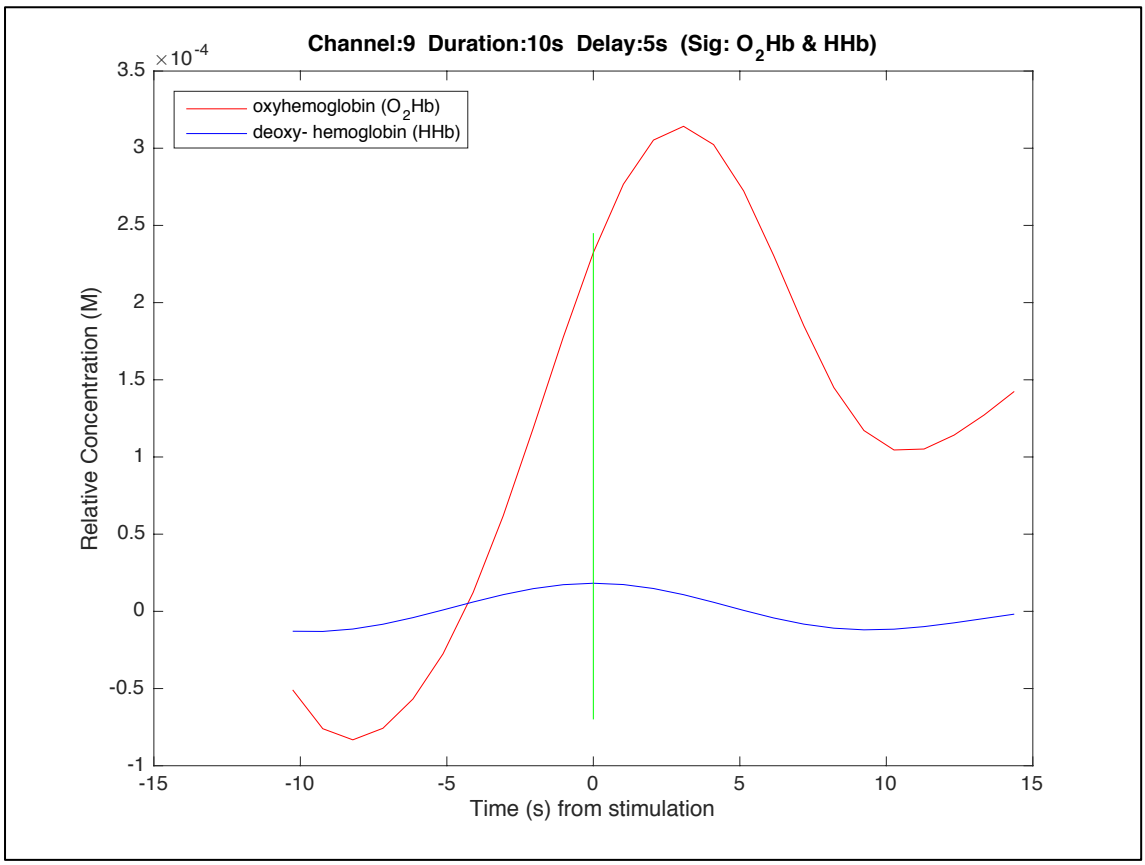
Channel:9 Duration:10s Delay:5s (Sig: O2Hb & HHb)
×10-4
oxyhemoglobin (O2Hb)
deoxy- hemoglobin (HHb)
Relative Concentration (M)
Time (s) from stimulation

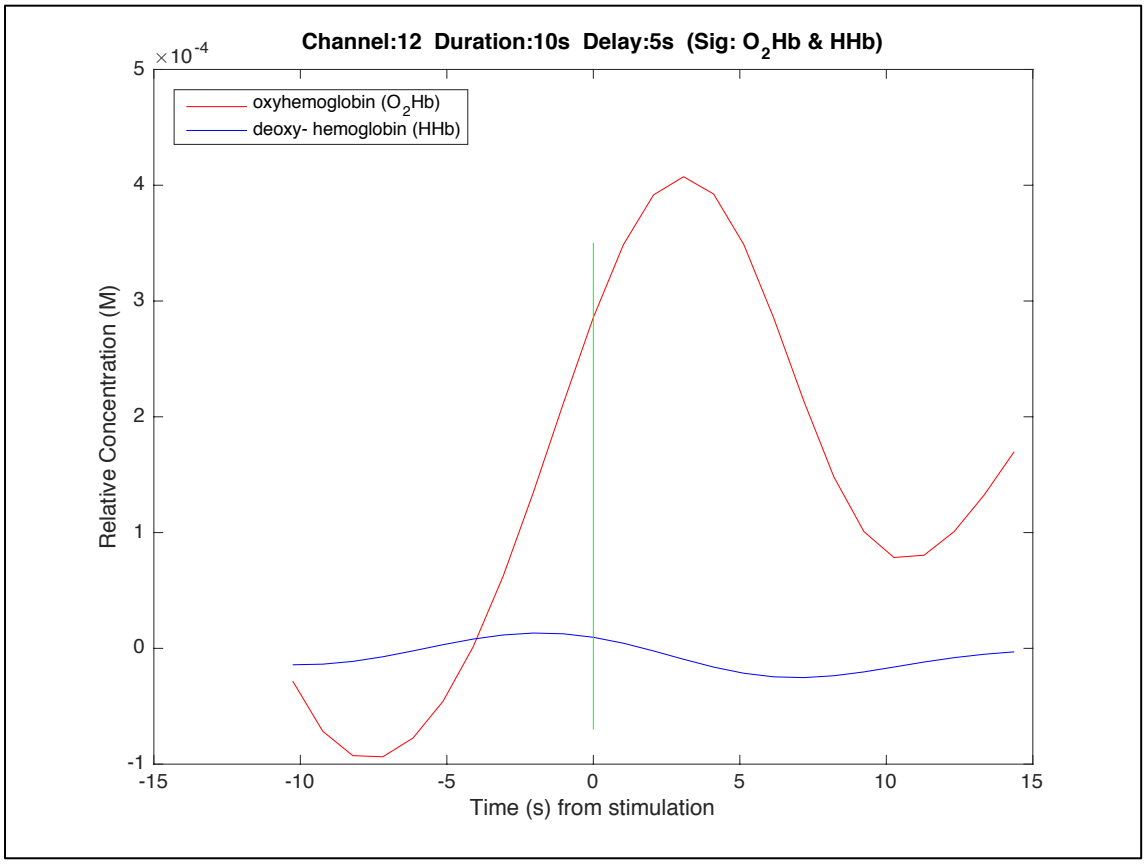
Channel:12 Duration:10s Delay:5s (Sig: O2Hb & HHb)
×10-4
oxyhemoglobin (O2Hb)
deoxy- hemoglobin (HHb)
Relative Concentration (M)
Time (s) from stimulation

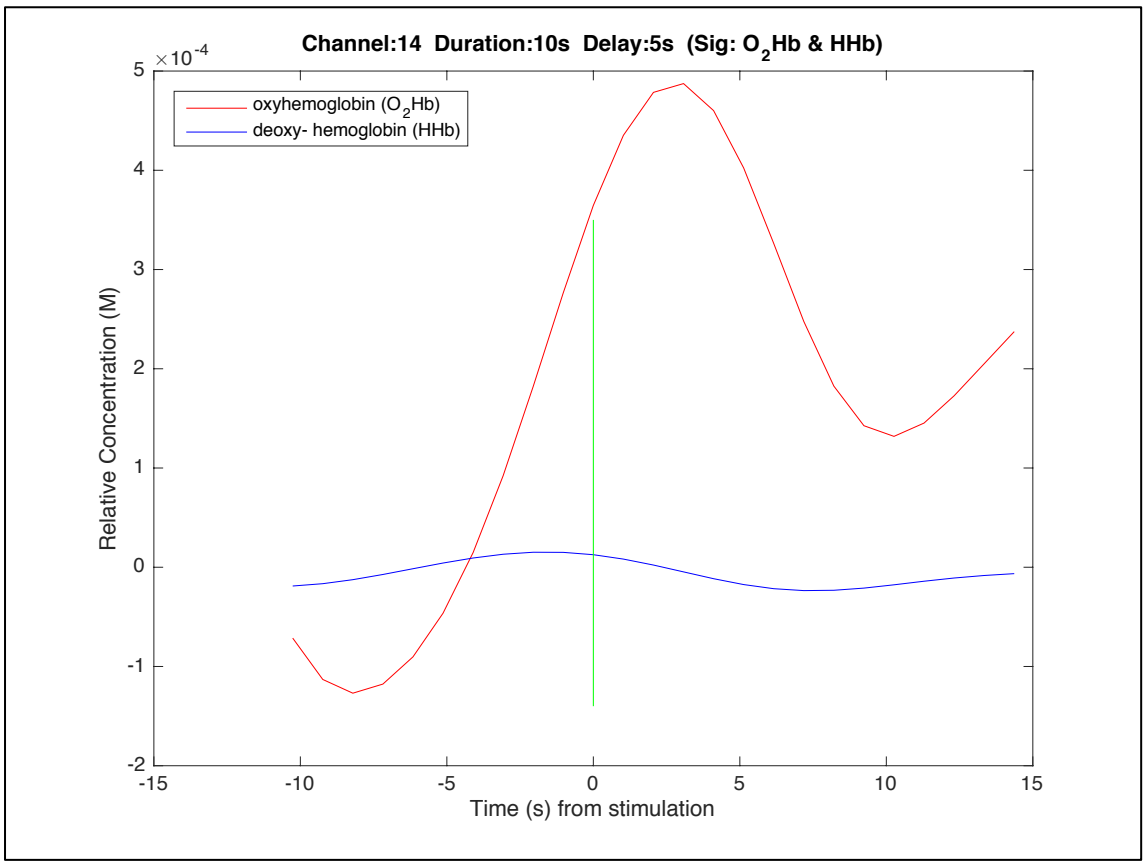
Channel:14 Duration:10s Delay:5s (Sig: O2Hb & HHb)
×10-4
oxyhemoglobin (O2Hb)
deoxy- hemoglobin (HHb)
Relative Concentration (M)
Time (s) from stimulation

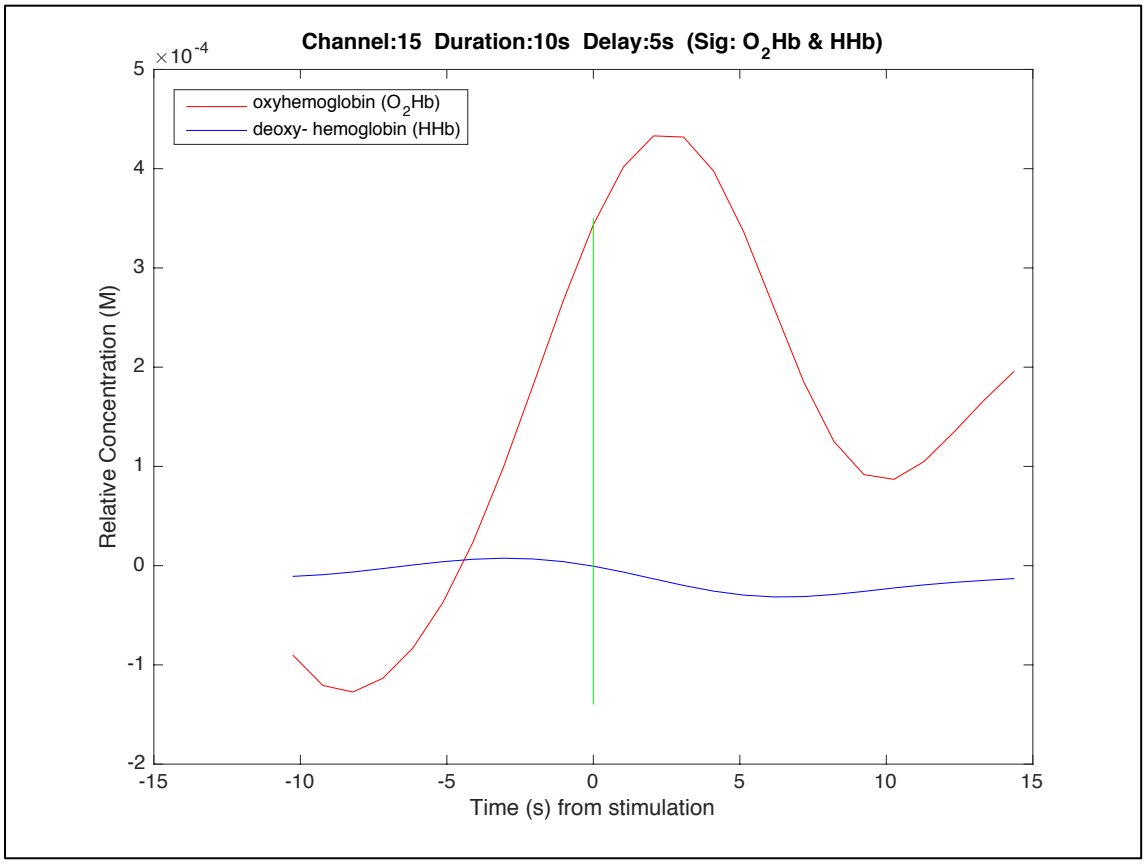
Channel:15 Duration:10s Delay:5s (Sig: O2Hb & HHb)
×10-4
oxyhemoglobin (O2Hb)
deoxy- hemoglobin (HHb)
Relative Concentration (M)
Time (s) from stimulation

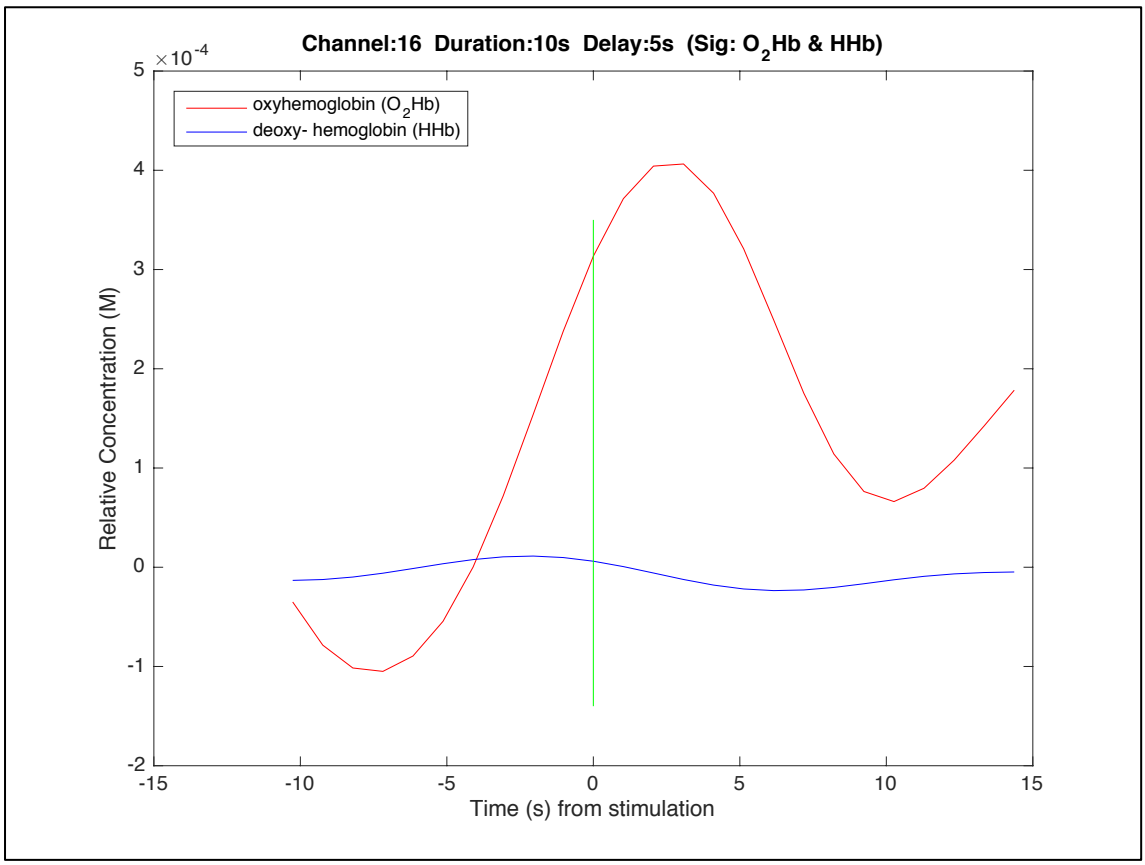
Channel:16 Duration:10s Delay:5s (Sig: O2Hb & HHb)
×10-4
oxyhemoglobin (O2Hb)
deoxy- hemoglobin (HHb)
Relative Concentration (M)
Time (s) from stimulation

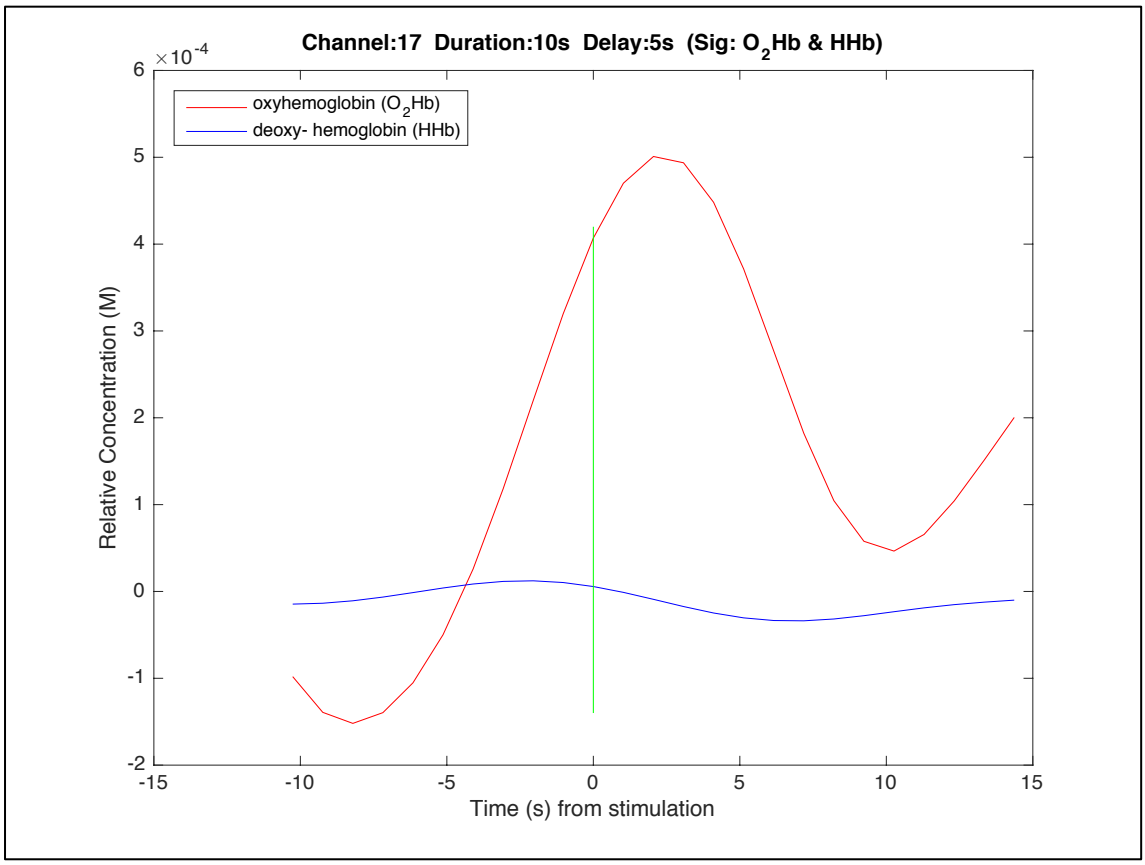
Channel:17 Duration:10s Delay:5s (Sig: O2Hb & HHb)
×10-4
oxyhemoglobin (O2Hb)
deoxy- hemoglobin (HHb)
Relative Concentration (M)
Time (s) from stimulation

Condition 2: Simultaneous Stimulation of 6 Quads

None of the optode channels showed a positive fNIRS response under Condition 2 stimulations in subject 51-003.

Condition 3: Sequential Stimulation of 6 Quads

None of the optode channels showed a positive fNIRS response under Condition 3 stimulations in subject 51-003.

51-005

None of the optode channels showed a positive fNIRS response under all of the 3 stimulation conditions in subject 51-005.

51-006

Condition 1: Foveal Quad Stimulation

None of the optode channels showed a positive fNIRS response under Condition 1 stimulations in subject 51-006.

Condition 2: Simultaneous Stimulation of 6 Quads

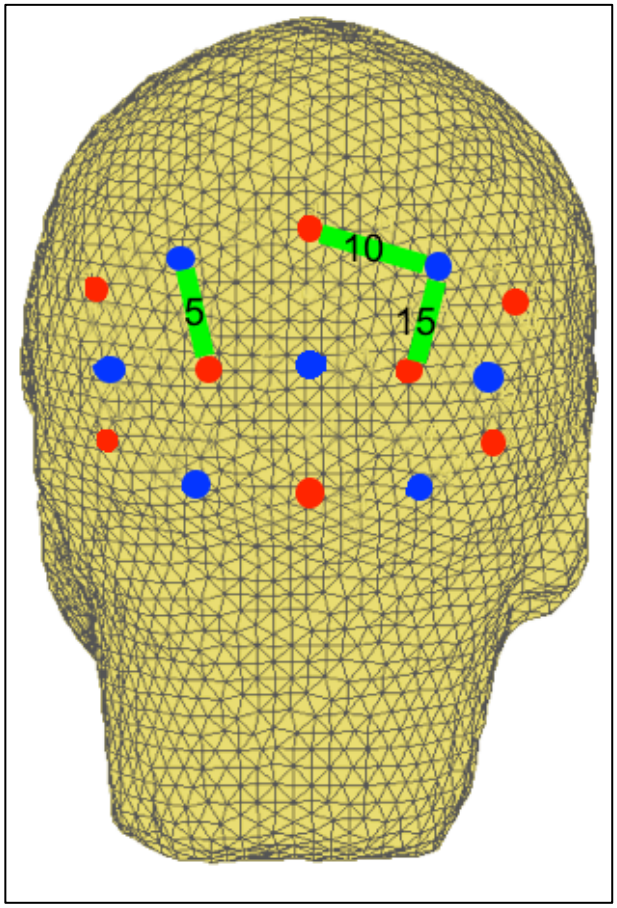

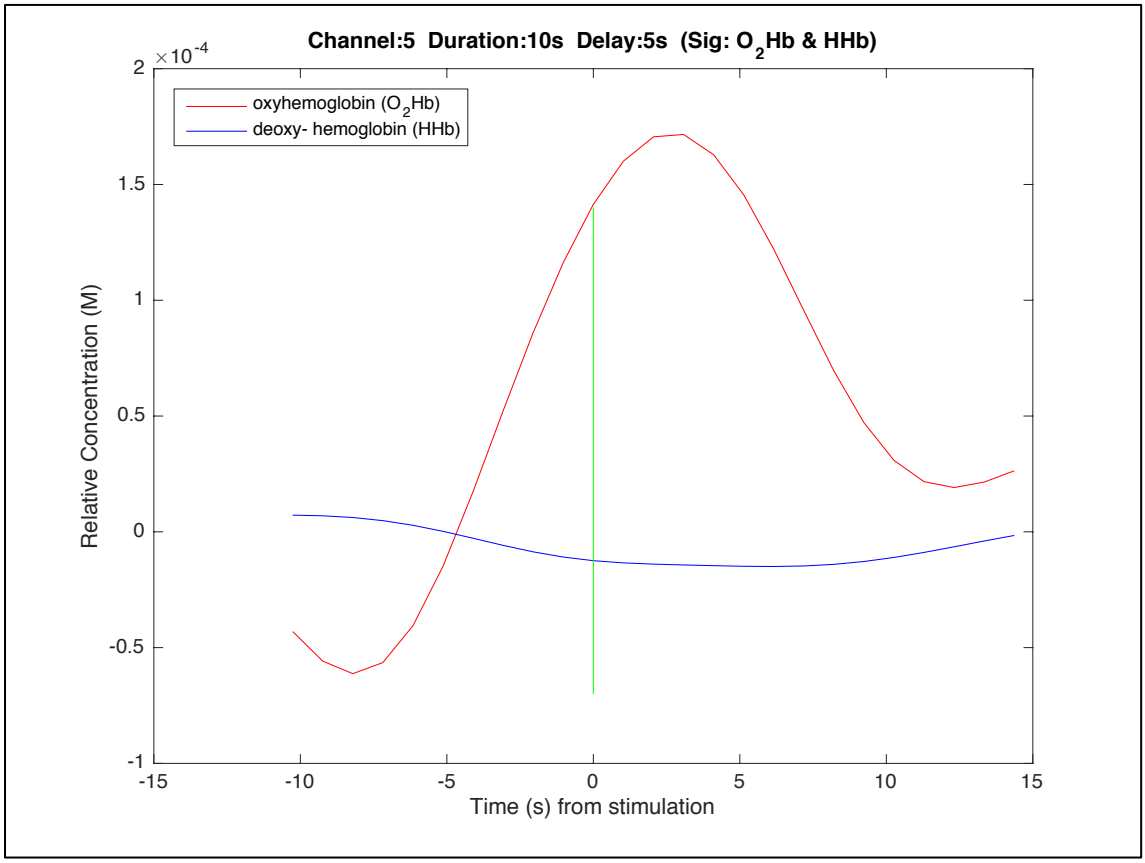

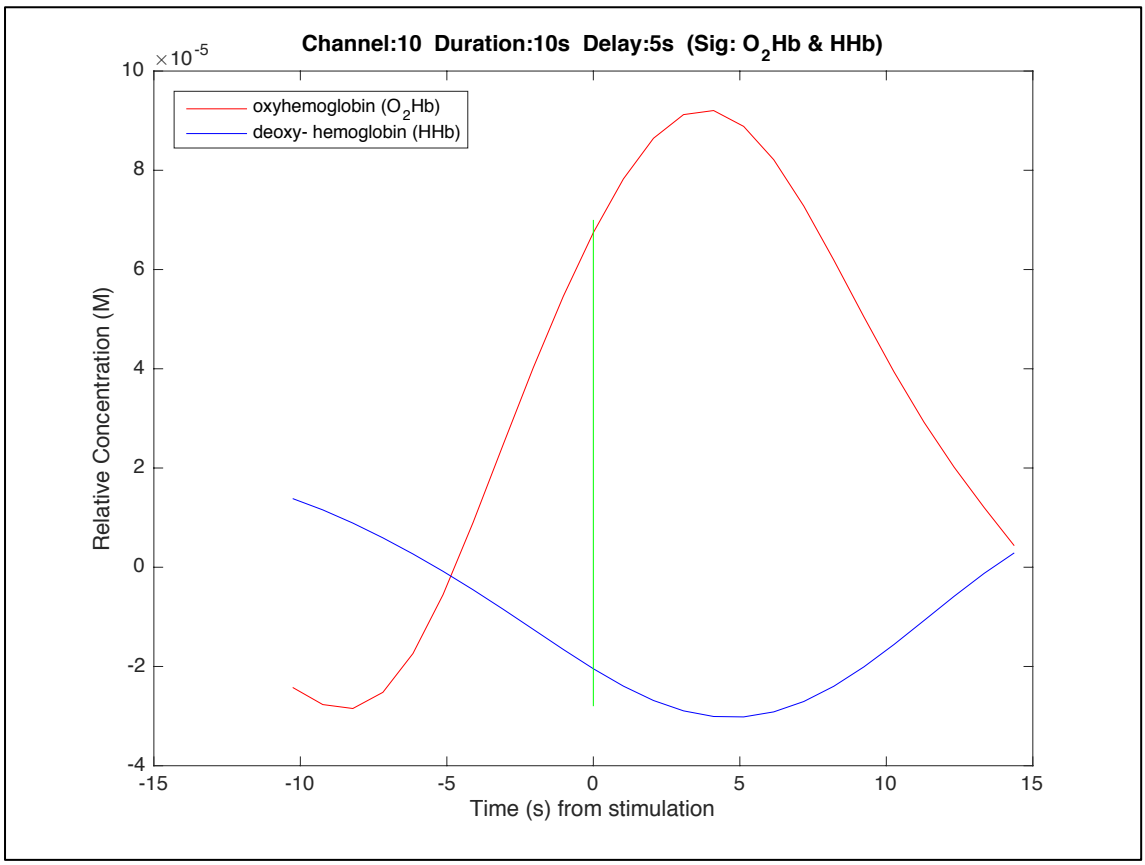
Channel:10 Duration:10s Delay:5s (Sig: O2Hb & HHb)
×10-5
oxyhemoglobin (O2Hb)
deoxy- hemoglobin (HHb)
Relative Concentration (M)
Time (s) from stimulation

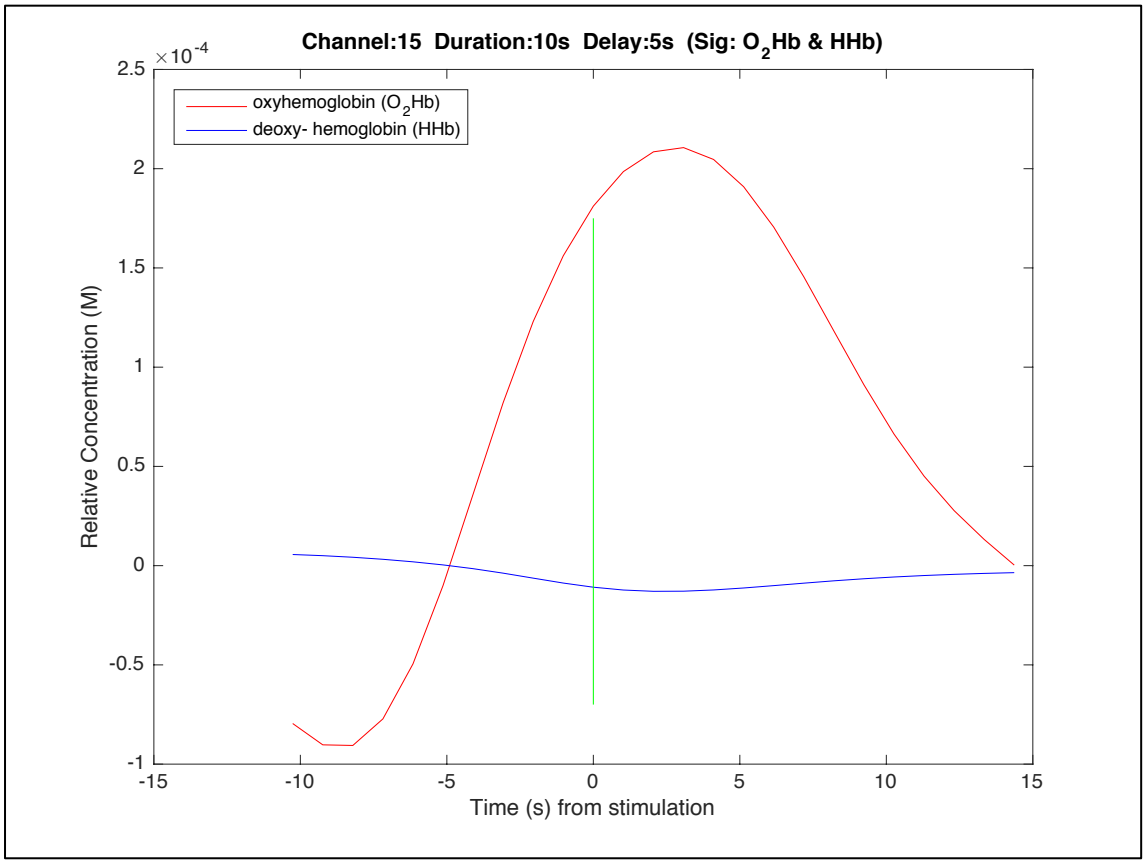
Channel:15 Duration:10s Delay:5s (Sig: O2Hb & HHb)
×10-4
oxyhemoglobin (O2Hb)
deoxy- hemoglobin (HHb)
Relative Concentration (M)
Time (s) from stimulation

Condition 3: Sequential Stimulation of 6 Quads

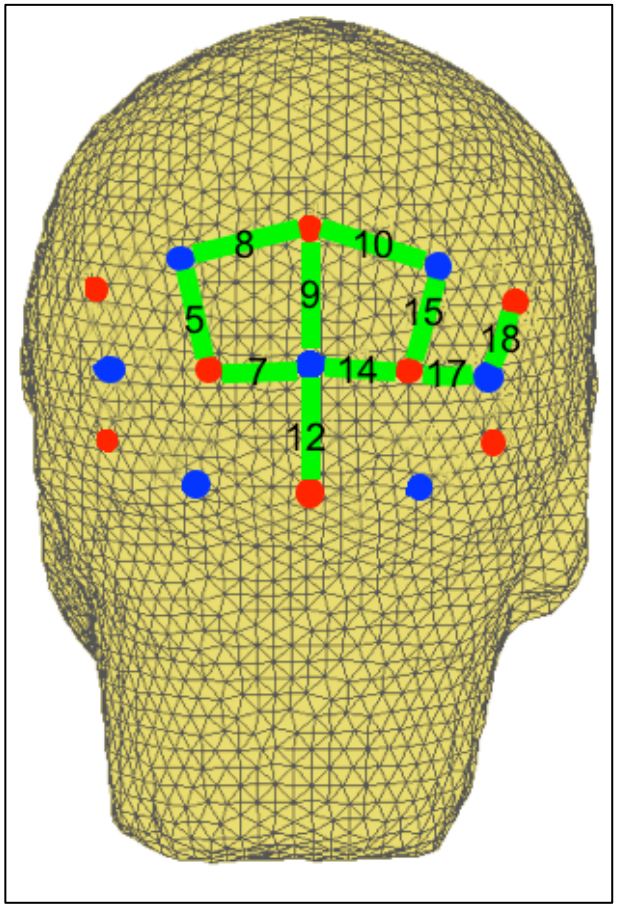

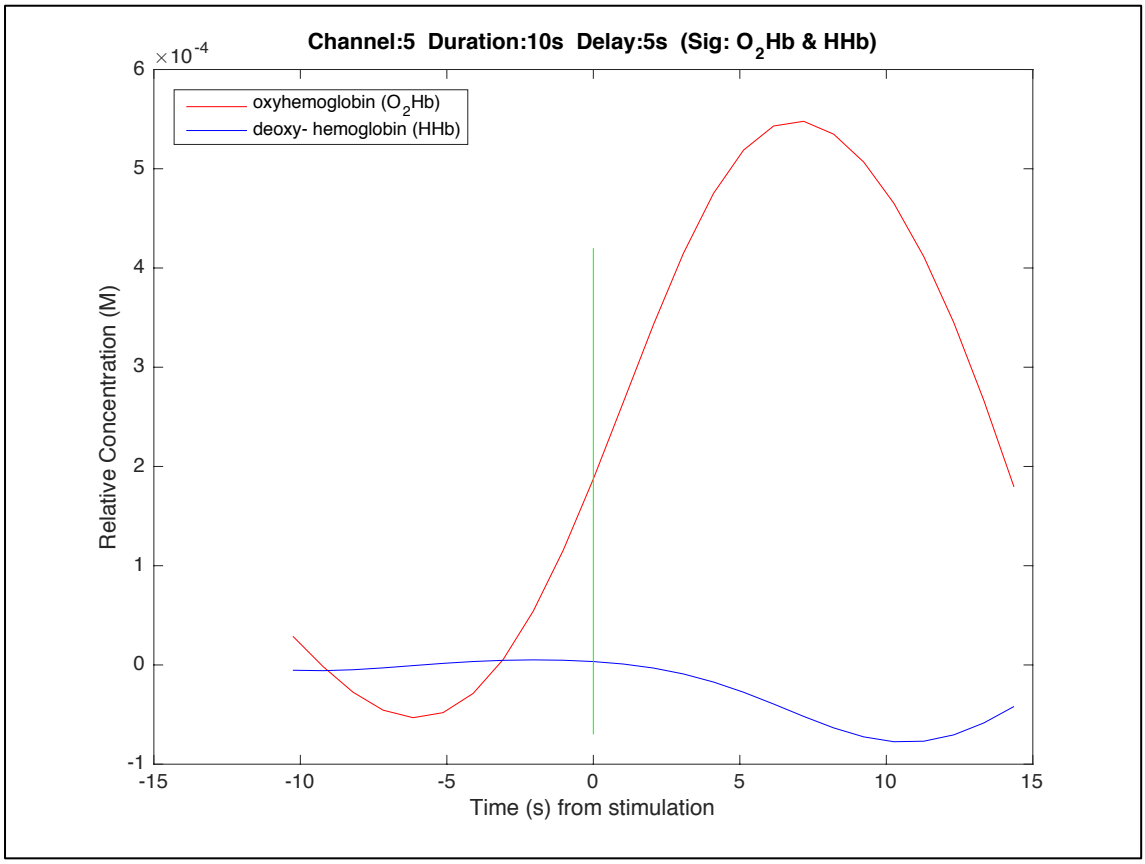

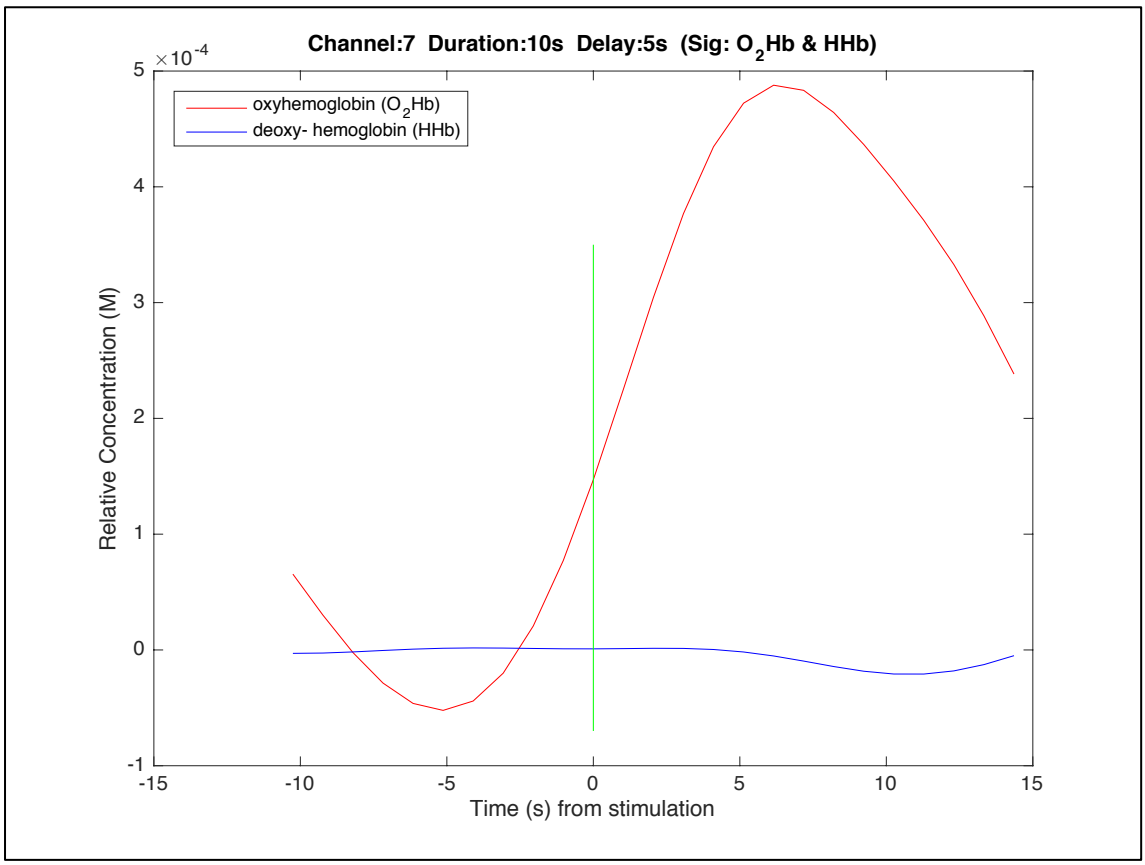
Channel:7 Duration:10s Delay:5s (Sig: O2Hb & HHb)
×10-4
oxyhemoglobin (O2Hb)
deoxy- hemoglobin (HHb)
Relative Concentration (M)
Time (s) from stimulation

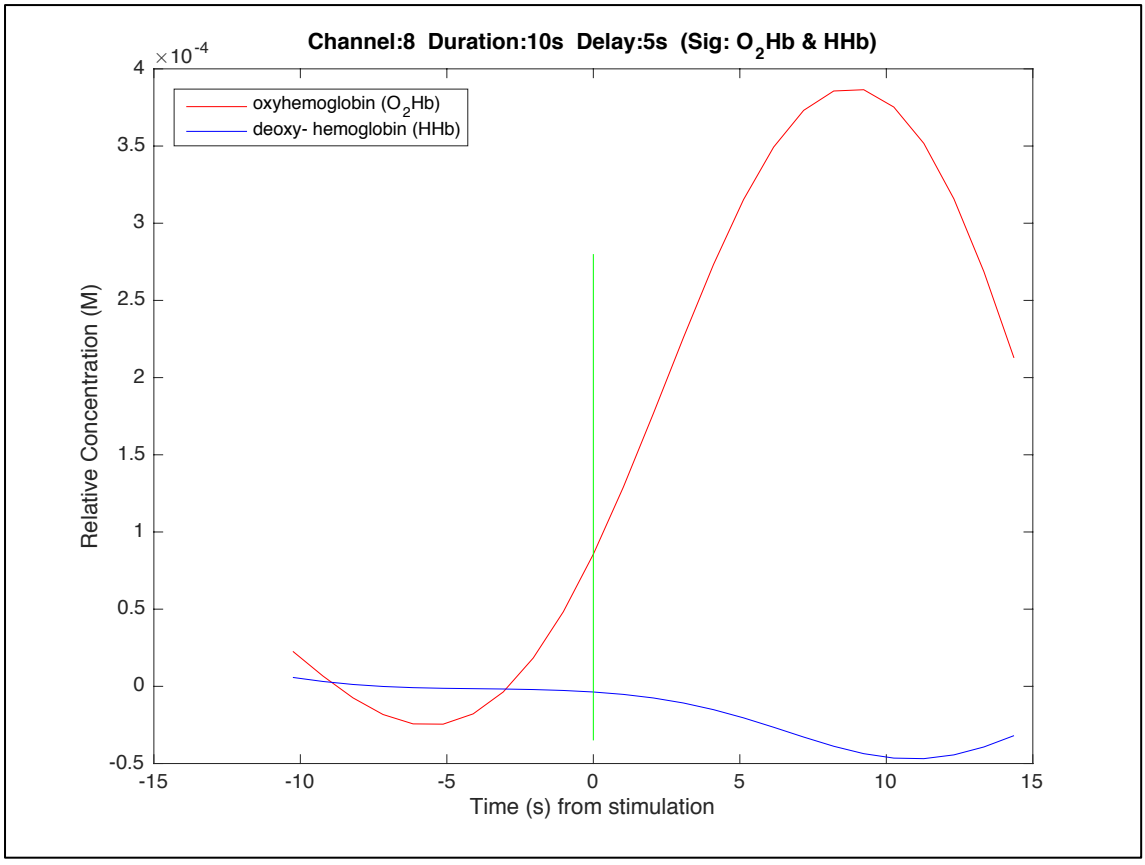
Channel:8 Duration:10s Delay:5s (Sig: O2Hb & HHb)
×10-4
oxyhemoglobin (O2Hb)
deoxy- hemoglobin (HHb)
Relative Concentration (M)
Time (s) from stimulation

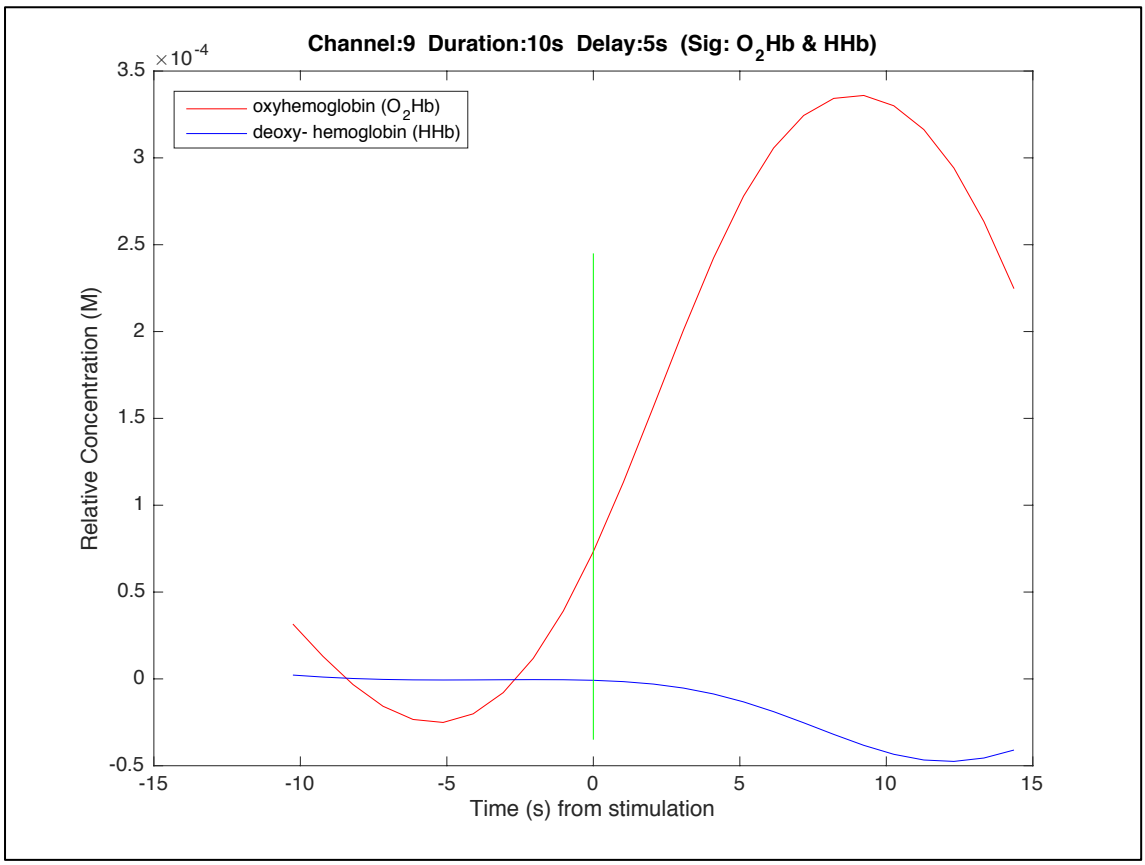
Channel:9 Duration:10s Delay:5s (Sig: O2Hb & HHb)
×10-4
oxyhemoglobin (O2Hb)
deoxy- hemoglobin (HHb)
Relative Concentration (M)
Time (s) from stimulation

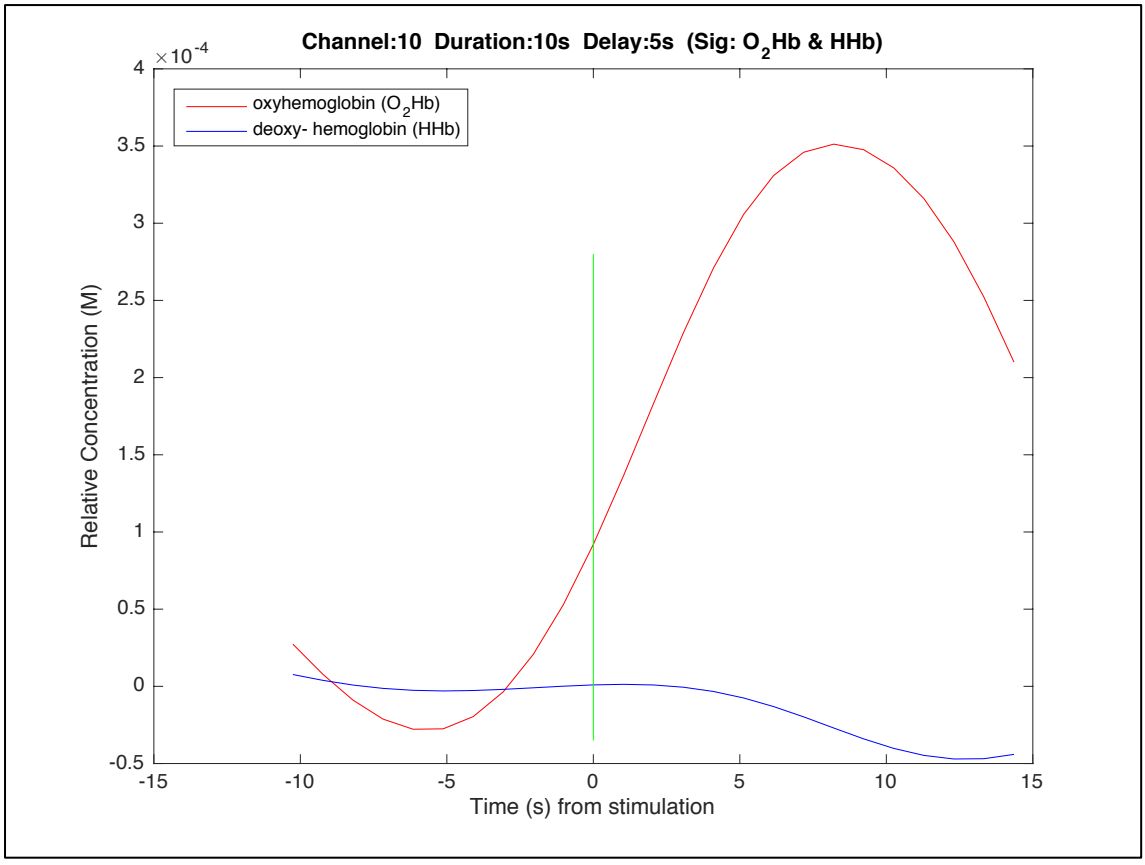
Channel:10 Duration:10s Delay:5s (Sig: O2Hb & HHb)
×10-4
oxyhemoglobin (O2Hb)
deoxy- hemoglobin (HHb)
Relative Concentration (M)
Time (s) from stimulation

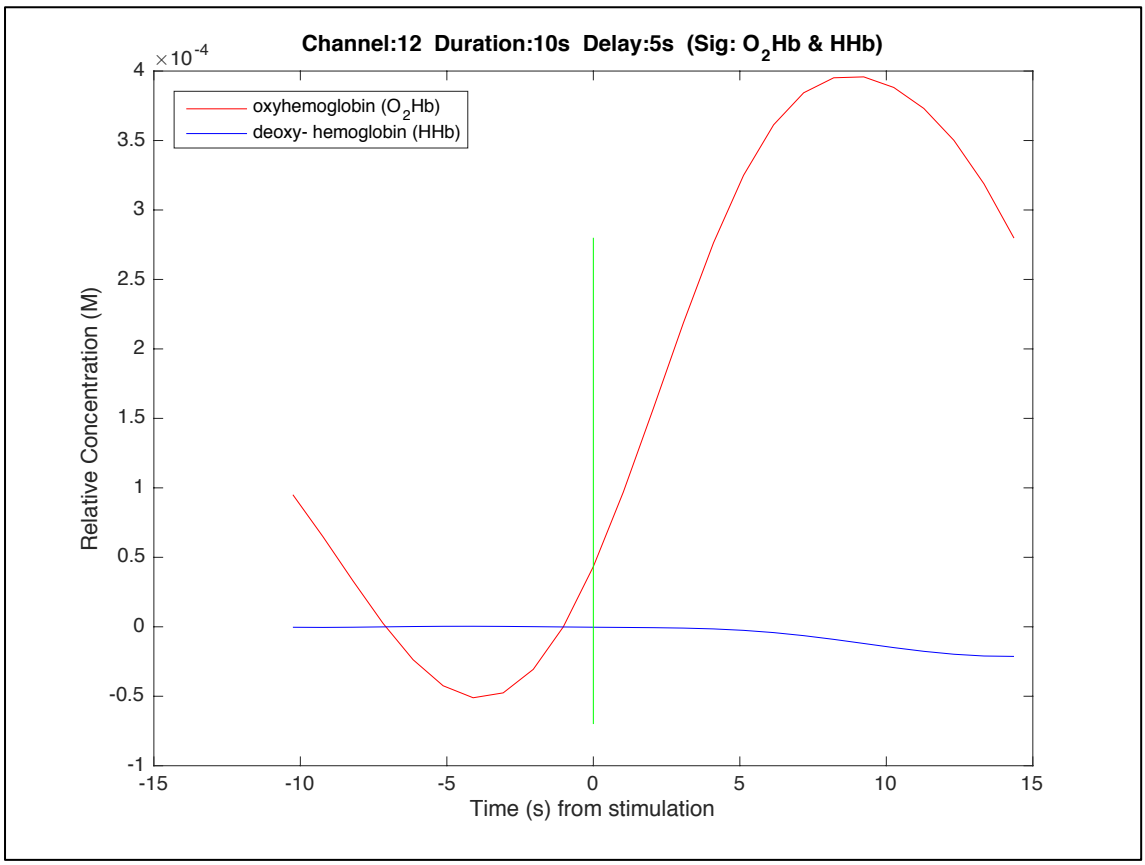
Channel:12 Duration:10s Delay:5s (Sig: O2Hb & HHb)
×10-4
oxyhemoglobin (O2Hb)
deoxy- hemoglobin (HHb)
Relative Concentration (M)
Time (s) from stimulation

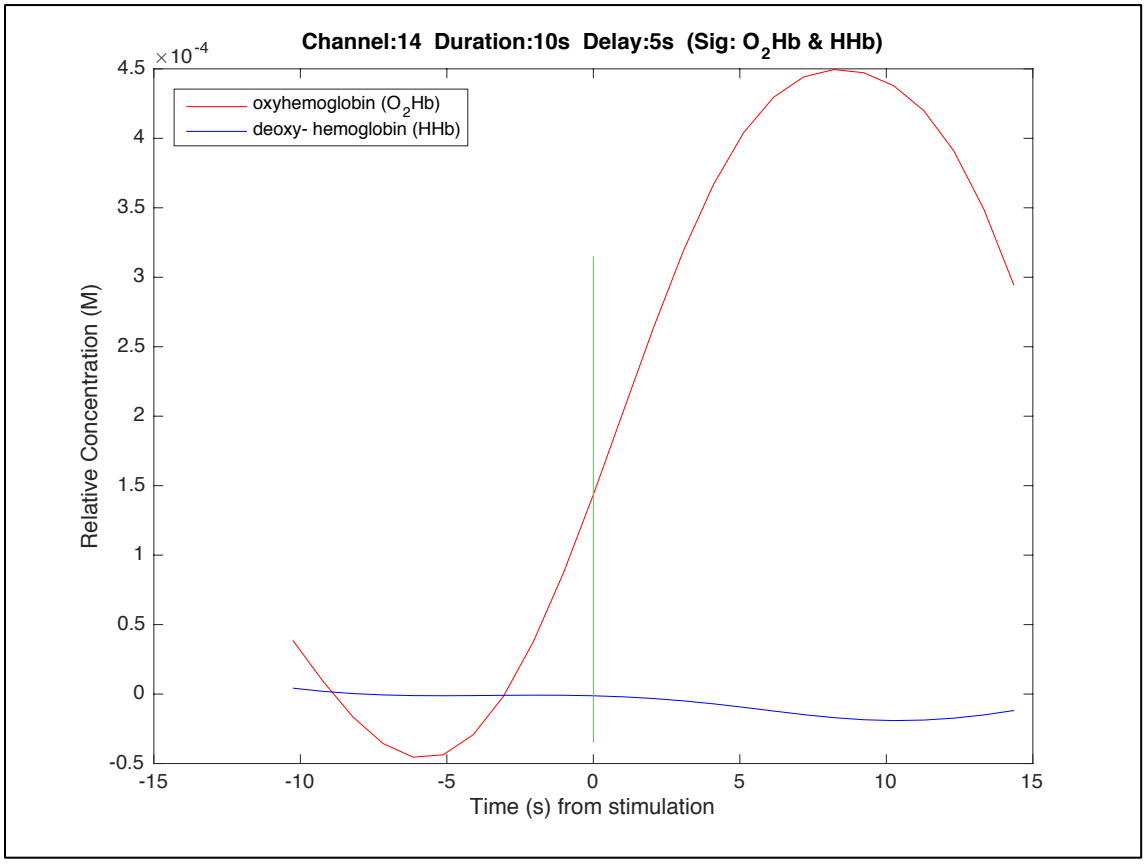
Channel:14 Duration:10s Delay:5s (Sig: O2Hb & HHb)
×10-4
oxyhemoglobin (O2Hb)
deoxy- hemoglobin (HHb)
Relative Concentration (M)
Time (s) from stimulation

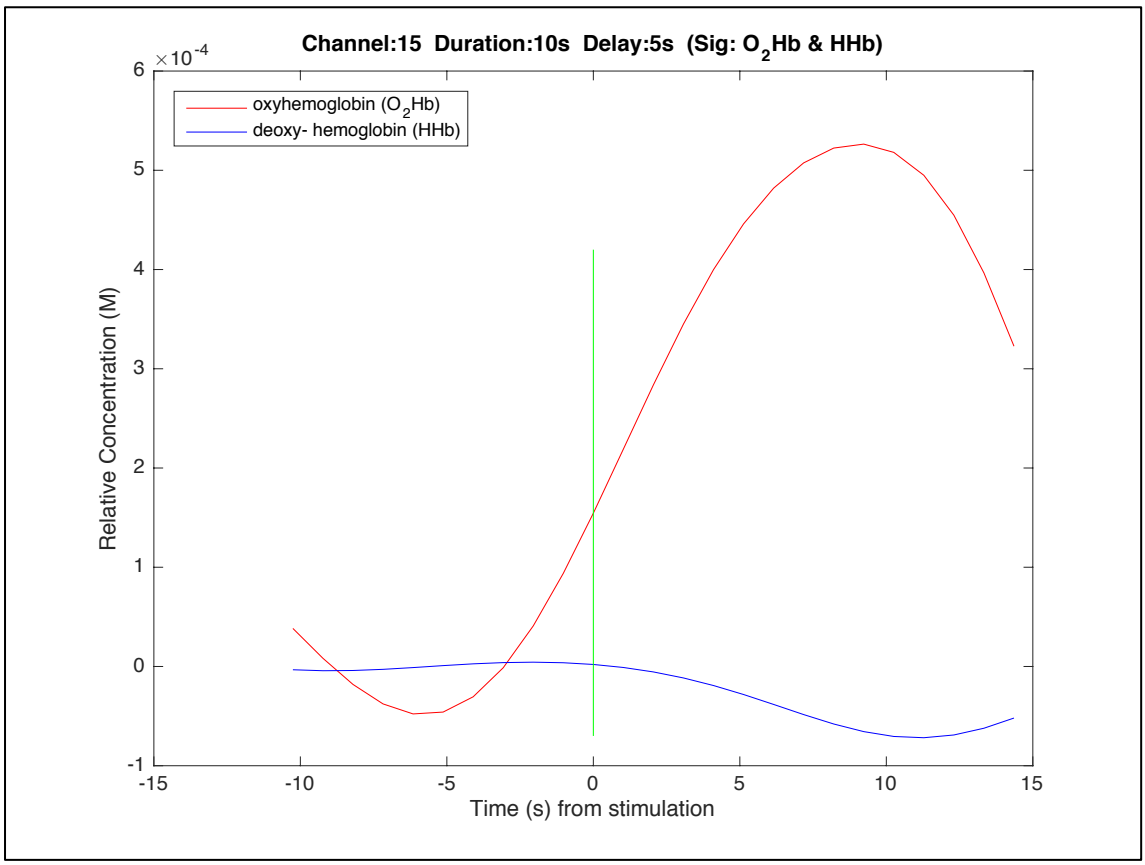
Channel:15 Duration:10s Delay:5s (Sig: O2Hb & HHb)
×10-4
oxyhemoglobin (O2Hb)
deoxy- hemoglobin (HHb)
Relative Concentration (M)
Time (s) from stimulation

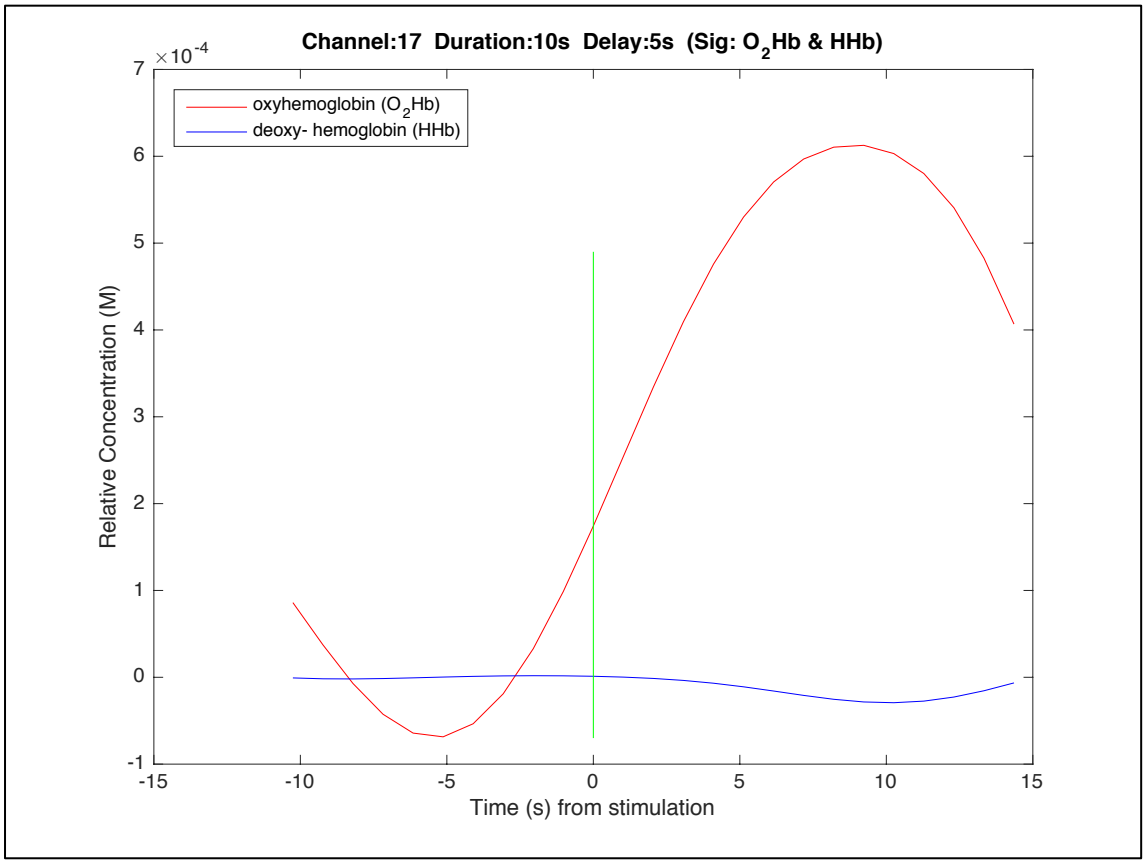
Channel:17 Duration:10s Delay:5s (Sig: O2Hb & HHb)
×10-4
oxyhemoglobin (O2Hb)
deoxy- hemoglobin (HHb)
Relative Concentration (M)
Time (s) from stimulation

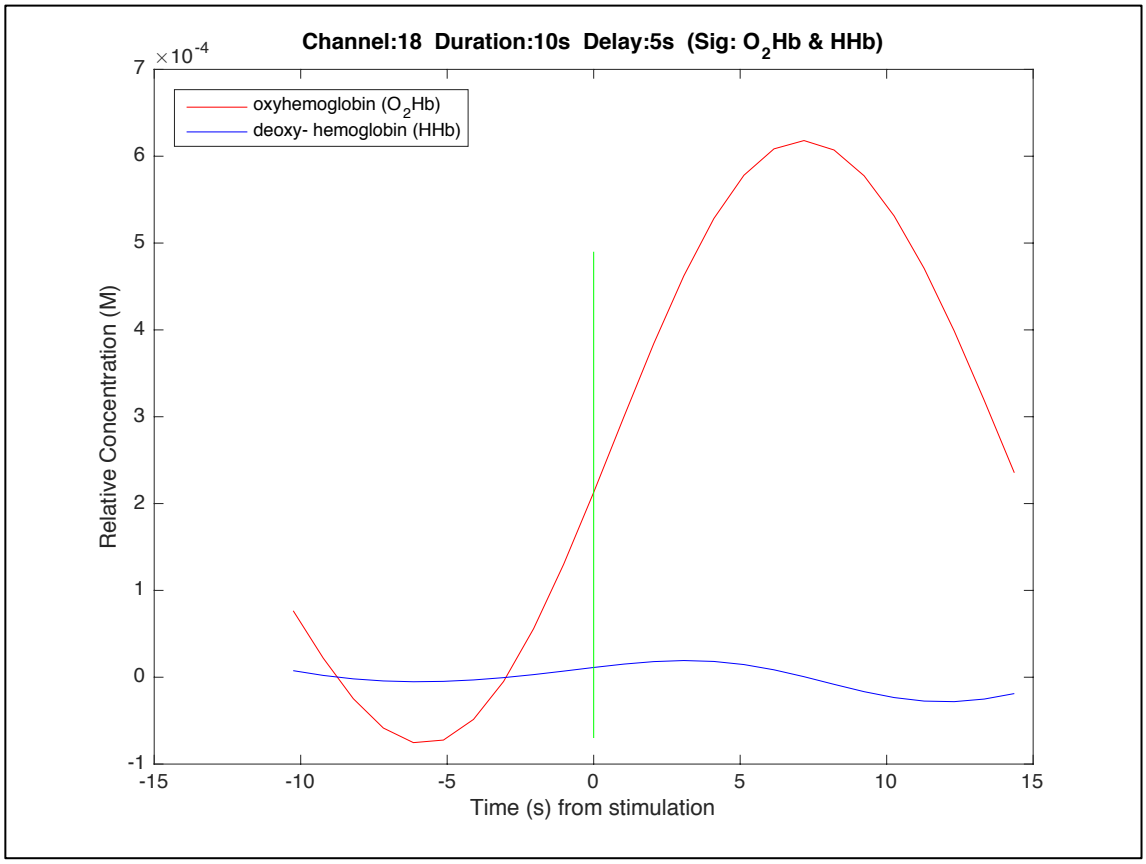
Channel:18 Duration:10s Delay:5s (Sig: O2Hb & HHb)
×10-4
oxyhemoglobin (O2Hb)
deoxy- hemoglobin (HHb)
Relative Concentration (M)
Time (s) from stimulation
7
6
5
4
3
2
1
0
-1
-15
-10
-5
0
5
10
15

51-007

Condition 1: Foveal Quad Stimulation

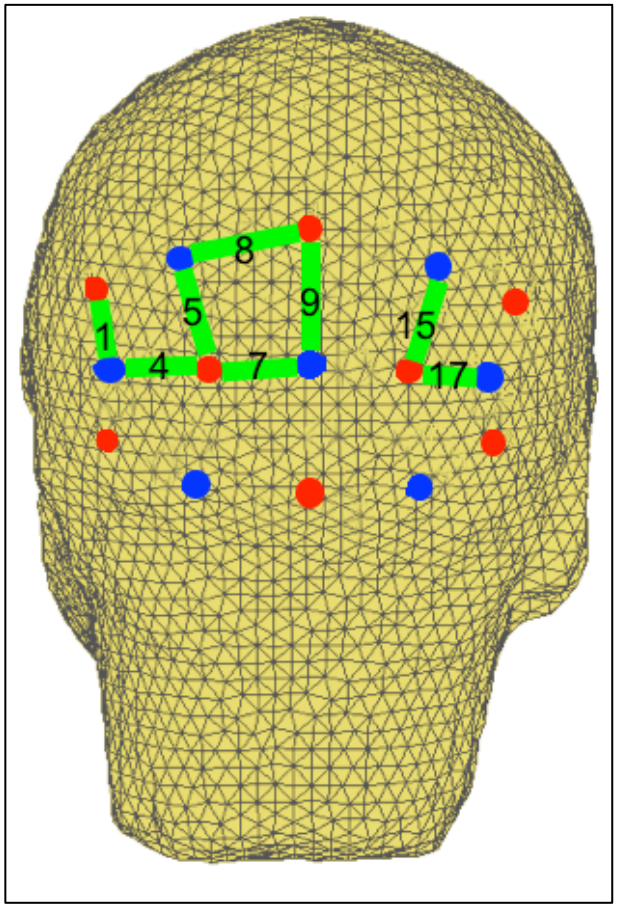

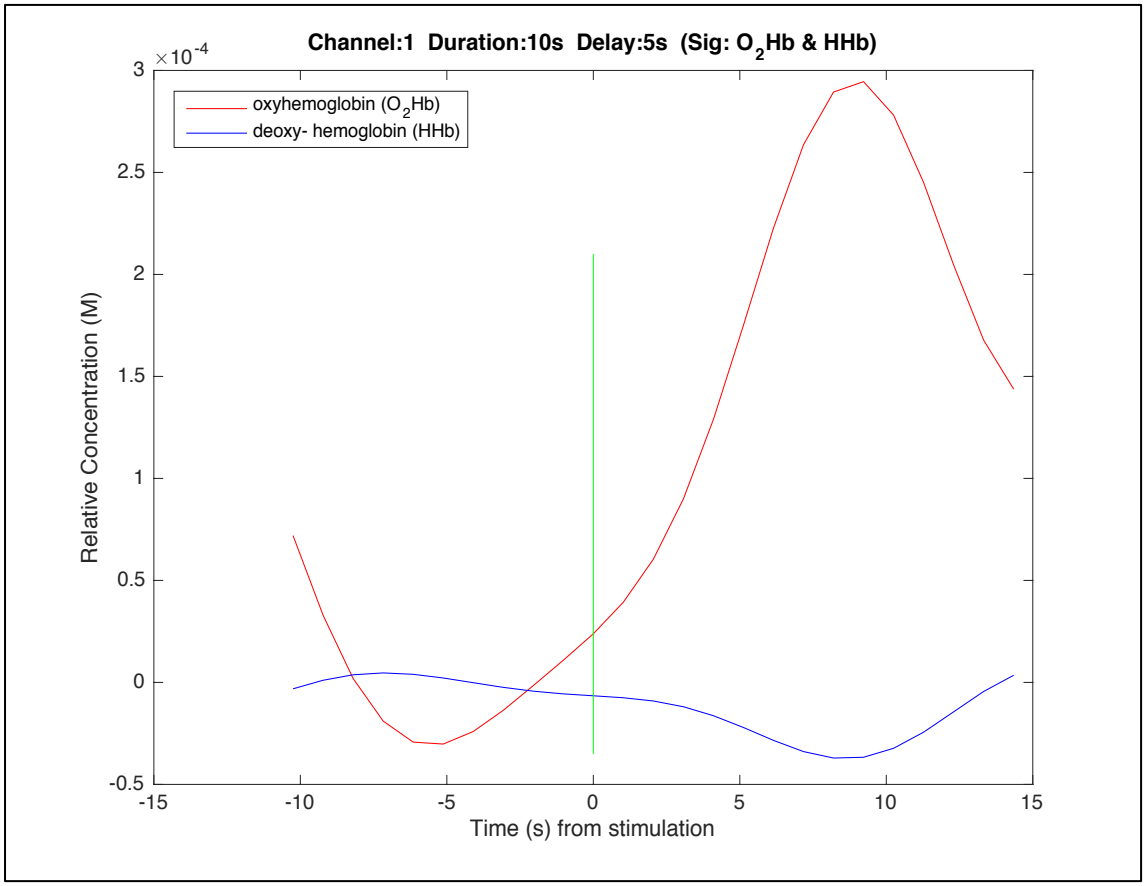

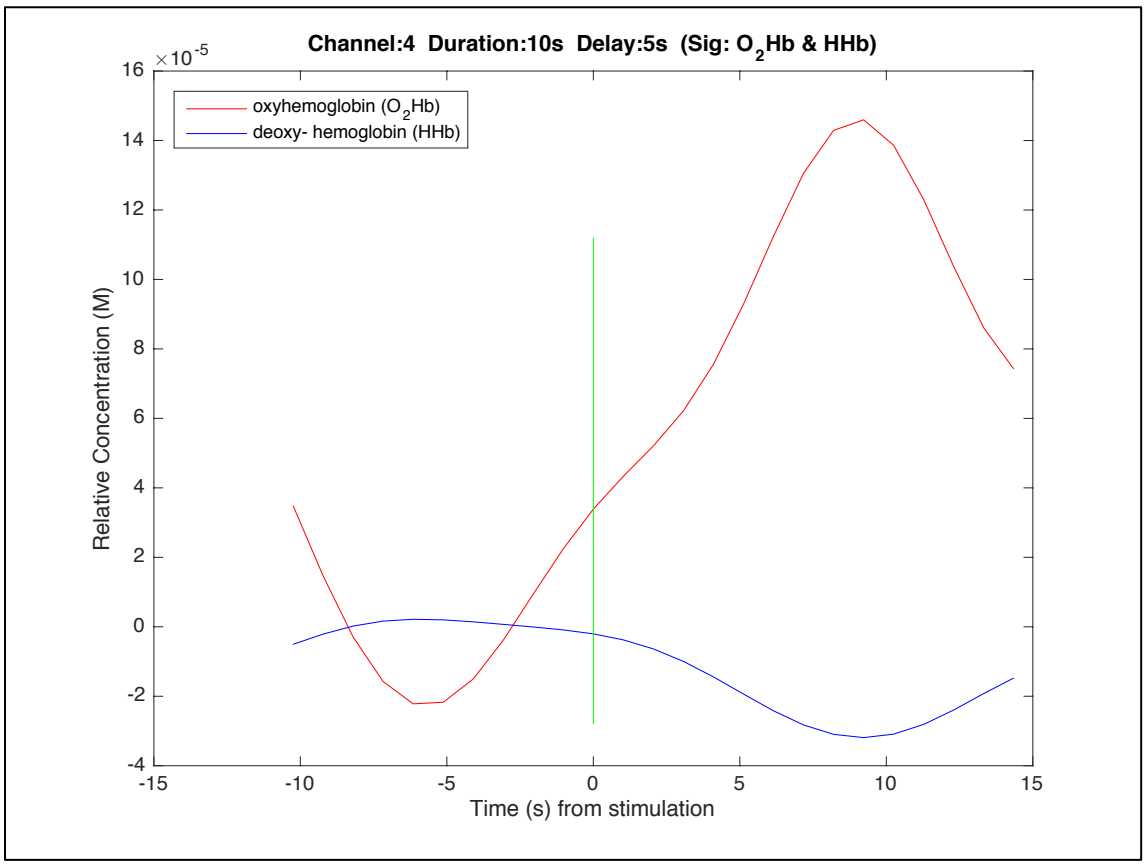
Channel:4 Duration:10s Delay:5s (Sig: O2Hb & HHb)
×10-5
oxyhemoglobin (O2Hb)
deoxy- hemoglobin (HHb)
Relative Concentration (M)
Time (s) from stimulation

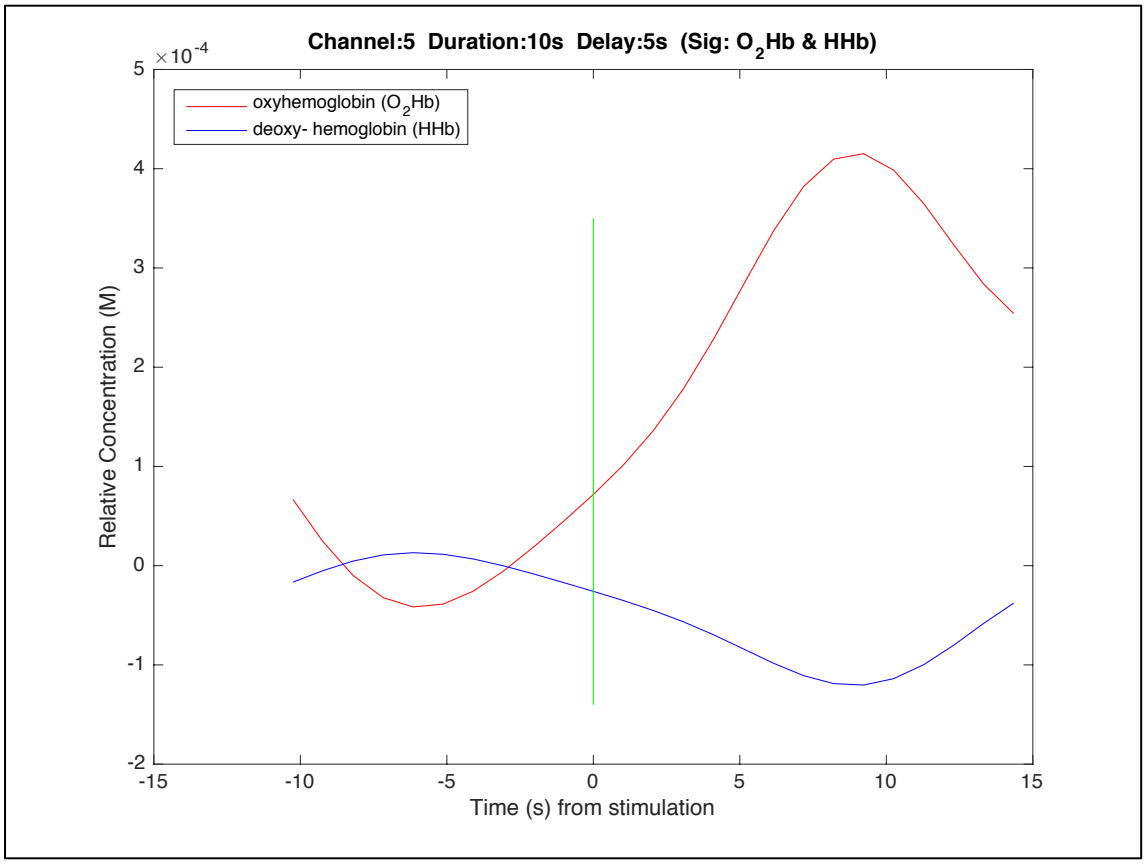
Channel:5 Duration:10s Delay:5s (Sig: O2Hb & HHb)
×10-4
oxyhemoglobin (O2Hb)
deoxy- hemoglobin (HHb)
Relative Concentration (M)
Time (s) from stimulation

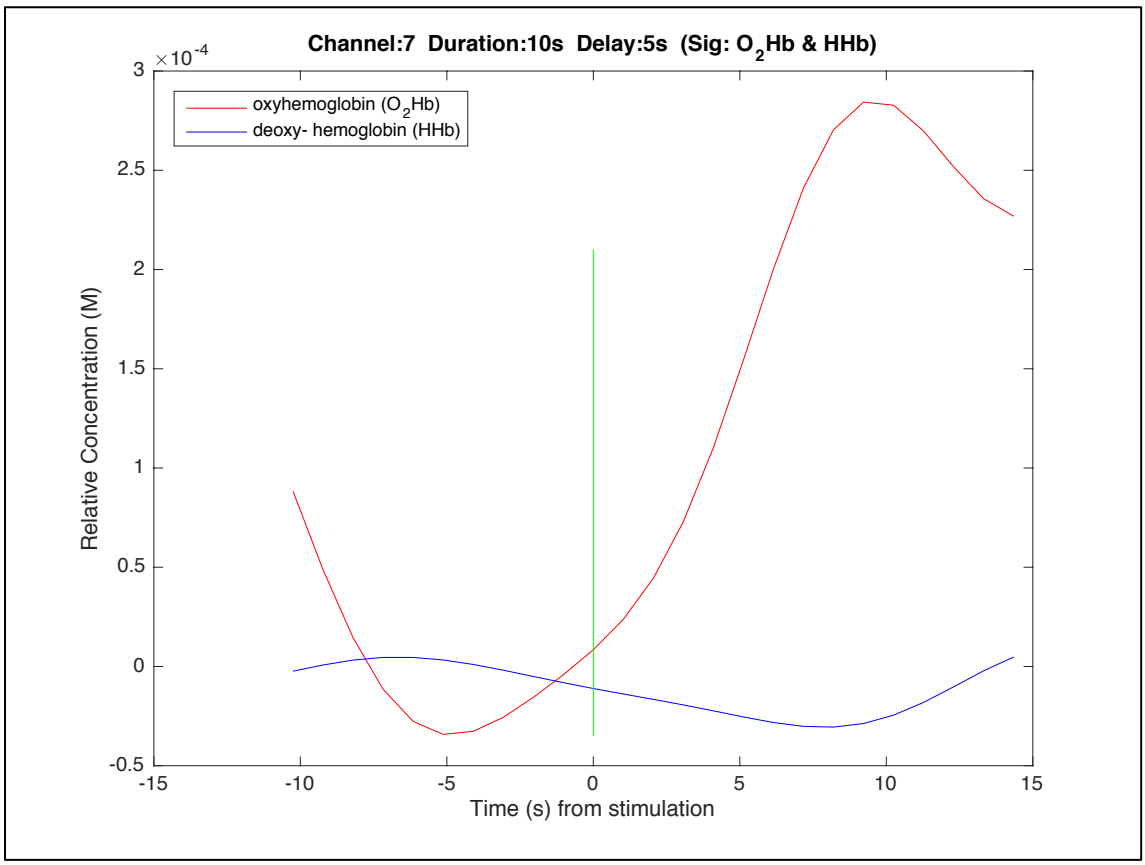
Channel:7 Duration:10s Delay:5s (Sig: O2Hb & HHb)
×10-4
oxyhemoglobin (O2Hb)
deoxy- hemoglobin (HHb)
Relative Concentration (M)
Time (s) from stimulation

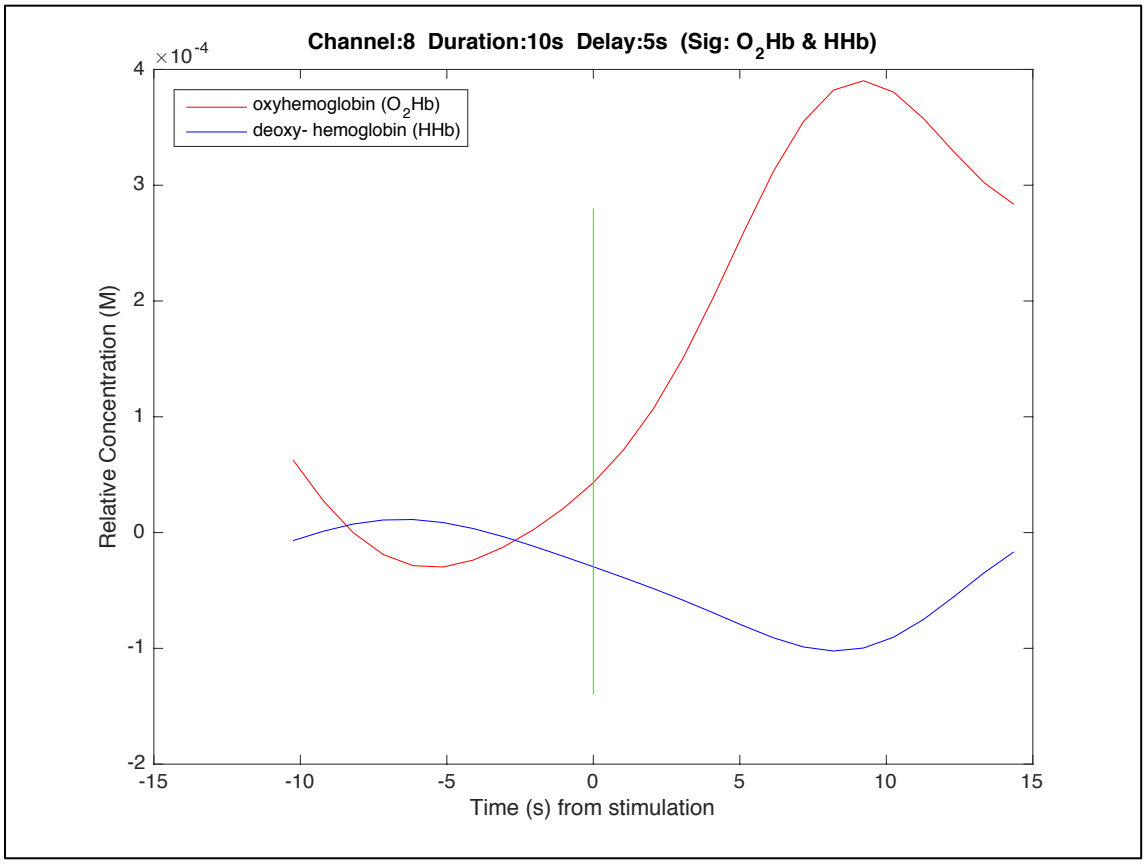
Channel:8 Duration:10s Delay:5s (Sig: O2Hb & HHb)
×10-4
oxyhemoglobin (O2Hb)
deoxy- hemoglobin (HHb)
Relative Concentration (M)
Time (s) from stimulation

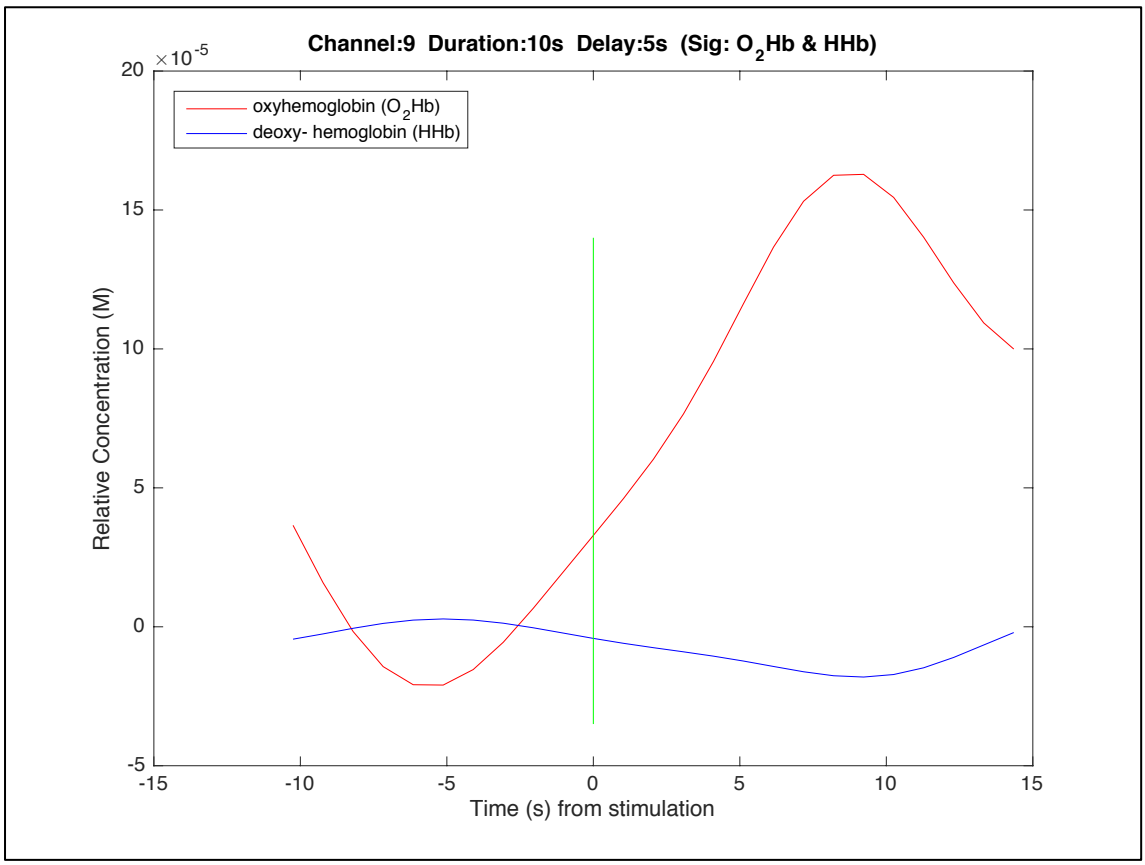
Channel:9 Duration:10s Delay:5s (Sig: O2Hb & HHb)
×10-5
20
15
10
5
0
-5
oxyhemoglobin (O2Hb)
deoxy- hemoglobin (HHb)
Relative Concentration (M)
-15
-10
-5
0
5
10
15
Time (s) from stimulation

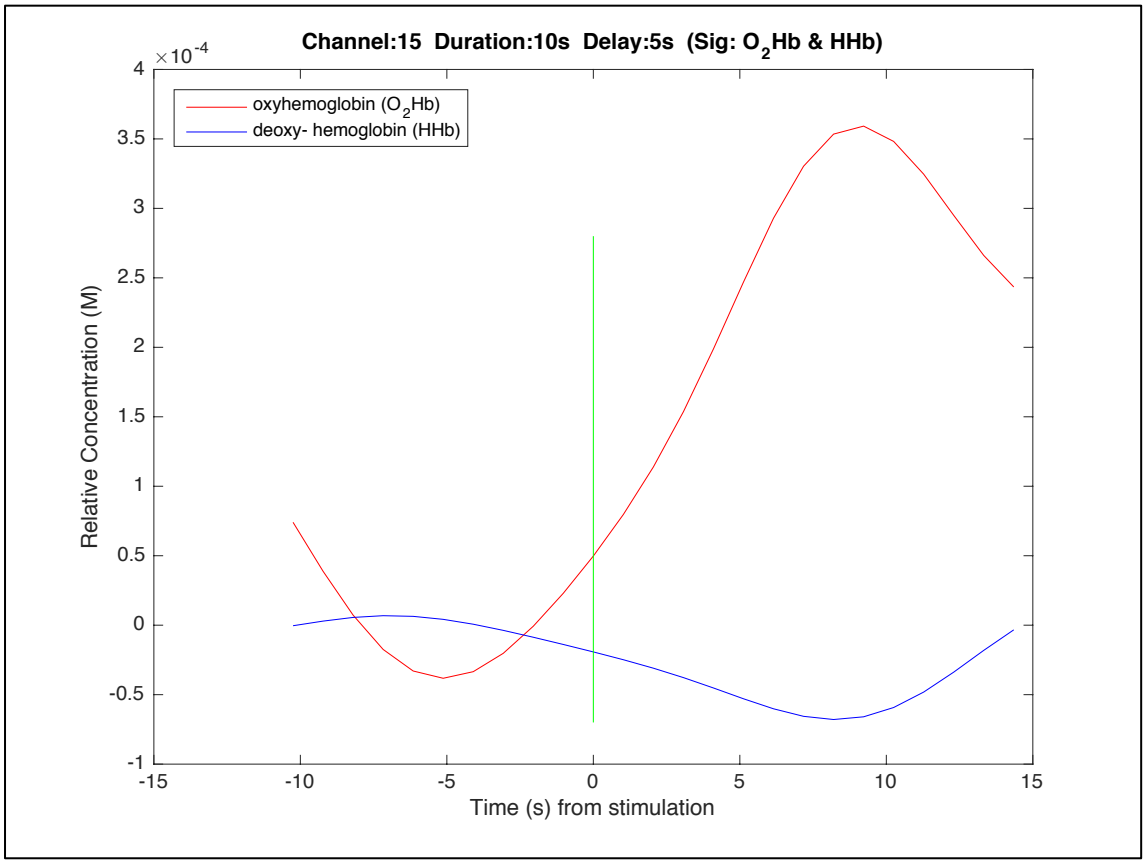
Channel:15 Duration:10s Delay:5s (Sig: O2Hb & HHb)
×10-4
4
3.5
3
2.5
2
1.5
1
0.5
0
-0.5
-1
oxyhemoglobin (O2Hb)
deoxy- hemoglobin (HHb)
Relative Concentration (M)
-15
-10
-5
0
5
10
15
Time (s) from stimulation

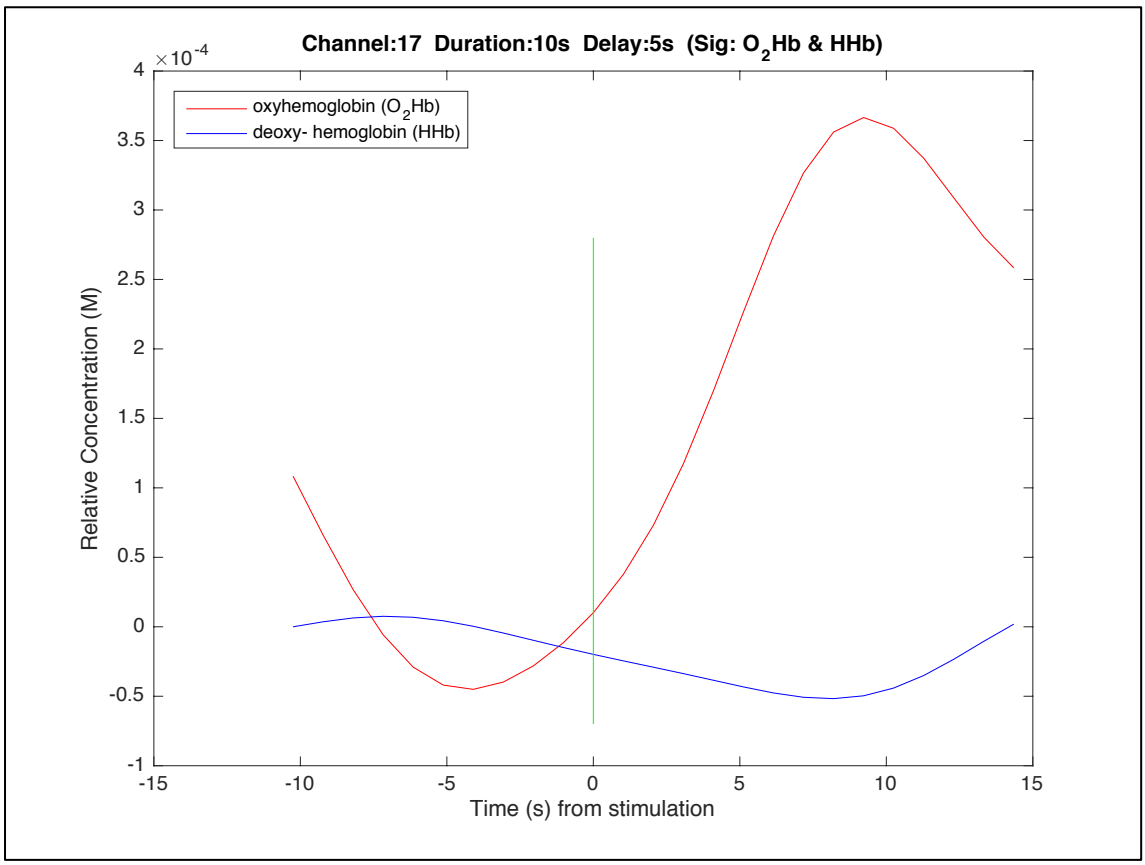
Channel:17 Duration:10s Delay:5s (Sig: O2Hb & HHb)
×10-4
oxyhemoglobin (O2Hb)
deoxy- hemoglobin (HHb)
Relative Concentration (M)
Time (s) from stimulation
4
3.5
3
2.5
2
1.5
1
0.5
0
-0.5
-1
-15
-10
-5
0
5
10
15

Condition 2: Simultaneous Stimulation of 6 Quads

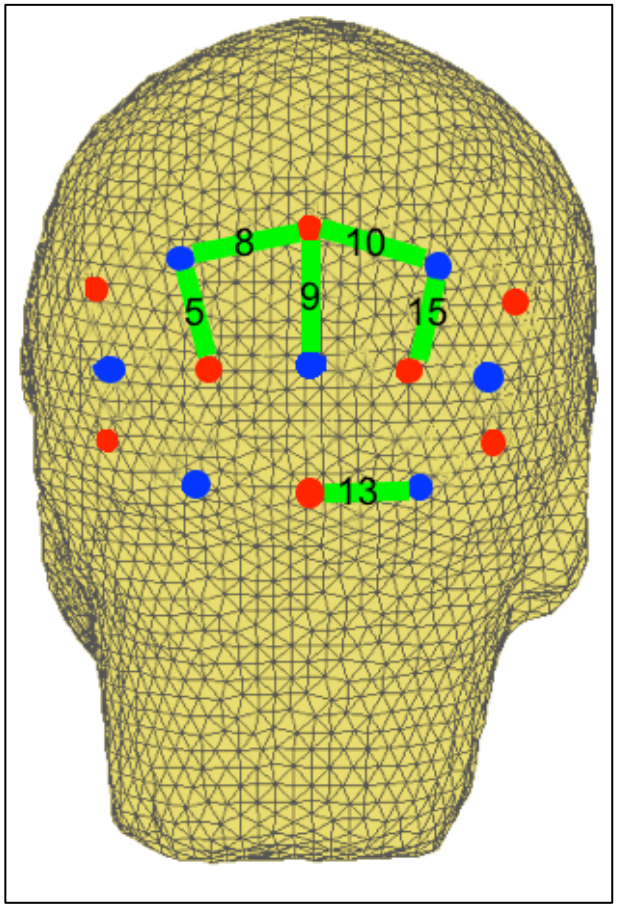

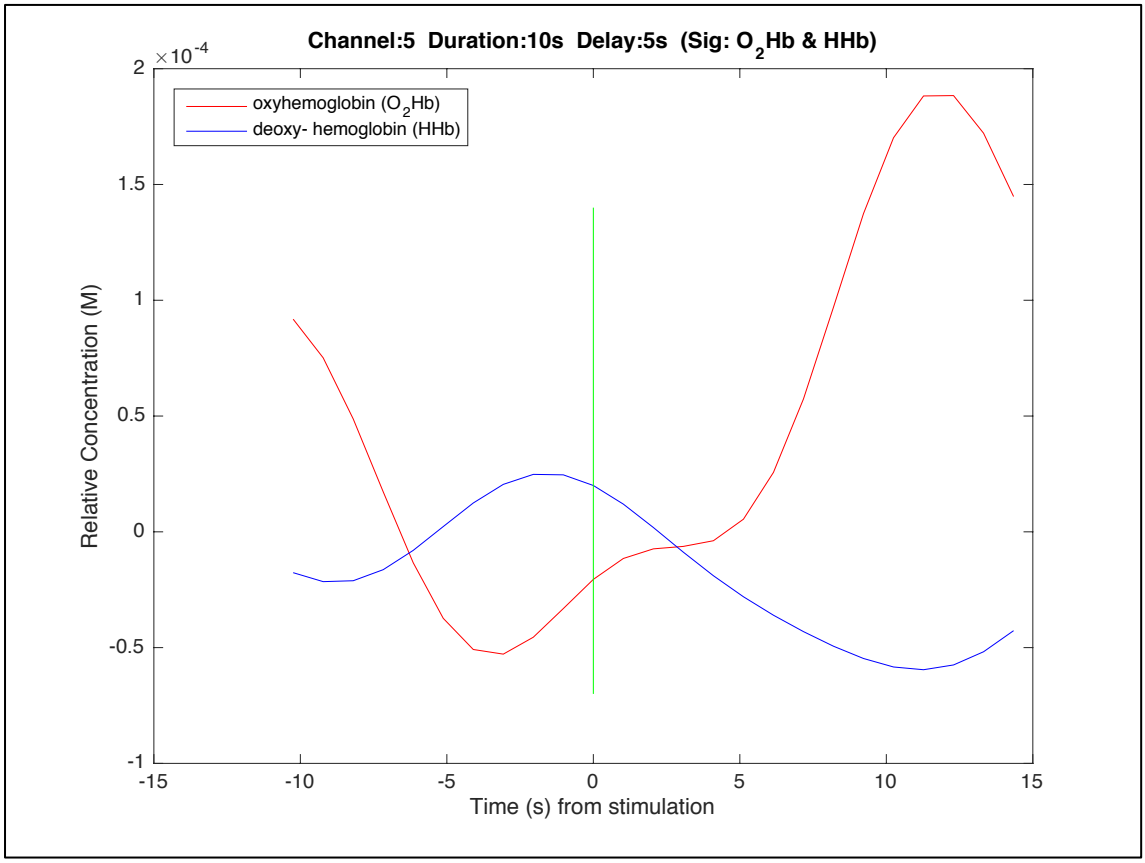

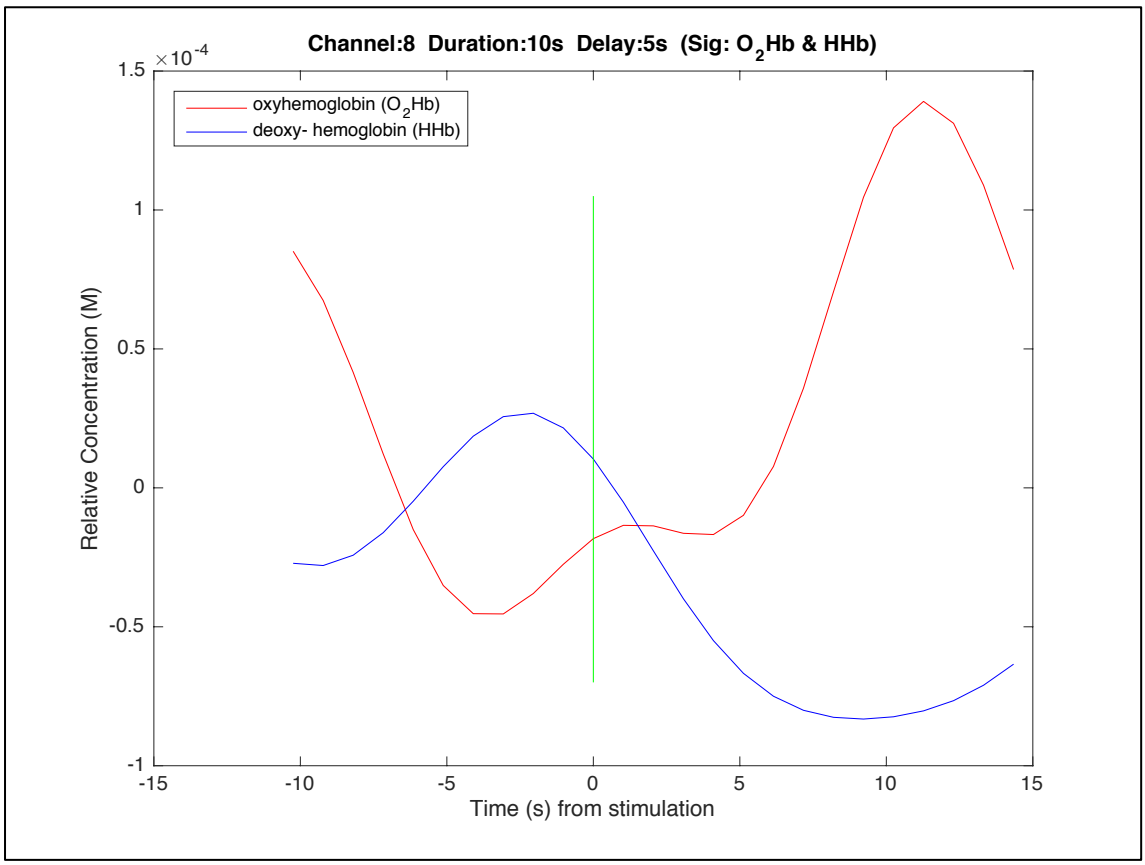
Channel:8 Duration:10s Delay:5s (Sig: O2Hb & HHb)
×10-4
1.5
1
0.5
0
-0.5
-1
oxyhemoglobin (O2Hb)
deoxy- hemoglobin (HHb)
Relative Concentration (M)
-15
-10
-5
0
5
10
15
Time (s) from stimulation

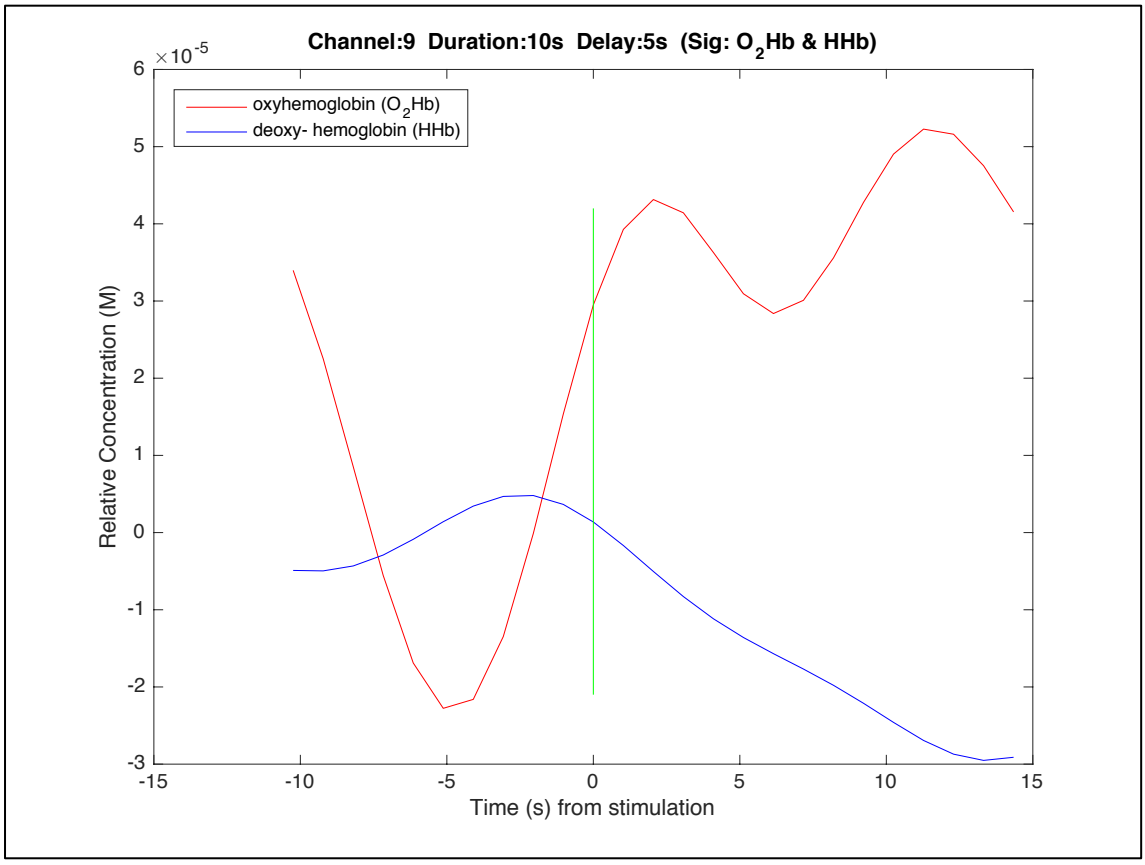
Channel:9 Duration:10s Delay:5s (Sig: O2Hb & HHb)
×10-5
6
5
4
3
2
1
0
-1
-2
-3
oxyhemoglobin (O2Hb)
deoxy- hemoglobin (HHb)
Relative Concentration (M)
-15
-10
-5
0
5
10
15
Time (s) from stimulation

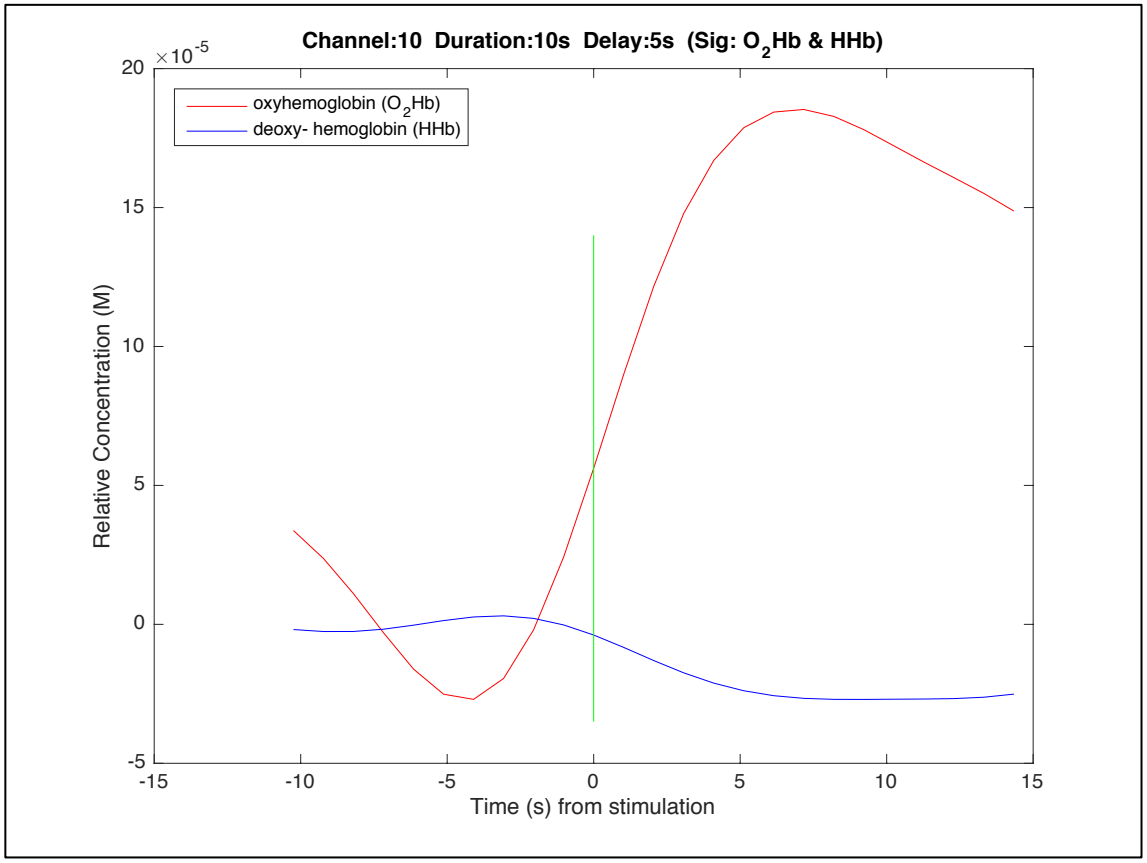
Channel:10 Duration:10s Delay:5s (Sig: O2Hb & HHb)
×10-5
20
15
10
5
0
-5
oxyhemoglobin (O2Hb)
deoxy- hemoglobin (HHb)
Relative Concentration (M)
-15
-10
-5
0
5
10
15
Time (s) from stimulation

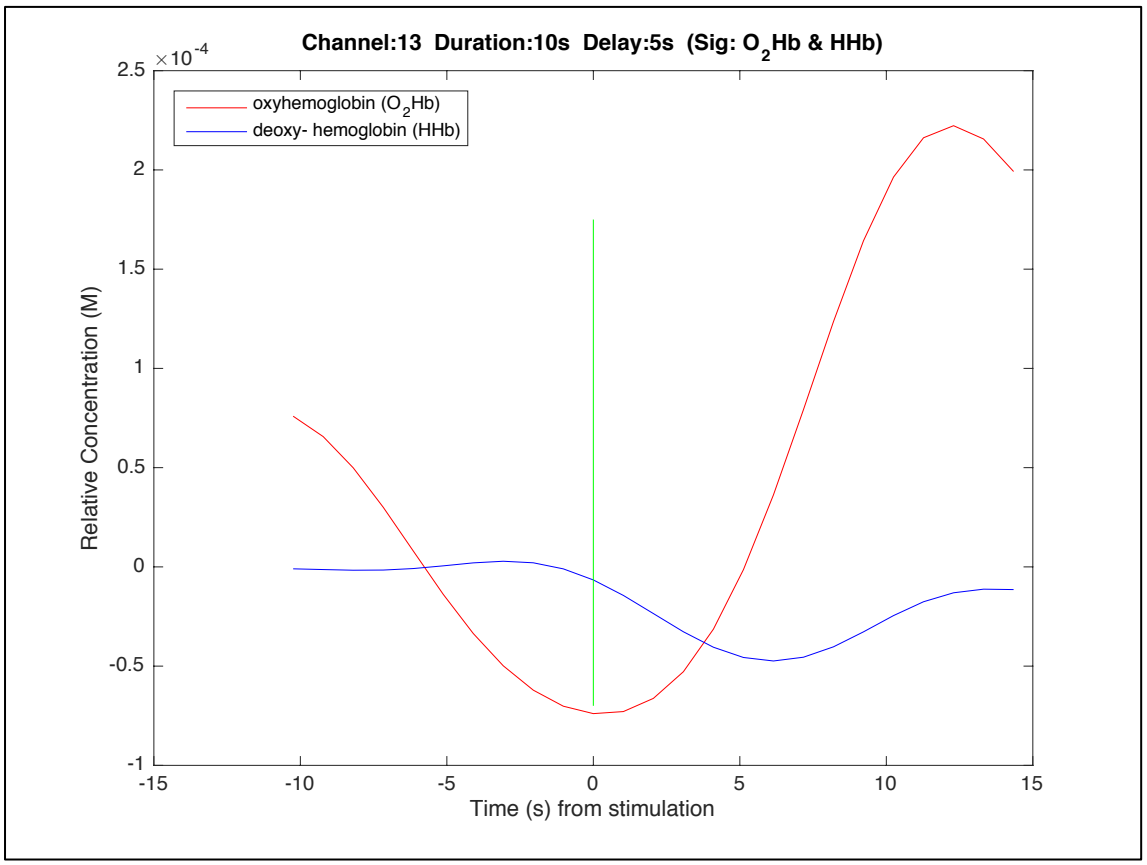
Channel:13 Duration:10s Delay:5s (Sig: O2Hb & HHb)
×10-4
2.5
2
1.5
1
0.5
0
-0.5
-1
oxyhemoglobin (O2Hb)
deoxy- hemoglobin (HHb)
Relative Concentration (M)
-15
-10
-5
0
5
10
15
Time (s) from stimulation

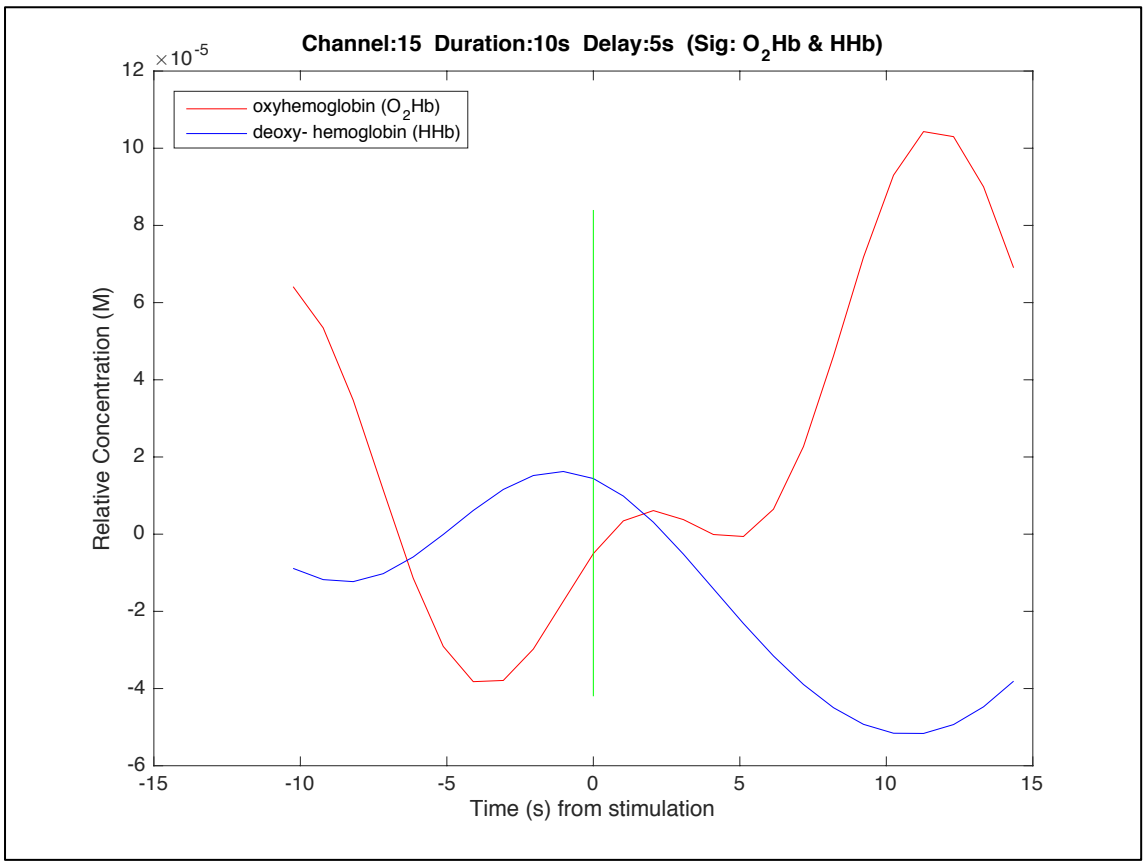
Channel:15 Duration:10s Delay:5s (Sig: O2Hb & HHb)
×10-5
12
10
8
6
4
2
0
-2
-4
-6
oxyhemoglobin (O2Hb)
deoxy- hemoglobin (HHb)
Relative Concentration (M)
-15
-10
-5
0
5
10
15
Time (s) from stimulation

Condition 3: Sequential Stimulation of 6 Quads

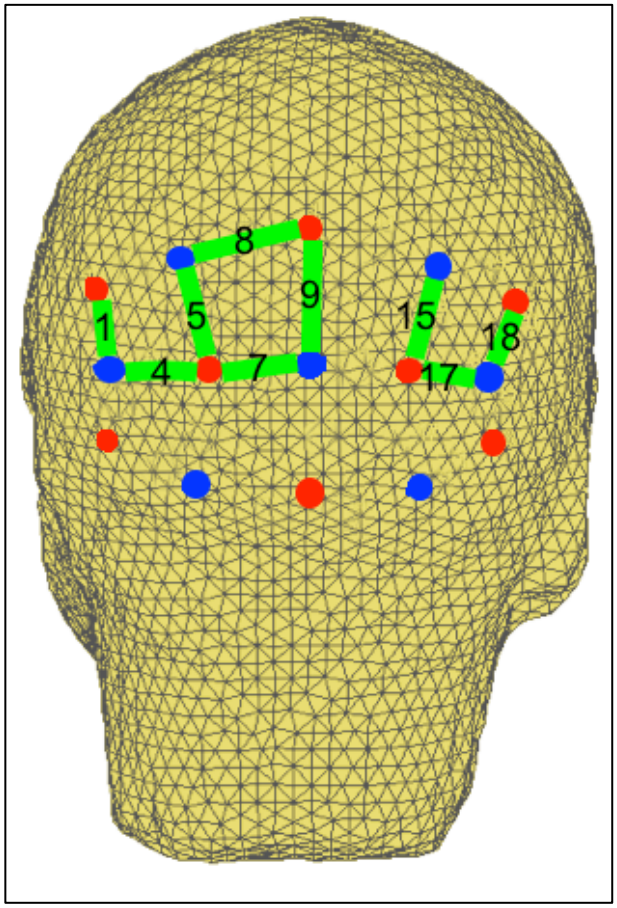

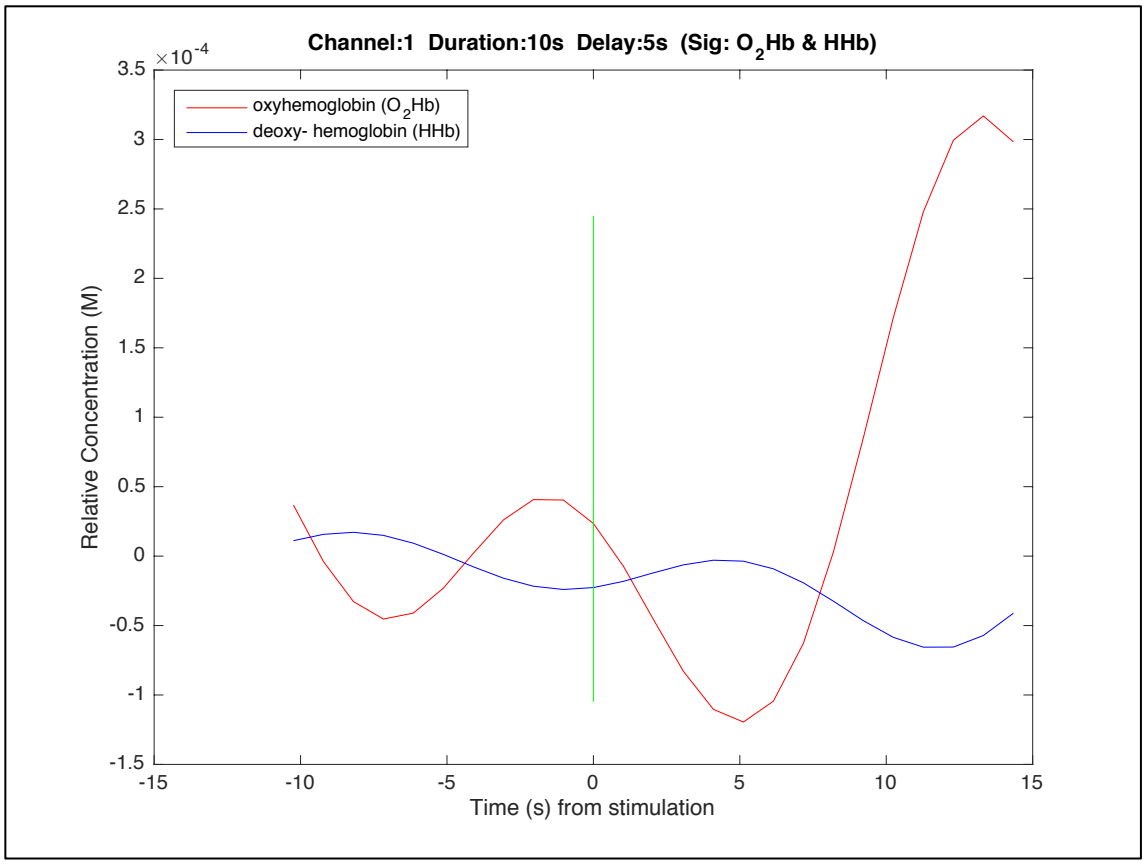

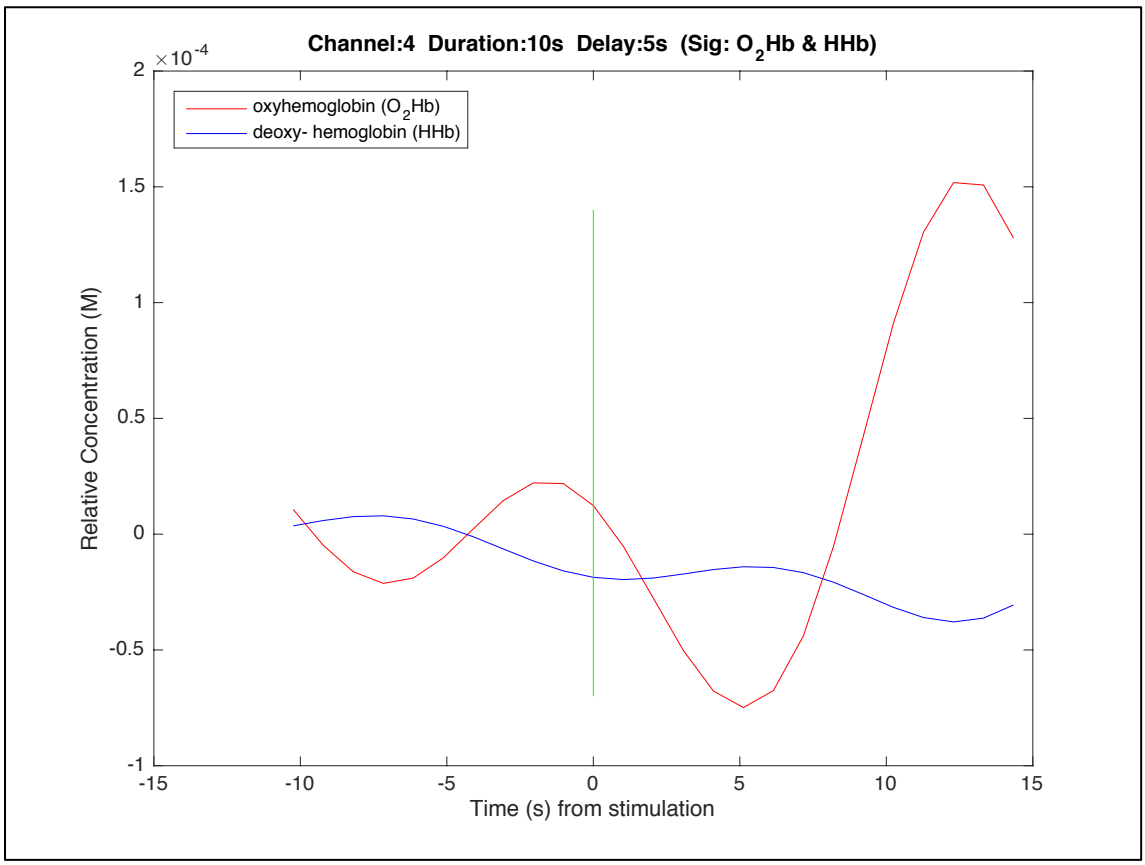
Channel:4 Duration:10s Delay:5s (Sig: O2Hb & HHb)
×10-4
oxyhemoglobin (O2Hb)
deoxy- hemoglobin (HHb)
Relative Concentration (M)
Time (s) from stimulation

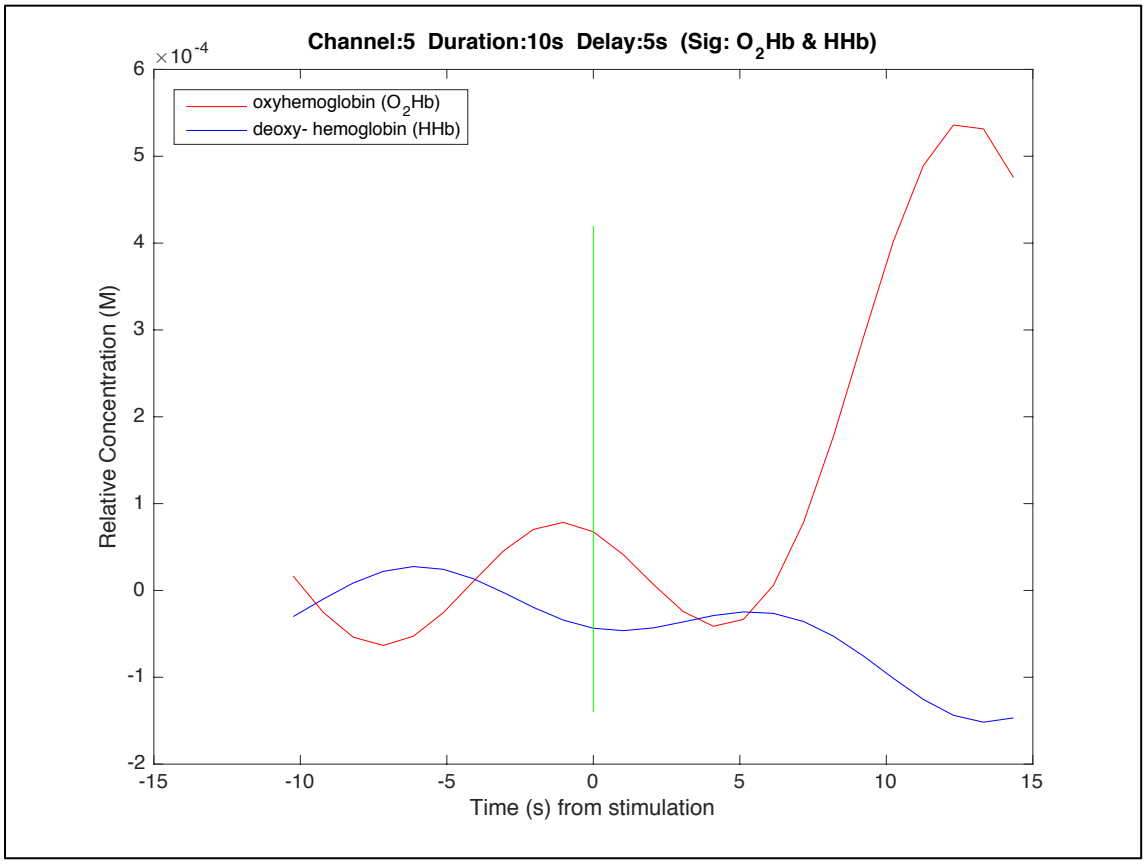
Channel:5 Duration:10s Delay:5s (Sig: O2Hb & HHb)
×10-4
oxyhemoglobin (O2Hb)
deoxy- hemoglobin (HHb)
Relative Concentration (M)
Time (s) from stimulation

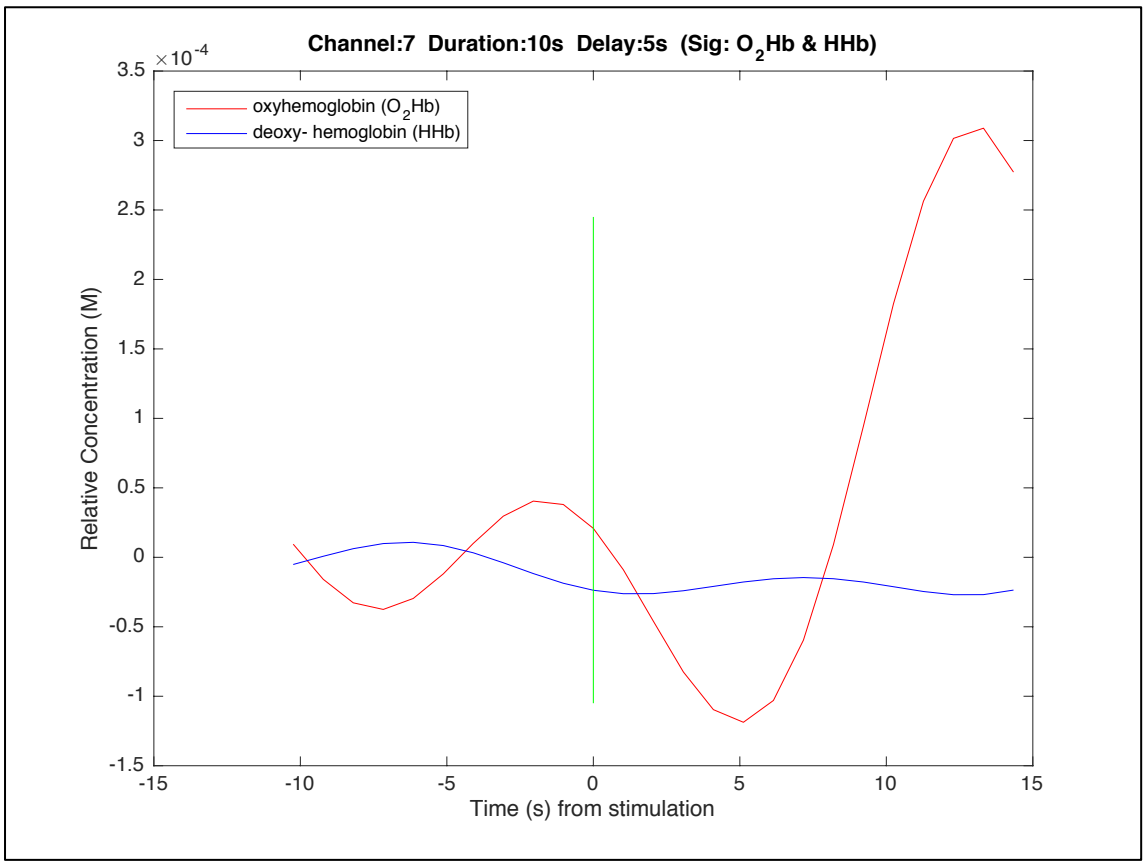
Channel:7 Duration:10s Delay:5s (Sig: O2Hb & HHb)
×10-4
oxyhemoglobin (O2Hb)
deoxy- hemoglobin (HHb)
Relative Concentration (M)
Time (s) from stimulation

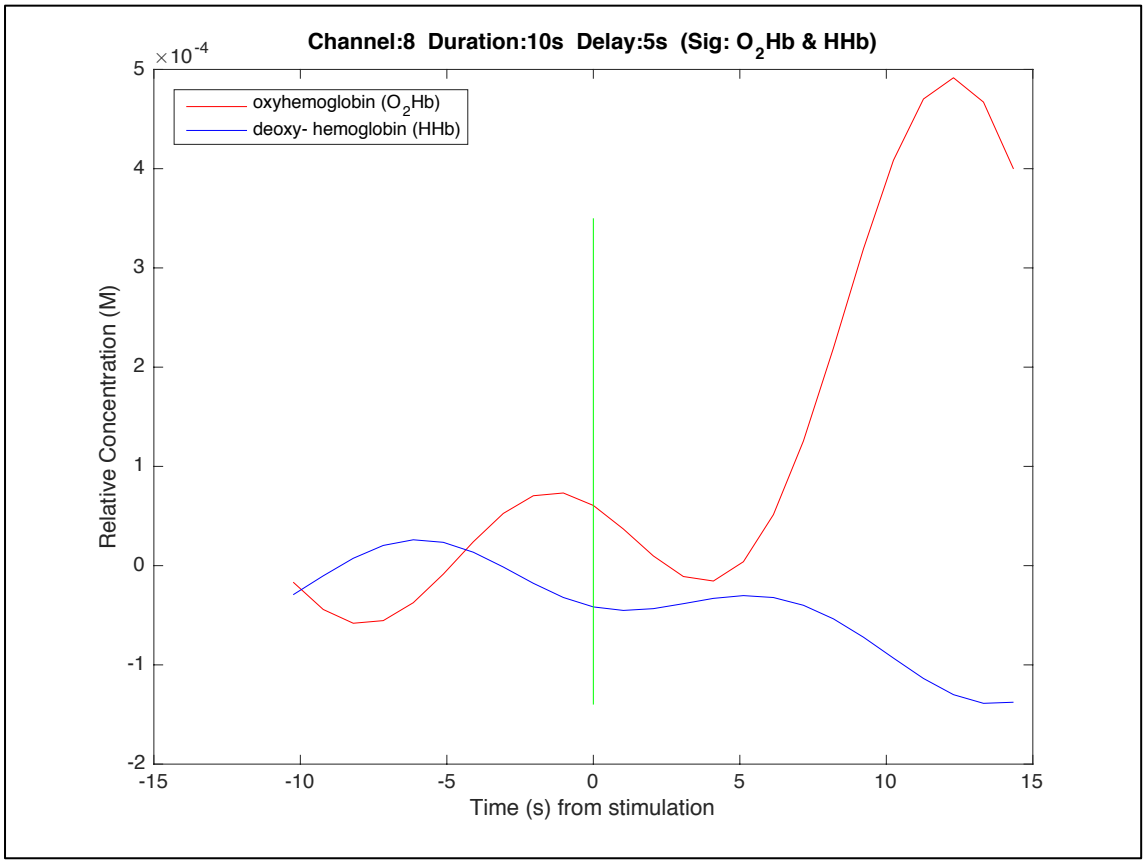
Channel:8 Duration:10s Delay:5s (Sig: O2Hb & HHb)
×10-4
oxyhemoglobin (O2Hb)
deoxy- hemoglobin (HHb)
Relative Concentration (M)
Time (s) from stimulation

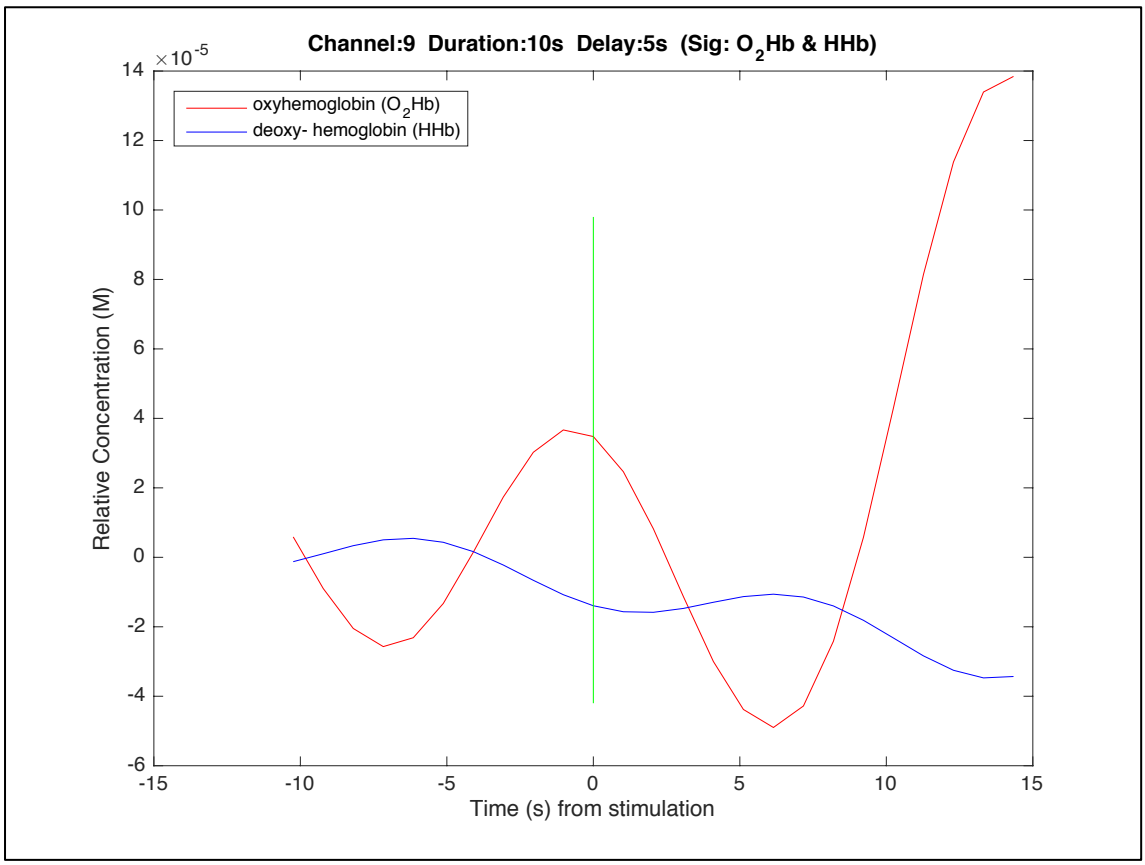
Channel:9 Duration:10s Delay:5s (Sig: O2Hb & HHb)
×10-5
oxyhemoglobin (O2Hb)
deoxy- hemoglobin (HHb)
Relative Concentration (M)
Time (s) from stimulation

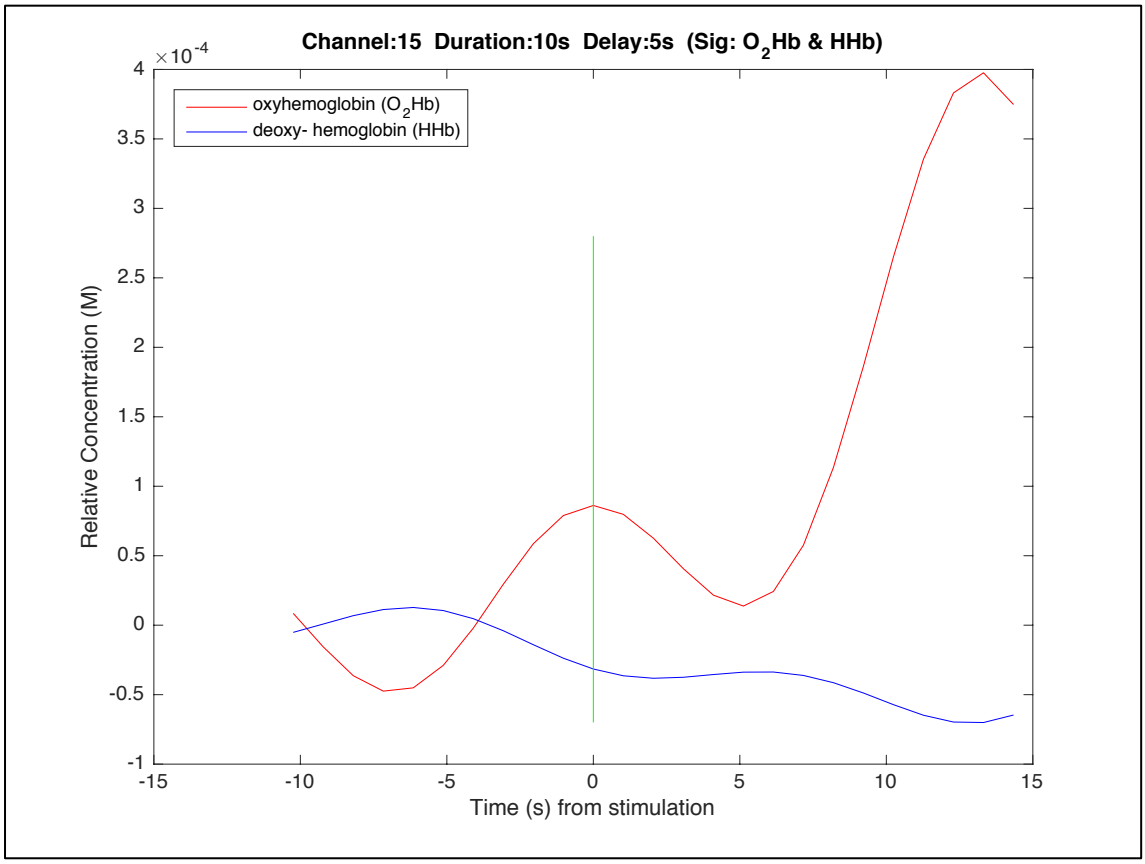
Channel:15 Duration:10s Delay:5s (Sig: O2Hb & HHb)
×10-4
oxyhemoglobin (O2Hb)
deoxy- hemoglobin (HHb)
Relative Concentration (M)
Time (s) from stimulation

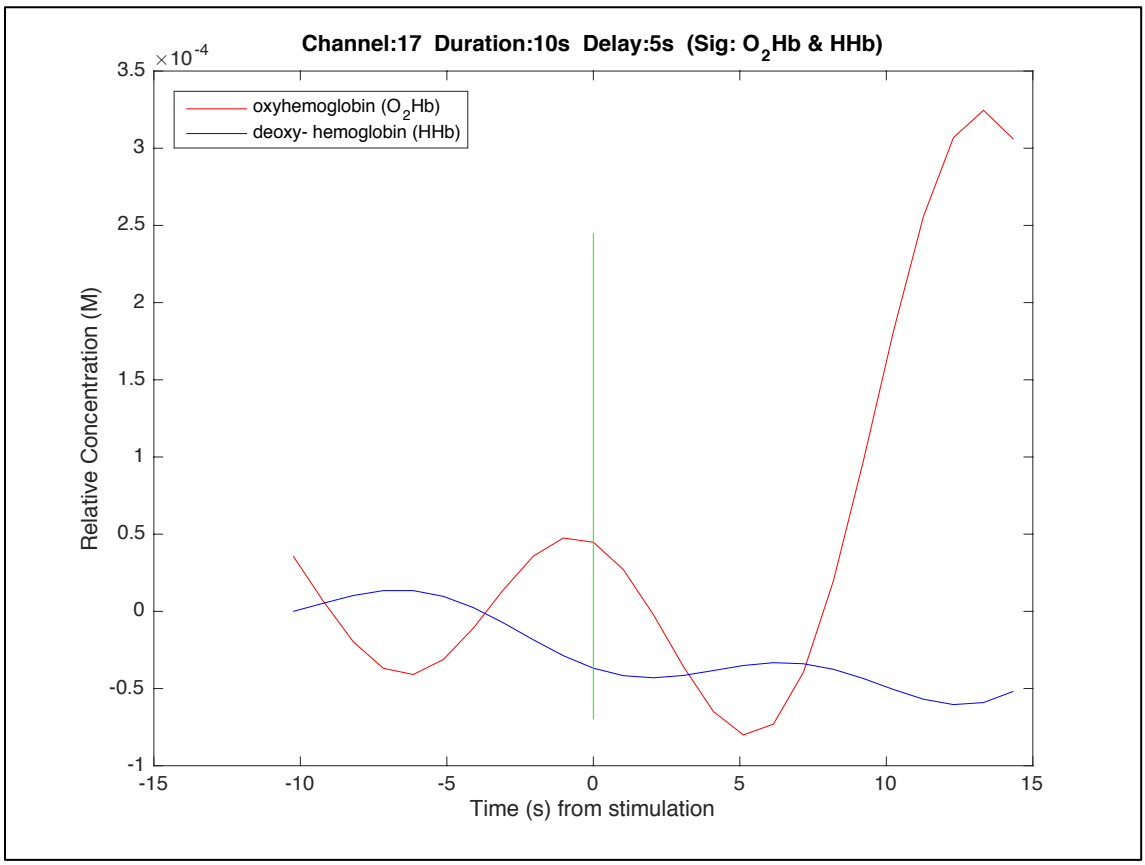
Channel:17 Duration:10s Delay:5s (Sig: O2Hb & HHb)
×10-4
oxyhemoglobin (O2Hb)
deoxy- hemoglobin (HHb)
Relative Concentration (M)
Time (s) from stimulation

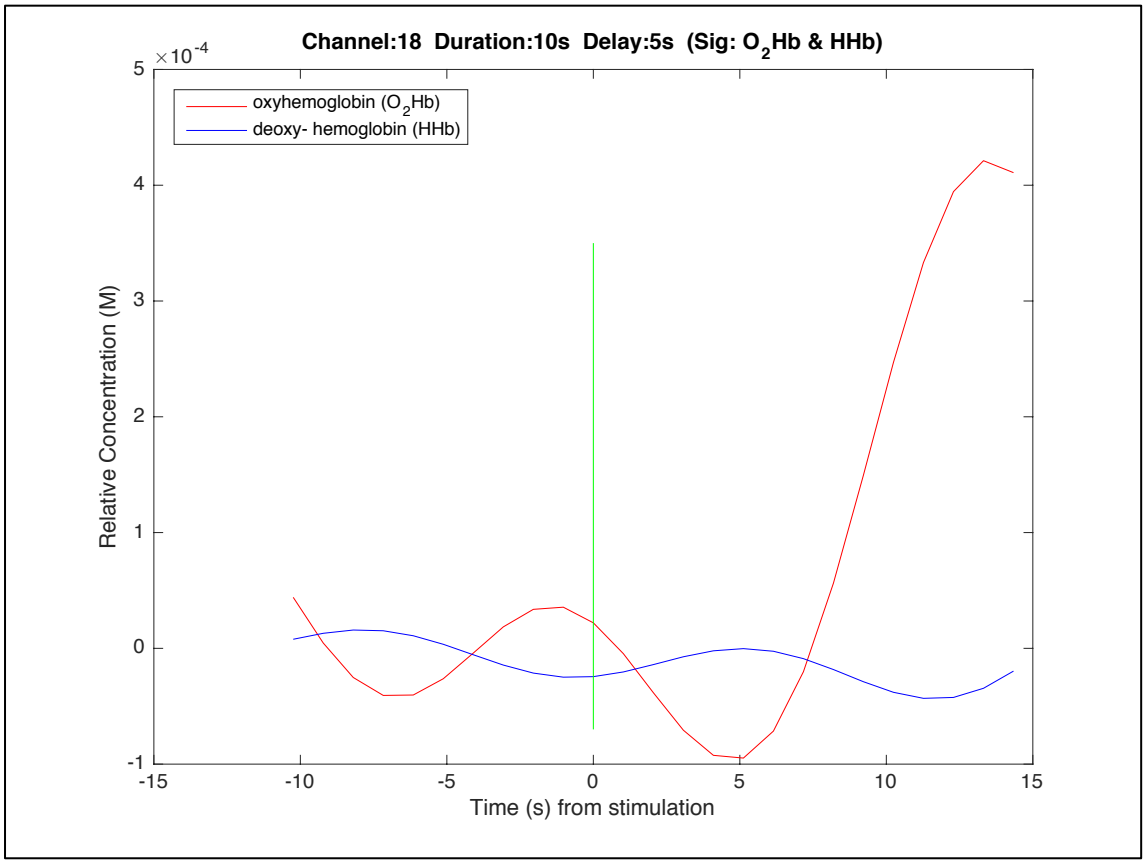
Channel:18 Duration:10s Delay:5s (Sig: O2Hb & HHb)
×10-4
oxyhemoglobin (O2Hb)
deoxy- hemoglobin (HHb)
Relative Concentration (M)
Time (s) from stimulation

51-009

Condition 1: Foveal Quad Stimulation

None of the optode channels showed a positive fNIRS response under Condition 1 stimulations in subject 51-009.

Condition 2: Simultaneous Stimulation of 6 Quads

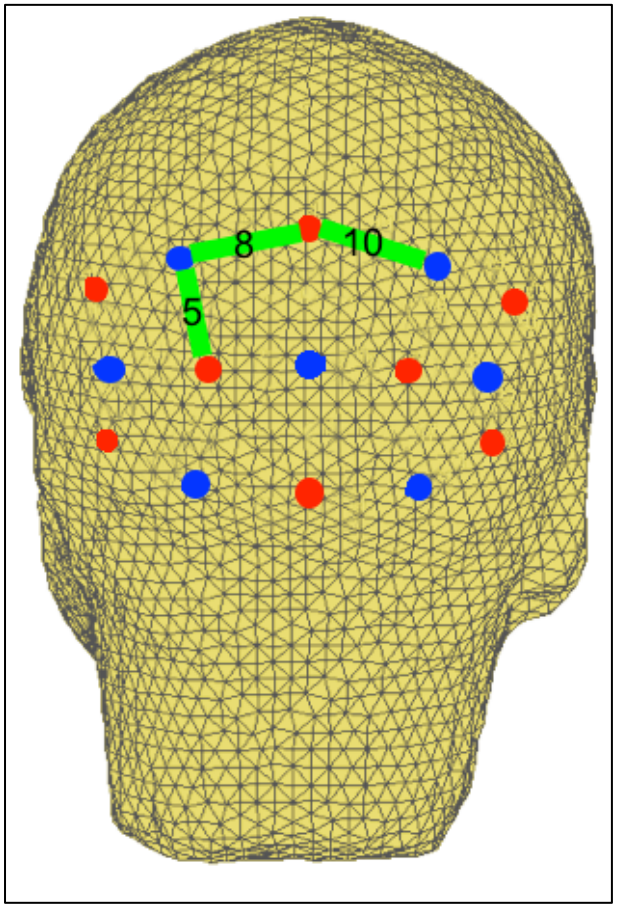

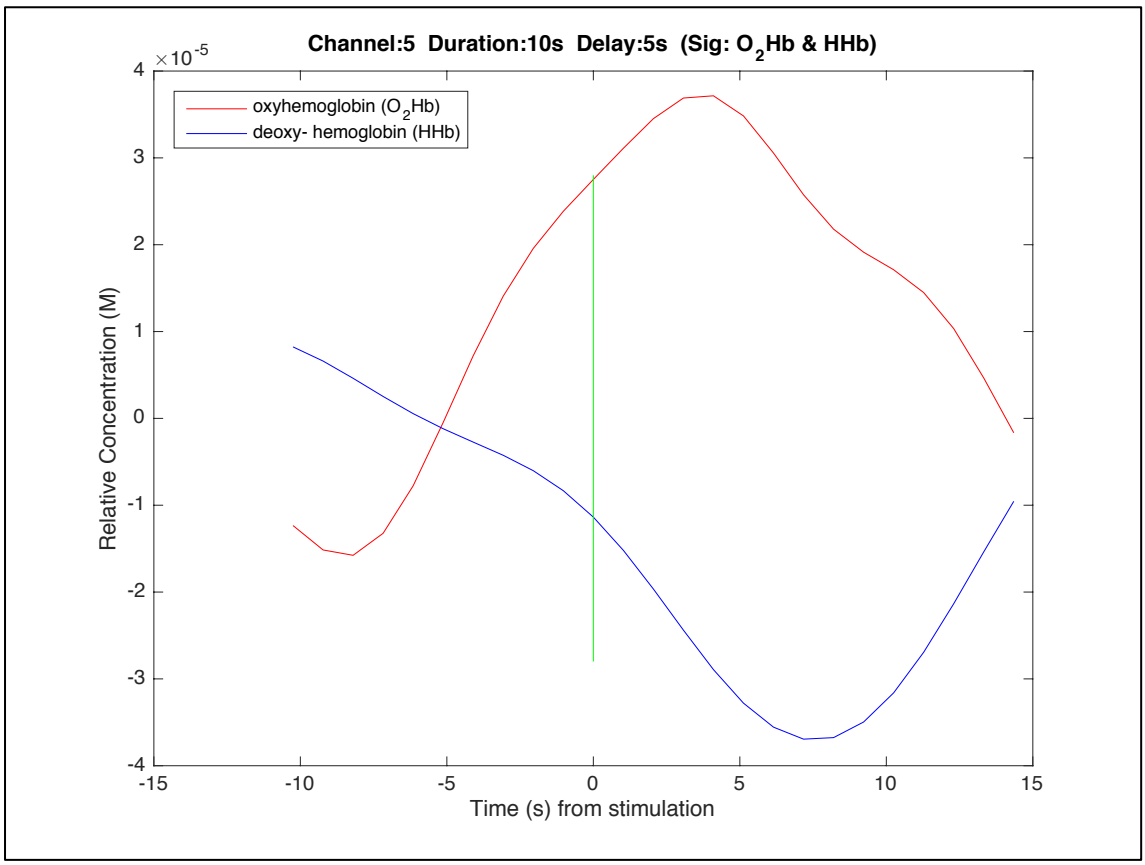
Channel:5 Duration:10s Delay:5s (Sig: O2Hb & HHb)
×10-5
oxyhemoglobin (O2Hb)
deoxy- hemoglobin (HHb)
Relative Concentration (M)
Time (s) from stimulation

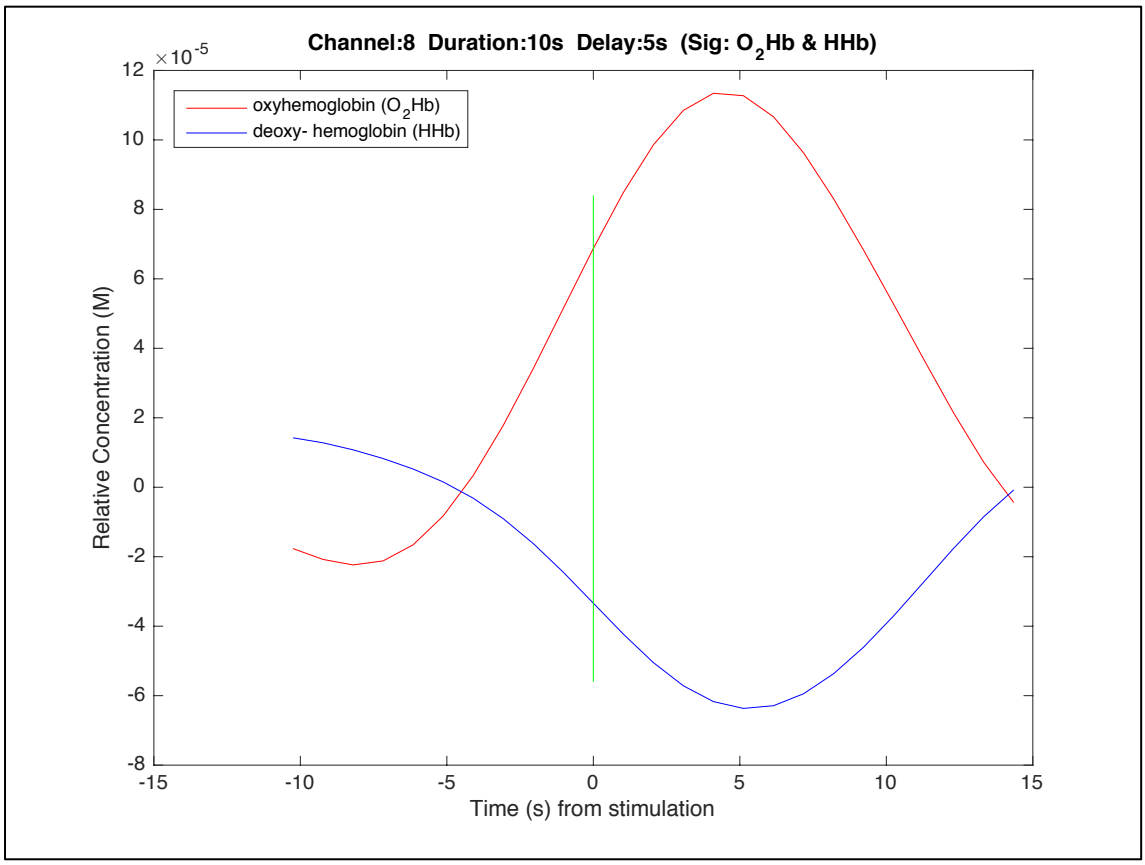
Channel:8 Duration:10s Delay:5s (Sig: O2Hb & HHb)
×10-5
oxyhemoglobin (O2Hb)
deoxy- hemoglobin (HHb)
Relative Concentration (M)
Time (s) from stimulation

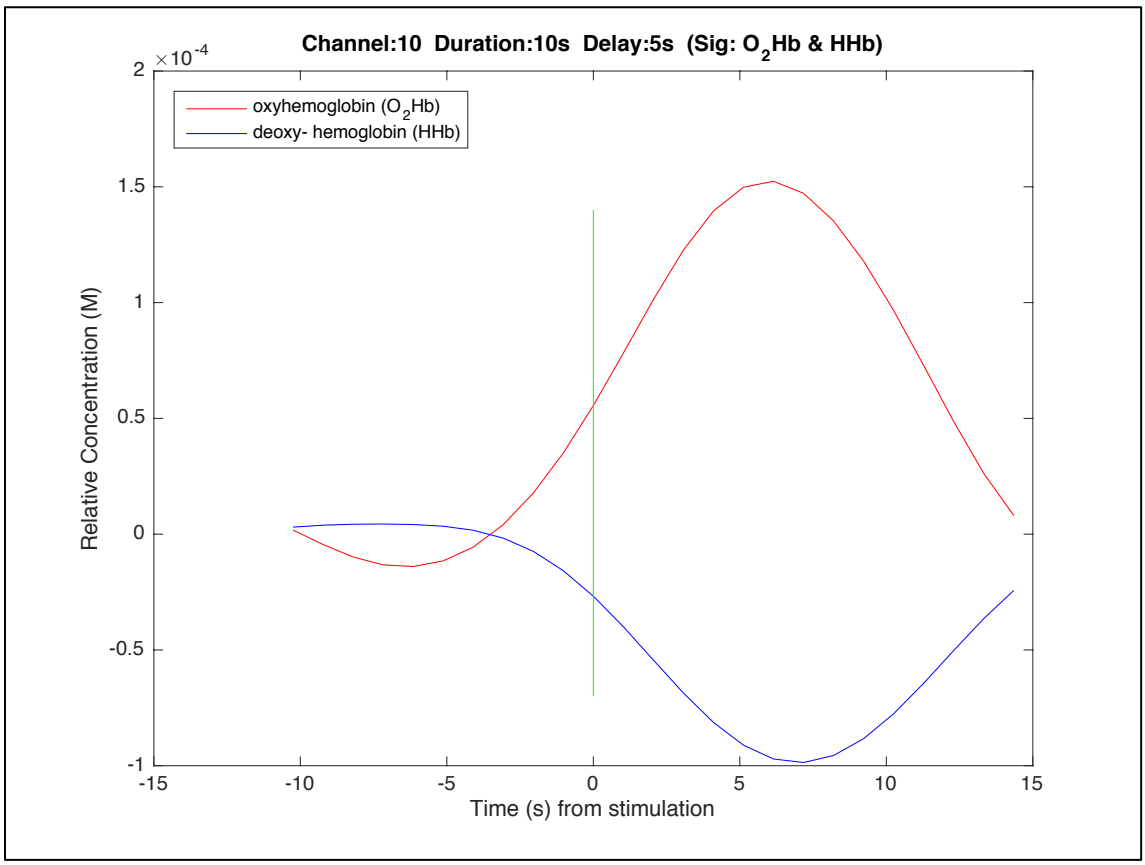
Channel:10 Duration:10s Delay:5s (Sig: O2Hb & HHb)
×10-4
2
1.5
1
0.5
0
-0.5
-1
oxyhemoglobin (O2Hb)
deoxy- hemoglobin (HHb)
Relative Concentration (M)
-15
-10
-5
0
5
10
15
Time (s) from stimulation

Condition 3: Sequential Stimulation of 6 Quads

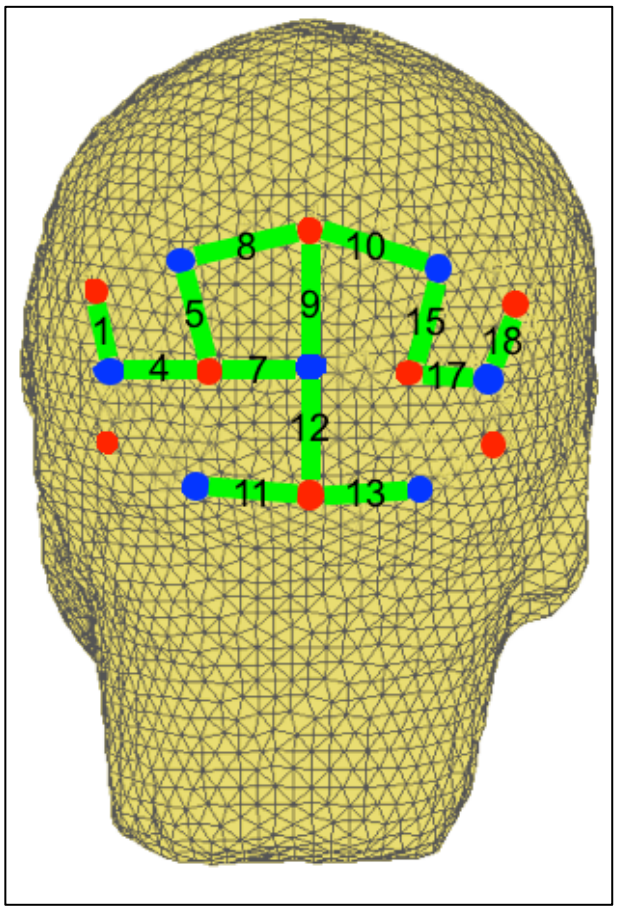

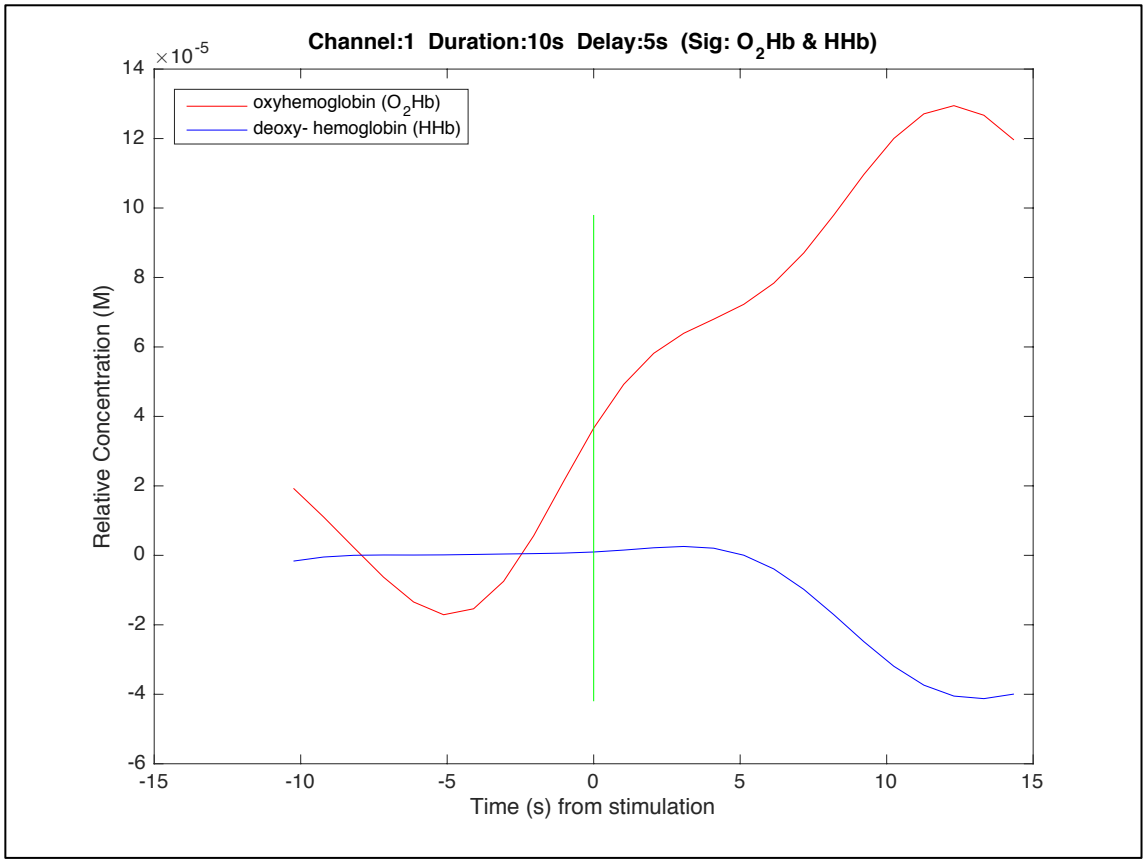

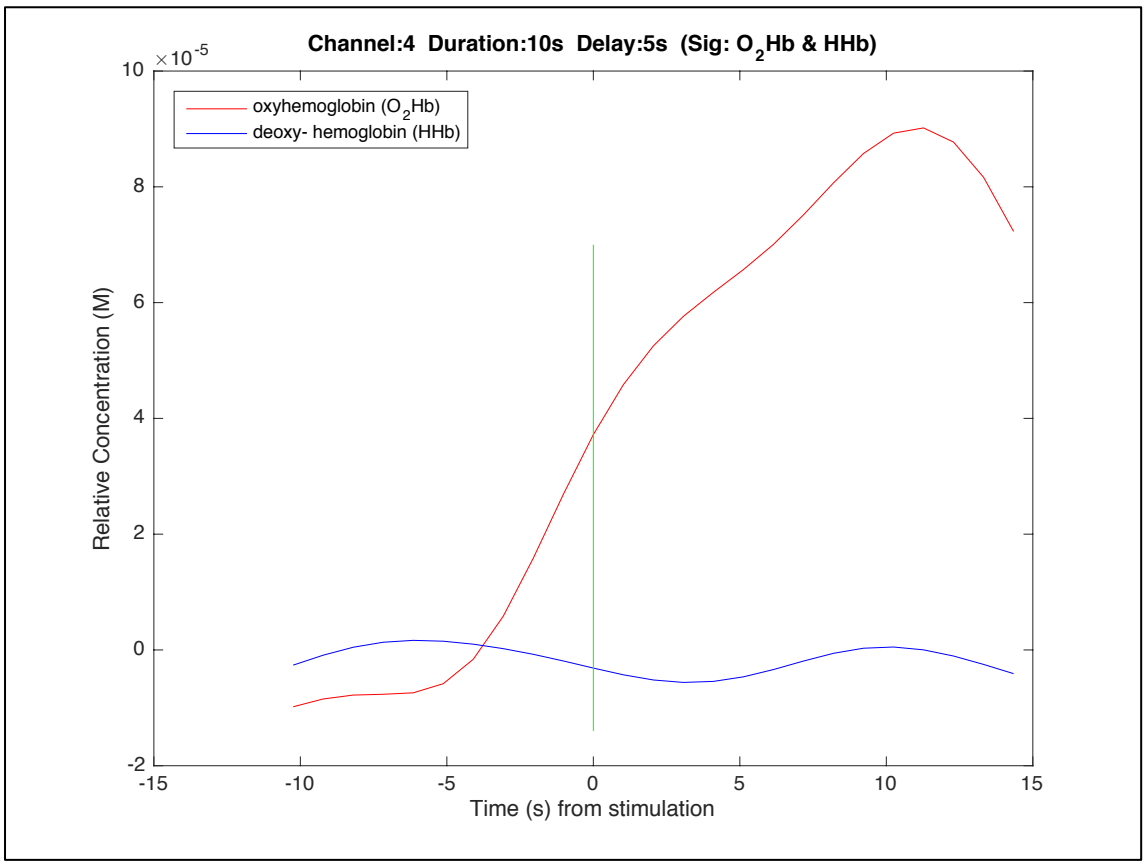
Channel:4 Duration:10s Delay:5s (Sig: O2Hb & HHb)
×10-5
oxyhemoglobin (O2Hb)
deoxy- hemoglobin (HHb)
Relative Concentration (M)
Time (s) from stimulation

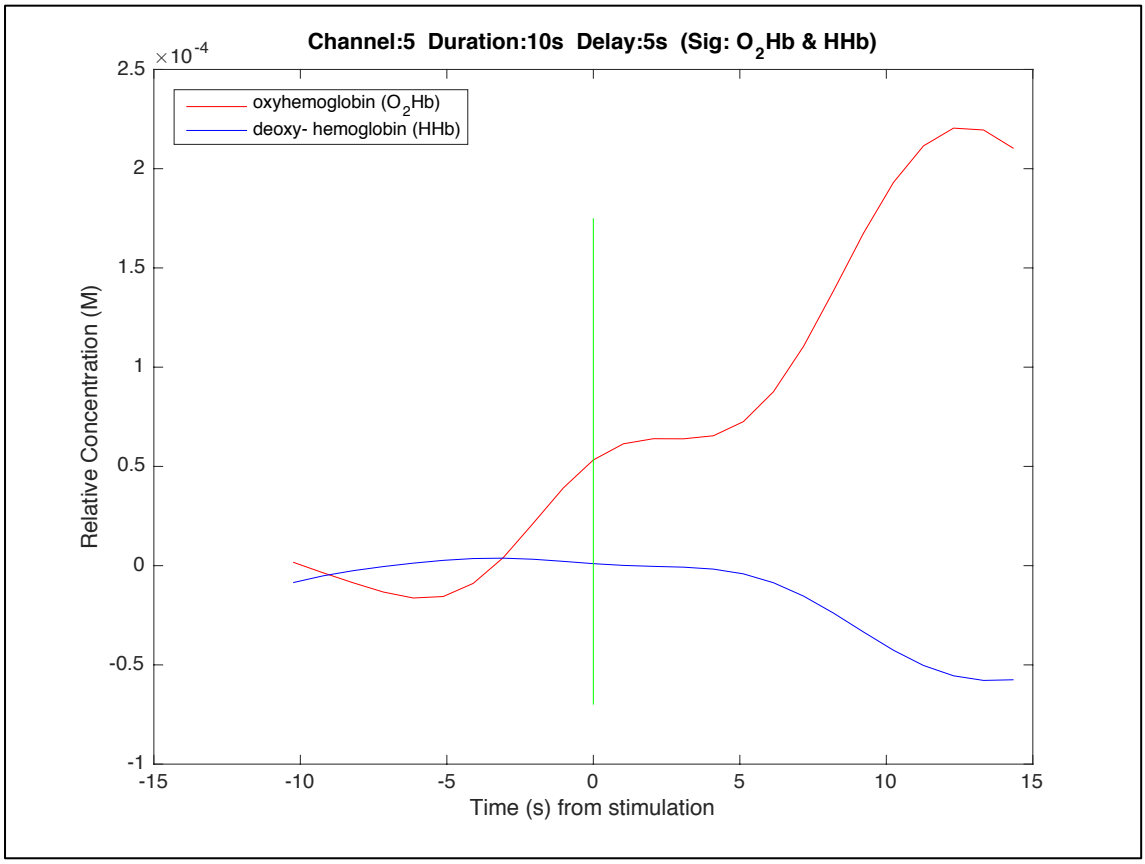
Channel:5 Duration:10s Delay:5s (Sig: O2Hb & HHb)
×10-4
oxyhemoglobin (O2Hb)
deoxy- hemoglobin (HHb)
Relative Concentration (M)
Time (s) from stimulation

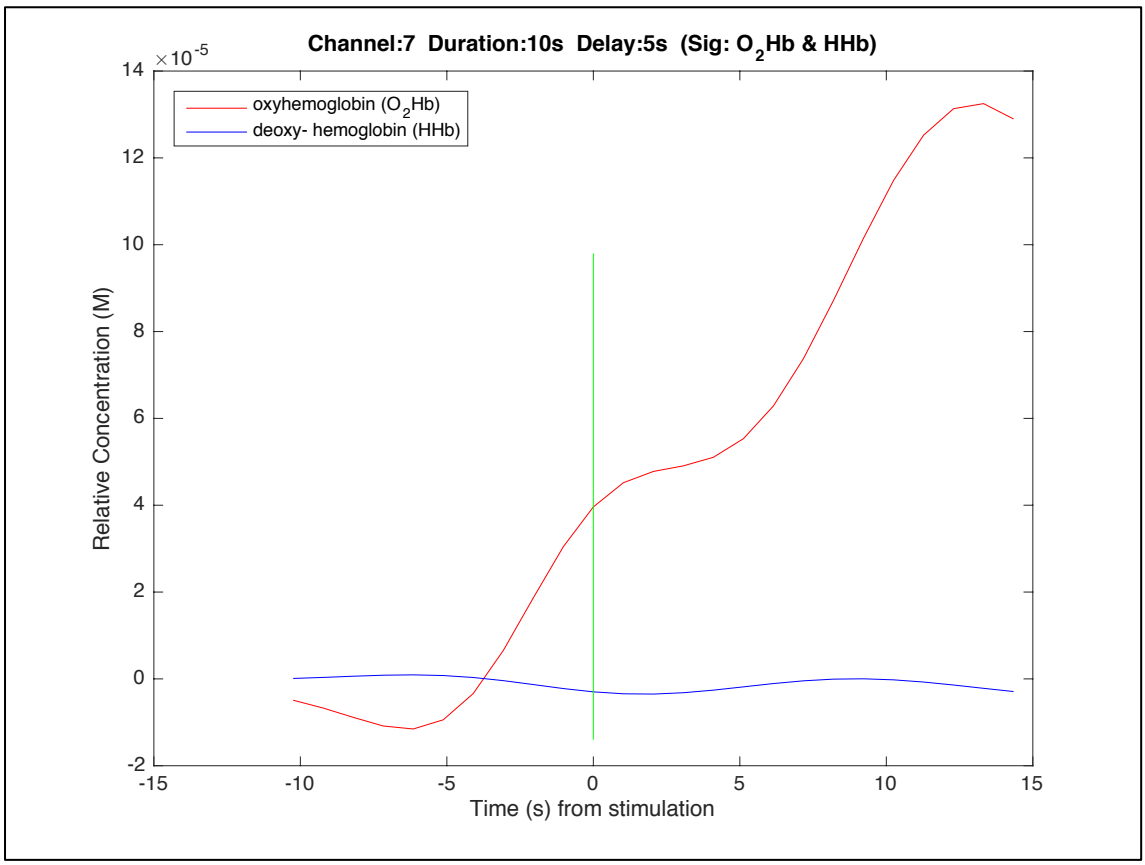
Channel:7 Duration:10s Delay:5s (Sig: O2Hb & HHb)
×10-5
oxyhemoglobin (O2Hb)
deoxy- hemoglobin (HHb)
Relative Concentration (M)
Time (s) from stimulation

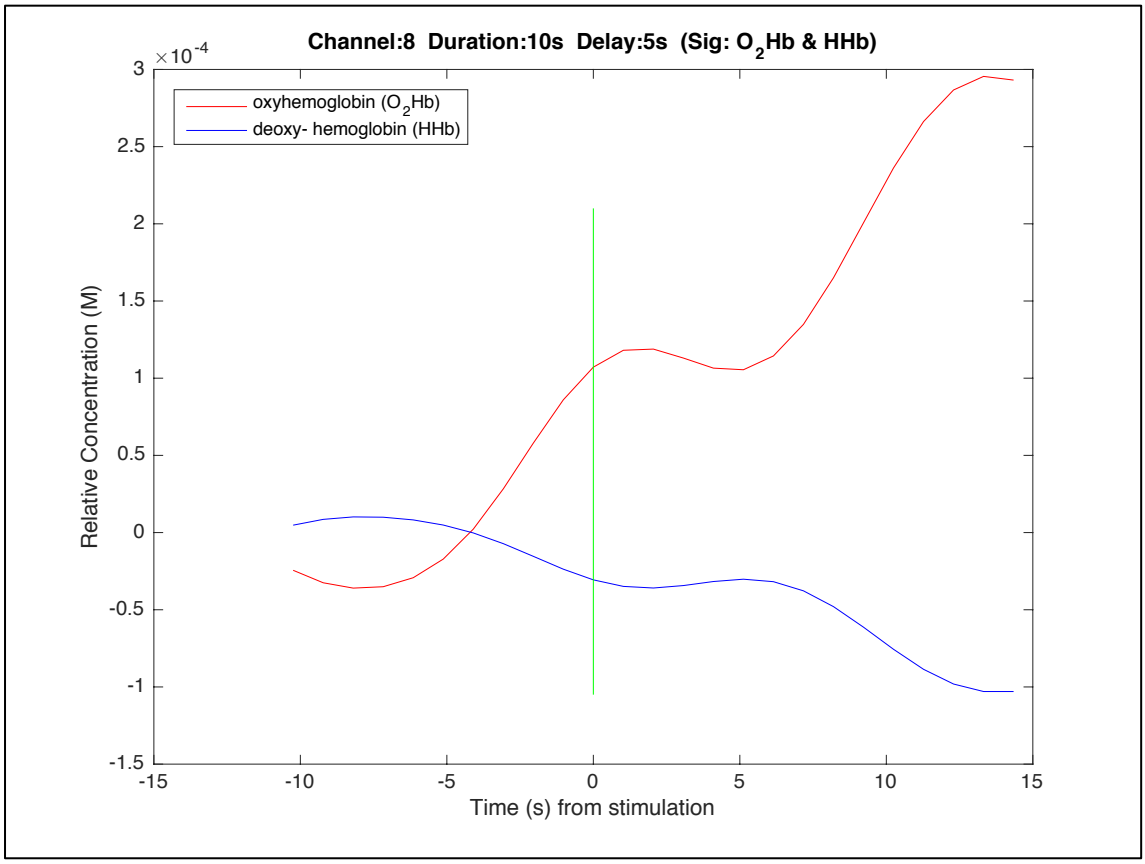
Channel:8 Duration:10s Delay:5s (Sig: O2Hb & HHb)
×10-4
oxyhemoglobin (O2Hb)
deoxy- hemoglobin (HHb)
Relative Concentration (M)
Time (s) from stimulation

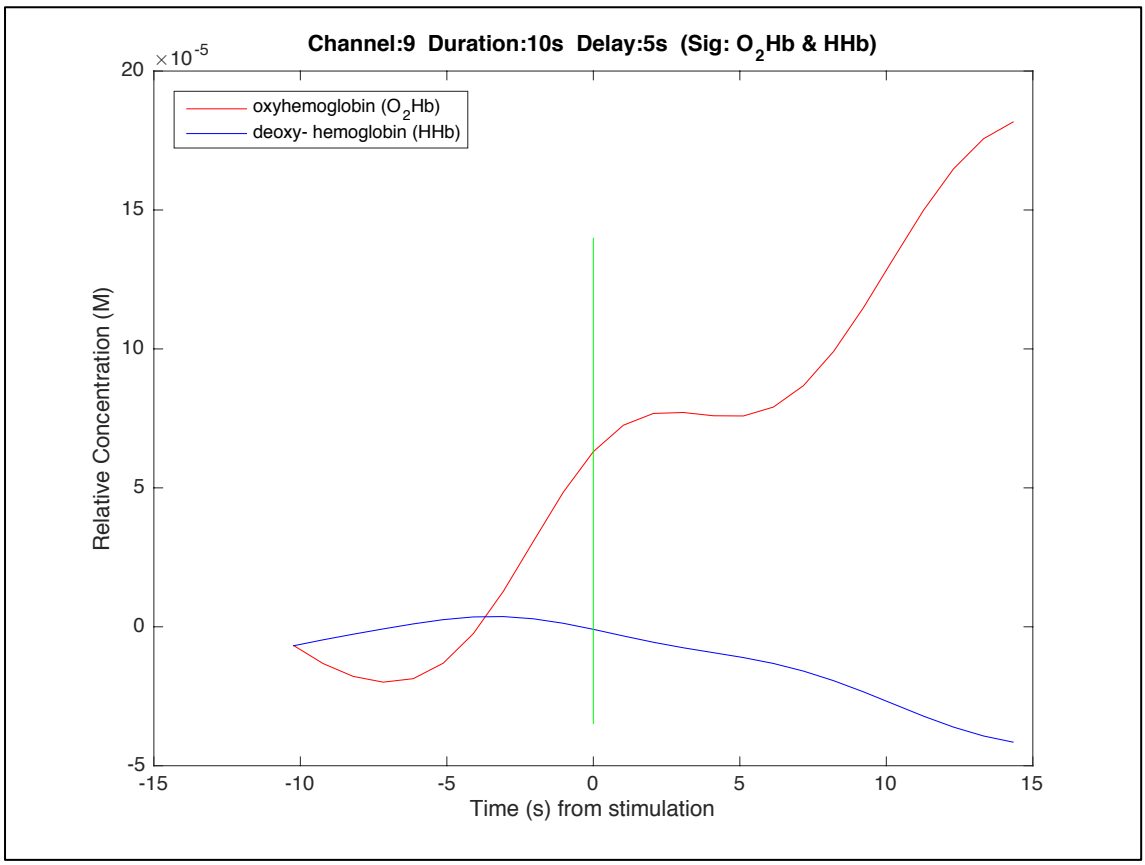
Channel:9 Duration:10s Delay:5s (Sig: O2Hb & HHb)
×10-5
oxyhemoglobin (O2Hb)
deoxy- hemoglobin (HHb)
Relative Concentration (M)
Time (s) from stimulation

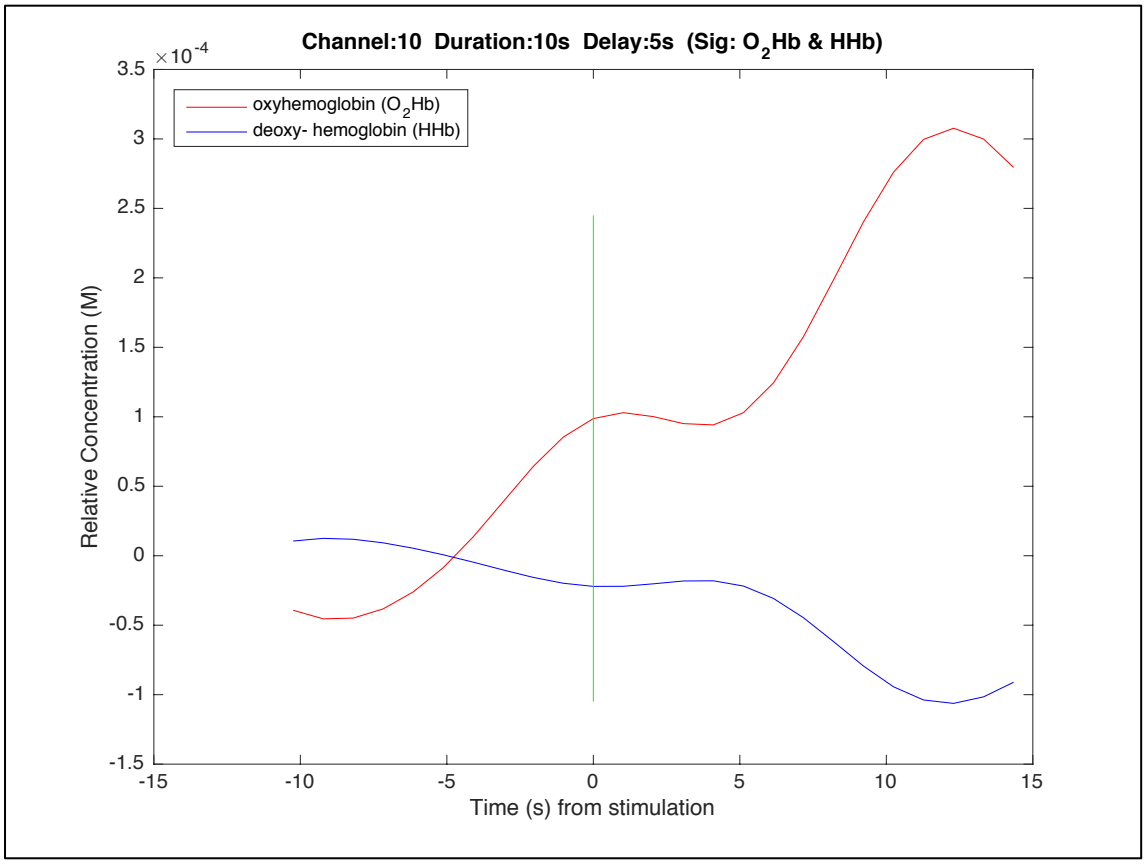
Channel:10 Duration:10s Delay:5s (Sig: O2Hb & HHb)
×10-4
oxyhemoglobin (O2Hb)
deoxy- hemoglobin (HHb)
Relative Concentration (M)
Time (s) from stimulation

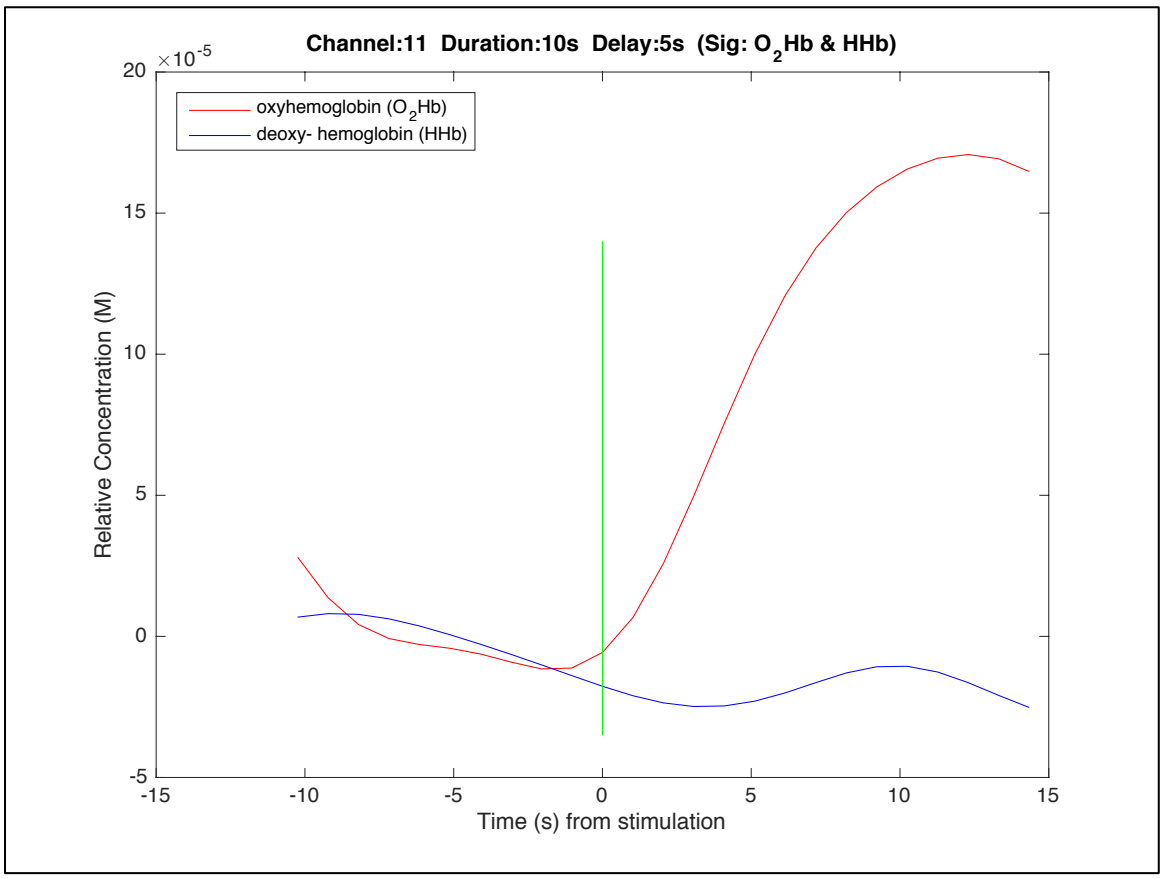
Channel:11 Duration:10s Delay:5s (Sig: O2Hb & HHb)
×10-5
oxyhemoglobin (O2Hb)
deoxy- hemoglobin (HHb)
Relative Concentration (M)
Time (s) from stimulation

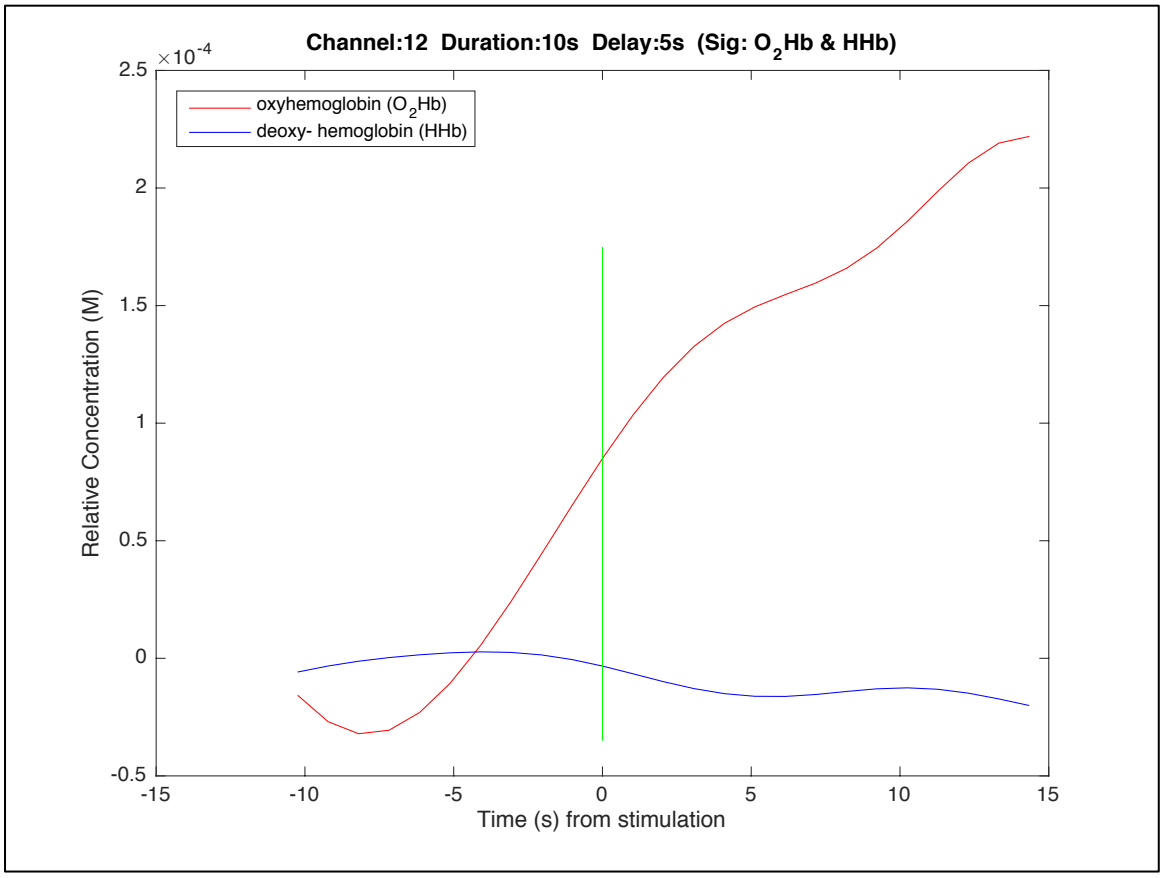
Channel:12 Duration:10s Delay:5s (Sig: O2Hb & HHb)
×10-4
oxyhemoglobin (O2Hb)
deoxy- hemoglobin (HHb)
Relative Concentration (M)
Time (s) from stimulation

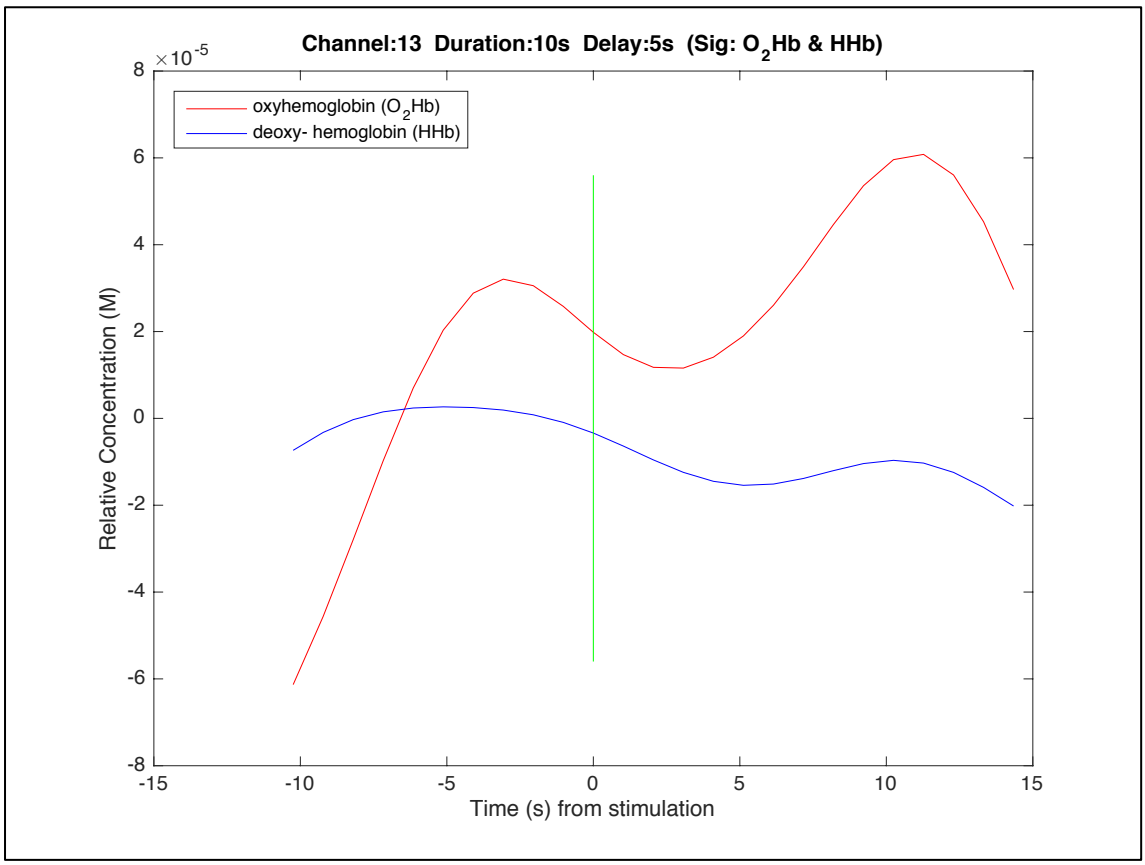
Channel:13 Duration:10s Delay:5s (Sig: O2Hb & HHb)
×10-5
oxyhemoglobin (O2Hb)
deoxy- hemoglobin (HHb)
Relative Concentration (M)
Time (s) from stimulation

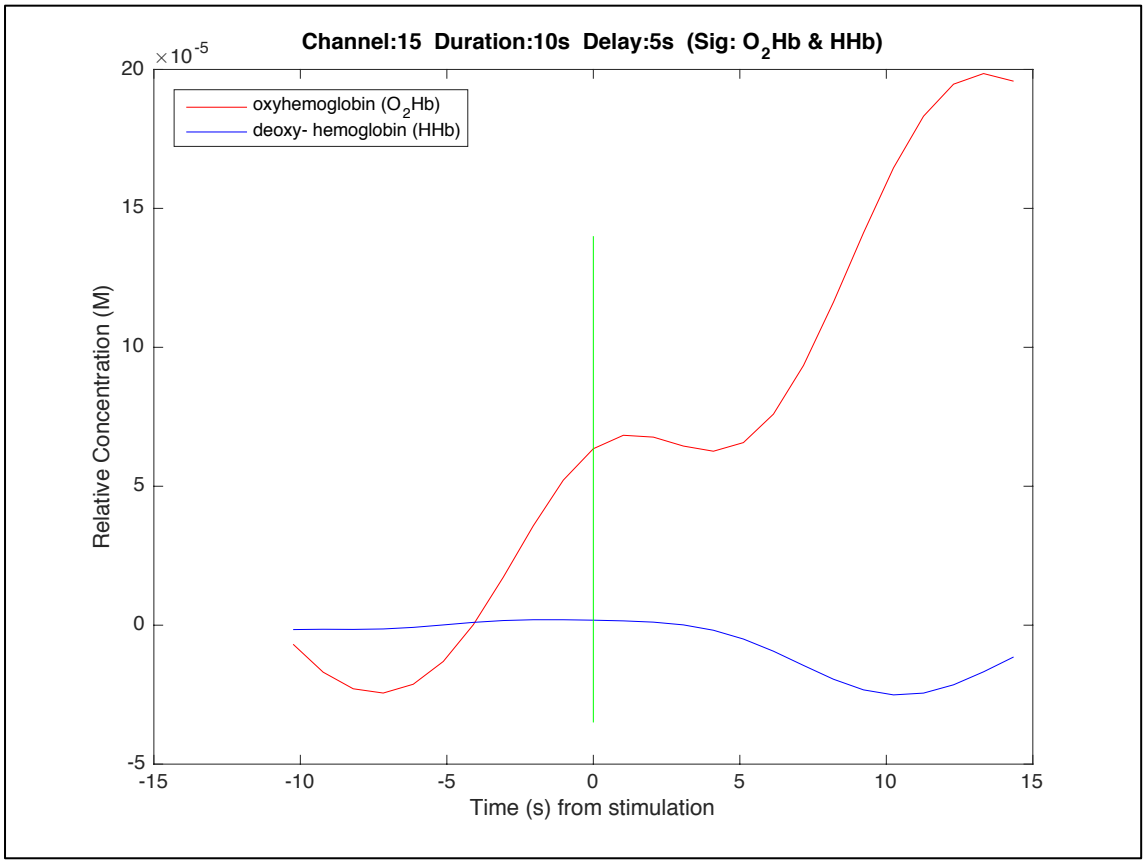
Channel:15 Duration:10s Delay:5s (Sig: O2Hb & HHb)
×10-5
oxyhemoglobin (O2Hb)
deoxy- hemoglobin (HHb)
Relative Concentration (M)
Time (s) from stimulation

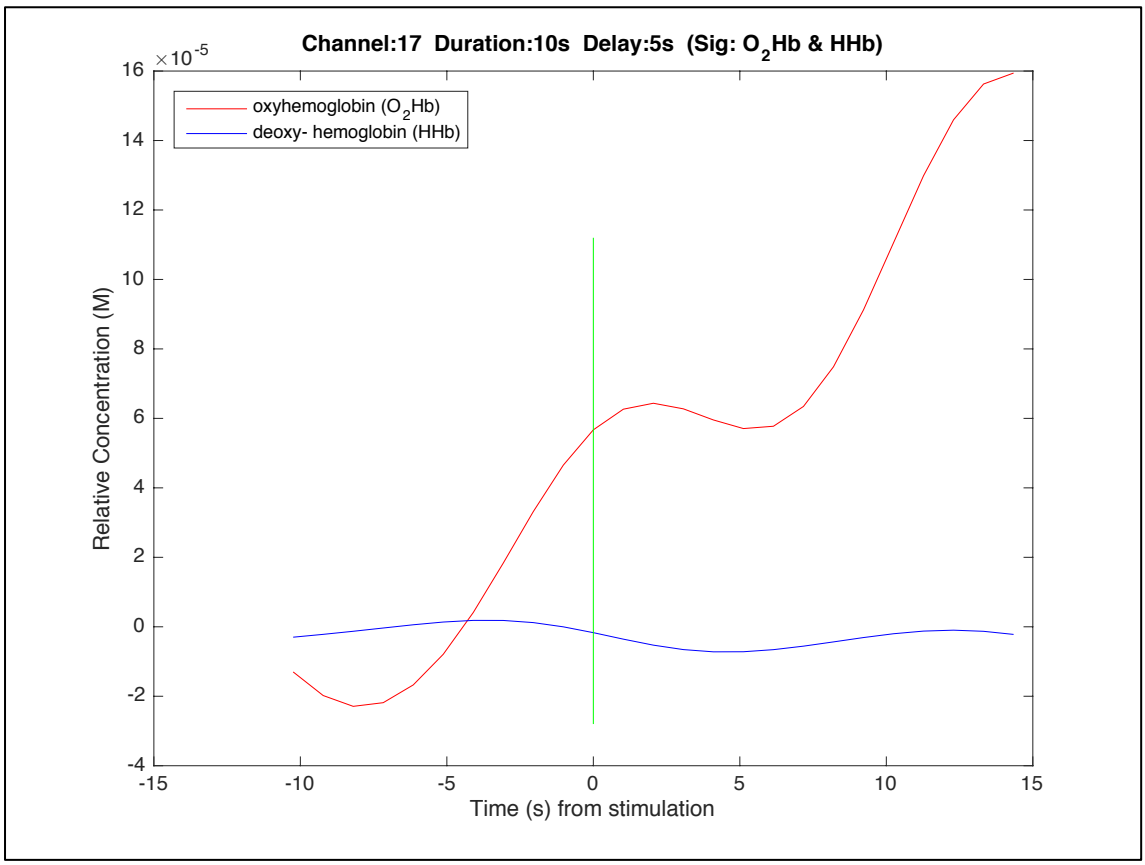
Channel:17 Duration:10s Delay:5s (Sig: O2Hb & HHb)
×10-5
oxyhemoglobin (O2Hb)
deoxy- hemoglobin (HHb)
Relative Concentration (M)
Time (s) from stimulation

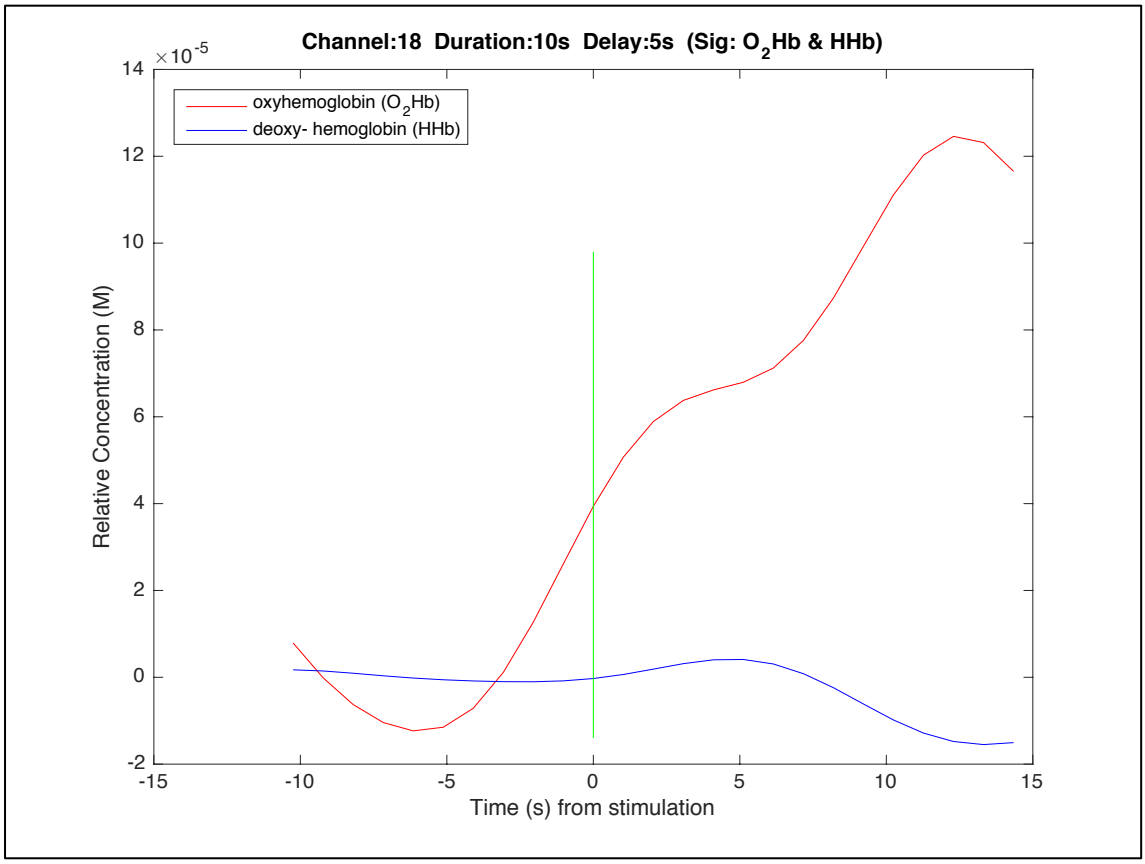
Channel:18 Duration:10s Delay:5s (Sig: O2Hb & HHb)
×10-5
oxyhemoglobin (O2Hb)
deoxy- hemoglobin (HHb)
Relative Concentration (M)
Time (s) from stimulation

7.3.2 Summary of Optode Channel Activation

The optode channels activated by the 3 stimulation conditions in each subject can be summarised as the table below:

Subject ID	Positive Optode Channels		
	Condition 1 (stim of foveal quad)	**Condition 2** (simultaneous stim of 6 quads)	**Condition 3** (sequential stim of 6 quads)
51-001	10, 11, 19	05, 10, 19	01, 18, 19, 20
51-003	01, 04, 05, 06, 07, 09, 12, 14, 15, 16, 17	none	none
51-005	none	none	none
51-006	none	5, 10, 15	05, 07, 08, 09, 10, 12, 14, 15, 17, 18
51-007	01, 04, 05, 07, 08, 09, 15, 17	05, 08, 09, 10, 13, 15	01, 04, 05, 07, 08, 09, 15, 17, 18
51-009	none	05, 08, 10	01, 04, 05, 07, 08, 09, 10, 11, 12, 13, 15, 17, 18

Table 7.4: Summary of all the optode channel number(s) showing a statistically significant change in the O_2Hb and HHb concentrations levels relative to baseline, for each of the 3 stimulation conditions in each subject.

For ease of comparison, the topographical maps of optode channel activation for all the subjects are tabulated as below:

Subject ID	Condition 1	Condition 2	Condition 3
51-001	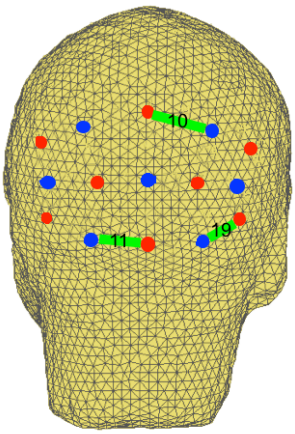	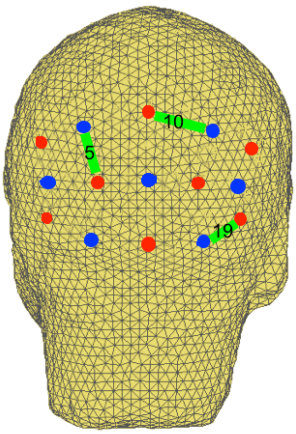	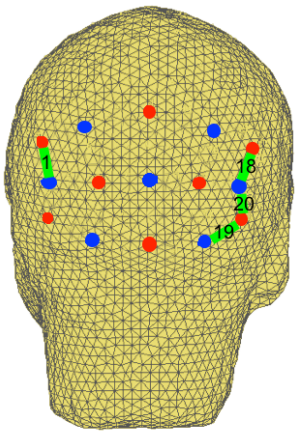
51-003	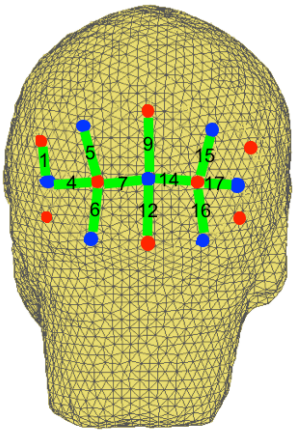	none	none
51-005	none	none	none

51-006	none	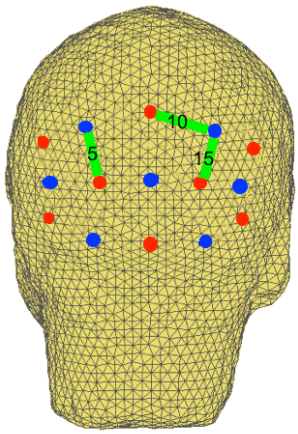	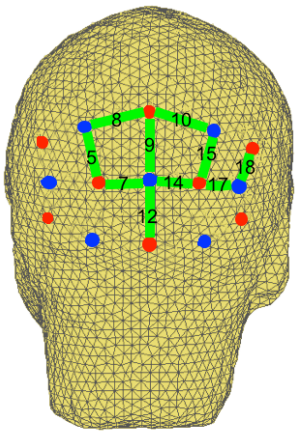
51-007	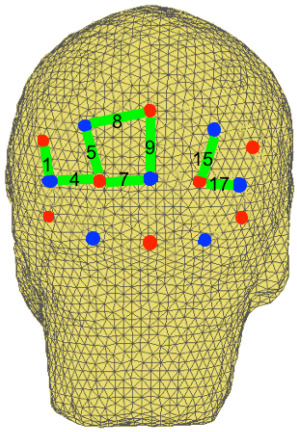	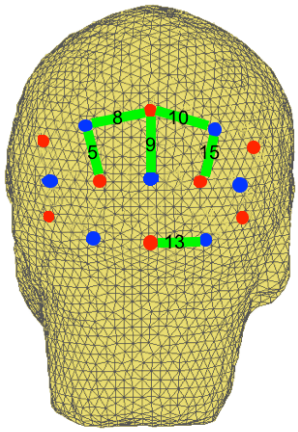	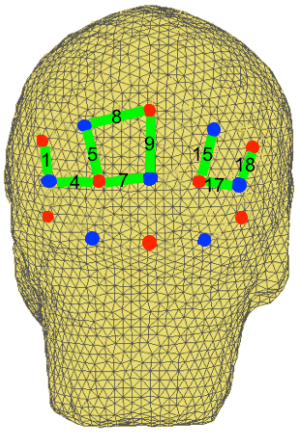
51-009	none	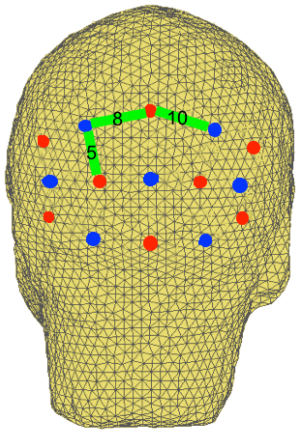	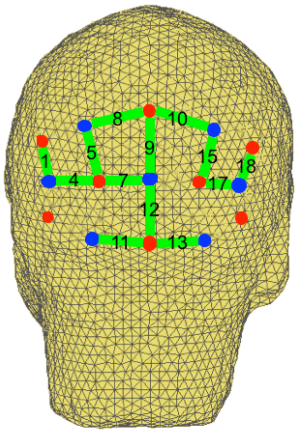

Table 7.5: Topographical maps of optode channel activation for each subject under the 3 stimulation conditions. The locations of the NIR sources were shown as red dots; the blue dots represented the locations of the detectors; and the active optode channels were shown as a green line labelled with the corresponding channel number. For each subject, the topographical map of optode channel activation and their respective O_2Hb and HHb concentration graphs were presented for all the 3 stimulation conditions.

Opotode channel activations were observed in 5 out of the 6 subjects (all except subject 51-005) in at least one of the stimulation conditions. In 4 subjects,

sequential stimulation of different electrode quads appeared to generate a larger area of primary visual cortex activation than simultaneous quad stimulation.

7.4 Discussion

Since the first description of functional MRI (fMRI) demonstrating NVC with activation of the visual cortex (Belliveau et al., 1991), research into non-invasive imaging of the cortical activities in the field of neuroscience has exploded. While fMRI relies on changes in the local deoxygenated haemoglobin (HHb) levels to generate the BOLD (blood oxygenation level-dependent) signals to detect cortical activation, fNIRS measures the changes in both oxygenated (O_2Hb) and deoxygenated haemoglobin (HHb) levels, and relies on changes in both parameters to detect cortical activation.

The main advantage of fMRI over fNIRS is spatial resolution. With fMRI, BOLD signal from each $4mm^3$ voxel samples activity from around 100,000 neurones. The 3D co-ordinates of each voxels are also well specified. In fNIRS with source-detector distances of 2 – 3 cm, each optode channel samples a much larger pool of neurones (perhaps 3 – 5 times larger) than a voxel (Gervain et al., 2011). Furthermore, owing to the relatively reduced tissue penetrance of NIR (in comparison to MRI), imaging of deeper cortical areas is limited. Despite these limitations, spatial resolution of as low as 1.7 cm with shifts of < 1 cm could be achieved (Zeff et al., 2007). Functional NIRS, on the other hand, has the advantage of high temporal resolution, with most machines capable of sampling rate of around 10Hz or much higher. By contrast, the temporal resolution of fMRI is around 0.5Hz. Other advantages of fNIRS imaging include the relatively low cost of the machine, as well as the portability of the system. In this study with a cohort of subjects implanted with the Argus® II retinal prosthesis, fNIRS has been particularly valuable as a tool of measuring cortical activities in the presence of real-time retinal stimulation using radiofrequency telemetry.

The use of fNIRS to measure visual cortex activation in normal sighted human adults and infants has been published extensively (Colier et al., 2001; Correia et al., 2012; Gratton et al., 1995; Kato et al., 1993; Lloyd-Fox et al., 2010; Obrig et al., 2000; Wenzel et al., 1996; Wijeakumar et al., 2012; Zeff et al., 2007), and

the correlation between fMRI and fNIRS is well established, especially for visual cortex activation (Eggebrecht et al., 2012; Obrig et al., 2000). In this study, we have demonstrated that haemodynamic responses of primary visual cortex activation (as seen in normal sighted adult humans, see Figure 7.1) could be detected and recorded in real-time in 5 out of 6 our patients with end-stage outer retinal dystrophy patients, implanted with Argus® II retinal prosthesis. All these patients have previously been blind and deprived of visual input for many decades. An unusual common feature seen in all these patients is that the decrease in HHb concentration levels is much smaller than that observed in normal sighted humans, despite achieving statistical significance. It is interesting to note that the 2 subjects who had the best form visual function (i.e. 51-007 and 51-009, see **chapter 3**) also have haemodynamic response curves most similar in appearance to that of normal sighted humans, with reasonable reduction in HHb concentration as well as a large increase in O_2Hb. This may be a reflection of the relative preservation the primary visual cortex integrity in these 2 subjects compared with the other subjects.

In order to assess the retinotopic localisation of signals, we compared the patterns of optode channel activation to the location of the stimulated quad relative to fovea (i.e. Condition 1) in each patient (see Table 7.6). The relative position of the stimulated quad to the presumed fovea location has previously been established (see **chapter 5**, Table 5.6) (Luo et al., 2016).

Subject ID	Active Optode Channels	Stimulated Quad	Quad Position Relative to Fovea
51-001	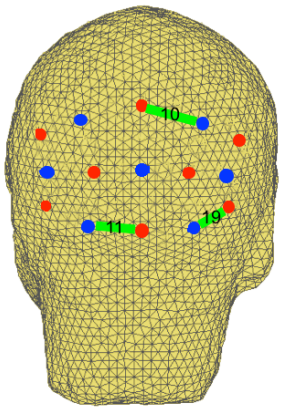	C07C08 D07D08	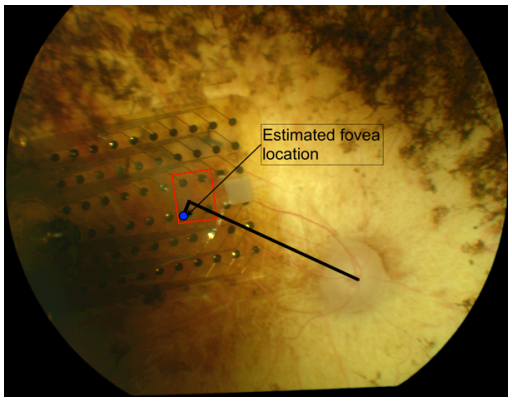
51-003	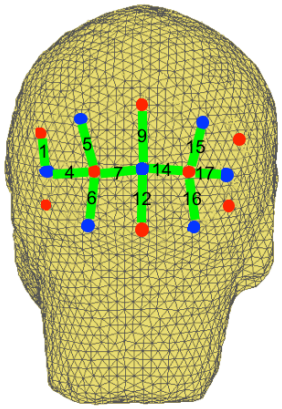	A07A08 B07B08	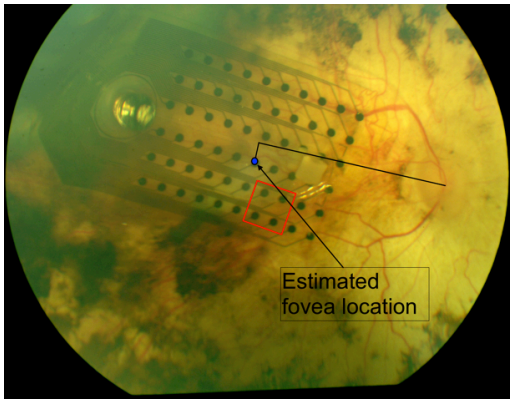
51-005	none	E05E06 F05F06	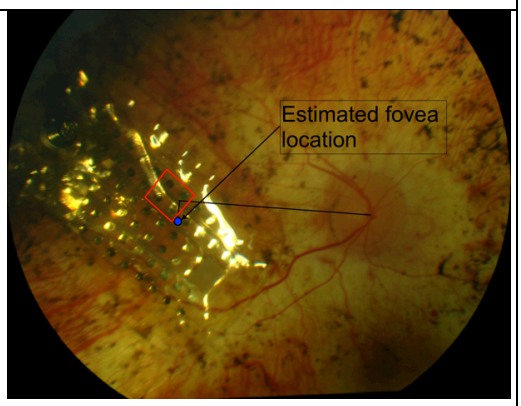
51-006	none	A07A08 B07B08	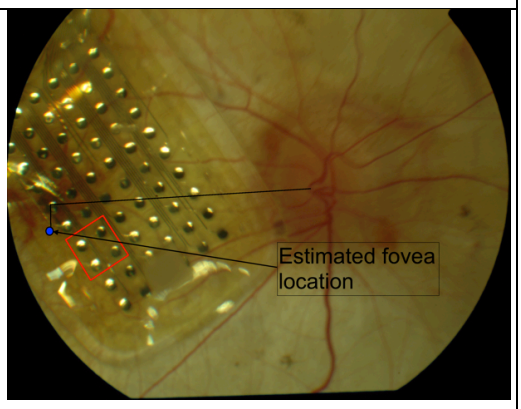

51-007	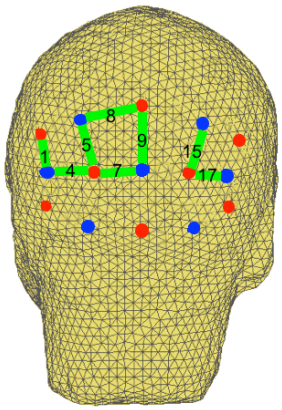	E07E08 F07F08	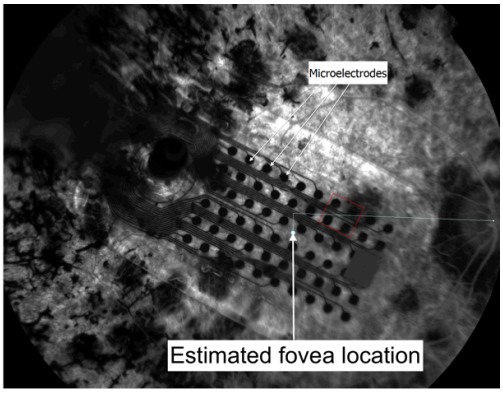
51-009	none	E07E08 F07F08	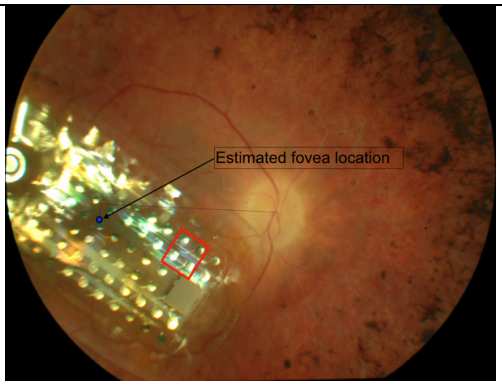

Table 7.6: Comparison of active optode channel patterns to the location of stimulated quad (relative to fovea) in each subject. The stimulated quad electrodes are enclosed in the red square. The fovea location is estimated as 15.5 ± 1.1° from the centre of the optic disc horizontally, and -1.5 ± 0.9° vertically (Rohrschneider, 2004), and labelled with an arrow.

Out of the 6 subjects, only 3 subjects showed positive optode channel activities with stimulation of foveal quad (condition 1), namely subject 51-001, 51-003 and 51-007. Their responses will be discussed individually in detail.

In subject 51-001, 3 optode channels (10, 11 and 19) were positive. Looking at the haemodynamic response curves for each channel, while channels 10 and 11 displayed good response curves for both O_2Hb and HHb concentration changes in keeping with the expected physiological NVC response, there is a mismatch in the timing of the increase in O2Hb levels and the decrease in HHb levels in channel 19. As such, we have discarded channel 19 as an active channel. The remaining 2 channels (10 and 11) corresponded to areas close to the midline in each hemisphere, which in turn corresponded to the foveal region (Dougherty et al., 2003). Given that the stimulated quad in 51-001 encompassed the estimated fovea, the optode channels activated were as expected.

In subject 51-003, multiple channels in both hemispheres were activated. This could be due to the spread of electrical charges to a much larger area of retina than the area of direct stimulation. In fact, the patient reported seeing “shimmering” light after the initial phosphene with each stimulation, which would spread out to the peripheral visual field, before fading out. Interestingly, none of the channels showed a positive response when the total number of electrodes stimulated was increased (i.e. in Condition 2 and 3), despite the subject reporting seeing brighter phosphenes, especially with stimulation under Condition 2.

In subject 51-007, while optode channels from both hemispheres were activated, there are many more channels activated in the left hemisphere (i.e. 6 active channels) compared with the right hemisphere (i.e. 2 active channels). Given that the stimulated quad lied superonasal to the estimated fovea location, one would expect the contralateral hemisphere to be predominantly activated, and this is as the pattern we have observed in subject 51-007.

Four subjects displayed positive optode channels with stimulation under Conditions 2 and 3, namely 51-001, 51-006, 51-007 and 51-009. With the exception of subject 51-001, all the other 3 subjects displayed more active channels under Condition 3 than Condition 2. This could be due to the fact that the simulating current applied to each quad in Condition 2 was much lower than in Condition 3 for safety concerns (as explained earlier). As such, some of the quads were probably stimulating at sub-threshold levels during the recording, resulting in less cortical activation. During Condition 3 stimulation, all the subjects also reported seeing moving phosphenes as the quads were stimulated sequentially. It is therefore plausible that some of the additionally activated optode channels could be related to activities in the dorsal stream for processing of motion perception (Goodale and Milner, 1992; Norman, 2002).

One subject (51-005) did not display any active optode channels despite perceiving phosphenes with retinal stimulation. One explanation for this is that thus far, we have assumed that the haemodynamic responses in these subjects are the same as those observed in normally sighted individuals. In reality, these subjects have been blind for decades and it is therefore possible that in subject 51-005, invasion of primary visual cortex by other sensory modalities has occurred as a result of cross-modal plasticity (Bavelier and Neville, 2002),

thereby disrupting the typical haemodynamic response we expected to see. In the future, we hope to be able to test for this by recording activities in the primary visual cortex while delivering auditory and / or touch stimuli, to investigate cross-sensory use of the cortex.

To our knowledge this is the first demonstration of real-time haemodynamic responses in the primary visual cortex, in response to retinal prosthesis stimulation. Though electrically elicited visual evoked potentials (eVEPs) in Argus® II subjects has previously been recorded (Stronks et al., 2013), this yielded eVEP waveforms with very low signal-to-noise ratios, which required much longer recording time and substantial signal processing afterwards. Furthermore, the authors reported that all the functioning electrodes were stimulated at a stimulus level approximately twice that of the subjective threshold to obtain the results. Functional NIRS by contrast, was able to record responses from individual quad stimulations, and could provide information on focal areas of visual cortex activation.

One limitation of this study is that presence of synchronous sound stimulation can suppress fNIRS signals to visual stimulus in the visual cortex compared to visual stimulus alone, due to cross-modality interactions in primary sensory cortices (Wiggins and Hartley, 2015). This effect may be particular pronounced or unexpectedly altered due to the presence cross-modal plasticity in this cohort of patients who have been blind for decades. During this study, we attempted to keep the sound and other stimuli to minimum by switching off all the lights in the room and leaving the subject alone in the room during the experiment. We also instructed the subjects to remain as still as possible during the experiments. However, we had no control over other noises in the background from the surrounding laboratory areas. Future experiments could be carried out in soundproof rooms to further reduce the interference from background noise.

Secondly, although this study had a small sample size, it has been sufficient to clearly demonstrate the feasibility of using this neuroimaging technique in this patient group. It is hoped that in the future as Argus® II retinal prostheses becomes more widespread in clinical use, more subjects would be available.

In conclusion, we have examined the feasibility of recording a cortical signal using fNIRS, following a retinal stimulus via the Argus® II retinal prosthesis

system. We have shown that consistent recording can be made and that it has a temporal and likely retinotopic association with the stimulus. As such, fNIRS appears to be a potentially useful and reliable method of recording cortical activities in this cohort of patients fitted with retinal prosthesis. This non-invasive and cost-effective imaging technique could be the method of choice for future studies involving other stimuli (e.g. sound) to assess cross-modality plasticity.

Chapter 8

Conclusion &

Future Development

8.1 Original Aims

This thesis aimed to: (1) examine certain aspects of long-term clinical and functional outcomes conferred by the Argus® II system in this early cohort of chronically implanted subjects; (2) to elucidate the characteristics of the artificial vision and its long-term repeatability and reproducibility in individual subjects; and (3) to explore the feasibility of real-time imaging of visual cortex activities in response to retinal stimulation using functional near infra-red spectroscopy. In the following sections, the key findings from **Chapters 3, 4, 5, 6** and **7** are described, the strengths and limitations of the studies are summarised, and a possible future roadmap for prosthetic vision research is outlined based on these findings.

8.2 Summary of Key Findings and Implications

Chapter 3 of the thesis showed that patients with end-stage RP or outer retinal dystrophy who were fitted with Argus® II retinal prosthesis are able to identify 2D distinct geometric shapes better with the device on than by chance. As well as this screen based, 2D form discrimination, patients were able to demonstrate a basic level of identification of 3D objects. Furthermore, the performance in identification of 2D and 3D testing was shown to improve by enhancing the outlines of the shape or object respectively. A wide inter-subject variation in the visual performance of form recognition has also been observed.

In **Chapter 4**, we demonstrated that in addition to being able to point at bright targets on a 2D screen (Ahuja et al., 2011), Argus® II subjects can also localise objects in 3D space and reach out and grasp the objects (prehension) using the device – a task which they could not achieve with their native vision alone. Despite the potential misalignment between the direction of the camera view for image acquisition (i.e. camera position) and the direction of gaze (i.e. eye position), Argus® II subjects appeared to have developed an effective compensatory mechanism with which they could localise targets in both 2D and 3D.

As an attempt to explain the observed wide inter-subject variations in visual performance, as well as to establish the feasibility of constructing predictable

pixelated patterns to achieve useful artificial vision, we set out to investigate the characteristics of phosphenes in these chronically implanted Argus® II subjects in **Chapter 5**. We established that there is a wide variation in the shapes and sizes of the phosphenes perceived by each subject for a given standardised stimulation. This may in part account for the inter-subject variation in the visual performance observed. Despite the differences in shapes and sizes, the characteristics of the phosphenes are consistently reproducible within each subject for the same stimulating parameters. Such consistency and reproducibility of phosphenes form an encouraging basis upon which more complex patterns of artificial vision could potentially be constructed by varying stimulating parameters.

Chapter 6 of the thesis looked at an important but unresolved issue about the use of the Argus® II system: the effect of undergoing MRI brain scan with internal components of the Argus® II retinal prosthesis in situ. Data on implant position (as evaluated by colour fundus photography, OCT scan and electrode impedances) and implant function (as evaluated by electrode thresholds) before and after the MRI scan were analysed and compared. We have concluded that MRI brain scans of up to 1.5-Tesla field strength appeared to have no detrimental effect on the subjects and their implant stability and function. The Argus® II implant produced an artifact of around 50mm x 50mm in size which would prevent visualisation of structures within the orbit, but visualisation of surrounding tissues outside this areas are unaffected. The demonstration of safety in MRI brain scanning was a prelude to, and had initially supported, our aim to analyse visual cortex activation using functional MRI (fMRI) in these patients. However, due to concerns of signal interference from the radiofrequency telemetry of the Argus® II system, and the impracticality of real-time retinal stimulation during image acquisition, an alternative novel method of neuroimaging was sought and detailed in **chapter 7**.

In **chapter 7**, we explored the feasibility of real-time imaging of visual cortex activation in response to retinal activation with Argus® II retinal prosthesis, using functional near-infrared spectroscopy (fNIRS). We have discovered that fNIRS is capable of detecting haemodynamic changes in the visual cortex in 5 out of 6 subjects, with stimulating parameters much lower than those required for electrically elicited visual evoked potentials (eVEPs) (Stronks et al., 2013). In 3 subjects, single pulse supra-threshold stimulation of one quad produced detectable cortical responses. In addition, as fNIRS imaging also provides

topographical activation maps of the cortex, this allows us to investigate further into signal localisation, as well as cross-modal plasticity in the future.

The work in this thesis has shown that Argus® II retinal prosthesis system could improve visual function both in terms of form recognition as well as object localisation in 3D in real-life settings, in a cohort of patients with end-stage RP or outer retinal dystrophies. The wide variation in the visual performance level observed could in part be attributable to the diversity in the features of the phosphenes perceived by these subjects. Nevertheless, the consistency and reproducibility with which these phosphenes could be elicited, with fixed stimulating parameters within each subject, provides an encouraging basis for the construction of more complicated pixelated images. Functional near-infrared spectroscopy is capable of real-time recording of visual cortex activation in response to retinal stimulation in these patients, and provides an exciting neuroimaging tool for future investigation into neuroplasticity and cross-modal plasticity. Future research into this area may prove to be the key in understanding the wide variation in visual performance in the Argus® II subjects observed so far, and in turn help us to devise better visual prosthesis to improve the patients' vision.

8.3 Appraisal of Limitations & Strengths

8.3.1 Strengths of the Thesis

The main strength of this work has been the ability to document objectively the presence of form vision and object localisation in 2D and 3D, with the use of the Argus® II retinal prosthesis system. Furthermore, this has been demonstrated in a cohort of subjects who underwent implantation in the original feasibility study. At the beginning of this research work, all the participating subjects had already had their Argus® II implant for more than 3 years. By the end of the reported studies, the patients who had received their implants in 2008 had had their devices for more than 6 years. Our findings represent the long-term clinical and functional outcomes achievable with this cohort of chronically implanted Argus® II subjects.

As the Argus® II device could be switched on and off, and the transmission signals could be artificially disorganised (i.e. scrambled mode, as described in **Chapter 3**), each subject acted as their on internal negative control (with device switched off), as well as positive control (with device in scrambled mode). The

studies described in **Chapter 3, Chapter 4** and **Chapter 5** are all prospective, internally controlled studies.

8.3.2 Limitations of the Thesis

Owing to the experimental nature of the initial phase I/II Argus® II retinal prosthesis feasibility clinical trial (clinicaltrials.gov identifier: NCT00407602), the number of patients who received the retinal implant during clinical trial and hence the number of available subjects for the subsequent functional studies, is limited. However as the Argus® II system has entered the commercial market and become available for clinical use world-wide, these data on long-term visual outcomes and functioning of the device are important to help both clinicians and potential patients make decisions on their treatment options.

Another limitation is the inclusion of patients with advanced disease in the initial clinical trial. As a phase I feasibility study with safety being the primary concern, the clinical protocol specified for vision of logMAR 2.9 (bare light perception) or worse as the inclusion criteria, to minimise any potential harm to the patients. At this level of advanced disease, intraretinal remodelling and / or rewiring with aberrant nerve regeneration occur (Jones et al., 2012; Luo and daCruz, 2014; Marc et al., 2007; 2003; Stingl et al., 2015), which further complicates the process of intrinsic visual processing. Theoretically, this could compromise the potential visual outcome of pixelated vision achievable with focal retinal stimulations, and limit our understanding of the relationship between retinal stimulation and the artificial vision it presents.

8.4 Future Work

Future work to determine the underlying factors influencing the perceived phosphene characteristics for individual Argus® II subjects, may allow for better prediction of functional outcome, which could in turn be useful for patient selection and tailored pre-operative counselling. For the subjects already implanted with the Argus® II system, further research into determining the suitable stimulating parameters for each electrode / quad stimulation may be required for individual subjects, to achieve the construction of useful, pixelated prosthetic vision.

In terms of future developments for the retinal prosthesis systems, plans for improvement have been described and envisaged at both the software level and the hardware level of the device.

8.4.1 Software Development

Without changing the current hardware configuration of the Argus® II System, adjustments to the image processing software have already been applied to improve the level of vision obtainable with the device. As described in **Chapter 3,** studies on shapes and objects recognition have shown an improvement in performance by enhancing the outlines of the targets, thereby maximising edge contrast. This finding has led to the on-going development of edge-detection and enhancement as part of image processing. Such innovation has shown the potential for future software changes to improve patient function, while using the existing device.

Another example of software improvement was recently presented by Sahel et al. (Sahel et al., 2013), who described an image processing software known as Acuboost™. Acuboost™ utilises a combination of image magnification and minimisation (zoom), as well as some image enhancement features to achieve a visual resolution that exceeds the limit set by the number of electrodes. Using 16x magnification, it allowed one Argus® II patient to achieve an equivalent vision of logMAR 1.0 (20/200) on gratings acuity measurement, while 4x magnification allowed the patient to read large-print (2.3 cm) letters from a notebook at 30cm.

Other image processing features under development include signal coding for facial or obstacle recognition, whereby the camera automatically recognises a face (or obstacle), and the image is processed such that the facial image is extracted from the rest of the visual scene and presented alone to the patient in a zoomed-out view. This allows efficient identification and localisation of the face by the patient, and in real-life situations, allows the patient to look at the other person's face during conversations (Stanga et al., 2013).

More experimentally, Horsager et al. (Horsager et al., 2011; 2010) described the spatiotemporal interaction between adjacent active electrodes. Through phase difference interference of the electromagnetic waves, it may be possible

to create intermediate stimulating signals, thereby effectively creating pseudo-electrodes (as observed in cochlear implants) to increase the potential resolution of the retinal implant.

8.4.2 Hardware Development

In terms of hardware development, increasing the number of electrodes with or without reducing the size of the electrodes, and increasing the area of retina stimulated and therefore visual field, are the most immediate areas of need.

The Second Sight Company has alluded to a next generation device with possibly 240 electrodes, with the possibility of adding peripheral electrodes to increase the visual field (Holmes, 1945; Stronks and Dagnelie, 2014). In terms of electrode size, the ultimate aim would be to have individual electrodes comparable in size to that of RGC soma so as to allow individual RGC activation. At present this is not possible as the charge density of an electrode, being inversely proportional to the surface area of the electrode (πr^2), renders this calibre of electrode unsafe.

Ahuja et al. have demonstrated that the most critical factor affecting the electrode threshold is the electrode-retina distance (Ahuja and Behrend, 2013; Ahuja et al., 2013). To minimise this electrode-retina distance, OCT-guided custom-made electrode arrays have been proposed, which take into account the different curvatures of individual patients' eyes to maximise array apposition (Opie et al., 2014). Researchers from California Institute of Technology, CA, USA have also described an origami implant design, whereby a 3D integration technique is employed to construct a spherical, 512-channel epiretinal implant conforming to the curvature of the macula. This would allow for larger areas of retina to be stimulated, while maintaining good electrode-retina contact (Y. Liu et al., 2013; Monge and Emami, 2014; Monge et al., 2013; Nakauchi et al., 2006; Ohta et al., 2007; Tokuda et al., 2009; Zhou et al., 2008).

To mitigate the misalignment between the glasses-mounted external camera position and a patient's eye position (as described in **Chapter 4**) and so as to improve the patient's perception of spatial localisation, intraocular cameras have been proposed (Hauer et al., 2009; Stiles et al., 2011). The intraocular camera would be placed within the capsular bag of the crystalline lens after

lensectomy, and the visual information could either be transmitted wirelessly to an external VPU for processing before being transmitting back to the epiretinal microelectrode array for stimulation, or the image processing could be performed entirely intraocularly. This has the potential advantage of controlling the direction of vision with eye movements rather than head movements, thereby allowing for the development of more natural hand-eye co-ordination.

8.4.3 Deciphering the Neural Code

Despite the effort to increase the number of stimulating electrodes (thereby improving the potential resolution of the prosthetic vision), and the use of various image processing techniques to maximise the vision obtainable with the current Argus® II System, the functional outcomes and resolution remains poor. The greatest obstacles to progress remain the lack of understanding of the electric field interaction between the active electrodes, the amplitude and frequency coding for signal transmission along the visual pathway to the visual cortex, and signal integration and interpretation at the cortical level. Without an understanding of the signal encoding and integration at this level, improvement in prosthetic vision synthesis would be limited irrespective of the number of electrodes available. This premise has already been demonstrated with the alpha-IMS subretinal implant which despite having 1500 channels in its stimulating array, does not have an appreciably greater acuity, only achieving a visual acuity of logMAR 1.43 (20/546) with Landolt C rings, and grating acuity of up to 3.3 cycles/degree at best (Stingl and Zrenner, 2013).

Nirenberg et al. (Nirenberg and Pandarinath, 2012) demonstrated the importance of encoding visual information into patterns of action potentials that could potentially be understood by the visual cortex. Using data generated from stimulation of normal mice retina as a model, they developed a signal encoder consisting of a linear-nonlinear (LN) cascade – to capture stimulus / response relations for a broad range of visual stimuli; and the Poisson spike generator – to convert the visual stimuli into corresponding action potential patterns. The signal encoder therefore worked as a retinal input / output model, performing the role of information processing, as would a normal retina.

Using blind *rd* mice and the Channelrhodopsin-2 (ChR2) optogenetic retinal prosthesis model, the authors showed that when visual scenes (captured by an

external camera) were presented to the *rd* mice using standard optogenetic retinal prosthesis stimulation without the signal encoder, the RGC firing patterns appeared haphazard. When the visual scenes were processed by the signal encoder first to generate the appropriate patterns for optogenetic prosthetic stimulation, the subsequent RGC firing patterns resembled that of the visual stimulation of a normal retina. Furthermore behaviourally, presentation of shifting sine wave gratings elicited optomotor eye tracking in normal mice as well as in blind *rd* mice stimulated with signal encoder-enhanced optogenetic prosthetic stimulation, but not when the standard optogenetic prosthetic stimulation (without the signal encoder) was applied.

Other groups have also described different models to mimic the intricate image processing carried out by the retina, in the hope of replicating the physiological, interpretable output sent to the visual cortex. Olmedo-Payá et al. (Olmedo-Payá et al., 2013) described the *RetinaStudio* model whereby processing of the visual scenes is broken down into 3 stages. The first stage involves splitting the images into the 3 colour channels, red, green and blue (R, G and B), mimicking the outer plexiform layer. The second stage involves spatial filtering using the *Difference of Gaussian (DoG)* filters, mimicking the inner plexiform layer. The third stage mimics the ganglion cell layer, using the “leaky-Integrate & Fire spiking neuron” model. More importantly, they have also shown that incorporation of the effects of natural eye movements such as micro-saccades, drifts and tremors, improved the modelling of visual processing with greater sensitivity to light changes and improved edge recognition. Lorach et al. (Lorach et al., 2012) on the other hand, focused on reproducing the spatial and temporal properties of the different major types of RGCs, using an event-based, asynchronous dynamic vision sensor (DVS) to mimic the fundamentally asynchronous nature of biological vision.

Perhaps more promisingly, Jepson et al. (Jepson et al., 2014) described a method of mapping spatio-temporal patterns of retinal activity in a group of identified RGCs, using a multi-electrode recording system in isolated primate (macaque monkey) retinas. It has been shown that ON parasol cells in particular could be electrically stimulated with high spatial and temporal precision to match the activity from visual stimuli.

Although an understanding and deciphering of the neural code may be useful, it needs to be remembered that intra-retinal remodelling and aberrant nerve regeneration in the degenerate retina may disrupt and interfere with normal spatio-temporal interaction (Alamusi et al., 2015; S. Liu et al., 2017; Marc et al., 2007; 2003). As such, it may be that the signal characteristics need to be individualised to account for the variance in disease and the state of the patient's residual retina, as exemplified by the widely varied phosphenes perceived by individuals as described in **Chapter 5**.

8.5 Conclusions

The Argus® II Retinal Prosthesis System has played an important role in establishing retinal prostheses as a viable and potentially beneficial treatment option in blinding outer retinal conditions. The ability of this device to provide stable, chronic retinal stimulation in a relatively safe manner over many years has been recognised and has led to regulatory approval across many countries. However, despite the increasing volume of published outcomes from clinical trials using the Argus® II device and a cumulative experience of over two hundred patient years, it still remains difficult to predict the outcome and usefulness of the device for a given patient. The future development of this treatment option will depend not only on improvements in the device hardware and software, but also on a greater understanding of retinal and central neural pathology. Functional near infra-red spectroscopy (fNIRS), as a real-time neuro-imaging tool, will enable future investigations into the differences in the cortical activities in response to different stimulations and in different subjects. This may in turn help us understand the variability in their visual performance, as well as to further explore the extent and effect of cross-modal plasticity at the cortical level. Furthermore, any scientific advances will have to address the specific functional needs of the recipient patient group, before the milestone achieved by the Argus® II as a first-generation retinal prosthesis consolidates into a routine treatment for blinding outer retinal diseases.

Bibliography

Abramian, M., Dokos, S., Morley, J.W., Lovell, N.H., 2010. Activation of ganglion cell axons following epiretinal electrical stimulation with hexagonal electrodes. Conf Proc IEEE Eng Med Biol Soc 2010, 6753–6756.

Abramian, M.M., Lovell, N.H.N., Morley, J.W.J., Suaning, G.J.G., Dokos, S.S., 2011. Activation of retinal ganglion cells following epiretinal electrical stimulation with hexagonally arranged bipolar electrodes. J Neural Eng 8, 035004–035004.

Addi, M.M., Dokos, S., Preston, P.J., Dommel, N., Wong, Y.T., Lovell, N.H., 2008. Charge recovery during concurrent stimulation for a vision prosthesis. Conf Proc IEEE Eng Med Biol Soc 2008, 1797–1800.

Ahuja, A.K., Behrend, M.R., 2013. The Argus™ II retinal prosthesis: Factors affecting patient selection for implantation. Prog Retin Eye Res 36, 1–23.

Ahuja, A.K., Dorn, J.D., Caspi, A., Filley, E., Dagnelie, G.G., Greenberg, R.J., McMahon, M.J., 2009. The Argus II Retinal Prosthesis Enables Blind Subjects to Identify the Direction of Motion. ARVO Meeting Abstracts 50, 4590.

Ahuja, A.K., Dorn, J.D., Caspi, A., McMahon, M.J., Dagnelie, G.G., daCruz, L., Stanga, P., Humayun, M.S., Greenberg, R.J., Argus, I.I.S.G., 2011. Blind subjects implanted with the Argus II retinal prosthesis are able to improve performance in a spatial-motor task. The British journal of ophthalmology 95, 539–543.

Ahuja, A.K., Yeoh, J., Dorn, J.D., Caspi, A., Wuyyuru, V., McMahon, M.J., Humayun, M.S., Greenberg, R.J., daCruz, L., 2013. Factors Affecting Perceptual Threshold in Argus II Retinal Prosthesis Subjects. Transl Vis Sci Technol 2, 1.

Alamusi, Matsuo, T., Hosoya, O., Tsutsui, K.M., Uchida, T., 2015. Vision maintenance and retinal apoptosis reduction in RCS rats with Okayama University-type retinal prosthesis (OUReP™) implantation. J Artif Organs 18, 264–271.

alpha-IMS of Retina Implant AG [WWW Document], n.d. alpha-IMS of Retina Implant AG [WWW Document]. retina-implant.de. URL http://retina-

implant.de/en/doctors/technology/default.aspx (accessed 4.12.13).

Apte, R.S., Scheufele, T.A., Blomquist, P.H., 2001. Etiology of blindness in an urban community hospital setting. Ophthalmology 108, 693–696.

Argus® II Retinal Prosthesis System [WWW Document], n.d. Argus® II Retinal Prosthesis System [WWW Document]. URL http://www.accessdata.fda.gov/cdrh_docs/pdf11/h110002c.pdf

Attebo, K., Mitchell, P., Smith, W., 1996. Visual acuity and the causes of visual loss in Australia. The Blue Mountains Eye Study. Ophthalmology 103, 357–364.

Barry, M.P., Dagnelie, G.G., Argus, I.I.S.G., 2012. Use of the Argus II Retinal Prosthesis to Improve Visual Guidance of Fine Hand Movements. Invest. Ophthalmol. Vis. Sci. 53, 5095–5101.

Bartholow, R., 1874. Experimental investigations into the functions of the human brain. The American Journal of the Medical Sciences 67, 305–313.

Bavelier, D., Neville, H.J., 2002. Cross-modal plasticity: where and how? Nat Rev Neurosci 3, 443–452.

Bear, M.F., Connors, B.W., Paradiso, M.A., 2015. Neuroscience: Exploring the Brain. Lippincott Williams \& Wilkins.

Beebe, X., Rose, T.L., 1988. Charge injection limits of activated iridium oxide electrodes with 0.2 ms pulses in bicarbonate buffered saline. IEEE Trans Biomed Eng 35, 494–495.

Behrend, M.R., Ahuja, A.K., Humayun, M.S., Chow, R.H., Weiland, J.D., 2011. Resolution of the epiretinal prosthesis is not limited by electrode size. IEEE Trans Neural Syst Rehabil Eng 19, 436–442.

Belliveau, J.W., Kennedy, D.N., McKinstry, R.C., Buchbinder, B.R., Weisskoff, R.M., Cohen, M.S., Vevea, J.M., Brady, T.J., Rosen, B.R., 1991. Functional mapping of the human visual cortex by magnetic resonance imaging. Science 254, 716–719.

Besch, D., Sachs, H., Szurman, P., Gulicher, D., Wilke, R., Reinert, S., Zrenner, E., Bartz-Schmidt, K.U., Gekeler, F., 2008. Extraocular surgery for implantation

of an active subretinal visual prosthesis with external connections: feasibility and outcome in seven patients. The British journal of ophthalmology 92, 1361–1368.

Bionic Vision Australia successfully completes clinical trial of retinal implant in retinitis pigmentosa : Bionic Vision Australia [WWW Document], n.d. Bionic Vision Australia successfully completes clinical trial of retinal implant in retinitis pigmentosa : Bionic Vision Australia [WWW Document]. bionicvision.org.au. URL http://bionicvision.org.au/media/archive/bionic_vision_australia_successfully_completes_trial_of_retinal_implant_in_retinitis_pigmentosa (accessed 5.11.17).

Brelén, M.E., De Potter, P., Gersdorff, M., Cosnard, G., Veraart, C., Delbeke, J., 2006. Intraorbital implantation of a stimulating electrode for an optic nerve visual prosthesis. Case report. J. Neurosurg. 104, 593–597.

Brindley, G.S., 1964. The Number Of Information Channels Needed For Efficient Reading. The Journal of physiology 46.

Brindley, G.S., Lewin, W.S., 1968. The sensations produced by electrical stimulation of the visual cortex. The Journal of physiology 196, 479–493.

Brummer, S.B., Turner, M.J., 1977. Electrochemical considerations for safe electrical stimulation of the nervous system with platinum electrodes. IEEE Trans Biomed Eng 24, 59–63.

Brummer, S.B.S., Robblee, L.S.L., Hambrecht, F.T.F., 1983. Criteria for selecting electrodes for electrical stimulation: theoretical and practical considerations. Ann N Y Acad Sci 405, 159–171.

Carpenter, R.H.S., Reddi, B., 2012. Neurophysiology: A Conceptual Approach. Hodder Arnold, London.

Caspi, A., Dorn, J.D., McClure, K.H., Humayun, M.S., Greenberg, R.J., McMahon, M.J., 2009. Feasibility study of a retinal prosthesis: spatial vision with a 16-electrode implant. Arch. Ophthalmol. 127, 398–401.

Cha, K., Horch, K., Normann, R.A., 1992a. Simulation of a phosphene-based visual field: visual acuity in a pixelized vision system. Ann Biomed Eng 20, 439–

449.

Cha, K., Horch, K.W., Normann, R.A., 1992b. Mobility performance with a pixelized vision system. Vision Res 32, 1367–1372.

Chader, G.J., Weiland, J., Humayun, M.S., 2009. Artificial vision: needs, functioning, and testing of a retinal electronic prosthesis. Prog. Brain Res. 175, 317–332.

Chai, X., Li, L., Wu, K., Zhou, C., Cao, P., Ren, Q., 2008. C-sight visual prostheses for the blind. IEEE Eng. Med. Biol. Mag. 27, 20–28.

Chen, L.-C., Sandmann, P., Thorne, J.D., Bleichner, M.G., Debener, S., 2016. Cross-Modal Functional Reorganization of Visual and Auditory Cortex in Adult Cochlear Implant Users Identified with fNIRS. Neural Plast. 2016, 4382656.

Chen, S.-J., Mahadevappa, M., Roizenblatt, R., Weiland, J., Humayun, M., 2006. Neural responses elicited by electrical stimulation of the retina. Trans Am Ophthalmol Soc 104, 252–259.

Choi, C.W., Kim, P.S., Shin, S.A., Yang, J.Y., Yang, Y.S., 2014. Lateral geniculate body evoked potentials elicited by visual and electrical stimulation. Korean J Ophthalmol 28, 337–342.

Chow, A.Y., Bittner, A.K., Pardue, M.T., 2010. The artificial silicon retina in retinitis pigmentosa patients (an American Ophthalmological Association thesis). Trans Am Ophthalmol Soc 108, 120–154.

Chow, A.Y., Packo, K.H., Pollack, J.S., Schuchard, R.A., 2003. Subretinal Artificial Silicon Retina Microchip Implantation in Retinitis Pigmentosa Patients: Long Term Follow-Up. ARVO Meeting Abstracts 44, 4205.

Chow, A.Y., Pardue, M.T., Chow, V.Y., Peyman, G.A., Liang, C., Perlman, J.I., Peachey, N.S., 2001. Implantation of silicon chip microphotodiode arrays into the cat subretinal space. IEEE Trans Neural Syst Rehabil Eng 9, 86–95.

Chow, A.Y., Pollack, J.S., Packo, K.H., Schuchard, R.A., 2005. The Artificial Silicon Retina Microchip for the Treatment of Retinitis Pigmentosa: 2 to 4 1/2 Year Update. Invest. Ophthalmol. Vis. Sci. 46, 1140–1140.

Clifton, R.K., Muir, D.W., Ashmead, D.H., Clarkson, M.G., 1993. Is Visually Guided Reaching in Early Infancy a Myth? Child Development 64, 1099–1110.

Colier, W.N., Quaresima, V., Wenzel, R., van der Sluijs, M.C., Oeseburg, B., Ferrari, M., Villringer, A., 2001. Simultaneous near-infrared spectroscopy monitoring of left and right occipital areas reveals contra-lateral hemodynamic changes upon hemi-field paradigm. Vision Res 41, 97–102.

Correia, T., Lloyd-Fox, S., Everdell, N., Blasi, A., Elwell, C., Hebden, J.C., Gibson, A., 2012. Three-dimensional optical topography of brain activity in infants watching videos of human movement. Phys Med Biol 57, 1135–1146.

daCruz, L., Coley, B.F., Dorn, J., Merlini, F., Filley, E., Christopher, P., Chen, F.K., Wuyyuru, V., Sahel, J., Stanga, P., Humayun, M., Greenberg, R.J., Dagnelie, G.G., Argus II Study Group, 2013. The Argus II epiretinal prosthesis system allows letter and word reading and long-term function in patients with profound vision loss. The British journal of ophthalmology 97, 632–636.

daCruz, L., Dorn, J.D., Humayun, M.S., Dagnelie, G.G., Handa, J., Barale, P.-O., Sahel, J.-A., Stanga, P.E., Hafezi, F., Safran, A.B., Salzmann, J., Santos, A.A., Birch, D., Spencer, R., Cideciyan, A.V., de Juan, E., Duncan, J.L., Eliott, D., Fawzi, A., Olmos de Koo, L.C., Ho, A.C., Brown, G., Haller, J., Regillo, C., Del Priore, L.V., Arditi, A., Greenberg, R.J., Argus II Study Group, 2016. Five-Year Safety and Performance Results from the Argus II Retinal Prosthesis System Clinical Trial. Ophthalmology 123, 2248–2254.

daCruz, L., Merlini, F., Arsiero, M., Anaflous, F., Caspi, A., Sahel, J.A., Stanga, P.E., Hafezi, F., Greenberg, R.J., Group, A.R.I.S., 2012. Subjects Blinded By Outer Retinal Dystrophies Are Able To Recognize Outlined Shapes Using The Argus(R) Ii Retinal Prosthesis System: A Comparison With The Full Shapes Recognition Task. ARVO Meeting Abstracts 53, 5507.

Dagnelie, G.G., Barnett, D., Humayun, M.S., Thompson, R.W., 2006. Paragraph text reading using a pixelized prosthetic vision simulator: parameter dependence and task learning in free-viewing conditions. Invest. Ophthalmol. Vis. Sci. 47, 1241–1250.

Dagnelie, G.G., Keane, P., Narla, V., Yang, L., Weiland, J., Humayun, M., 2007.

Real and virtual mobility performance in simulated prosthetic vision. J Neural Eng 4, S92–101.

Deisseroth, K., 2011. Optogenetics. Nature Methods 8, 26–29.

Delbeke, J., Wanet-Defalque, M.C., Gerard, B., Troosters, M., Michaux, G., Veraart, C., 2002. The Microsystems Based Visual Prosthesis for Optic Nerve Stimulation. Artificial Organs 26, 232–234.

Delpy, D.T., Cope, M., van der Zee, P., Arridge, S., Wray, S., Wyatt, J., 1988. Estimation of optical pathlength through tissue from direct time of flight measurement. Phys Med Biol 33, 1433–1442.

Dimitrov, P.N., Mukesh, B.N., McCarty, C.A., Taylor, H.R., 2003. Five-year incidence of bilateral cause-specific visual impairment in the Melbourne Visual Impairment Project. Invest. Ophthalmol. Vis. Sci. 44, 5075–5081.

Dobelle, W.H., 2000. Artificial Vision for the Blind by Connecting a Television Camera to the Visual Cortex. ASAIO Journal 46, 3.

Dobelle, W.H., Mladejovsky, M.G., Girvin, J.P., 1974. Artifical vision for the blind: electrical stimulation of visual cortex offers hope for a functional prosthesis. Science 183, 440–444.

Dobelle, W.H., Quest, D.O., Antunes, J.L., Roberts, T.S., Girvin, J.P., 1979. Artificial vision for the blind by electrical stimulation of the visual cortex. Neurosurgery 5, 521–527.

Dobelle, W.H., 1998. Willem J. Kolff and Artificial Vision for the Blind. Artificial Organs 22, 966–968.

Dorn, J.D., Ahuja, A.K., Caspi, A., daCruz, L., Dagnelie, G.G., Sahel, J.-A., Greenberg, R.J., McMahon, M.J., Group, F.T.A.I.S., 2013. The Detection of Motion by Blind Subjects With the Epiretinal 60-Electrode (Argus II) Retinal ProsthesisBlind Subjects and Motion Detection. JAMA Ophthalmol 131, 183–189.

Dougherty, R.F., Koch, V.M., Brewer, A.A., Fischer, B., Modersitzki, J., Wandell, B.A., 2003. Visual field representations and locations of visual areas V1/2/3 in

human visual cortex. Journal of Vision 3, 1.

Eckmiller, R., Neumann, D., Baruth, O., 2005. Tunable retina encoders for retina implants: why and how. J Neural Eng 2, S91–S104.

Eggebrecht, A.T., White, B.R., Ferradal, S.L., Chen, C., Zhan, Y., Snyder, A.Z., Dehghani, H., Culver, J.P., 2012. A quantitative spatial comparison of high-density diffuse optical tomography and fMRI cortical mapping. Neuroimage 61, 1120–1128.

Ferrari, M., Quaresima, V., 2012. A brief review on the history of human functional near-infrared spectroscopy (fNIRS) development and fields of application. Neuroimage 63, 921–935.

Foerster, O., 1929. Beiträge zur Pathophysiologie der Sehbahn und der Sehsphäre. J Psychol Neurol 463–485.

Friedman, M.W., 1958. The scleral buckling procedure. Trans Pac Coast Otoophthalmol Soc Annu Meet 39, 319–27; discussion 327–8.

Garcia, S., Petrini, K., da Cruz, L., Rubin, G., Nardini, M., 2014. Cue combination with a new sensory signal: multisensory processing in blind patients with a retinal prosthesis. Journal of Vision 14, 1132–1132.

Gervain, J., Mehler, J., Werker, J.F., Nelson, C.A., Csibra, G., Lloyd-Fox, S., Shukla, M., Aslin, R.N., 2011. Near-infrared spectroscopy: a report from the McDonnell infant methodology consortium. Dev Cogn Neurosci 1, 22–46.

Ghazi, N.G., Abboud, E.B., Nowilaty, S.R., Alkuraya, H., Alhommadi, A., Cai, H., Hou, R., Deng, W.-T., Boye, S.L., Almaghamsi, A., Saikhan, Al, F., Al-Dhibi, H., Birch, D., Chung, C., Colak, D., LaVail, M.M., Vollrath, D., Erger, K., Wang, W., Conlon, T., Zhang, K., Hauswirth, W., Alkuraya, F.S., 2016. Treatment of retinitis pigmentosa due to MERTK mutations by ocular subretinal injection of adeno-associated virus gene vector: results of a phase I trial. Hum. Genet. 135, 327–343. Goodale, M.A., Milner, A.D., 1992. Separate visual pathways for perception and action. Trends Neurosci.

Goodale, M.A., Milner, A.D., 1992. Separate visual pathways for perception and action. Trends Neurosci.

Gratton, G., Corballis, P.M., Cho, E., Fabiani, M., Hood, D.C., 1995. Shades of gray matter: noninvasive optical images of human brain responses during visual stimulation. Psychophysiology 32, 505–509.

Gratton, G., Maier, J.S., Fabiani, M., Mantulin, W.W., Gratton, E., 1994. Feasibility of intracranial near-infrared optical scanning. Psychophysiology 31, 211–215.

Greenberg, R.J., Velte, T.J., Humayun, M.S., Scarlatis, G.N., de Juan, E., 1999. A computational model of electrical stimulation of the retinal ganglion cell. IEEE Trans Biomed Eng 46, 505–514.

Grover, S.S., Fishman, G.A.G., Anderson, R.J.R., Tozatti, M.S.M., Heckenlively, J.R.J., Weleber, R.G.R., Edwards, A.O.A., Brown, J.J., 1999. Visual acuity impairment in patients with retinitis pigmentosa at age 45 years or older. Ophthalmology 106, 1780–1783.

Guadagni, V., Novelli, E., Piano, I., Gargini, C., Strettoi, E., 2015. Pharmacological approaches to retinitis pigmentosa: A laboratory perspective. Prog Retin Eye Res.

Guo, T., Lovell, N.H., Tsai, D., Twyford, P., Fried, S., Morley, J.W., Suaning, G.J., Dokos, S., 2014. Selective activation of ON and OFF retinal ganglion cells to high-frequency electrical stimulation: a computational modeling study. Conf Proc IEEE Eng Med Biol Soc 2014, 6108–6111.

Güven, D., Weiland, J.D., Fujii, G., Mech, B.V., Mahadevappa, M., Greenberg, R., Roizenblatt, R., Qiu, G., Labree, L., Wang, X., Hinton, D., Humayun, M.S., 2005. Long-term stimulation by active epiretinal implants in normal and RCD1 dogs. J Neural Eng 2, S65–73.

Halverson, H.M., 1943. The development of prehension in infants., in: Barker, R.G., Kounin, J.S., Wright, H.F. (Eds.), Child Behavior and Development: a Course of Representative Studies. McGraw-Hill, New York, NY, US, pp. 49–65.

Hamel, C., 2006. Retinitis pigmentosa. Orphanet J Rare Dis 1, 40.

Hartong, D.T., Berson, E.L., Dryja, T.P., 2006. Retinitis pigmentosa. Lancet 368, 1795–1809.

Hauer, M.C., edu, M.L., edu, H.U., 2009. Intraocular camera for retinal prostheses: refractive and diffractive lens systems.

Hayes, J.S., Yin, V.T., Piyathaisere, D., Weiland, J.D., Humayun, M.S., Dagnelie, G.G., 2003. Visually guided performance of simple tasks using simulated prosthetic vision. Artificial Organs 27, 1016–1028.

Henderson, D.C., Evans, J.R., Dobelle, W.H., 1979. The Relationship between Stimulus Parameters and Phosphene Threshold/ Brightness, during Stimulation of Human Visual Cortex. ASAIO Journal 25, 367.

High-Acuity device - Bionic Vision Australia [WWW Document], n.d. High-Acuity device - Bionic Vision Australia [WWW Document]. bionicvision.org.au. URL http://www.bionicvision.org.au/eye/prototypes/high_acuity (accessed 4.11.13).

Ho, A.C., Humayun, M.S., Dorn, J.D., daCruz, L., Dagnelie, G.G., Handa, J., Barale, P.-O., Sahel, J.-A., Stanga, P.E., Hafezi, F., Safran, A.B., Salzmann, J., Santos, A.A., Birch, D., Spencer, R., Cideciyan, A.V., de Juan, E., Duncan, J.L., Eliott, D., Fawzi, A., Olmos de Koo, L.C., Brown, G.C., Haller, J.A., Regillo, C.D., Del Priore, L.V., Arditi, A., Geruschat, D.R., Greenberg, R.J., Argus II Study Group, 2015. Long-Term Results from an Epiretinal Prosthesis to Restore Sight to the Blind. Ophthalmology 122, 1547–1554.

Hodgkin, A.L., Huxley, A.F., 1952. A quantitative description of membrane current and its application to conduction and excitation in nerve. The Journal of physiology 117, 500–544.

Hohlstein, R.R., 1982. The development of prehension in normal infants. Am J Occup Ther 36, 170–176.

Holmes, G., 1945. Ferrier Lecture: the organization of the visual cortex in man. Presented at the Proceedings of the Royal Society of London Series B.

Hornig, R., Zehnder, T., Velikay-Parel, M., Laube, T., Feucht, M., Richard, G., 2007a. Artificial Sight, Artificial Sight. Springer New York, New York, NY.

Hornig, R., Zehnder, T., Velikay-Parel, M., Laube, T., Feucht, M., Richard, G., 2007b. The IMI Retinal Implant System, in: Humayun, M.S., Weiland, J.D., Chader, G., Greenbaum, E. (Eds.), Artificial Sight: Basic Research, Biomedical

Engineering, and Clinical Advances, Artificial Sight: Basic Research, Biomedical Engineering, and Clinical Advances. Springer New York, New York, NY, pp. 111–128.

Horsager, A., Boynton, G.M., Greenberg, R.J., Fine, I., 2011. Temporal interactions during paired-electrode stimulation in two retinal prosthesis subjects. Invest. Ophthalmol. Vis. Sci. 52, 549–557.

Horsager, A., Greenberg, R.J., Fine, I., 2010. Spatiotemporal interactions in retinal prosthesis subjects. Invest. Ophthalmol. Vis. Sci. 51, 1223–1233.

Horsager, A., Greenwald, S.H., Weiland, J.D., Humayun, M.S., Greenberg, R.J., McMahon, M.J., Boynton, G.M., Fine, I., 2009. Predicting visual sensitivity in retinal prosthesis patients. Invest. Ophthalmol. Vis. Sci. 50, 1483–1491.

Humayun, M.S., 2001. Intraocular retinal prosthesis. Trans Am Ophthalmol Soc 99, 271.

Humayun, M.S., de Juan, E., Dagnelie, G.G., Greenberg, R.J., Propst, R.H., Phillips, D.H., 1996. Visual perception elicited by electrical stimulation of retina in blind humans. Arch. Ophthalmol. 114, 40–46.

Humayun, M.S., de Juan, E., Weiland, J.D., Dagnelie, G.G., Katona, S., Greenberg, R., Suzuki, S., 1999. Pattern electrical stimulation of the human retina. Vision Res 39, 2569–2576.

Humayun, M.S., Dorn, J.D., daCruz, L., Dagnelie, G.G., Sahel, J.-A., Stanga, P.E., Cideciyan, A.V., Duncan, J.L., Eliott, D., Filley, E., Ho, A.C., Santos, A.A., Safran, A.B., Arditi, A., Del Priore, L.V., Greenberg, R.J., Argus II Study Group, 2012. Interim Results from the International Trial of Second Sight's Visual Prosthesis. Ophthalmology 119, 779–788.

Humayun, M.S., Freda, R., Fine, I., Roy, A., Fujii, G., Greenberg, R.J., Little, J., Mech, B., Weiland, J.D., de Juan, E.J., 2005. Implanted Intraocular Retinal Prosthesis in Six Blind Subjects. ARVO Meeting Abstracts 46, 1144.

Humayun, M., Propst, R., de Juan, E., McCormick, K., Hickingbotham, D., 1994. Bipolar surface electrical stimulation of the vertebrate retina. Arch. Ophthalmol. 112, 110–116.

Humayun, M.S., Weiland, J.D.J., Fujii, G.Y.G., Greenberg, R.R., Williamson, R.R., Little, J.J., Mech, B.B., Cimmarusti, V.V., Van Boemel, G.G., Dagnelie, G.G., de Juan, E.E., 2003. Visual perception in a blind subject with a chronic microelectronic retinal prosthesis. Vision Res 43, 2573–2581.

Humayun, M.S., Dorn, J.D., daCruz, L., Dagnelie, G.G., Sahel, J.-A., Stanga, P.E., Cideciyan, A.V., Duncan, J.L., Eliott, D., Filley, E., Ho, A.C., Santos, A.A., Safran, A.B., Arditi, A., Del Priore, L.V., Greenberg, R.J., Argus II Study Group, 2012. Interim Results from the International Trial of Second Sight's Visual Prosthesis. Ophthalmology 119, 779–788.

Jacobson, S.G., Cideciyan, A.V., Ratnakaram, R., Heon, E., Schwartz, S.B., Román, A.J., Peden, M.C., Alemán, T.S., Boye, S.L., Sumaroka, A., Conlon, T.J., Calcedo, R., Pang, J.-J., Erger, K.E., Olivares, M.B., Mullins, C.L., Swider, M., Kaushal, S., Feuer, W.J., Iannaccone, A., Fishman, G.A., Stone, E.M., Byrne, B.J., Hauswirth, W.W., 2012. Gene Therapy for Leber Congenital Amaurosis Caused by RPE65 Mutations: Safety and Efficacy in 15 Children and Adults Followed Up to 3 Years. Arch. Ophthalmol. 130, 9–24.

Jensen, R.J., Rizzo, J.F., Ziv, O.R., Grumet, A., Wyatt, J., 2003a. Thresholds for activation of rabbit retinal ganglion cells with an ultrafine, extracellular microelectrode. Invest. Ophthalmol. Vis. Sci. 44, 3533–3543.

Jensen, R.J., Ziv, O.R., Rizzo, J.F., 2003b. Thresholds for Direct and Indirect Activation of Ganglion Cells With an Epiretinal Electrode: Effect of Stimulus Duration and Electrode Size. ARVO Meeting Abstracts 44, 5048.

Jepson, L.H., Hottowy, P., Mathieson, K., Gunning, D.E., Dabrowski, W., Litke, A.M., Chichilnisky, E.J., 2013. Focal electrical stimulation of major ganglion cell types in the primate retina for the design of visual prostheses. J. Neurosci. 33, 7194–7205.

Jepson, L.H., Hottowy, P., Weiner, G.A., Dąbrowski, W., Litke, A.M., Chichilnisky, E.J., 2014. High-fidelity reproduction of spatiotemporal visual signals for retinal prosthesis. Neuron 83, 87–92.

Jobsis, F.F., 1977. Noninvasive, infrared monitoring of cerebral and myocardial oxygen sufficiency and circulatory parameters. Science.

Jones, B.W., Kondo, M., Terasaki, H., Lin, Y., McCall, M., Marc, R.E., 2012. Retinal remodeling. Japanese journal of ophthalmology 56, 289–306.

Jones, B.W., Marc, R.E., 2005. Retinal remodeling during retinal degeneration. Exp. Eye Res.

Jurcak, V., Tsuzuki, D., Dan, I., 2007. 10/20, 10/10, and 10/5 systems revisited: their validity as relative head-surface-based positioning systems. Neuroimage 34, 1600–1611.

Kato, T., Kamei, A., Takashima, S., Ozaki, T., 1993. Human visual cortical function during photic stimulation monitoring by means of near-infrared spectroscopy. J. Cereb. Blood Flow Metab. 13, 516–520.

Kim, E.T., Seo, J.-M., Woo, S.J., Zhou, J.A., Chung, H., Kim, S.J., 2008. Fabrication of Pillar Shaped Electrode Arrays for Artificial Retinal Implants. Sensors (Basel) 8, 5845–5856.

Klaver, C.C.W., Wolfs, R.C.W., Vingerling, J.R., Hofman, A., de Jong, P.T.V.M., 1998. Age-Specific Prevalence and Causes of Blindness and Visual Impairment in an Older Population: The Rotterdam Study. Arch. Ophthalmol. 116, 653–658.

Klein, R., Wang, Q., Klein, B.E., Moss, S.E., Meuer, S.M., 1995. The relationship of age-related maculopathy, cataract, and glaucoma to visual acuity. Invest. Ophthalmol. Vis. Sci. 36, 182–191.

Kolb, H., 2003. How the Retina Works. American Scientist 91, 28–35.

Kotecha, A., Zhong, J., Stewart, D., daCruz, L., 2014. The Argus II prosthesis facilitates reaching and grasping tasks: a case series. BMC Ophthalmol 14, 71.

Krause, F., Schum, H., Boshamer, K., Lysholm, E., Bruns, von, P., 1932. Die spezielle Chirurgie der Gehirnkrankheiten.

Krumpaszky, H.G., Lüdtke, R., Mickler, A., Klauss, V., Selbmann, H.K., 1999. Blindness Incidence in Germany. Ophthalmologica 213, 176–182.

Lee, D.S., Lee, J.S., Oh, S.H., Kim, S.K., Kim, J.W., Chung, J.K., Lee, M.C., Kim, C.S., 2001. Cross-modal plasticity and cochlear implants. Nature 409, 149–150.

Liew, G., Michaelides, M., Bunce, C., 2014. A comparison of the causes of blindness certifications in England and Wales in working age adults (16–64 years), 1999–2000 with 2009–2010. BMJ Open 4, e004015.

Light and shadow centroids | GIMP Plugin Registry [WWW Document], n.d. Light and shadow centroids | GIMP Plugin Registry [WWW Document]. URL http://registry.gimp.org/node/27529

Lilly, J.C., Hughes, J.R., Alvord, E.C., Galkin, T.W., 1955. Brief, Noninjurious Electric Waveform for Stimulation of the Brain. Science 121, 468–469.

Liu, S., Matsuo, T., Hosoya, O., Uchida, T., 2017. Photoelectric Dye Used for Okayama University-Type Retinal Prosthesis Reduces the Apoptosis of Photoreceptor Cells. Journal of Ocular Pharmacology and Therapeutics 33, 149–160.

Liu, Y., Park, J., Lang, R.J., Emami-Neyestanak, A., Pellegrino, S., Humayun, M.S., Tai, Y.-C., 2013. Parylene origami structure for intraocular implantation, in:. Presented at the 2013 Transducers & Eurosensors XXVII: The 17th International Conference on Solid-State Sensors, Actuators and Microsystems (TRANSDUCERS & EUROSENSORS XXVII), IEEE, pp. 1549–1552.

Lloyd-Fox, S., Blasi, A., Elwell, C.E., 2010. Illuminating the developing brain: The past, present and future of functional near infrared spectroscopy. Neuroscience & Biobehavioral Reviews.

Lovell, N.H., Dokos, S., Preston, P., Lehmann, T., Dommel, N., Lin, A., Wong, Y.T., Opie, N., Hallum, L.E., Chen, S., Suaning, G.J., 2005. A Retinal Neuroprosthesis Design Based on Simultaneous Current Injection, in:. Presented at the 2005 3rd IEEE/EMBS Special Topic Conference on Microtechnology in Medicine and Biology, IEEE, pp. 98–101.

Lorach, H., Benosman, R., Marre, O., Ieng, S.-H., Sahel, J.A., Picaud, S., 2012. Artificial retina: the multichannel processing of the mammalian retina achieved with a neuromorphic asynchronous light acquisition device. J Neural Eng 9, 066004–066004.

Luo, Y.H.-L., daCruz, L., 2014. A review and update on the current status of

retinal prostheses (bionic eye). Br. Med. Bull. 109, 31–44.

Luo, Y.H.-L., daCruz, L., 2016. The Argus® II Retinal Prosthesis System. Prog Retin Eye Res 50, 89–107.

Luo, Y.H.-L., Davagnanam, I., daCruz, L., 2013. MRI Brain Scans in Two Patients with the Argus II Retinal Prosthesis. Ophthalmology 120, 1711–1711.e8.

Luo, Y.H.-L., Zhong, J.J., Clemo, M., daCruz, L., 2016. Long-term Repeatability and Reproducibility of Phosphene Characteristics in Chronically Implanted Argus® II Retinal Prosthesis Subjects. Am. J. Ophthalmol.

Luo, Y.H.-L., Zhong, J.J., daCruz, L., 2015. The use of Argus® II retinal prosthesis by blind subjects to achieve localisation and prehension of objects in 3-dimensional space. Graefe's archive for clinical and experimental ophthalmology = Albrecht von Graefes Archiv fur klinische und experimentelle Ophthalmologie 253, 1907–1914.

Machemer, R., Buettner, H., Norton, E.W., Parel, J.M., 1971. Vitrectomy: a pars plana approach. Transactions -- American Academy of Ophthalmology and Otolaryngology 75, 813–820.

Machemer, R., Parel, J.M., Norton, E.W., 1972. Vitrectomy: a pars plana approach. Technical improvements and further results. Transactions -- American Academy of Ophthalmology and Otolaryngology 76, 462–466.

MacLaren, R.E., Bennett, J., Schwartz, S.D., 2016. Gene Therapy and Stem Cell Transplantation in Retinal Disease: The New Frontier. Ophthalmology 123, S98–S106.

MacLaren, R.E., Groppe, M., Barnard, A.R., Cottriall, C.L., Tolmachova, T., Seymour, L., Clark, K.R., During, M.J., Cremers, F.P.M., Black, G.C.M., Lotery, A.J., Downes, S.M., Webster, A.R., Seabra, M.C., 2014. Retinal gene therapy in patients with choroideremia: initial findings from a phase 1/2 clinical trial. Lancet.

Marc, R.E., Jones, B.W., Anderson, J.R., Kinard, K., Marshak, D.W., Wilson, J.H., Wensel, T., Lucas, R.J., 2007. Neural reprogramming in retinal

degeneration. Invest. Ophthalmol. Vis. Sci. 48, 3364–3371.

Marc, R.E., Jones, B.W., Watt, C.B., Strettoi, E., 2003. Neural remodeling in retinal degeneration. Prog Retin Eye Res 22, 607–655.

Market Research MRI products [WWW Document], n.d. Market Research MRI products [WWW Document]. imvinfo.com. URL http://www.imvinfo.com/index.aspx?sec=mri&sub=dis&itemid=200023 (accessed 11.17.12).

Mathieson, K., Loudin, J., Goetz, G., Huie, P., Wang, L., Kamins, T.I., Galambos, L., Smith, R., Harris, J.S., Sher, A., Palanker, D., 2012. Photovoltaic retinal prosthesis with high pixel density. Nature Photon 6, 391–397.

Menzel-Severing, J.J., Laube, T.T., Brockmann, C.C., Bornfeld, N.N., Mokwa, W.W., Mazinani, B.B., Walter, P.P., Roessler, G.G., 2012. Implantation and explantation of an active epiretinal visual prosthesis: 2-year follow-up data from the EPIRET3 prospective clinical trial. Eye (Lond) 26, 501–509.

Michaelides, M., Hunt, D.M., Moore, A.T., 2003. The genetics of inherited macular dystrophies. J. Med. Genet. 40, 641–650.

Milam, A.H., Li, Z.Y., Fariss, R.N., 1998. Histopathology of the human retina in retinitis pigmentosa. Prog Retin Eye Res 17, 175–205.

Mokwa, W.W., Goertz, M.M., Koch, C.C., Krisch, I.I., Trieu, H.K.H., Walter, P.P., 2008. Intraocular epiretinal prosthesis to restore vision in blind humans. Conf Proc IEEE Eng Med Biol Soc 2008, 5790–5793.

Monge, M., Emami, A., 2014. Design considerations for high-density fully intraocular epiretinal prostheses. 2014 IEEE Biomedical Circuits and Systems Conference (BioCAS) 224–227.

Monge, M., Raj, M., Nazari, M.H., Chang, H.-C., Zhao, Y., Weiland, J.D., Humayun, M.S., Tai, Y.-C., Emami, A., 2013. A fully intraocular high-density self-calibrating epiretinal prosthesis. IEEE Trans Biomed Circuits Syst 7, 747–760.

Muñoz, B., West, S.K., Rubin, G.S., Schein, O.D., Quigley, H.A., Bressler, S.B.,

Bandeen-Roche, K., 2000. Causes of blindness and visual impairment in a population of older Americans: The Salisbury Eye Evaluation Study. Arch. Ophthalmol. 118, 819–825.

Nadig, M.N., 1999. Development of a silicon retinal implant: cortical evoked potentials following focal stimulation of the rabbit retina with light and electricity. Clin Neurophysiol 110, 1545–1553.

Nakauchi, K., Fujikado, T., Terasawa, Y., Saito, T., Kanda, H., Ohta, J., Hirakata, A., Tano, Y., 2006. Threshold Current for Retinal Damage by Artificial Retina With Chronic Suprachroidal-transretinal Stimulation. ARVO Meeting Abstracts 47, 3197.

Nanduri, D., 2011. Prosthetic vision in blind human patients: predicting the percepts of epiretinal stimulation :: University of Southern California Dissertations and Theses. University of Southern California.

Nanduri, D., Dorn, J.D., Humayun, M.S., Greenberg, R.J., Weiland, J.D., 2011. Percept Properties of Single Electrode Stimulation in Retinal Prosthesis Subjects. ARVO Annual Meeting Abstract Search and Program Planner 2011, 442–442.

Nanduri, D., Fine, I., Horsager, A., Boynton, G.M., Humayun, M.S., Greenberg, R.J., Weiland, J.D., 2012. Frequency and amplitude modulation have different effects on the percepts elicited by retinal stimulation. Invest. Ophthalmol. Vis. Sci. 53, 205–214.

Nanduri, D., Humayun, M.S., Greenberg, R.J., McMahon, M.J., Weiland, J.D., 2008. Retinal prosthesis phosphene shape analysis. Conf Proc IEEE Eng Med Biol Soc 2008, 1785–1788.

Naples, G.G., Mortimer, J.T., Scheiner, A., Sweeney, J.D., 1988. A spiral nerve cuff electrode for peripheral nerve stimulation. IEEE Trans Biomed Eng 35, 905–916.

Neuroscience for Kids: the visual pathway Interesting information on what can happen if there's any damage | Teaching: Physics - Vision | Pinterest | Pathways… [WWW Document], n.d. Neuroscience for Kids: the visual pathway

Interesting information on what can happen if there's any damage | Teaching: Physics - Vision | Pinterest | Pathways… [WWW Document]. pinterest.com. URL https://www.pinterest.com/pin/462463455457839221/ (accessed 8.15.16).

New trial for wet AMD [WWW Document], n.d. New trial for wet AMD [WWW Document]. moorfields.nhs.uk. URL http://www.moorfields.nhs.uk/news/new-trial-wet-amd (accessed 5.14.17).

Nirenberg, S., Pandarinath, C., 2012. Retinal prosthetic strategy with the capacity to restore normal vision. Proceedings of the National Academy of Sciences of the United States of America 109, 15012–15017.

Norman, J., 2002. Two visual systems and two theories of perception: An attempt to reconcile the constructivist and ecological approaches. Behavioral and brain sciences.

Normann, R.A., Greger, B., House, P., Romero, S.F., Pelayo, F., Fernandez, E., 2009. Toward the development of a cortically based visual neuroprosthesis. J Neural Eng 6, 035001.

Obrig, H., Wenzel, R., Kohl, M., Horst, S., Wobst, P., Steinbrink, J., Thomas, F., Villringer, A., 2000. Near-infrared spectroscopy: does it function in functional activation studies of the adult brain? Int J Psychophysiol 35, 125–142.

OECD, 2012. Magnetic resonance imaging (MRI) exams, total 2012/2. oecd-ilibrary.org. doi:10.1787/mri-exam-total-table-2012-2-en

Ohta, J., Tokuda, T., Kagawa, K., Sugitani, S., Taniyama, M., Uehara, A., Terasawa, Y., Nakauchi, K., Fujikado, T., Tano, Y., 2007. Laboratory investigation of microelectronics-based stimulators for large-scale suprachoroidal transretinal stimulation (STS). J Neural Eng 4, S85–91.

Oldfield, R.C., 1971. The assessment and analysis of handedness: the Edinburgh inventory. Neuropsychologia 9, 97–113.

Olmedo-Payá, A., Martínez-Álvarez, A., Cuenca-Asensi, S., Ferrández-Vicente, J.M., Fernandez, E., 2013. Modeling the Effect of Fixational Eye Movements in Natural Scenes, in: Natural and Artificial …, Lecture Notes in Computer Science. Springer Berlin Heidelberg, Berlin, Heidelberg, pp. 332–341.

Opie, N.L., Ayton, L.N., Apollo, N.V., Ganesan, K., Guymer, R.H., Luu, C.D., 2014. Optical coherence tomography-guided retinal prosthesis design: model of degenerated retinal curvature and thickness for patient-specific devices. Artificial Organs 38, E82–94.

Palanker, D., Huie, P., Vankov, A., Aramant, R., Seiler, M., Fishman, H., Marmor, M., Blumenkranz, M., 2004. Migration of Retinal Cells through a Perforated Membrane: Implications for a High-Resolution Prosthesis. Invest. Ophthalmol. Vis. Sci. 45, 3266.

Panetsos, F., Diaz-De Cerio, E., Sanchez-Jimenez, A., Herrera-Rincon, C., 2009. Thalamic visual neuroprostheses: Comparison of visual percepts generated by natural stimulation of the eye and electrical stimulation of the thalamus, in:. Presented at the Neural Engineering, 2009. NER '09. 4th International IEEE/EMBS Conference on, pp. 56–59.

Panetsos, F., Sanchez-Jimenez, A., Cerio, E.D.-D., Diaz-Guemes, I., Sanchez, F.M., 2011. Consistent phosphenes generated by electrical microstimulation of the visual thalamus. An experimental approach for thalamic visual neuroprostheses. Frontiers in Neuroscience 5, 84.

Pardue, M.T., Phillips, M.J., Hanzlicek, B., Yin, H., Chow, A.Y., Ball, S.L., 2006. Neuroprotection of Photoreceptors in the RCS Rat After Implantation of a Subretinal Implant in the Superior or Inferior Retina, in: Hollyfield, J.G., Anderson, R.E., LaVail, M.M. (Eds.), Retinal Degenerative Diseases, Retinal Degenerative Diseases. Springer US, Boston, MA, pp. 321–326.

Pérez Fornos, A., Sommerhalder, J., daCruz, L., Sahel, J.-A., Mohand-Said, S., Hafezi, F., Pelizzone, M., 2012. Temporal properties of visual perception on electrical stimulation of the retina. Invest. Ophthalmol. Vis. Sci. 53, 2720–2731.

Perry, J.W., Morton, D., 1992. Laboratory Manual for Starr & Taggart's Biology. Singular.

Pezaris, J.S., Eskandar, E.N., 2009. Getting signals into the brain: visual prosthetics through thalamic microstimulation. Neurosurg Focus 27, E6.

Pezaris, J.S., Reid, R.C., 2007. Demonstration of artificial visual percepts

generated through thalamic microstimulation. Proceedings of the National Academy of Sciences of the United States of America 104, 7670–7675.

Potts, A.M., Inoue, J., 1970. The Electrically Evoked Response of the Visual System (EER) III. Further Contribution to the Origin of the EER. Invest. Ophthalmol. Vis. Sci.

Potts, A.M., Inoue, J., 1969. The electrically evoked response (EER) of the visual system. II. Effect of adaptation and retinitis pigmentosa. Invest Ophthalmol 8, 605–612.

Potts, A.M., Inoue, J., Buffum, D., 1968. The electrically evoked response of the visual system (EER). Invest. Ophthalmol. Vis. Sci.

qualisys.com, n.d. qualisys.com. URL http://www.qualisys.com (accessed 2.28.14).

Research Randomizer: Free Random Sampling and Random Assignment [WWW Document], n.d. Research Randomizer: Free Random Sampling and Random Assignment [WWW Document]. randomizer.org. URL http://www.randomizer.org/ (accessed 8.18.13).

Resnikoff, S., Pascolini, D., Etya'ale, D., Kocur, I., Pararajasegaram, R., Pokharel, G.P., Mariotti, S.P., 2004. Global data on visual impairment in the year 2002. Bull. World Health Organ. 82, 844–851.

Rizzo, J.F., Wyatt, J., Loewenstein, J., Kelly, S., Shire, D., 2003a. Methods and perceptual thresholds for short-term electrical stimulation of human retina with microelectrode arrays. Invest. Ophthalmol. Vis. Sci. 44, 5355–5361.

Rizzo, J.F., Wyatt, J., Loewenstein, J., Kelly, S., Shire, D., 2003b. Perceptual efficacy of electrical stimulation of human retina with a microelectrode array during short-term surgical trials. Invest. Ophthalmol. Vis. Sci. 44, 5362–5369.

Rizzo, S., Belting, C., Cinelli, L., Allegrini, L., Genovesi-Ebert, F., Barca, F., Di Bartolo, E., 2014. The Argus II retinal prosthesis: 12-month outcomes from a single-study center. Am. J. Ophthalmol. 157, 1282–1290.

Roessler, G., Laube, T., Brockmann, C., Kirschkamp, T., Mazinani, B., Goertz,

M., Koch, C., Krisch, I., Sellhaus, B., Trieu, H.K., Weis, J., Bornfeld, N., Röthgen, H., Messner, A., Mokwa, W., Walter, P., 2009. Implantation and explantation of a wireless epiretinal retina implant device: observations during the EPIRET3 prospective clinical trial. Invest. Ophthalmol. Vis. Sci. 50, 3003–3008.

Roessler, G., Laube, T., Brockmann, C., Kirschkamp, T., Mazinani, B., Menzel-Severing, J., Bornfeld, N., Walter, P., EPIRET Group, 2011. Angiographic findings following tack fixation of a wireless epiretinal retina implant device in blind RP patients. Graefe's archive for clinical and experimental ophthalmology = Albrecht von Graefes Archiv fur klinische und experimentelle Ophthalmologie 249, 1281–1286.

Rohrschneider, K., 2004. Determination of the location of the fovea on the fundus. Invest. Ophthalmol. Vis. Sci. 45, 3257–3258.

Rose, T.L., Robblee, L.S., 1990. Electrical stimulation with Pt electrodes. VIII. Electrochemically safe charge injection limits with 0.2 ms pulses (neuronal application). IEEE Trans Biomed Eng 37, 1118–1120.

Sabbah, N., Authie, C.N., Sanda, N., Mohand-Said, S., Sahel, J.-A., Safran, A.B., 2014. Importance of eye position on spatial localization in blind subjects wearing an Argus II retinal prosthesis. Invest. Ophthalmol. Vis. Sci. 55, 8259–8266.

Sahel, J., Mohand-Said, S., Stanga, P., Caspi, A., Greenberg, R., Argus II Study Group, 2013. Acuboost™: Enhancing the maximum acuity of the Argus II Retinal Prosthesis System. ARVO Meeting Abstracts 54, 1389.

Sakaguchi, H., Kamei, M., Fujikado, T., Yonezawa, E., Ozawa, M., Cecilia-Gonzalez, C., Ustariz-Gonzalez, O., Quiroz-Mercado, H., Tano, Y., 2009. Artificial vision by direct optic nerve electrode (AV-DONE) implantation in a blind patient with retinitis pigmentosa. J Artif Organs 12, 206–209.

Sakaguchi, H., Kamei, M., Nishida, K., Terasawa, Y., Fujikado, T., Ozawa, M., Nishida, K., 2012. Implantation of a newly developed direct optic nerve electrode device for artificial vision in rabbits. J Artif Organs 15, 295–300.

Sandman, C.A., O'Halloran, J.P., Isenhart, R., 1984. Is there an evoked vascular response? Science 224, 1355–1357.

Santos, A.A., 1997. Preservation of the Inner Retina in Retinitis Pigmentosa. Arch. Ophthalmol. 115, 511.

Schepens, C.L., 1957. The Scleral Buckling Procedures. AMA Arch Ophthalmol 58, 797–811.

Scholkmann, F., Kleiser, S., Metz, A.J., Zimmermann, R., Mata Pavia, J., Wolf, U., Wolf, M., 2014. A review on continuous wave functional near-infrared spectroscopy and imaging instrumentation and methodology. Neuroimage 85 Pt 1, 6–27.

Schwartz, S.D., Hubschman, J.-P., Heilwell, G., Franco-Cardenas, V., Pan, C.K., Ostrick, R.M., Mickunas, E., Gay, R., Klimanskaya, I., Lanza, R., 2012. Embryonic stem cell trials for macular degeneration: a preliminary report. Lancet 379, 713–720.

Schwartz, S.D., Regillo, C.D., Lam, B.L., Eliott, D., Rosenfeld, P.J., Gregori, N.Z., Hubschman, J.-P., Davis, J.L., Heilwell, G., Spirn, M., Maguire, J., Gay, R., Bateman, J., Ostrick, R.M., Morris, D., Vincent, M., Anglade, E., Del Priore, L.V., Lanza, R., 2015. Human embryonic stem cell-derived retinal pigment epithelium in patients with age-related macular degeneration and Stargardt's macular dystrophy: follow-up of two open-label phase 1/2 studies. The Lancet 385, 509–516.

Sekirnjak, C., 2006. Electrical Stimulation of Mammalian Retinal Ganglion Cells With Multielectrode Arrays. Journal of Neurophysiology 95, 3311–3327.

Sekirnjak, C., Hottowy, P., Sher, A., Dabrowski, W., Litke, A.M., Chichilnisky, E.J., 2008. High-resolution electrical stimulation of primate retina for epiretinal implant design. J. Neurosci. 28, 4446–4456.

Sekirnjak, C., Hulse, C., Jepson, L.H., Hottowy, P., Sher, A., Dabrowski, W., Litke, A.M., Chichilnisky, E.J., 2009. Loss of Responses to Visual But Not Electrical Stimulation in Ganglion Cells of Rats With Severe Photoreceptor Degeneration. Journal of Neurophysiology 102, 3260–3269.

Slide Show: The Neural Control of Vision D-1 [WWW Document], n.d. Slide

Show: The Neural Control of Vision D-1 [WWW Document]. web.mit.edu. URL http://web.mit.edu/bcs/schillerlab/research/A-Vision/A4-1.html (accessed 4.29.17).

Sommerhalder, J., Oueghlani, E., Bagnoud, M., Leonards, U., Safran, A.B., Pelizzone, M., 2003. Simulation of artificial vision: I. Eccentric reading of isolated words, and perceptual learning. Vision Res 43, 269–283.

Sommerhalder, J., Rappaz, B., de Haller, R., Fornos, A.P., Safran, A.B., Pelizzone, M., 2004. Simulation of artificial vision: II. Eccentric reading of full-page text and the learning of this task. Vision Res 44, 1693–1706.

Sommerhalder, J.R., Perez Fornos, A., Chanderli, K., Colin, L., Schaer, X., Mauler, F., Safran, A.B., Pelizzone, M., 2006. Minimum Requirements for Mobility in Unpredictible Environments. ARVO Meeting Abstracts 47, 3204.

Special Senses [WWW Document], n.d. Special Senses [WWW Document]. droualb.faculty.mjc.edu. URL http://droualb.faculty.mjc.edu/Lecture%20Notes/Unit%205/special_senses%20Spring%202007%20with%20figures.htm (accessed 8.15.16).

Stanga, P., Sahel, J., Mohand-Said, S., daCruz, L., Caspi, A., Merlini, F., Greenberg, R., Argus II Study Group, 2013. Face Detection using the Argus(R) II Retinal Prosthesis System. ARVO Meeting Abstracts 54, 1766.

Sterling, T.D., ACM, A.F.C.M., 1971. Visual Prosthesis, the Interdisciplinary Dialogue: 2nd Conference, Chicago, June 1969, Proceedings. Academic Press.

Stiles, N.R.B., McIntosh, B.P., Nasiatka, P.J., Hauer, M.C., Weiland, J.D., Humayun, M.S., Tanguay, A.R., Jr, 2011. An Intraocular Camera for Retinal Prostheses: Restoring Sight to the Blind, in: Serpengüzel, A., Poon, A.W. (Eds.), An Intraocular Camera for Retinal Prostheses: Restoring Sight to the Blind. Optical Processes in Microparticles and Nanostructures, p. 385.

Stingl, K., Bach, M., Bartz-Schmidt, K.U., Braun, A., Bruckmann, A., Gekeler, F., Greppmaier, U., Hörtdörfer, G., Kusnyerik, A., Peters, T., Wilhelm, B., Wilke, R., Zrenner, E., 2013a. Safety and efficacy of subretinal visual implants in humans: Methodological aspects. Clin Exp Optom 96, 4–13.

Stingl, K., Bartz-Schmidt, K.U., Besch, D., Braun, A., Bruckmann, A., Gekeler,

F., Greppmaier, U., Hipp, S., Hörtdörfer, G., Kernstock, C., Koitschev, A., Kusnyerik, A., Sachs, H., Schatz, A., Stingl, K.T., Peters, T., Wilhelm, B., Zrenner, E., 2013b. Artificial vision with wirelessly powered subretinal electronic implant alpha-IMS. Proceedings. Biological sciences / The Royal Society 280, 20130077.

Stingl, K., Bartz-Schmidt, K.U., Besch, D., Chee, C.K., Cottriall, C.L., Gekeler, F., Groppe, M., Jackson, T.L., MacLaren, R.E., Koitschev, A., Kusnyerik, A., Neffendorf, J., Nemeth, J., Naeem, M.A.N., Peters, T., Ramsden, J.D., Sachs, H., Simpson, A., Singh, M.S., Wilhelm, B., Wong, D., Zrenner, E., 2015. Subretinal Visual Implant Alpha IMS - Clinical trial interim report. Vision Res 111, 149–160.

Stingl, K., Zrenner, E., 2013. Electronic approaches to restitute vision in patients with neurodegenerative diseases of the retina. Ophthalmic Res. 50, 215–220.

Stone, J.L., 1992. Morphometric Analysis of Macular Photoreceptors and Ganglion Cells in Retinas With Retinitis Pigmentosa. Arch. Ophthalmol. 110, 1634.

Stronks, H.C., Barry, M.P., Dagnelie, G.G., 2013. Electrically elicited visual evoked potentials in Argus II retinal implant wearers. Invest. Ophthalmol. Vis. Sci. 54, 3891–3901.

Stronks, H.C., Dagnelie, G.G., 2014. The functional performance of the Argus II retinal prosthesis. Expert Rev Med Dev 11, 23–30.

Stone, J.L., 1992. Morphometric Analysis of Macular Photoreceptors and Ganglion Cells in Retinas With Retinitis Pigmentosa. Arch. Ophthalmol. 110, 1634.

The Primary Visual Cortex by Matthew Schmolesky – Webvision [WWW Document], n.d. The Primary Visual Cortex by Matthew Schmolesky – Webvision [WWW Document]. webvision.med.utah.edu. URL http://webvision.med.utah.edu/book/part-ix-psychophysics-of-vision/the-primary-visual-cortex/ (accessed 4.29.17).

Terasawa, Y., Fujikado, T., Yagi, T., 2001. Simulation of visual prosthesis in

virtual space. International Journal of Applied Electromagnetics and Mechanics 15, 431–436.

The Argus II Retinal Prosthesis (“Bionic Eye”) Receives Medicare Approval - VisionAware Blog - VisionAware [WWW Document], n.d. The Argus II Retinal Prosthesis (“Bionic Eye”) Receives Medicare Approval - VisionAware Blog - VisionAware [WWW Document]. visionaware.org. URL http://www.visionaware.org/blog/visionaware-blog/the-argus-ii-retinal-prosthesis-bionic-eye-receives-medicare-approval/12 (accessed 5.14.17).

Thompson, R.W., 2003. Facial Recognition Using Simulated Prosthetic Pixelized Vision. Invest. Ophthalmol. Vis. Sci. 44, 5035–5042.

Tokuda, T., Takeuchi, Y., Noda, T., Sasagawa, K., Nishida, K., Kitaguchi, Y., Fujikado, T., Tano, Y., Ohta, J., 2009. Light-controlled retinal stimulation on rabbit using CMOS-based flexible multi-chip stimulator. Conf Proc IEEE Eng Med Biol Soc 2009, 646–649.

Twyford, P., Cai, C., Fried, S., 2014. Differential responses to high-frequency electrical stimulation in ON and OFF retinal ganglion cells. J Neural Eng 11, 025001.

Uji, A., Matsuo, T., Ishimaru, S., Kajiura, A., Shimamura, K., Ohtsuki, H., Dan-oh, Y., Suga, S., 2005. Photoelectric dye-coupled polyethylene film as a prototype of retinal prostheses. Artificial Organs 29, 53–57.

Uji, A., Matsuo, T., Uchida, T., Shimamura, K., Ohtsuki, H., 2006. Intracellular Calcium Response and Adhesiveness of Chick Embryonic Retinal Neurons to Photoelectric Dye-coupled Polyethylene Films as Prototypes of Retinal Prostheses. Artificial Organs 30, 695–703.

Vaidya, A., Borgonovi, E., Taylor, R.S., Sahel, J.-A., Rizzo, S., Stanga, P.E., Kukreja, A., Walter, P., 2014. The cost-effectiveness of the Argus II retinal prosthesis in Retinitis Pigmentosa patients. BMC Ophthalmol 14, 49.

Velikay-Parel, M., Ivastinovic, D., Georgi, T., Hornig, R., 2010. Perceptual threshold and neuronal excitability as long-term safety evaluation in retinal implants. Acta Ophthalmologica 88, 0–0.

Velikay-Parel, M., Ivastinovic, D., Georgi, T., Richard, G., Hornig, R., 2013. A test method for quantification of stimulus-induced depression effects on perceptual threshold in epiretinal prosthesis. Acta Ophthalmologica 91, e595–602.

Velikay-Parel, M., Ivastinovic, D., Langmann, G., Hornig, R., Georgi, T., Wedrich, A., 2009. First experience with The IRIS retinal implant system. Acta Ophthalmologica 87.

Veraart, C., Raftopoulos, C., Mortimer, J.T., Delbeke, J., Pins, D., Michaux, G., Vanlierde, A., Parrini, S., Wanet-Defalque, M.C., 1998. Visual sensations produced by optic nerve stimulation using an implanted self-sizing spiral cuff electrode. Brain Res. 813, 181–186.

Veraart, C., Wanet-Defalque, M.-C., Gérard, B., Vanlierde, A., Delbeke, J., 2003. Pattern recognition with the optic nerve visual prosthesis. Artificial Organs 27, 996–1004.

Walter, P., Heimann, K., 2000. Evoked cortical potentials after electrical stimulation of the inner retina in rabbits. Graefe's archive for clinical and experimental ophthalmology = Albrecht von Graefes Archiv fur klinische und experimentelle Ophthalmologie 238, 315–318.

Walter, P., Kisvárday, Z.F., Görtz, M., Alteheld, N., Rössler, G., Stieglitz, T., Eysel, U.T., 2005. Cortical Activation Via an Implanted Wireless Retinal Prosthesis. Invest. Ophthalmol. Vis. Sci. 46, 1780–1785.

Wang, L., Yang, L., Dagnelie, G.G., 2008. Virtual Wayfinding Using Simulated Prosthetic Vision in Gaze-locked Viewing. Optom Vis Sci 85, E1057–E1063.

Weiland, J.D., Anderson, D.J., Humayun, M.S., 2002. In vitro electrical properties for iridium oxide versus titanium nitride stimulating electrodes. IEEE Trans Biomed Eng 49, 1574–1579.

Weiland, J.D., Faraji, B., Greenberg, R.J., Humayun, M.S., Shellock, F.G., 2012. Assessment of MRI issues for the Argus II Retinal Prosthesis. Magnetic Resonance Imaging 30, 382–389.

Weiland, J.D., Humayun, M.S., Dagnelie, G.G., de Juan, E., Greenberg, R.J.,

Iliff, N.T., 1999. Understanding the origin of visual percepts elicited by electrical stimulation of the human retina. Graefe's archive for clinical and experimental ophthalmology = Albrecht von Graefes Archiv fur klinische und experimentelle Ophthalmologie 237, 1007–1013.

Wenzel, R., Obrig, H., Ruben, J., Villringer, K., Thiel, A., Bernarding, J., Dirnagl, U., Villringer, A., 1996. Cerebral blood oxygenation changes induced by visual stimulation in humans. J Biomed Opt 1, 399–404.

Wide-View device - Bionic Vision Australia [WWW Document], n.d. Wide-View device - Bionic Vision Australia [WWW Document]. bionicvision.org.au. URL http://www.bionicvision.org.au/eye/prototypes/wide_view (accessed 4.11.13).

Wiggins, I.M., Hartley, D.E.H., 2015. A Synchrony-Dependent Influence of Sounds on Activity in Visual Cortex Measured Using Functional Near-Infrared Spectroscopy (fNIRS). PLOS ONE 10, e0122862.

Wijeakumar, S., Shahani, U., Simpson, W.A., McCulloch, D.L., 2012. Localization of hemodynamic responses to simple visual stimulation: an fNIRS study. Invest. Ophthalmol. Vis. Sci. 53, 2266–2273.

Wilke, R., Gabel, V.P., Sachs, H., Bartz-Schmidt, K.U., Gekeler, F., Besch, D., Szurman, P., Stett, A., Wilhelm, B., Peters, T., Harscher, A., Greppmaier, U., Kibbel, S., Benav, H., Bruckmann, A., Stingl, K., Kusnyerik, A., Zrenner, E., 2011. Spatial resolution and perception of patterns mediated by a subretinal 16-electrode array in patients blinded by hereditary retinal dystrophies. Invest. Ophthalmol. Vis. Sci. 52, 5995–6003.

Wong, Y.T., Chen, S.C., Kerdraon, Y.A., Allen, P.J., McCombe, M.F., Morley, J.W., Lovell, N.H., Suaning, G.J., 2008. Efficacy of supra-choroidal, bipolar, electrical stimulation in a vision prosthesis, in:. Presented at the 2008 30th Annual International Conference of the IEEE Engineering in Medicine and Biology Society, IEEE, pp. 1789–1792.

Wong, Y.T., Dommel, N., Preston, P., Hallum, L.E., Lehmann, T., Lovell, N.H., Suaning, G.J., 2007. Retinal neurostimulator for a multifocal vision prosthesis. IEEE Trans Neural Syst Rehabil Eng 15, 425–434.

Wurtz, R.H., Kandel, E., 2013. 27. Central Visual Pathways & 28. Perception of Motion, Depth, and Form, in: Principles of Neural Science. McGraw Hill Professional, pp. 524–571.

Yagi, T., 2009. Biohybrid visual prosthesis for restoring blindness. Int'l J of Applied Biomedical Engineering.

Yanai, D., Weiland, J.D., Mahadevappa, M., Fujii, G.Y., de Juan, E.J., Greenberg, R.J., Williamson, R., Cimmarusti, V., Humayun, M.S., 2003. Visual Perception in Blind Subjects with Microelectronic Retinal Prosthesis. ARVO Meeting Abstracts 44, 5056.

Yong, V.K., Morgan, W.H., Cooper, R.L., Shaw, M., Bremner, A.P., Bulsara, M., Yu, D.-Y., 2006. Trends in registered blindness and its causes over 19 years in Western Australia. Ophthalmic Epidemiol 13, 35–42.

Zeff, B.W., White, B.R., Dehghani, H., Schlaggar, B.L., Culver, J.P., 2007. Retinotopic mapping of adult human visual cortex with high-density diffuse optical tomography. Proceedings of the National Academy of Sciences of the United States of America 104, 12169–12174.

Zhou, J.A., Woo, S.J., Park, S.I., Kim, E.T., Seo, J.M., Chung, H., Kim, S.J., 2008. A suprachoroidal electrical retinal stimulator design for long-term animal experiments and in vivo assessment of its feasibility and biocompatibility in rabbits. J. Biomed. Biotechnol. 2008, 547428.

Zhou, D.D., Dorn, J.D., Greenberg, R.J., 2013. The Argus® II retinal prosthesis system: An overview, in:. Presented at the Multimedia and Expo Workshops (ICMEW), 2013 IEEE International Conference on, pp. 1–6.

Zrenner, E., Bartz-Schmidt, K.U., Benav, H., Besch, D., Bruckmann, A., Gabel, V.-P., Gekeler, F., Greppmaier, U., Harscher, A., Kibbel, S., Koch, J., Kusnyerik, A., Peters, T., Stingl, K., Sachs, H., Stett, A., Szurman, P., Wilhelm, B., Wilke, R., 2011. Subretinal electronic chips allow blind patients to read letters and combine them to words. Proceedings. Biological sciences / The Royal Society 278, 1489–1497.

Zrenner, E., Stett, A., Weiss, S., Aramant, R.B., Guenther, E., Kohler, K.,

Miliczek, K.D., Seiler, M.J., Haemmerle, H., 1999. Can subretinal microphotodiodes successfully replace degenerated photoreceptors? Vision Res 39, 2555–2567.

Appendix

Publications